Imperial College of Science, Technology and Medicine
Department of Chemistry

Conformationally-Fixed Conjugated Polymers *via* Aldol Polymerisation for Organic Semiconducting Applications

Nkechinyerem Adannaya Uzoamaka Onwubiko

Submitted in part fulfilment of the requirements for the degree of
Doctor of Philosophy in Chemistry, Imperial College London
Sep 2019

Abstract

There is copious potential for carbon-based semiconductors to compliment inorganic materials and open-up a range of applications to technology, as well as offer economic and environmental advantages for both manufacturers and consumers. These organic semiconducting materials are inexpensive and flexible with tunable properties due to covalent bonding within the molecules and intermolecular Van der Waals interactions. Through property-structure led strategic design these lightweight materials can be solution processed at ambient temperatures and high-throughput volumes to minimise energy consumption, expand their compatibility with plastic and flexible substrates and lower manufacturing costs.

The organic semiconducting field includes materials such as organic photovoltaic materials, organic light emitting diodes, photodetectors, radio-frequency identification tags and transistors, the focus of this thesis. Polymeric materials for organic field-effect transistors are generally prepared by transition metal mediated coupling reactions that often involve highly reactive, functional group sensitive or toxic reagents. These coupling reactions generate polymers where aromatic units are connected by carbon-carbon single bonds and are therefore subject to arbitrary rotation along the polymer spine. Torsional strain along the polymer spine increases conformational and energetic disorder in the polymer. In addition to this, defects from mis-coupling reactions during polymerisation results in higher degrees of disorder in the polymers. Disorder along the polymer backbone has been shown to hinder efficient charge transport and the formation of closely stacked polymer chains and extended crystalline domains for charge mobility.

To elicit coplanar, conjugated polymers and facilitate close $\pi - \pi$ stacking between polymer chains, we synthesised conformationally-fixed polymers by linking monomer units by carbon-carbon double bonds. Our polymers were prepared *via* metal-free, acid catalysed aldol polymerisation, an environmentally benign synthesis compared to traditional polymerisation reactions. The monomer structures used generated electron deficient polymers with extended delocalised frontier orbitals, near infrared absorption and good ambient stable electron charge transport. We also explored common property-design strategies of elongating the aromatic centres, side-chain engineering and reducing torsional strain to optimise the charge transport properties.

Acknowledgements

I would like to extend my sincere appreciation to Prof. Iain McCulloch for accepting me to join his research group and part-take in this challenging and refreshingly new project direction in the field of organic semiconductors.

I am grateful for having Dr Pascal Hayoz of BASF Basel as my second supervisor. He is unassuming, encouraging and impressively creative in adding to the direction of the project.

I am incredibly thankful to have collaborated, worked and laughed with a talented and welcoming group of scientists across the McCulloch and Heeney groups. I have many joyous memories from my time with those mentioned here: Dan-tiberiu Sbircea, Dr Hung-Yang Chen, Dr Wan Yue, Dr Astrid-Caroline Knall, Dr B. Purushothaman, Dr Mark Little, Dr James Ponder, Dr Karl Thorley, Dr Fei Zhuping, Dr Rolf Andernach, Dr Jessica Shaw, Dr Joshua Green, Dr Cameron Jellett, Petruta Maria, Matthew Bidwell, Dr Adam Marsh, Adam Marks, Maximilian Moser and Wenmin Xu. I have special appreciation for Dan-tiberiu Sbircea without whom I would never have considered joining the McCulloch group nor laughed or cried as much as I did during my PhD.

Many sincere thanks to the Imperial College Department of Chemistry technical staff, notably Dr Lisa Haigh, Mr Peter Haycock and Dr Andrew White, who enabled this work through their expertise and use of their instruments.

My family was my rock and foundation throughout my PhD and I would like to express my deepest gratitude to my mother, Ihedinma Onwubiko, and sister, Josephine Onwubiko, who answered my numerous calls whenever I called.

Many thanks to the many individuals who impacted my life up to this point and more specifically my life during my PhD: Prof. Phil Parson, Dr Lewis Allen, Dr Filip Sebest, Dr Christian Loftus, Dr Candice Palmer, Dr Bruno Loubière and Dr Kofo Saromi. It is impossible to name everyone here since many people have contributed to my story.

Last but not least, I am so thankful to God for opening doors of opportunities and strengthening me to grab life with my two hands.

This thesis is lovingly dedicated to Ihedinma and Josephine Onwubiko.

Declaration of Originality

The work described in this thesis was carried out in Imperial College London between October 2014 and November 2018. Unless otherwise stated the work was carried out by the author.

Copyright Notice

Imperial College of Science, Technology and Medicine
Department of Chemistry
Conformationally-Fixed Conjugated Polymers *via* Aldol Polymerisation for Organic Semiconducting Applications

Nkechinyerem.onwubiko09@imperial.ac.uk

Ada Nkechinyerem Onwubiko
Department of Chemistry
Imperial College London
Exhibition Road
London
SW7 2AZ
UK
www.imperial.ac.uk

Funding

We acknowledge funding from BASF, as well as FP7 Marie Curie IEF (622187), EPSRC Project EP/G037515/1, EP/M005143/1, EC FP7 Project SC2 (610115), EC FP7 Project ArtESun (604397), EC FP7 POLYMED (612538), EC H2020 and Project SOLEDLIGHT (643791) for financial support. Dr Mahesh Kumar Ravva and Professor Jean-Luc Brédas thank the generous internal competitive funding from KAUST; they are grateful to the KAUST IT Research Computing Team and Supercomputing Laboratory for providing continuous assistance as well as computational and storage resources. We thank the State Key Laboratory of Luminescent Materials and Devices, South China University of Technology, for the single crystal XRD experiments of NIID. Mingfei Xiao thanks the Cambridge Overseas Trust and Chinese Scholarship Council for PhD funding.

Contributions

Dr Wan Yue synthesised the initial C8C10 naphthalene bisisatin and polymerised it with C12 naphthalene bisoxindole monomer prepared by the author to furnish polymer P5.

Dr Cameron Jellett synthesised C8C10 naphthalene bisoxindole and used this along with the C8C10 naphthalene prepared by the author to produce polymer P4.

Dr Hung-Yang Chen synthesised the initial thieno[3,2-*b*]thiophene bisisatin monomer.

Dr Balaji Purushothaman contributed notably by synthesising further batches of thieno[3,2-*b*]thiophene bisisatin monomer.

Dr Mahesh Kumar Ravva under the supervision of Prof J. L. Brédas performed DFT calculations on the conformationally-fixed polymer systems and analysed the DFT calculations.

David A. Hanifi under the supervision of Prof Alberto Salleo measured and analysed GIWAXS data.

Mingfei Xiao under the supervision of Prof Henning Sirringhaus fabricated transistor devices and analysed the data obtained and Dr Mark Nikolka conducted the experiments to extract the Urbach energies.

Publications

Synthesis and Properties of Isoindigo and Benzo[1,2-*b*:4,5-*b*']bis[*b*]benzothiophene Oligomers. H. Liao, C. Xiao, M. K. Ravva, Y. Wang, M. Little, M. V. C. Jenart, A. Onwubiko, Z. Li, Z. Wang, J.-L. Brédas, I. McCulloch and W. Yue, *Chem. Commun.*, 2018, **54**, 11152-11155.

Fused Electron Deficient Semiconducting Polymers for Air Stable Electron Transport. A. Onwubiko, W. Yue, C. Jellett, M. Xiao, H.-Y. Chen, M. K. Ravva, D. A. Hanifi, A.-C. Knall, B. Purushothaman, M. Nikolka, J.-C. Flores, A. Salleo, J.-L. Brédas, H. Sirringhaus, P. Hayoz and I. McCulloch, *Nat. Commun.*, 2018, **9**, 416.

A Thieno[2,3-*b*]pyridine-Flanked Diketopyrrolopyrrole Polymer as an n-Type Polymer Semiconductor for All-Polymer Solar Cells and Organic Field-Effect Transistors. H.-Y. Chen, M. Nikolka, A. Wadsworth, W. Yue, A. Onwubiko, M. Xiao, A. J. P. White, D. Baran, H. Sirringhaus and I. McCulloch, *Macromolecules*, 2018, **51**, 71-79.

Diazaisoindigo Bithiophene and Terthiophene Copolymers for Application in Field-effect Transistors and Solar Cells. W. Yue, C. Li, X. Tian, W. Li, M. Neophytou, H. Chen, W. Du, C. Jellett, H.-Y. Chen, A. Onwubiko and I. McCulloch, *J. Polym. Sci. Part A: Polym. Chem.*, 2017, **55**, 2691-2699.

Azaisoindigo Conjugated Polymers for High Performance n-Type and Ambipolar Thin Film Transistor Applications. W. Yue, M. Nikolka, M. Xiao, A. Sadhanala, C. Nielsen, B. Christian, A. J. White, H.-Y. Chen, A. Onwubiko, H. Sirringhaus and I. McCulloch, *J. Mater. Chem. C*, 2016, **4**, 41, 9704-9710.

An Approach to the Core of Lactonamycin. P. J. Parsons, D. R. Jones, L. J. Walsh, L. A. T. Allen, A. Onwubiko, L. Preece, J. Board, and A. J. P. White, *Org. Lett.*, 2017, **19**, 10, 2533-2535.

Semiconducting Polymer. J.-C. Flores, P. Hayoz, I. McCulloch, N. Onwubiko, D. Kaelblein, W. Yue, H.-Y. Chen and A.-C. Knall, WO2017148864A, 2017, Pub: Feb 14, 2019, BASF SE.

Abbreviations

^{o} - Degree

μ_h - Hole mobility

μ_e - Electron mobility

Å - Angstrom

BDP - Benzodipyrrolidone

calc. - Calculated

CB - Chlorobenzene

CdSe - Cadmium selenide

δ - Chemical shift

μ - Micro

A - Amperes (amps)

aq. - Aqueous

BT - Benzothiazole

C - Celsius

cm - Centimetres

CV - Cyclic Voltametry

$C\#$ - $C_{\#}H_{2\#+1}$ Linear alkyl chain

$C\#C\#'$ - Branched alkyl chain

o-DCB - *o*-Dichlorobenzene

DCM - Dichloromethane

DFT - Density Functional Theory

DMF - Dimethylformamide

DMSO - Dimethylsulfoxide

DPP - Diketopyrrolopyrrole

DSC - Differential Scanning Calorimetry

e.g. - Exempli gratia (for example)

E_g - Band gap

EI - Electron ionisation

ES - Electrospray ionisation

eq. - Equivalents

eV - Electron volts

Feb - February

g - Grams

GC - Gas Chromatography

Ge - Germanium

GIWAXS - Grazing-incidence Wide-angle X-ray scattering

GPC - Gel Permeation Chromatography

HOMO - Highest Occupied Molecular Orbital

I_D - Drain current

$I_{on/off}$ - on/off Current ratio

IR - Infrared

InSb - Indium antimonide

J - Coupling constant

L - Channel length

L - Litre

LDA - Lithium diisopropylamide

LUMO - Lowest Unoccupied Molecular Orbital

λ - Wavelength

m - Milli or metres

M - Molar

mins - Minutes

M_n - Number average molecular weight

MS - Mass spectrometry

M_W - Weight average molecular weight

m/z - Mass-to-charge ratio

NBS - *N*-Bromosuccinimide

NIR - Near-infrared

nm - Nanometres

NMR - Nuclear Magnetic Resonance

o - *ortho*

OFET - Organic field-effect transistor

OPV - Organic photovoltaic

OS - Organic semiconductor

P3HT - Poly(3-hexylthiophene)

PBTTT - Poly(2,5-bis(3-hexylthiophen-2yl)thieno(3,2-b)thiophene)

PE - Petroleum ether

PET - Polyethylene terephthalate

PESA - Photoelectron spectroscopy in air

ppm - Part per million

Pub - Published

rt - Room temperature

s - Seconds

sat. - Saturated

SMOS - Small molecule organic semiconductor

t - tertiary (*tert*)

TCE - Tetrachloroethane

Te - Tellurium

THF - Tetrahydrofuran

TLC - Thin layer chromatography

ToF - Time of flight

UV - Ultraviolet

UV-vis - Ultraviolet-visible

V - Voltage (volts)

V_D - Drain voltage

V_G - Gate voltage

V_{th} - Threshold voltage

W - Channel width

XRD - X-ray diffraction

Contents

List of Tables

List of Figures

Chapter 1

Introduction

1.1 Motivations for Organic Semiconductors

Technology and electronics are integral to every facet of 21^{st} Century living. It is important for research, analysis, communication and progression of all aspects of modern day living. And currently, there is a drive for integration of platforms, amalgamation of services and collection of big data for discerning markets and product opportunities. All these interests push forward the frontier of electronics, perpetually changing and evolving it.

Part of this progression is the incorporation of soft electronics, organic semiconductors, into technology due to their physical properties, economic and environmental advantages. Organic semiconductors are composed largely of non-metals, carbon, sulfur and oxygen atoms that are inexpensive to obtain. They have a great propensity for solution, high-frequency manufacturing techniques that lower costs compared to inorganic materials.[1] Furthermore, the potential for colour variability, lightweight and flexible electronics appeals both to producers and consumers of electronics.[2,3] Organic materials are increasing utilised in the Energy sector as organic photovoltaics (OPV).[4,5] Other applications for organic semiconductors include organic light emitting diodes (OLEDs),[6] photodetectors, radio frequency identification tags (RFID) and bio-electronics.[7–10]

Displays, ubiquitous in technology, require pixels to give information to users, and for all its various applications and functionality, it is the dominant application of thin film transistors. Flat panel displays (FPD) are a common type of display used in smartphones, tablet computers, televisions and more. Types of FPD include liquid crystal displays, plasma panels, electroluminescent panels and organic light-emitting diodes.[11] With the FPD market projected to be worth $135 billion in 2020, there is a strong monetary motivation for new organic semiconducting transistors.[12,13] Along with this large industry comes the need for thin film transistors (TFT) to control the pixels. Inorganic materials such as single crystal silicon, polycrystalline silicon and amorphous silicon oxides are prevalent in transistors. Other inorganic materials such as metal oxides of tellurium (Te), cadmium selenide (CdSe), germanium (Ge) and indium antimonide (InSb) are also used.[14] Although current display technology is dominated by amorphous silicon semiconductors, there are a number of shortfalls to using silicon-based materials in transistors. Crystalline or polycrystalline silicon are expensive to manufacture due to the multiple high energy processes involved in their production. As much as 50 % of the cost associated with manufacturing displays is attributed to the production of silicon-based semiconductors.[15] These high costs fuel a demand for low-cost electronics and therefore research into cheaper materials such as hydrated amorphous silicon, amorphous metal oxides and organic semiconductors.

Polycrystalline silicon benefit from high charge mobilities in the range of 30-300 $cm^2V^{-1}s^{-1}$. However, it's main liability is the high production costs from high temperature processing and multiple production steps.[16] Also, the non-uniform nature of polycrystalline silicon results in multiple grain boundaries that limit charge transport in devices.[15] Hydrogenated amorphous silicon (a-Si:H) was developed as a semiconductor material after polycrystalline silicon. Amorphous silicon was introduced in the 1970s and continues to be the predominant technology used in most TFT devices.[17,18] Although, the low mobility of a-Si:H, in the range of 1 $cm^2V^{-1}s^{-1}$, is borderline sufficient for it's use in displays, there are TFT applications in which its mobility is insufficient and new materials would be more suitable. Amorphous silicon has limited charge carrier density due to the covalent bonds to hydrogen atoms, in addition to its amorphous nature, this lowers its charge mobility. It also suffers from high current leakage that increases the power consumption of electronics. The stability of a-Si:H is also questionable, with significant

threshold voltage drifting in certain conditions. Amorphous silicon is the prevailing semiconducting material, as in the past there was and continues to be a demand for improved materials with fewer defective properties and more nuanced characteristics for FPD applications.

There is also an interest to make more lightweight, larger and or flexible electronics. Silicon-based TFT are generally deposited on heavy and brittle glass substrates.. Rather than use glass substrates, the industry would like to exploit flexible, plastic substrates. Plastic substrates, though, necessitate lower processing temperatures. Polycrystalline silicon is deposited at temperatures above 500 ^oC and produced at even higher temperatures, whilst a-Si:H is deposited at approximately 300 ^oC, but organic semiconductors will enable the use of temperatures closer to ambient levels.[19] Crucially, low processing temperatures allow the use of flexible, plastic substrates because they require low deposition temperatures. The nature of flexible plastic would infer properties such as rollability and foldability of electronics, that are incompatible with polycrystalline silicon or a-Si:H.[9] The vapor deposition method used in a-Si:H and polycrystalline silicon devices also limit the ability to produce large area devices.

Transistors made from amorphous metal-oxides (AMOS) can fulfill several physical properties present in organic semiconductors.[20] Furthermore, they display high charge mobilities, and could therefore be used in large area application unlike a-Si:H. TFT of indium-gallium-zinc oxide ($InGaZnO_4$) was commercialised in 2012 although they were first reported in literature in 1996. AMOS can be transparent, flexible and could be fabricated at room temperature and therefore onto plastic substrates such as polyethylene terephthalate (PET) to produce uniform devices that do not require post-deposition annealing.[21]

Typically though, AMOS contain poisonous and environmentally damaging metals. Considering the potential damage of the accumulative billions of waste phones in landfill, this is a significant concern. The quantity of phones being manufactured in China reached 1.2 billion in 2012.[22] The global quantity of mobile phones manufactured in 2012 is higher still since China accounts for 81 % of manufactured phones. This number is projected to rise. The quantity of cadmium in one mobile phone battery can pollute 600,000 L of water.[23] In addition to the physiology benefits of recycling mobile phones, there are also economic benefits as the resources

lost in waste phones can be recovered and utilised. Given that 80 % of the components of mobile phones can be recycled the billions of phones discarded each year are a true loss.[24] In addition to the physiological benefits of recycling mobile phones, the economic benefits are also underappreciated. From 1 ton of mobile phones, about 130 kg of copper, 3.5 kg of silver, 340 g of gold and 140 g of palladium can be recovered.[25] Since only 4 % of mobile phones are recycled globally further use of toxic metals in electronics should be avoided or minimised.[26] The replacement of these metals with organic semiconductors or the use of organic semiconductors to compliment inorganic semiconductors can only be environmentally beneficial.

1.2 Introductions to Organic Field-Effect Transistors

Organic semiconductors are grouped into two broad categories; discrete molecular compounds and polymers. The molecular size of these materials generally directs the material processing method, which in turn, determines manufacturing costs. Polymers are suitable for solution processing and incompatible with high energy batch gas deposition techniques. Small molecules, though, are often processed by vapor deposition techniques such as sublimation in addition to solution processing. Given that polymers are solution processed, they are preferred because high-throughput solution manufacturing techniques offer more cost savings compared to batch production. Solution processes such as printing, spraying or coating can be continuous processes.[27,28] Whats more, these processes do not require vacuum chambers and are less expensive deposition methods.

Regardless of their differences, small molecules and polymers must be conjugated; consist of congruent π-bonds that alternate with σ bonds. The sp^2-hybridised carbon atoms are linked by strong σ bonds and weaker π-bonds perpendicularly to the single bonds. The small molecules and polymers interact with each other by weak Van der Waals forces, that imparts the desirable physical characteristic such as flexibility to organic semiconductors. Conversely, amorphous silicon is inherently stronger and brittle because its atoms are connected throughout by strong covalent bonds. The different bonding mechanisms in organic and inorganic semiconductors

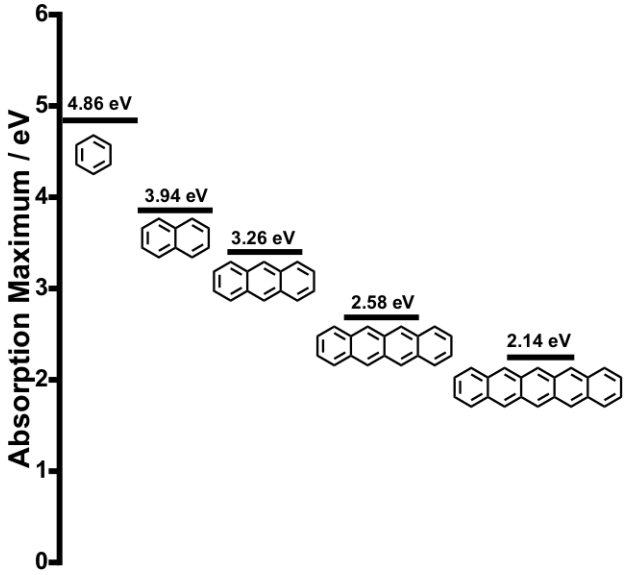

Figure 1.1: A graphical illustration of the effect of acene size on light absorption. Acene conjugation length increases with its size therefore pushing up its HOMO with higher electron density and producing a smaller optical gap and lower energy absorption maximum.

prescribe the mode of charge transport in the materials and much of the observed differences in their properties.

In inorganic semiconductors, the molecular orbitals extend across the bulk of the material due to the large network of covalent bonds. The frontier orbitals in organic semiconductors, though, delocalise along the molecule or polymer to a limited degree. The π-bonding orbital of a molecule is called the highest occupied molecular orbital, HOMO. Whilst the π^* orbital is the lowest unoccupied molecular orbital, LUMO. In bulk organic semiconducting material, the HOMO and LUMO are more precisely labelled the ionisation potential (IP) and the electron affinity (EA) respectively, however the terms HOMO and LUMO are often used to refer to the bulk OS. The energy difference between the HOMO and LUMO is an approximation of the fundamental gap.[29] Electrons are excited into the LUMO when they absorb photons of energy equal to or greater than the fundamental gap, leaving a hole in the HOMO. In the HOMO, sequential intramolecular and intermolecular charge transfer process of either the electron or the hole enables charge transport in the material. The energy of these frontier orbitals are determined by the conjugation length in the organic compound, which are in turn determined by the molecular structure. As conjugation increases, the optical gap narrows (Fig. 1.1). The optical gap decreases in energy because there is greater electron density in the delocalised

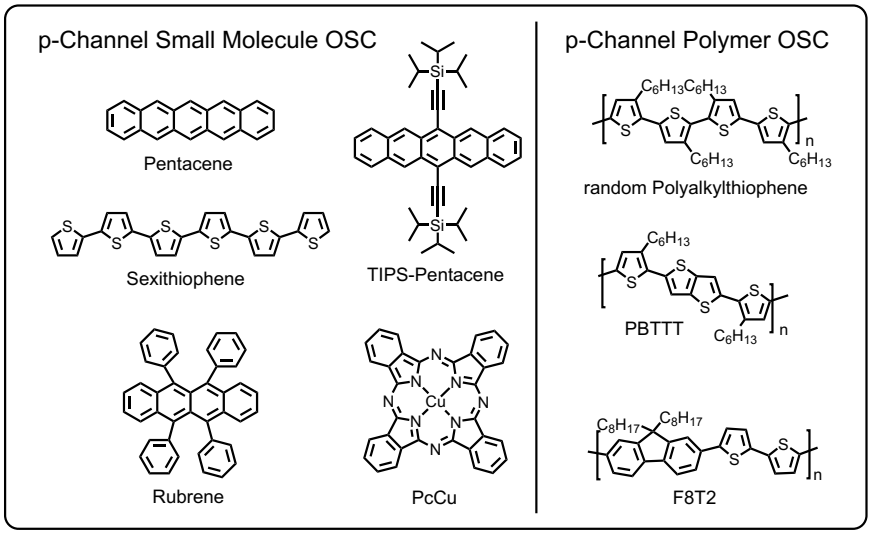

Figure 1.2: A selection of p-type charge transport small molecules and polymers that are foundational to the field of organic semiconductors.

molecular HOMO that pushes the HOMO level up. Introducing anti-bonding character in the molecule, such as interrupting the conjugation (cross-conjugation) would localise the frontier orbitals, lower the HOMO and widen the optical gap. Narrowing the optical gap can also be achieved by stabilising the LUMO relative to the HOMO. Spatially separating the π^* orbitals and introducing electron withdrawing units stabilises the LUMO. The acene homologous series (Fig. 1.1) shows how increasing the conjugation length changes the optical gap. However, narrowing of the optical gap does not continue indefinitely until the LUMO and HOMO merge to create a conduction band like in metals where electrons require no addition energy for free movement. Longuet-Higgins and Salem illustrated that fully delocalised, infinitely large cyclic polyene become unstable due to anti-symmetrical distortion as the conjugation length tends to infinity.[30] This Peierl's distortion ensures that the optical gaps tends toward a discrete value.

1.2.1 A Selection of Organic Semiconductors

An introduction to the field of organic semiconductors is incomplete without a summary of the veteran molecules and polymers that built the field.[31,32] Figure 1.2 shows common structures and materials with p-channel transport. A discussion of these highlight the charge transport parameters that are generally associated with these materials. In applications of transistors,

anthracene was one of the first molecules used for p-channel conduction in OFETS.[33] Considering the nature of how transistors function and the typical structural features required of its molecules, it is obvious that anthracene is a good potential moiety for use in OFETs. Other acenes, particularly pentacene and its derivatives such as TIPS-pentacene, have also shown wide functionality in TFT devices.[34–36]

Pentacene, perhaps the most researched small molecules for OFET applications, is presently commercially available products. It is polycrystalline, but can produce single crystals with the molecules packed into herring bone pattern when grown through vapor deposition. Due to its strong aggregation and tight solid state packing, p-type charge transport in pentacene-based transistors are moderately stable to oxygen and light, for the same reason pentacene is highly insoluble, making it difficult to process. It is subsequently deposited onto substrates by high temperature, batch-process vapor deposition. Soluble pentacene precursors can be solution processed and post deposition treatment such as heating can release pentacene onto the device and circumvent the use of vapor deposition. Lin *et al.* reported high mobilities of 1.5 $cm^2V^{-1}s^{-1}$ for pentacene with devices displaying on/off current ratio $> 10^8$, near zero threshold voltage and sub-threshold swing of $< 1.6\ V/decade$.[37] There are many methods available in transistor manufacturing to optimise transistor devices, and pentacene devices have achieved mobilities greater than 3.0 $cm^2V^{-1}s^{-1}$. Although, pentacene is a p-type semiconductor, n-transport is possible when it is doped. Iodine-(alkaline metal-)doped pentacene is an ambipolar semiconductor.[38,39]

In addition to acenes, thiophene-based oligomers are another common class of small molecule organic semiconductors (SMOS).[40] Figure 1.3 gives a short selection of these molecular semiconductors. Sexithiophene is a good example of this class of semiconductors. Their mobilities are typically lower than that of pentacene based SMOS. Thiophene-based FETs achieved mobilities of 0.002 $cm^2V^{-1}s^{-1}$.[41] These results suggest, long range order and crystallinity promote high charge mobility in the TFT. Within this class of molecules, regio-regularity of the side chains is crucial and affects the solid-sate arrangement of the molecules. Regio-irregularly substituted thiophene molecules are less able to stack together in a way that promotes charge transport.

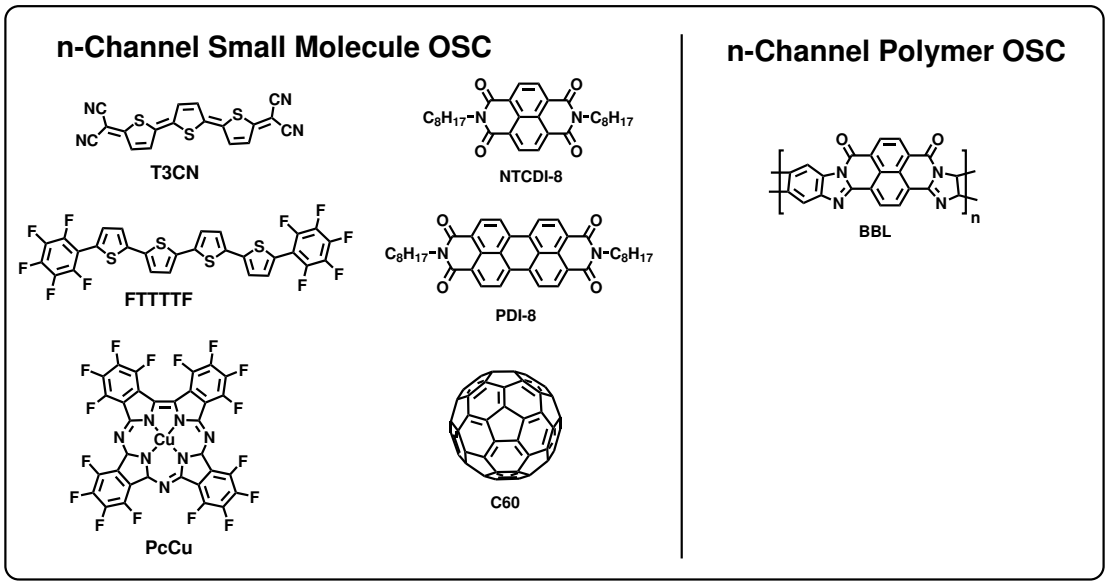

Figure 1.3: A selection of n-type charge transport small molecules and a polymer that is foundational to the field of organic semiconductors.

The p-channel polymeric workhorse material, poly(3-hexylthiophene) (P3HT), is an extension of thiophene-based small molecules.[42,43] It also suffers significantly from the issues of regio-regularity of the side-chains. In regio-random P3HT, side-chains are arranged both head-to-head and head-to-tail randomly along the polymer. The steric repulsion in head-to-head side chains arrangements results in misalignment of adjacent thiophene units along the polymer. The resulting torsional twists limits conjugation length along the polymer spine and forces polymer chains apart in the solid state since the polymers cannot not stack effectively. The disorder in the arrangement of the polymer cause the solid state morphology to be less effective for charge transport.[44] P3HT has application in transistors, but predominantly in OPV. Other polymers of note include PBTTT[45] and F8T2.[46,47]

From this small selection it is clear that thiophene and benzene rings are central to the materials in organic semiconductors. In addition to p-type materials, electron transporting materials are also required for complementary logic circuits for example. Fig. 1.3 gives a selection of n-type small molecules and polymers for OFET. Materials for n-type OS are less common than p-type materials. This is because they suffer from intrinsic and extrinsic factors that limit charge injection and promote energy level instabilities when electrons are present in the LUMO.[48]

N-type materials are typically characterised by molecules or polymers containing significant

quantities of electron withdrawing groups or building blocks. A common method for stabilising the LUMO is the replacement of hydrogen atoms in the polymer backbone with electron withdrawing fluorine or other halogens.[49] Another strategy toward n-channel transport is to modify the dielectric material to eliminate electron traps. This method has transformed primarily p-channel material to n-channel transport semiconductors[32,50,51] This also enhances the electron mobility of established n-type materials. Similarly to p-type materials, thiophene-based small molecules or polymers are a prominent class of n-channel transport material, particularly when modified to have lower frontier orbitals. A popular approach is to substitute hydrogen atoms on thiophene units with fluorine and cyano groups or attach flanking perflouroalkyl or aryl groups.[52–54] Antonio and colleagues reported perfluorohexylsubstituted thiophene oligomers with mobilities of 0.24 $cm^2V^{-1}s^{-1}$.[55]

Another group of n-type materials are fused naphthalene and perylene[54,56,57] acenes. Molecules such as PDI-8[58,59] and NTCDI-8[60,61] benefit from strongly electron withdrawing carbodiimide groups that lower the LUMO. Fullerenes have also been shown to display electron transport properties. Mixtures of $C_{60}-C_{90}$ produce isotropic solids when deposited at ultra high vacuums achieved mobilities of 0.08 $cm^2V^{-1}s^{-1}$.[62] Ladder type materials are another important class of n-channel polymers, we will discuss this in more detail later in the thesis. The archetypal ladder type polymer, BBL, has demonstrated mobilities of < 0.1 $cm^2V^{-1}s^{-1}$.[63]

1.2.2 Organic Field-Effect Transistors (OFET)

The first transistor device is credited to Schokley *et al.* in 1949.[64] Although the concept of metal-insulator field-effect transistor was present in 1928, it was in the 1960s that the design and development of inorganic semiconductor in thin-film transistors really began to grow.[18,65] Thin-film transistors are a niche of field effect transistors where a thin film of active layer material is structured with a dielectric material and contacts to create a transistor.[66] Transistors can be produced in a variety of architectures, depending on the application, desired device characteristics and the relative processing conditions of the components. There is a wealth of literature on the fundamental physics of organic field-effect transistors.[67–69] Organic transistors

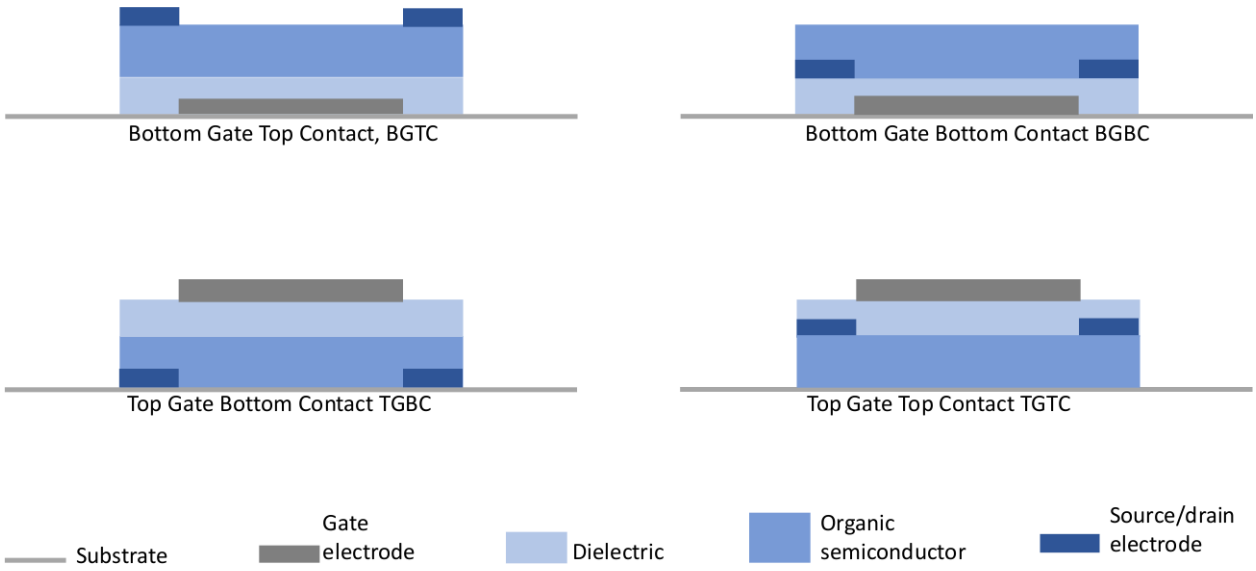

Figure 1.4: Four transistor device structures. Depending on the deposition order of the different components a range of transistor architectures are possible.

are composed of: gate electrode, dielectric material, organic semiconductor, source and drain electrodes. The gate electrode can be positioned either atop the device, Top-Gate (TG), or at the bottom of the device, Bottom-Gate (BG). Of these two categories, the Bottom Gate geometry is most common in the literature even though the TG structure is inherently more stable due to self-encapsulation of the contacts and semiconductor by the dielectric material and gate electrode. Figure 1.4 depicts the four main devices geometries. In BGTC device, the dielectric material is layered atop the gate electrode, followed by the organic semiconductor. The source and drain contacts are then patterned onto the semiconductor *via* vapor-phase evaporation of the contacts. This methodology poses the risk of damaging the semiconductor layer even though it is highly advantageous in imparting lower contact resistance because it offers a close contact between the electrodes and the semiconductors. Lower contact resistance is beneficial for maximising charge mobility. In BGBC devices, the source and drain electrodes are sandwiched between the dielectric and the organic semiconductor. In this case, the dielectric surface can be disturbed by the source and drain electrode deposition and the devices subject to greater contact resistance. BGBC, for this reason, often has lower measured charge mobilities. Notwithstanding, this geometry is more amenable to cost-effective, high-throughput manufacturing. In TGBC device geometry the dielectric and gate materials are deposited on top of the organic semiconductor respectively, shielding it from the external environment. When the

source and drain contacts are deposited first then a TGBC architecture is obtained and when they are deposited after the organic semiconductor a TGTC geometry is achieved.

When the gate electrode is subjected to a potential difference it modulates the HOMO and LUMO level of the organic semiconductor through the dielectric layer *via* the field-effect phenomenon. Silicon dioxide is a standard dielectric material although other oxides and polymeric insulators are used. Deposited on top of the gate, the dielectric layer allows a capacitance to develop between the gate and the organic semiconductor. Consequently, an applied positive gate voltage results in the accumulation of negative charges, electrons, at the organic semiconductor insulator interface, creating an n-type charge transport channel. Conversely, when a negative potential difference is applied to the gate electrode, holes, positive charge carriers, concentrate in the lower layers of the organic semiconductor. A potential difference between the source and drain electrode then enables charge to flow. It follows, then, that charge transport is controlled by gate voltage and the source-drain potential difference.

Figure 1.5 illustrates the field-effect phenomenon that governs charge transport in OFETs. At $V_G = 0$, and $V_D = 0$ HOMO and LUMO level of the organic semiconductor is at their solid state energy levels relative to the contact electrodes. In an electron transport material, applied positive gate voltage pulls frontier orbitals down, more importantly, it lowers the LUMO. When the LUMO energy matches the Fermi levels of the source and drain contacts (part b Figure 1.5), a difference in the source-drain voltage allows charge to move (part d Figure 1.5). The gate voltage at which the LUMO matches the contact energy level is effectively the threshold voltage. Ideally, the transistor is off when $V_G = 0$, however this is often not the case. From the threshold voltage incremental increases in the gate voltage results in a sharp rise in the current, this is the subthreshold regime, shown in Figure 1.6 in the transfer curve. Now, when a positive V_D is applied, current flows between the source and drain electrodes. Inversely, negative gate voltage elevate the HOMO level, until it matches the Fermi level of the contacts. At this point, a source-drain potential difference allows hole charge transport between the electrodes.

Two main types of graphical data are obtained from transistor devices; an output curves and transfer curves referring to the $I_D - V_D$ and $I_D - V_G$ relationships respectively. The output

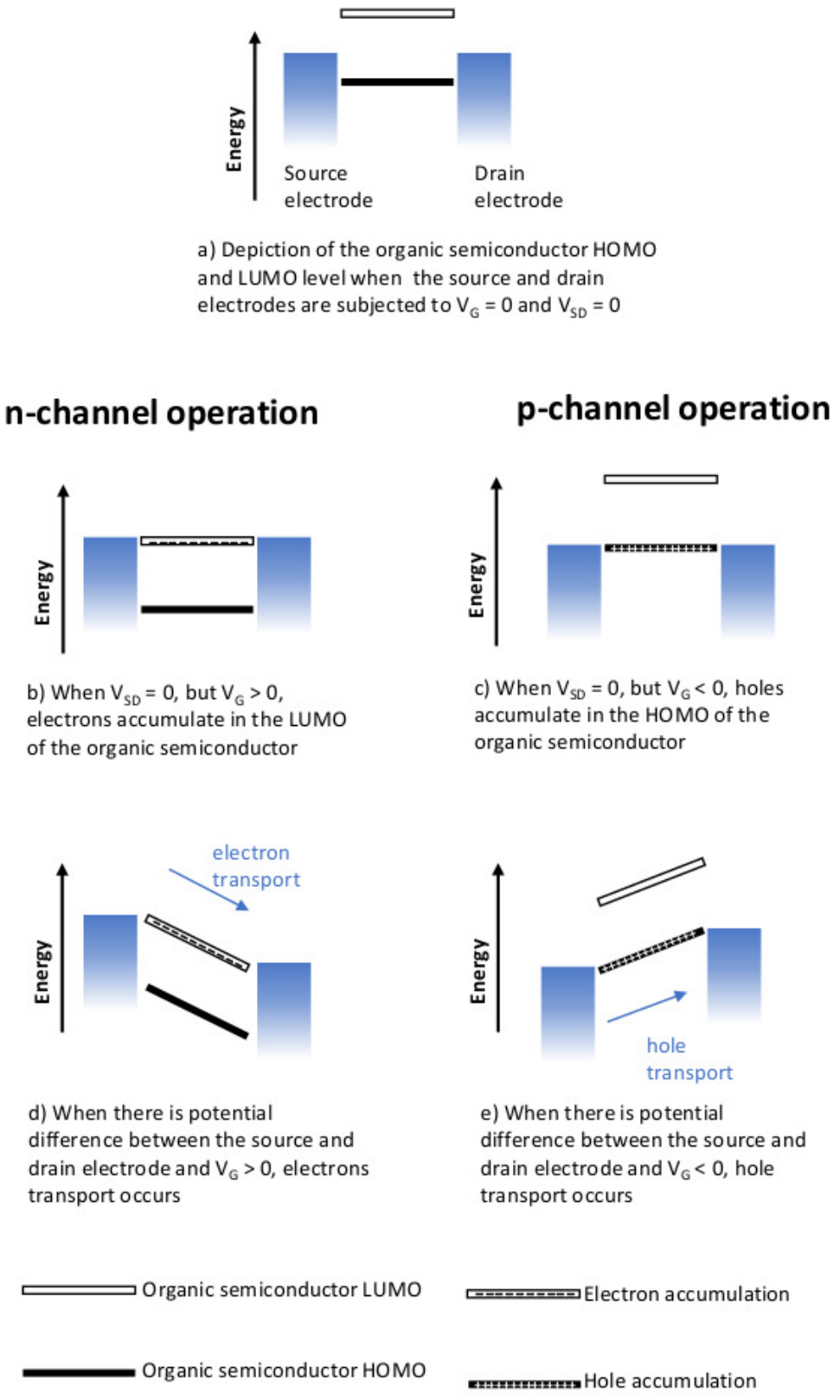

Figure 1.5: A schematic demonstrating the mechanism of n-channel and p-channel transport based on the energy levels of the transistor components.[70]

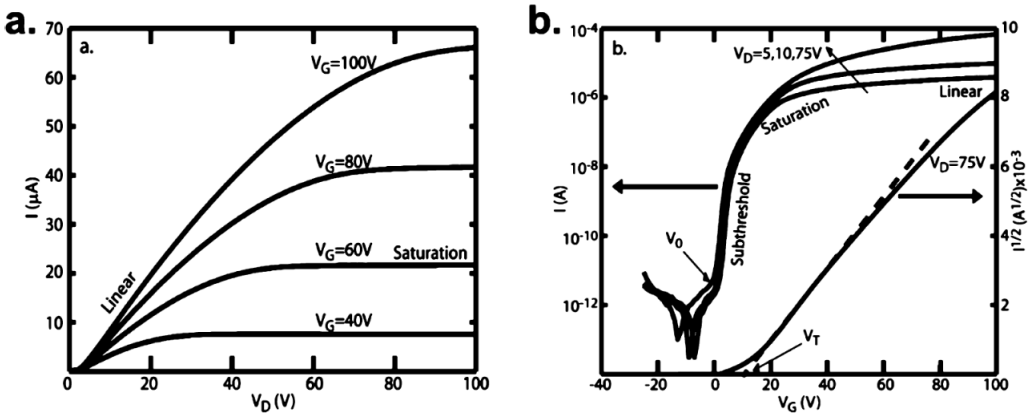

Figure 1.6: Examples of data output from n-channel transistors. a) $I_D - V_D$, output curve,shows variation of device current with source-drain voltage at different gate voltages. b) A transfer curve, $I_D - V_G$, displaying current changes with respect to gate voltage at different source-drain voltages. This image was reproduced with permission, copyright 2004 American Chemical Society.[70]

curve shows the variation of current with drain voltage. The curve is composed of a linear and saturation regime. Upon applying a positive drain voltage V_D, the current (μA) through the semiconductors increases linearly with voltage. As the voltage continues to increase the current begins to plateau into the saturation regime. The current rise per voltage increase is determined by the gate voltage and therefore changing the gate voltage increases the gradient of the linear region and increases the voltage at which the current reaches saturation. Meanwhile, the transfer curve shows the relationship of the current and gate voltage, V_G. The region near zero gate voltage and current changes is the sub-threshold region. The sub-threshold regime begins at $V_D = 0$. In n-type material, small positive increase V_G considerably raises the current in the sub-threshold region. The current continues to increase several orders of magnitude (Linear regime), before it starts to saturate and plateau (Saturation regime). Negative gains on V_G also results in the same changes for a hole-transporting material. If the material is ambipolar then it would also display current increases as the gate voltage is made more negative or more positive.

The different regimes can also be visualised in the illustration in Figure 1.6 part a) and b). This figure (part a) also shows the charge carrier accumulated in the transport channel at either a hole and electron transport channel. When the gate voltage is equal to the source-drain voltage then a current flows in the linear region. Due to depletion of charge carriers, current cannot

rise indefinitely.

The charge carrier mobility (μ), current modulation ratio (I_{on}/I_{off}) and threshold voltage (V_t) are the defining parameters to extract from OTFT devices. The mobility describes the drift of charge per area per electric field and it is also temperature dependent as temperature affects the charge transport mode. The I_{on}/I_{off} is the ratio of the current between the source and drain electrodes when the gate voltage is high and the device is on, compared to when the gate voltage is zero and the device is off. It gives an indication of the material purity and propensity to atmospheric doping. The threshold voltage is the gate voltage when the device can function dependent on the source-drain potential. Traps in the material cause an increase in threshold voltage because the traps must be filled before the device can be turned on. These parameters are obtained from the OTFT output and transfer curves. The charge carrier mobility (μ) and threshold voltage (V_{Th}) in the saturated and linear region can be calculated from the output characteristics from the equations below

$$Saturation\ regime \qquad I_{SD} = \mu_{sat}\frac{WC}{2L}(V_G - V_{Th})^2 \tag{1.1}$$

$$Linear\ regime \qquad I_{SD} = \mu_{lin}\frac{WC}{L}(V_G - V_{Th})V_{SD} \tag{1.2}$$

Equation 1.1 describes the standard saturated regime current, whilst equation 1.2 describes the linear regime current in the output curve, shown where $V_D < (V_G - V_{Th})$, where I_D is the current between the source and drain electrodes, W is the channel width, L is the channel length and C_{ox} is the capacitance of the dielectric material. These equations show that the current measured in a transistor is dependent on the capacitance of the dielectric layer in addition to the dimensions of the device and the applied potential voltages. The mobility is generally obtained from the saturation region because the linear mobility is subject to high contact resistance depending that can dominate the device performance. The threshold voltage can be obtained from the intercept of a line drawn through the linear region of $I_{D,sat}^{1/2}$ *vs* V_G plot.

In addition to transistor devices, other forms of measuring charge transport in organic semi-

conductors include Time of Flight measurements, Space-charge limited current-voltage, space-charge limited dark injection. Using different measurement techniques allows for a fuller picture of the material property of the organic semiconductor to be observed.

Time of Flight (ToF) measurements are a bulk material measurement that require a sandwich-type geometry where the semiconductor is sandwiched between two metal contacts. The anode is grounded and a voltage is applied at the cathode. To carry out the measurement, a short pulse is applied to one of the semi-transparent non-injecting electrode contact. The single layer of charge generated then drifts across the thick layer of material, and the movement of the charge is measured mobility in a ToF experiment is given by: $\mu = \frac{d^2}{t_{tr}V}$ Space charge limited current-voltage experiment is run similarly to that of ToF measurements. The set-up is also like a sandwich and the material thickness is approximately 100 nm. The mobility in this case though is calculated with the equation: $\mu = \frac{8Jd^3}{9V^2\epsilon\epsilon_0}$ When the contact is non-ohmic, the current, J, is limited by injection rate rather than mobility. The data produced is difficult to analyse for disperse transport and different devices are required to study electrons and holes.

1.2.3 Charge Transport

Charge transport in solid state organic materials describe the transfer of electrons or holes from a charged ionic molecular state to a neutral molecular state. A hole is created when an electron is removed from a neutral molecule to generate a cation, M+ (Fig. 1.7). The transfer of this hole occurs when the molecular cation, receives an electron from an adjacent neutral molecule. Similarly for electron transfer, an electron is injected into a neutral molecule to generate an anion, M-. The transfer of an electron from the negatively charged molecule to a neutral molecule is electron transport. The language used thus far is for discrete molecules, for polymers the charged states are referred to as positive or negative polarons.[71] In conjugated polymers, positive and negative polarons are delocalised along the a certain length of the polymer. The energies of the charged state is different depending on the energy level of polymer segment and its surrounding. This polarisation is stabilised by converse polarisation energies in the solid state.

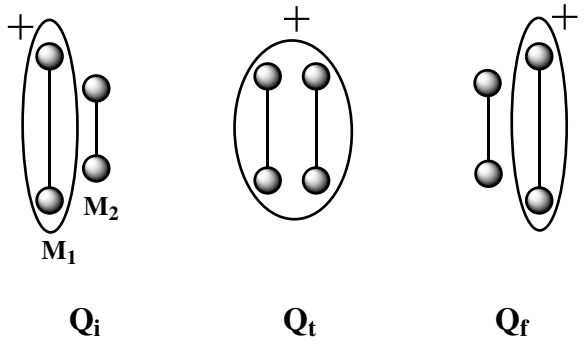

Figure 1.7: Simplification of a hole charge transfer process between a cationic molecule and an adjacent neutral molecule, passing through an intermediate labeled Q_t. Q_i and Q_f respectively refer to the initial and final state of the systems.

Charge transport occurs *via* two mechanisms; band transport or hopping transport.[72] These can takes place to varies degrees within a material, making it difficult to correlate the charge mobility. Band transport, present in inorganic semiconductors, is prominent in single molecular crystals at low temperatures. In molecular crystals, the bandwidth is small due to the weak electronic delocalisation, and mobilities are in the order of 1-10s $cm^2V^{-1}s^{-1}$. There are fundamental differences in the composition of organic semiconductors and inorganic semiconductors. Atoms in inorganic semiconductors are all bonded by covalent bonds, consequently electronic states are extended across the whole material. As the frontier wave function of the atoms all overlap and interconnect to form a band structure for charge transport. This also means that the dielectric permittivity in inorganic semiconductors is high and electron binding energy is low. The converse is true for organic semiconductors, they have localised electronic states, low dielectric permittivity and low binding energy. The atoms are covalently bonded in organic semiconductors to give finite molecules small molecules or polymers that interact with each other by Van der Waals interaction. This means that charge has to hop between discrete electronic states. The charge transport is therefore orders of magnitudes lower in organic semiconductors (10^{-7} - 10 $cm^2V^{-1}s^{-1}$) compared to inorganic materials (10 - 10^4 $cm^2V^{-1}s^{-1}$).

The presence of traps allow deviations from this transport mode. In extremely amorphous materials, charges hop from site to site because there is no band structure. This leads to much lower mobility values of around 10^{-3} $cm^2V^{-1}s^{-1}$. The mobility is then dependent on both temperature and the applied electric field strength. The temperature dependency of

the mobility varies for different charge transport models. Space charge trapping effects and charge carrier injection mechanisms considerably affect the ability of charge to comply with the inverse power dependence of mobility on temperature. In terms of the bulk material, the current through the materials is given by the charge carrier density (n), the elemental charge (e), and the velocity (ν). The velocity can be expressed as mobility multiplied by electric field strength (F).

$$j = en\nu = en\mu F \tag{1.3}$$

There are multiple aspects of charge transport in organic semiconductors. Overall though, charge transport in semiconductors consist of moving charges from one energy state to another energy state. It is therefore necessary to consider the energy of the sites and their spatial relationships. The precise location and energy levels of sites are important for small systems. But in large systems, where charge transport involves a large number of sites, the exact topology is best described by a statistical distribution function. In organic semiconductor materials where the materials are on a macroscopic scale a statistical function is sufficient to describe the energy site topology. There are numerous steps involved in charge transport in transistor devices: charge injection, charge channel formation, charge accumulation, charge transport and charge collection.[70,72] Each stage of the processes is governed by the relationship of the different electronic states in many deviations of the molecule or polymer from equilibrium, such as addition or removal of charge causes bond length, bond angles, charge and spin density variability.

There are two modes of charge transport in organic semiconductors: fast band-like transport within the polymer due to its strong electronic coupling and hopping-mechanism, intermolecularly, or between segments of conjugated polymers. The rate of charge transport is described by non-adiabatic Marcus theory. Charge transport is essentially a multiple charge transfer processes from a polaron to an adjacent polymer or polymer segment. The main parameters that control charge transfers are reorganisation energy, electronic transfer integral and the energy difference between the initial and final energy state of the relevant components.

The intermolecular charge transport can be modelled by considering the charge transfer of an

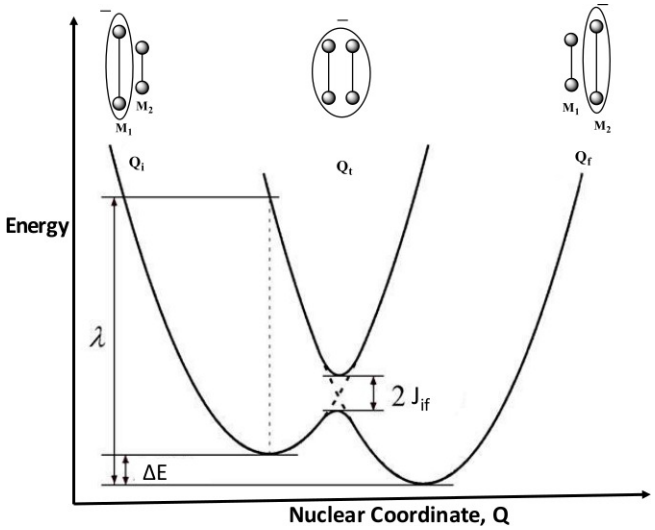

Figure 1.8: An illustration of the potential energy surface changes during charge transfer. The original image was modified to highlight the roles of transfer integral and reorganisation energy in charge transfer.[73]

electron from a negative polaron M_1^- to a neutral molecule M_2, Figure 1.8. The Hamiltonian is used to describe electronic states. The energies of the initial and final states can be given by the parabolic potential energy surfaces. At equilibrium, the molecule sits at the bottom of the energy surface however, the system experiences perturbation from equilibrium due to absorbing thermal energy and vibration of the system move it away from energy minima.

Both systems, the ionic molecule and the neutral molecule, have their own optimum nuclei positions that allow for each molecule to be at its lowest energy. The potential final system consisting of the two molecule is also subject to perturbations. The energy surfaces of initial and final set of molecules intersect when the atoms in the systems occupy the same relative positions and have the same energy. At this intersection point the charge is delocalised over the two molecules. We can imagine another set of systems within these crossing parabolic energy surface representations, Figure 1.8. The system where the charge is delocalised over the two molecules and the two molecules experience perturbation of their nuclear position. Meanwhile the bottom curve presents a condition where charge is localised on one molecule or the other.

When the system is strongly coupled, as in the two molecules have large orbital overlap there is a large distance between the two parabolas.[51,70] The reverse case, though, is primarily true in organic semiconductors, where it is more likely to have a small overlap between the molecules

and ergo weak coupling in the system.The potential energy difference between the energy of the system when the charge is on either molecule or when the charge is delocalised over both molecules is called the transfer integral J_{if}. The energy required for charge to move from one molecule in the system to reside on both molecules at the same nuclei position is called the reorganisation energy. In order to calculate the charge transfer rate, a number of assumption is considered. Firstly, in this model system for describing the charge transfer, we are considering the Su-Schrieffer-Heeger (SSH) approximation.[74–77] This approximation ignores the electron-electron interactions and the electron-nuclei interaction in the Hamilitonian equation. The Franck-Condon principle assumes that the nuclear coordination are invariant during the charge transfer. Therefore charge transfer occurs at the intersection, retaining the conservation of energy. The Born Oppenhiemer approximation allows the assumption that electrons move much faster than nuclei consequently the electronic and nuclei contributions to the wavefunctions can be separated. If both surfaces are approximately parabolic and have the same curvature, then the probability of the system having the coordinates suitable for a charge transfer process is proportion to $e^{-\delta E/kT}$. With these assumptions, and considering Fermi's Golden Rule that the rate of charge transfer is dependent on the orbital overlap. In the weak coupling regime, the equation for charge transfer rate according to the non-adiabatic Marcus Theory. The reorganization energy is defined as the energy required for all structural adjustments (in the reactants and the surrounding solvent molecules) that are needed for the acceptor and donor molecule to assume the configuration necessary for charge transfer. The equation for electron transfer rate according to non-adiabatic Marcus theory:

$$\Gamma_{if} = \frac{|J_{if}|^2}{\hbar}\sqrt{\frac{\pi}{\lambda kT}}exp[-(\Delta E + \lambda)^2/4\lambda kT] \tag{1.4}$$

1.2.4 Factors that Affect Charge Transport in OFET

There are a number of factors that affect charge transport in OFET devices. These factors are pervasive throughout all features of the organic semiconductor: molecular shape and structure, inter-molecular interactions, macro-molecular structure, morphology and at material interfaces

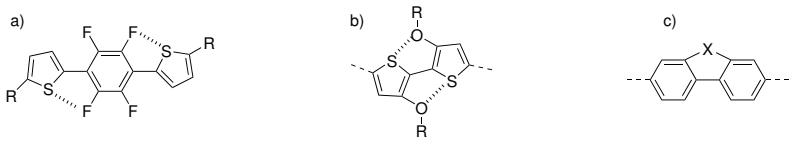

Figure 1.9: Methods for planarising adjacent aromatic units on a polymer backbone. a) Planarising short contact between sulfur and fluoride atoms, b) sulfur and oxygen atoms planarise monomer units in a polymer. c) Bridging atoms between six-membered aromatic rings can force adjacent monomers into co-planar conformation.

in the device.[78–81] These factors are introduced right at the onset of polymer design. Monomers incorporated into the polymers or are chosen or design to infer a certain material property to the polymer. Typically the aim is to either modulate the frontier orbitals of the bulk materials and to move the morphology of the material along the amorphous to crystalline spectrum. Close packing is generally the preferred morphology for optimum charge transport in a material.

Given the theoretical background that govern the rate of charge transfer, clearly the stronger the orbital overlap in the polymers the larger the transfer integral and the higher the charge mobility. Frontier orbital overlap is largest when the polymers approach each other closely and therefore stack in an orderly manner. Ordered stacking therefore leads to crystalline domains that can exhibit short and long range order. Clearly, in inorganic semiconductors, more crystalline materials with larger and better aligned crystal domains display higher charge mobilities. Crystalline silicon achieves mobility in hundreds of $cm^2V^{-1}s^{-1}$ whilst amorphous-silicon has mobility around 1 $cm^2V^{-1}s^{-1}$.[15,19]

At the molecular level a number of methods are used to promote crystallinity in polymer morphology. To start with, the polymers are designed to have long conjugation lengths. Therefore monomer units that lead to cross-conjugation are avoided. Flat, monomers that can be co-planar with other units promote conjugation. Short contacts between monomers along the polymer backbone planarise the polymer.[44,82] Short contacts are possible between sulfur and fluorine or sulfur and oxygen atoms or hydrogen bonding between monomers. When monomers in a polymer are connected by single carbon-carbon bonds, there is the potential for bond rotation in the solution phase and twists in the dihedral angles are then frozen into the polymer in the solid state when the solvent evaporates. Short contacts as shown in Fig. 1.10, increase the activation energy to rotation and promotes planarisation of monomers along the polymer.

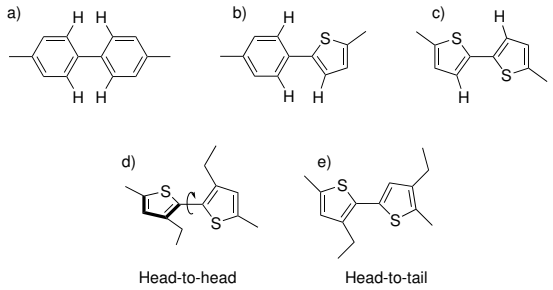

Figure 1.10: An illustration of interactions of substituent on adjacent units along a polymer backbone. a) Ortho substituents between adjacent six-member aromatic rings result in torsional strain and a large dihedral angle between the units. b) Introduction of a five-member ring eliminates one ortho substituent repulsion and c) steric repulsion is lowest between two adjacent five membered aromatic rings. d) Head-to-head coupled thiophene monomers have a dihedral angle between the two units due to ortho-hydrogen steric repulsions, in a head-to-tail coupling this steric interaction is removed.

Introducing steric repulsion between monomers is a simple way to prevent coplanarity between monomers in the polymers. Steric strain is introduced in typically two ways; bulky side chains and clashing side groups in head-to-head interactions. Connected six-membered aromatic rings suffer from steric repulsion of ortho hydrogen atoms, these create torsional strain on connected monomers which result in twists in the polymer backbone. Moving from six-membered monomers to five-membered monomers allows the alleviation of dihedral twists by increasing the distance between ortho atoms. Side-chains in the ortho positions can though cause repulsions that would twist aromatic cores out of the plane. Figure 1.10 shows the head-to-head repulsion in thiophene oligomers, head-to-tail thiophene organisation on the other hand allows the oligomers to planarise. The size and branching point of side-chains in the monomers, if they don't affect the coplanarity of the monomers, may prevent polymers from stacking because they occupy more space over or below the flat polymer backbone and thus increase polymer lamellar stacking distance. Increasing the aromatic core is a fine method for increasing conjugation length. This thesis attempts to achieve co-planarity in the polymers mentioned here for its benefits to the film morphology and in turn charge transport. The strategy used here is different from that in literature. Typically polymers in organic semiconductors are all structurally similar. They consist of monomers connected by single carbon-carbon bonds. These bonds allow for single bond rotation and therefore twists in the polymer backbone. Here the monomers are forced into a fixed conformation by connecting them with double bonds. The

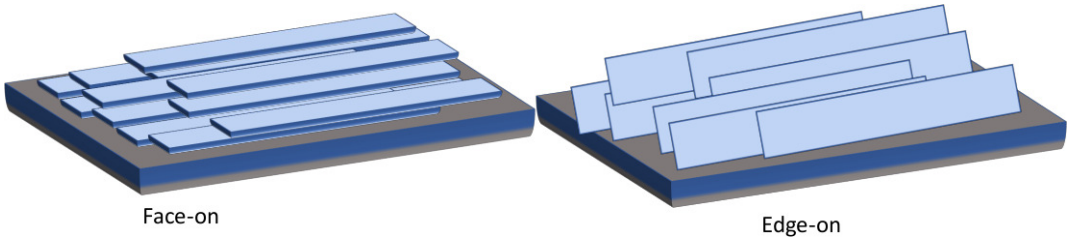

Figure 1.11: An illustration of face-on and edge-on packing on a substrate.

double bonds, theoretically disallow bond twisting. If the monomers can not twist out of plane from each other the conjugated polymer may take the structure of a ribbon or sheet that is sufficiently flat to facilitate close packing of polymers and therefore long range packing and crystallinity and consequently enhanced mobility. There are challenges with designing and implementing organic semiconductors.[83] The arrangement of the sheets of polymer may take on an edge-on or face-on orientation with respective to the substrate. These orientations greatly impact the observed charge transport in transistor devices. Edge on packing is significantly beneficial for the lateral charge transport between the source and drain electrodes in transistor devices, whilst face-on packing is ideal for vertical charge transport.[84] Annealing films after deposition has been shown to improve charge transport properties because the polymer chains rearrange to be more ordered relative to the substrate for transport.[85,86]

1.2.5 Diketopyrrolopyrrole-based Organic Semiconductors

Diketopyrrolopyrrole (DPP) is a pigment that transitioned into use in organic semiconductors. DPP consists of two five-membered lactam ring in the configuration shown in Figure 1.12. It often exists with flanking aromatic units due to its synthesis and the fact that it is highly insoluble and unstable. Diphenyl-DPP is the pigment responsible for the iconic Ferrari red car color. Turbiez first introduced DPP as a monomer for use in organic semiconductors in 2005.[87] Although, the first DPP-based FET achieved low charge transport properties, the charge mobilities of DPP-based organic semiconductors has since improved through a number of strategies. DPP-based polymers are now commonly accepted as higher performing and stable polymers in transistor applications as well as OPV devices.[88] Figure 1.12 gives the structure of diaryl-DPP moiety, different flanking units include phenyl groups, thiophenes and furans. A

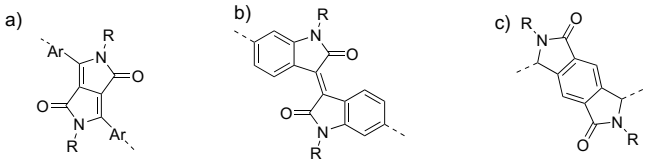

Figure 1.12: a) General structure of diaryl substituted DPP, b) N-alkyl substituted isoindigo and c) benzodipyrrolidone (BDP).

major advantage of DPP-based polymer for TFT polymers are the strong aggregating properties of DPP polymers. The fixed polarity of the lactam rings order the polymer chains in the solid state due to intermolecular dipolar, and hydrogen bonding interactions. Large solubilising chains are therefore necessary to produce polymers that can be solution processed.

Large solubilising alkyl chain density, though, has been shown to limit large charge transport performances.[89] In addition to reducing the alkyl chain density, literature shows that decreasing the steric repulsion between the lactam oxygen and the α-hydrogen in the flanking ring improves FET property. This steric repulsion prevents co-planarisation of the DPP core with the flanking group and results in a 27 ^{o} dihedral twist between the units. This influences the $\pi - \pi$ stacking distance of the polymer chains and therefore lowers the degree of short and long range order in the polymer films. For this reason, diphenyl-DPP-based polymers are generally more amorphous than dithienyl-DPP-based polymers. The five membered ring of thiophene space the lactam oxygen away from the thiophene α-hydrogen. This results in shorter $\pi - \pi$ distance and promotes crystallinity in the materials and generally higher charge transport. Naturally, the comonomer in these polymers influences the charge transporting properties. Dithienyl-DPP copolymerised with thienothiophene gives the polymer DPPT-TT (Figure 1.13) that outperforms the corresponding dithienyl-DPP-bithiophene polymer (DPPT-2T).[90] Interesting in their report, Zhang and coworkers found that the mobility of DPPT-T exceeded that of DPPT-TT and DPPT-2T in both TGBC and BGTC devices because it had a higher molecular weight. Also when the size of the aromatic core was increased by copolymerising naphthalene with dithienyl-DPP, even higher hole mobilities were obtained.[91] The naphthalene ring provided an extended aromatic plane that can stack with adjacent polymers. The use of different aromatic cycles imparts the possibility of favourable solid state arrangement of the polymers.

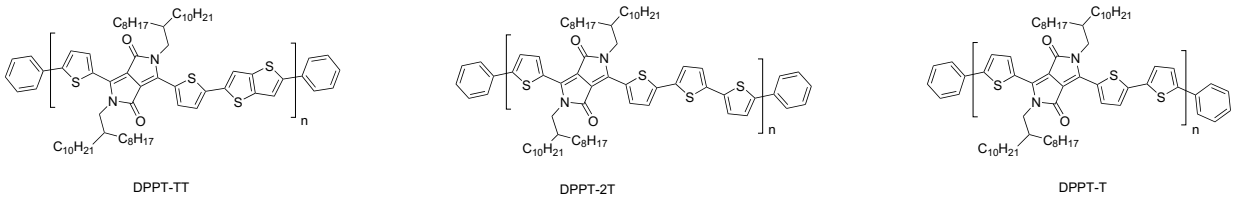

Figure 1.13: The structure of the resulting polymers when dithienyl-DPP is polymerised with thienothiophene (DPPT-TT), bithiophene (DPPT-2T) and thiophene (DPPT-T).

The effect of crystallinity on charge transport is not linear. When there are multiple crystal domains that are incongruent and misaligned, each fracture line slows down charge transport between the domains. The film mobility is then limited by the slow charge transfer between the domains.[92] Single crystal molecules regularly achieve mobilities higher than amorphous silicon.[68]

The electron transporting DPP-based polymers often include electron-poor comonomers such benzothiadiazole, BT. In hole transporting materials, the HOMO is extended much along the polymer spine, but the LUMO is localised on electron deficient monomers. A major prerequisite for electron transport is to have low LUMO for electron injection. Delocalisation of the LUMO then enables electron transport along the polymer and charge transfer between polymer chains.

1.2.6 Isoindigo-based Organic Semiconductors

Isoindigo, another pigment, is an isomer of the common blue indigo dye, and is now a well recognised organic semiconductor building moiety. As a member of the indigoid dyes, isoindigo can be extracted from Isatis tinctoria leaves.[93,94] Isoindigo is not new to the scientific field. It also has a long history in medicinal properties and research in biologically active compounds.[95,96] There are commercially available anticancer, antipyschotic and HIV protease inhibitor drugs that incorporate isatin moieties.[97,98] In the field of organic semiconductors, isoindigo falls into the group of lactam containing molecules, Figure 1.12, such as DPP and benzodipyrrolidone (BDP). These have been extensively studied in the past few years, particularly as electron accepting units for donor-acceptor conjugated polymers for hole transport, as well as amibipolar transport and electron transport as these units are electron deficient.[88] Reynolds *et al.*

Table 1.1: Summary of optoelectronic properties of isoindigo-bithiophene polymers.

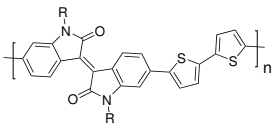

R Group	Name	Highest Mobility /$cm^2V^{-1}s^{-1}$	HOMO/LUMO /eV
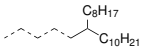	IIDDT	1.06	-5.70 / -3.70
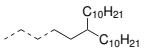	IIDDT-C2	0.40	-5.60 / -3.70
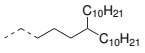	IIDDT-C3	3.62	-5.52 / -3.74
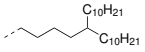	IIDDT-C4	1.76	-5.50 / -3.74

As the branching point of the polymer side chain is moved from C1, C2, C3 and C4 position, the hole mobility tends to increase.[106,107]

first introduced isoindigo in 2011 as an acceptor unit in the field of organic semiconductors.[99] Isoindigo is easily synthesised by acid catalysed condensation of isatin and oxindole. Unsubstituted isoindigo is very insoluble due to its hydrogen bonding ability similarly to DPP, therefore the solubility of the the monomer is controlled by alkylating the nitrogen atom. Typically the longer the alkylation chains or the more branched the group the greater the solubility of the resulting monomer and polymer. Isoindigo has been shown in a number of polymers to produce highly coplanar polymers.[100] However, the crystal structure of N,N'-dimethyl-isoindigo shows a dihedral twist of 22.3^{o} along the central double bond plane.[101] Computational studies, though, showed that the same isoindigo compound at B3LYP/6-31G(d) DFT level theory has two stationary points. One stationary point is completely planar and the other is has a slight twist of approximately 15^{o} between the two oxindole units. Compared to DPP, isoindigo has a slightly higher affinity for oxygen; it has a LUMO level of -3.5 eV compared to -3.4 eV for DPP but lower electron affinity than naphthalene diimide (-3.6 eV).[88,100,102]

Isoindigo monomers are linked at the 6,6' position rather than 5,5' position. Polymerisation of 5,5' substitution isoindigo results in curved polymers that are morphologically inferior for efficient charge transport.[103] Halogen substitution in isoindigo at 5,5' or 7,7' positions, though, can be used to fine tune the polymer electronic properties.[104,105] Isoindigo units have found uses in both small molecules and polymers for organic photovoltaics and OFET applications. Thiophene, bithophene and thioeno[2,3-*b*]thiophene units are common electron donating co-monomers for polymers. Pei and co-workers published results of isoindigo-based polymers,

Table 1.1, where they systematically moved the alkyl chain branching position away from the polymer backbone.[107] A number of conclusions can be drawn from the data. Moving the branching point away from the polymer backbone generally increased the hole mobility and the HOMO and LUMO level of the polymers. The isoindigo-bithiophene polymer with 4-decyltetradecyl achieved the highest electron mobility of 3.62 $cm^2V^{-1}s^{-1}$ amongst the polymers. Pei and coworkers argued that as the branch point is moved away from the polymer spine, the polymers are able to stack closer. Interestingly, the mobility drops when the branching point is moved to the C4 position. The HOMO level increase as the mobility drops, pointing to other complex conflicting contribution of the large alkyl chain to mobility. As well as moving the branch point, the overall number of carbons in the alkyl chain is also increased and this increase may also affect charge transport. In fact, the $\pi - \pi$ stacking distance was found to have fallen steadily from 3.75 to 3.57 nm. The improved packing of the polymers raised the HOMO energy level, as there is more orbital overlaps that elevates the overall electron density on the material. The polymer packing also has a limited effect in stabilising the LUMO of the polymers.

In addition to alkyl branching point, the symmetry of the monomers affects charge transport by influencing curvature in the resulting polymer.[108,109] Pei *et al.* found that isoindigo co polymerised with centro-symmetric monomers such as bi-thiophene and thienothiophene exhibit higher mobility than polymers of isoindigo with axi-symmetric co-monomers.[106] Similar results were observed by Osaka *et al.* in naphthodithiophene (NDT)-derived polymers.[110] Although Osaka *et al.* theorised that the linear NDT monomers would produce polymers with the highest mobility in comparison to angular NDT monomers. The reverse was true because the angular NDT monomers produced more linear polymers that packed effectively for higher charge mobility. The resulting polymer spine curvature is the determining factor for the polymer morphology and subsequently charge transport, not just the nature of the monomer. The curvature therefore prevents regular packing and crystallinity in the polymer microstructure.

Along with the optoelectronic properties of organic semiconducting polymers, there are a number of physical parameters such as ambient stability that are desirable for commercialisation of the materials. Isoindigo polymer was able to achieve a water stable long acting device function.[111] As mentioned previously, tuning the material frontier energy level is important in

designing materials for organic semiconductors. This is of particular importance for matching the energy level of the semiconductor to the source and drain electrodes to minimise barriers in injection. Tuning the energy levels is also important in determining the nature of the charge transported and the ambient stability of the material.

The energy level of isoindigo unit itself was tuned by replacing the flanking phenyl rings with other aromatic cycles and heterocycles. McCulloch *et al.*, for example, published results of ambipolar thienoisoindigo-benzothiadiazole polymer.[112] Substituting the phenyl ring in isoindigo for thiophene made the monomer a more electron donating unit. The HOMO level is markedly higher for this monomer compared to isoindigo. The use of thienoisoindigo also reduces steric replusion between the thienoisoindigo and the neighbouring monomer as we outlined previously. Extending the size of the heterocycle to thieno[3,2-*b*]thiophene isoindigo improved both the hole and electron mobility of the polymers. A range of small isoindigo-based molecules were also synthesised that exhibited impressive charge transport mobilities.[113,114]

1.2.7 Ladder-type Polymers for Organic Semiconductors

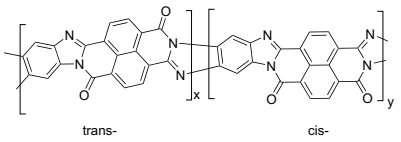

Figure 1.14: The structure of BBL, which exist as a statistical distribution of its trans and cis-isomeric repeating units.

Ladder-type polymers are a clear attempt at making coplanar, ribbon-like rigid polymers for ideal edge-on macromolecular arrangement of polymers on a substrate for charge transport. They consist of internally fused molecular sections that are connected to other fused molecular units. The fused ring in conventional ladder polymers restricts free-torsional motion between aromatic sections. These molecular units in the polymer, though, often display non-zero dihedral angles perhaps due to steric interactions between the units or thermal agitation in the material. This is a thorough review of the ladder-type polymer field landscape.[115]

Fully conjugated ladder polymers (cLPs) are a subtype of ladder-type polmyers where the fused aromatic sections in the polymer backbone are forced into coplanarity in multiples ways such as connecting them by two single bonds. Ladder polymers, courtesy of their highly fused nature, have high thermal, mechanical and chemical stability. They also suffer from solubility difficulties as a consequence of their planar nature. Poly(benzimidazole benzophenan-throline) (BBL) is the poster-molecule of ladder polymers since it publication in the 1960s.[116] Since then, numerous ladder-type polymers have been reported. Given their highly fused nature, one can envisage the impressive organo-synthetic feat necessary to produce them. There are limited synthetic pathways as well as limited precursors for their synthesis. Furthermore, highly selective and efficient conversion reactions are needed for the annulation reactions that produce ladder-type polymers.

Ladder-type polymer synthesis can be described in two ways, either a step-wise synthesis or a one-pot synthesis. In a stepwise synthesis, the monomers undergo an annulation reaction to furnish a polymer with reactive units. This reactive intermediates undergo post-polymerisation reactions to generate the polymer. In the one pot synthesis strategy, monomers react in a bidirectional fashion to generate the fused ladder-like polymer. Due to the complex nature of the reactions, there is a high probability of side reactions, misscoupling, and unreacted groups remaining in the final polymer. Intrachain hole mobility of ladder-type poly(para-phenylene)s (LPPPs)[117] with an average repeat unit of 54 have reached remarkable values of 600 $cm^2V^{-1}s^{-1}$.[118] LPPs are commonly more soluble than cLPs.

The low device mobilities measured in ladder-type polymers is a consequence of slow interchain charge transport in the bulk material. There is yet chance to enchance the synthesis of high mobility charge transport ladder-type polymers, or optimise already available polymers. Studies into BBL were able to increase its low transport mobility from 10^{-6} - $10^{-4}cm^2V^{-1}s^{-1}$ in the 1980s to 0.1 $cm^2V^{-1}s^{-1}$ in 2003[63] through doping and processing of the polymers with methane-sulfonic acid (MSA). Electron diffraction techniques suggested more crystalline material when BBL was processed with MSA. Other methods of processing BBL with MSA produced BBL nanobelts[119] that displayed ambient stability over four years, well exceeding the air stability of P3HT.[120] Charge transport in BBL and ladder-type polymers, though, continues to remain low,

and their stability and synthetic difficulties make it hard to establish larger scale applications of the material.

1.2.8 Motivations for N-type Organic Semiconductors

N-type organic semiconductors are required to complement hole transport in complementary metal oxide (CMOS)-like logic circuits.[8] However, there is a much smaller selection of electron transport OS compared to p-channel materials. One reason for fewer electron transport materials is the limited number of electron deficient building blocks for OS polymers. Polymers for electron transport require LUMO levels of approximately -4 eV.[48] At this frontier energy level, electron charge injection on to the LUMO is possible, furthermore, the electrons are less available for unwanted reactions with oxygen and ambient moisture as well as available hydroxyl groups from silicon dioxide a common dielectric. Reactions of water and oxygen with polymers produce charge traps that limit charge transport. LUMO levels much lower than -3.8 eV are less susceptible to these reactions however, the resulting spontaneous electron injection disrupts the semiconducting characteristics of the polymer.

The best performing hole and electron transport materials are often D-A polymers due to the push-pull effect on the frontier orbitals. If the electron withdrawing co-monomer in these polymers lowers the LUMO sufficiently for electron injection whilst the HOMO remains high enough for hole injection, ambipolar transport is achieved. In principle, such materials are ideal for CMOS logic circuits, however, experimentally they have been shown to exhibit higher off current (I_{off}) that results in low on/off current ratios (I_{on}/I_{off}) that are detrimental to the device performance.

There are still many hindrances to widespread commercialisation of organic semiconducting transistors. It would be difficult to displace an already established technology with the infrastructure and systems tailored to optimise production of silicon transistors. There are also the practical issues hindering adoption of organic semiconductors such as ambient stability; utilisation of expensive catalysts in the synthetic routes; material batch-to-batch variation and variation in solid-state morphology especially over a large area.

From the wide range of applications of organic semiconductors, this thesis focuses on the use of organic semiconductors as transistors and their application in displays. New materials to the field can potentially further open up the application of TFT in detectors and in integrated drivers and logic circuits into display back-planes. Other TFT applications include radio frequency tags, sensing devices, bio-sensing devices disposable electronics.[7,121] The new material should, at minimum, match the properties of amorphous silicon or ideally exceed them in terms of mobility, stability and uniformity. Alternative, organic semiconductors can compliment silicon and inorganic technologies in electronics.

Chapter 2

Conformationally-Fixed Polymers

2.1 Motivations and Objectives

The initial idea for conformationally-fixed polymers began organically within the McCulloch group, primarily in the PhD project undertaken by Joseph Rumer.[122] Rumer's research highlighted the potential of bislactam-containing monomers (DPIT and DPID, Figure 2.1) in organic semiconductors.[122–127] In 2013, he reported a new monomer synthesised from dihydropyrroloindoledione (DPID) and 5-bromo-2-thiophenecarboxaldehyde in a two-directional Knoevenagel reaction. This brominated monomer, Figure 2.1, was copolymerised with two different monomers in Suzuki and Stille coupling reactions to give two polymers. Both polymers displayed broad absorption spectra from 500 to 750 nm, making them ideal for OPV applications.[123] These polymers also displayed low optical gaps aided by their planar nature. B3LYP/6-31G* level studies on the polymer oligomers suggested the polymers to be highly planar (with dihedral angles between 0 and 4 degrees). The planar characteristics of the polymers was explained by the vinyl linkages that enabled planarising sulfur-oxygen interactions.[123]

The McCulloch group went on to produce more monomers and polymers based on DPID, and the incorporation of further thiophene comonomers resulted in improved absorption profile as well as charge transport properties of the materials.[126] Thiophene-flanked benzodipyrrolidone (BPT)-based alternating copolymers were also synthesised from dihydropyrroloindoletetraone

(DPIT), a bislactam tetraone monomer.[127] Rumer *et al.* also reported ambipolar DPIDT-2T polymer with hole and electron charge mobilities of 0.09 and 0.04 $cm^2V^{-1}s^{-1}$.[126] This supports the concept that increased planarity facilitates beneficial solid-state polymer stacking. Coplanar polymers may resemble sheets or ribbons that are capable of regular macro arrangement. Closely stacked polymers enable efficient charge transfer processes between polymer chains.

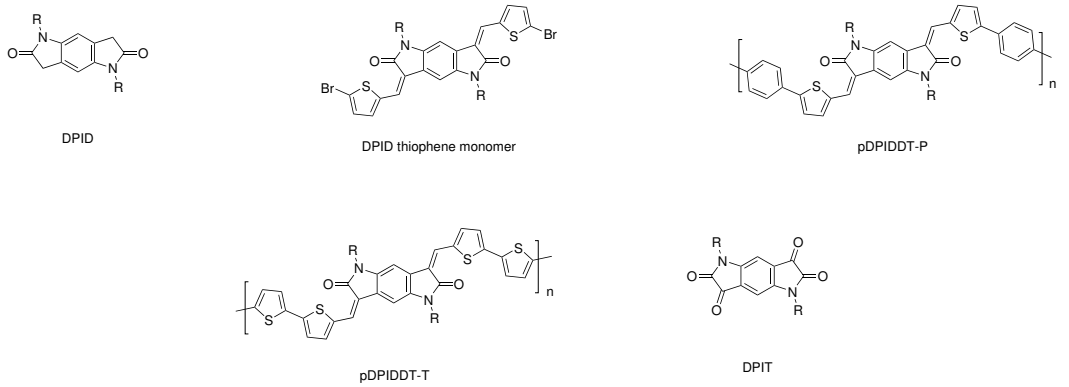

Figure 2.1: Rumer and coworker's seminal DPID-based polymers.[123,126] The alkyl chain label R represents 2-octyldodecyl.

The ideal was to produce conformationally-fixed polymers based on the promising DPID and DPIT monomers. An aldol reaction, related to the Knoevenagel condensation utilised by Rumer, offered a route to conformationally-fixed polymers with the monomers connected by carbon-carbon double bonds. The aldol reaction, however, would require both DPID and DPIT for a bidirectional condensation to furnish the polymers. Lawesson's reagent can also be used to generate the same polymer. In Figure 2.2 the spheres represent different aromatic centers. The monomer structures, bisisatins and bisoxindoles, can take on other aromatic centres to enable preparation of a selection of polymers. In literature we found that the bisisatin monomer can also undergo self-condensation with tris(diethylaamino)phosphine to give a series of polymers.[128] In this case though, the polymer synthesised from tris(diethylamino)phosphine can only be a homopolymer.

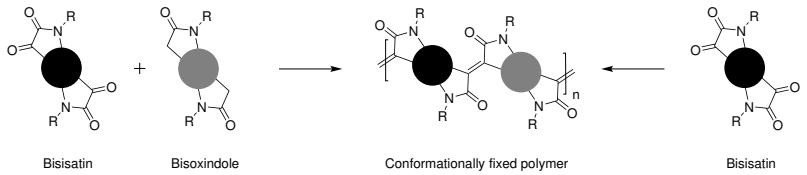

Figure 2.2: A schematic showing two synthetic routes to conformationally-fixed polymers. Route a, left, indicates condensation of a bisisatin and bisoxindole molecules and route b, right, shows self-condensation of a bisisatin molecule to generate a homopolymer.

Tris(diethylamino)phosphine, although useful in a number of other transformations such as transamination reactions, is a potential reagent for achieving self-condensation of bisisatin. This deoxygenation reaction of tris(diethylamino)phosphine ($P(NEt_2)_3$)was actually first reported in 2010, in the synthesis of substittuted isoindigo (3,3'-bisindolinylidene-2,2'-diones) from bisisatin molecules.[128] We attempted to polymerise phenylbisisatin with ($P(NEt_2)_3$). A polymerisation of DPIT at 60 ^oC using ($P(NEt_2)_3$) only generated oligomers, a green solution with very low molecular weight (Mn 2.4 kDa). This may be due to the carbene nature of the reaction mechanism generating side products at a relatively high a temperature. Figure 2.3 illustrates the proposed carbene mechanism as reported by Bogdanov and colleagues of tris(diethylamino)phosphine in the self-condensation of phenylisatin .[128] Tris(diethylamino)phosphine undergoes thermally activated homolytic bond cleavage to leave a free-radical on the phenylisatin. Its radical cation bonds to the β-carbonyl before reducing the isatin to a carbene intermediate. Dimerisation of the carbene intermediate furnishes the desired isoindigo structure. Bidirectional propagation of the mechanism in phenylbisisatin (DPIT) would generate a conformationally-fixed polymer. Such a polymerisation technique would have been ideal because it only requires one monomer, and therefore circumvents the requirement of careful stoichiometric control as predicted by Carothers' equation.

Lawesson's reagent was another potential method of achieving a conformationally-fixed polymer using one substituted glyoxal or bisisatin monomer. Lawesson's reagent, a phosphorus decasulfide compound that exits as a dimer, is useful in various reactions to thionate ketones, esters and amides.[129] It is particularly useful for substituting oxygen with sulfur atoms, rearrangement reactions and heterocyclisations. Lawesson's reagent can also form carbon-carbon double bonds between carbonyl groups.[130] Literature examples abound where one equivalent of

Lawesson's reagent couples two isatin molecules to generate isoindigo.[131] The reaction mechanism is thought to proceed with an initial thionisation of the secondary carbonyl group. Two of these thionated intermediates dimerise with each other before collapsing to extrude sulfur and furnish the coupled molecule. Figure 2.5 illustrates the mechanism for the coupling of phenylbisisatin using Lawesson's reagent. Again this method would allow the generation of a polymer with only one monomer.

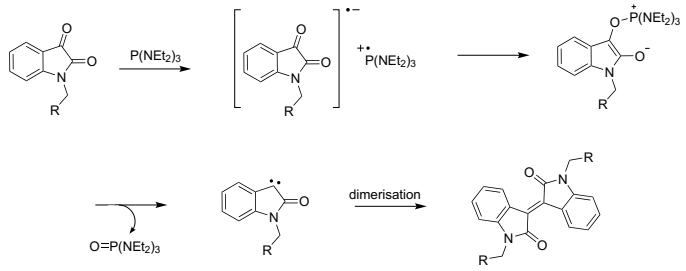

Figure 2.3: Proposed mechanism for the dimerisation of bisisatin to isoindigo.[128]

We carried out the polymerisation using one equivalent of Lawesson's reagent and phenylbisisatin heated at 120 ^oC for 32 hours in o-xylene. After this time, a red solution was obtained. GPC analysis of the polymer showed that it had Mn 2.8 kDa. The UV-vis spectrum of the polymer is presented in Figure 2.4. The high energy absorption peak is slightly red shifted relative to the high energy absorption of the monomer and its lower energy absorption peak is blue shifted relative to the dodecylphenylbisisatin. The polymerisation reaction was clearly unsuccessful from the absorption profile of the resulting polymer.

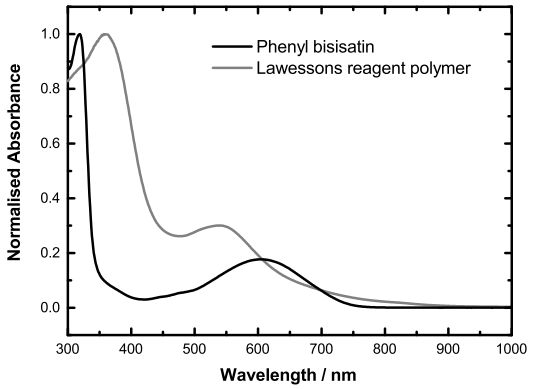

Figure 2.4: UV-vis spectrum of the polymerisation product from Lawesson's reagent and C10C12 phenylbisisatin. The polymer absorption spectrum resembles the starting material due to unwanted reactions.

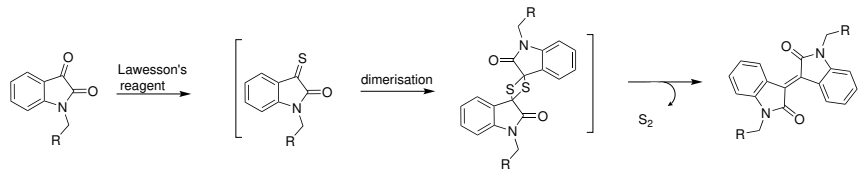

Figure 2.5: A proposed mechanism for isoindigo synthesis using Lawesson's reagent, adapted from literature.[130]

At this point, we decided to deviate from one monomer polymerisation reactions to polymerisation conditions using the two monomers, a bisisatin (DPIT) and a bisoxindole (DPID). Bisoxindole is a complementary monomer to phenylbisisatin that allows for a polymer with double bonds between the monomer units as shown in Figure 2.2. Aldol condensation of phenylbisisatin and phenylbisoxindole gives conformationally-fixed polymers. First reported by Kane in 1838,[132,133] the aldol condensation is a well established and important synthetic protocol for carbon-carbon bond formation reactions. The reaction broadly covers reactions between enolisable carbonyls and another ketones or aldehydes.[134] Carbonyl groups are permanently polarised due to the electronegativity of the oxygen atom relative to carbon, this results in the α-methylene group adjacent to carbonyls being acidic, with pKa of approximately 16-21. Subsequently, in basic conditions aldehydes and ketones with available α-methylene hydrogen atoms undergo tautomerism to give enolates. And in acidic solvents the carbonyl can tautomerise to enols. The enolate and enol exist in equilibrium with the starting carbonyl group and can perform nucleophilic addition to a carbonyl group in other aldehydes, ketones or itself to generate a β-hydroxyl aldol product, Figure 2.6. The name aldol comes from an amalgamation of the functional groups present in this product - aldehyde and alcohol.

The aldol reaction is the prevailing method for making isoindigo molecules in literature. When the polymerisation of phenylbisisatin and phenylbisoxindole was carried out in toluene with p-toluenesulfonic acid, the reaction yielded a deep purple polymer.[96] The polymers obtained were conformationally rigid polymers where monomers are linked by carbon-carbon double bonds. From this description, already one can image some deviations in reaction products. The two-directional aldol condensation progresses as outlined in Figure 2.6. *p*-Toluenesulfonic acid, with pKa -2.8 in water, drives the equilibrium of the phenylbisoxindole to tautomerise to the enol. This enol nucleophilically adds to the α-carbonyl of the phenylbisisatin, as it is the more

election deficient position. Figure 2.6 shows this mechanism for synthesising the polymers. In this case, there is only one enol possible. The α-hydroxy carbonyl is dehydrated to give the α, β-unsaturated functional group that links the two monomers together.

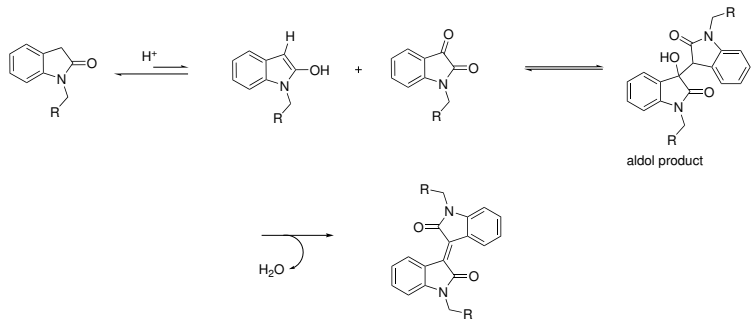

Figure 2.6: Mechanism for aldol condensation of isatin and oxindole to give isoindigo. The bidirectional reaction produces conformationally-fixed polymers.

In asymmetrical ketones, there is a potential for two possible enolates or enols that can add to an available carbonyl in the reaction medium. This leads to issues in controlling regioselectivity in reaction. For reactions where stereospecificity is required, the face on which the enolate adds to must be controlled. Furthermore, β-hydroxyl carbonyls can dehydrate to reveal α, β-unsaturated aldehydes or ketones, that can also then undergo Michael additions with the existing enolates or enols in the reaction. In basic conditions another side reaction is possible, aldehydes can undergo disproportionation to give both carboxcylic acid alcohol (Cannizzaro disproportion) or to form the ester (Tischenko reaction). What's more, enolates can also add to the carbonyl carbon or oxygen. Multiple aldol condensation modifications address the different side reactions mentioned here.[135]

Base-catalysed aldol reactions are more common than acid-catalysed aldol reactions. Consequently, there are more studies on base-catalysed reactions and more studies on the kinetics. The literature consensus is that base-catalysed reactions generate more side products than acid-catalysed reactions and stronger bases generate a greater proportion and number of side products.[136,137] Thomke *et al.* published mechanisms showing multiple secondary reactions from acetone.[137] They obtained C7 and C10 cyclic compounds from aldol reactions of acetone in gaseous conditions at elevated temperatures, 200 - 400 ^oC. Considering that the polymerisation conditions in this thesis occur under acidic conditions and at relatively lower temperatures,

secondary reactions and products should be minimal. There is also the question whether the aldol condensation reaction generates a cis or trans carbon double bond. In our literature search,there were no examples of cis isoindigo structures formed from aldol condensation with p-toluene sulfonic acid. The crystal structure of an isoindigo molecule made in the group only displayed trans double bond geometry therefore we are confident of having predominantly trans double bond geometry in our polymers. The aldol polymerisation reaction is metal-free, cheap, environmentally benign and has shown itself reliable in generating high molecular weight polymers. It is advantageous over polymerisation procedures that require precious transition metals, air and moisture sensitive reagents as in Grignard metathesis polymerisation or pernicious organometal such as organotin or organonickel reagents. Consequently, our polymers prepared by aldol polymerisation are easily amenable to biological applications.

Chapter 3

Size of Aromatic Centre in Conformationally-fixed Polymers

3.1 Motivations and Objectives

Property-design strategy in organic semiconductors frequently involves elongation or extension of the aromatic centre of monomers used in a polymer. In studies of acenes naphthalene, anthracene, tetracene, pentacene and hexacene, elongation of the aromatic centre have been shown to significantly reduce the polymer or small molecule reorganisation energy and increase the transfer integral.[138] These changes result in higher charge transport in the longer, extended acenes. Similar trends have been observed in other monomer structures used in conjugated polymers for organic field effect transistors.[45,109] The acene size is related to other optoelectronic properties of the monomer and consequently the polymer. Increasing the electron density in the monomer aromatic centre and subsequently the polymer tends to lower polymer stability to ambient conditions. It is then necessary to incorporate electron-withdrawing units on the aromatic core to modulate the material energy levels and improve other aspects of device function such as the light absorption profile and charge injection.[104] Elongating the aromatic centres also generates a larger flat surface for interchain $\pi - \pi$ stacking or molecular docking of the polymers that can then infer more short range and long range order in the macro-

morphology of the bulk material. As discussed previously, this is beneficial in increasing the transfer integral and therefore facilitates efficient intermolecular charge transport. Given that intermolecular charge transfer is often a limiting factor to charge mobility, faster intermolecular charge transport can greatly improve charge mobility.

Presented here is the series of polymers we synthesised where we enhanced the polymer transport properties by elongating the aromatic core in addition to reducing the alkyl chain density. The effects of these changes were analysed in the UV-vis spectrum, electronic and thermal properties of the polymers, TGA and DSC, in addition to the transistor output and transfer curves. X-ray diffraction results and computational data further elucidated the properties observed in these polymers.

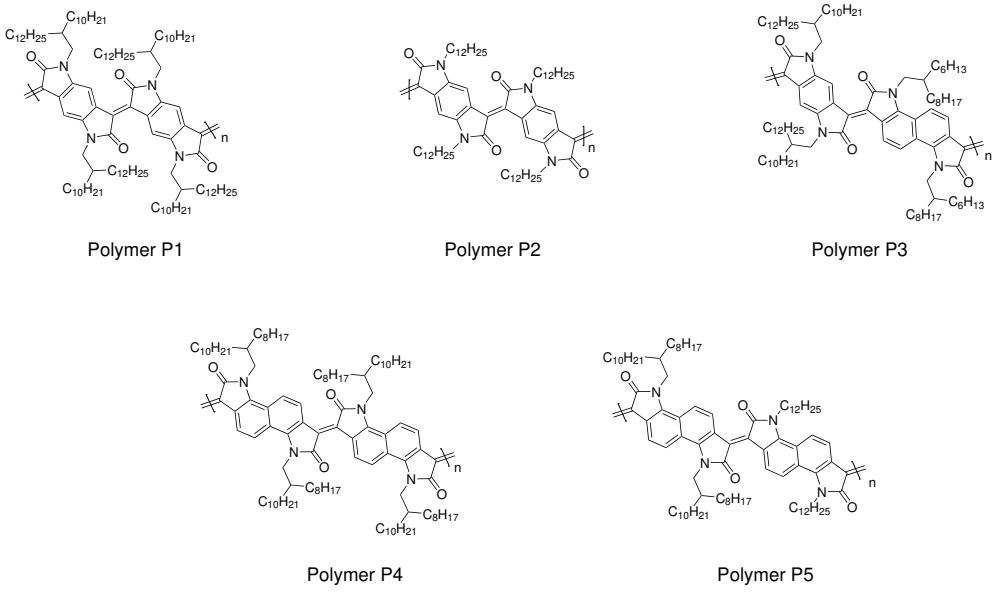

Figure 3.1: A series of polymers, P1 to P5, exploring the effect of aromatic size on conformationally-fixed polymers.

3.2 Results and Discussion

3.2.1 Monomer Synthesis

Synthesis of Phenyl-Based Monomers

Two monomers were synthesised for each of the polymers in Figure 3.1, bisisatin and a bisoxindole monomer. For polymer P1, C10C12 phenyl bisisatin and C10C12 phenyl bisoxindole were prepared. C10C12 refers to the carbon-2 branched 2-decyl-1-tetradecane; all the branched alkyl chains used in this thesis are branched at the C2 position unless otherwise specified. Synthesis of both monomers began with acylation of 1,4-benzenediamine using 2-decyltetradecanoyl chloride in DCM in the presence of triethylamine.[122,123] Upon addition of 2-decyltetradecanoyl chloride, the diacetamide product, structure 3.3 in Figure 3.2, immediately precipitated out of the reaction mixture as white flakes. This highly insoluble intermediate was isolated by filtration and oven dried under low pressure for 16 hours. The diacetamide was then reduced to the diamine, using lithium aluminum hydride in THF to furnish a brown/red solid as the product. Another acylation reaction on this diamine with acetoxyacetyl chloride produced the diacetate intermediate, structure 3.5, which was hydrolysed to dihydroxyacetamide. Thus far, the synthetic transformations were straight forward, high yielding and facile, if not cumbersome in terms of the lithal reduction workup. The next transformation of Swern[139–141] oxidation of the dihydroxyacetamide to bisglyoxamides was often difficult and unreliable.[142] A deep aqua colour change was observed upon successful formation of the activated alcohol intermediate, but no colour changes occurred when the reaction was unsuccessful.

Swern oxidation is the typical reaction condition for activating DMSO to oxidise alcohols to their corresponding carbonyl. Regardless of the activating reagent, DMSO activation mechanisms invariably progress in the same manner. DMSO reacts with the activating reagent to generate a sulfonium cation that consists of positively charged dimethylsulfonium ion with a leaving group attached. A chloride ion is the leaving group in a Swern oxidation reaction. The substrate alcohol displaces the leaving group to give an alkoxydimethylsulfonium salt - the activated

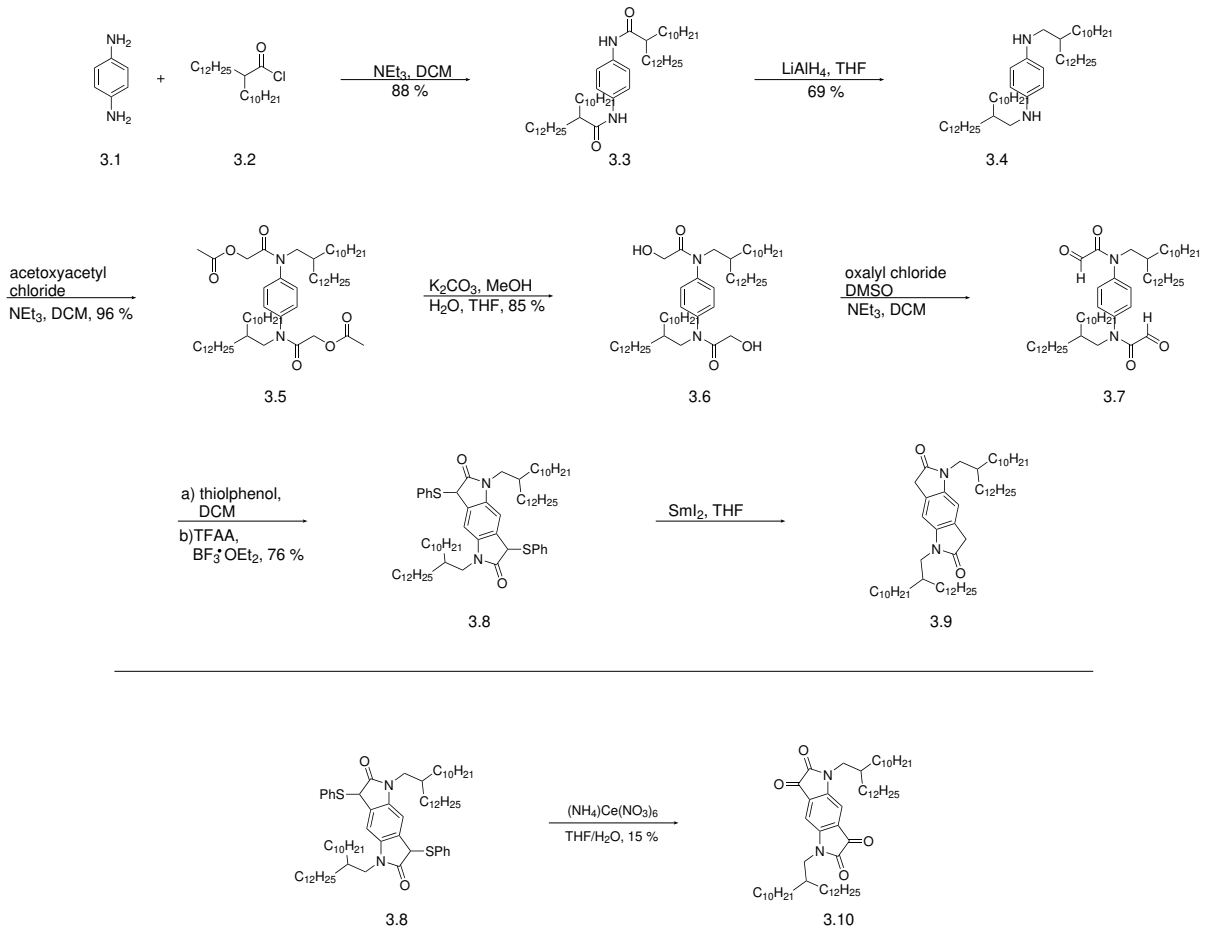

Figure 3.2: Synthetic route to phenyl bisoxindole and phenyl bisisatin monomers.

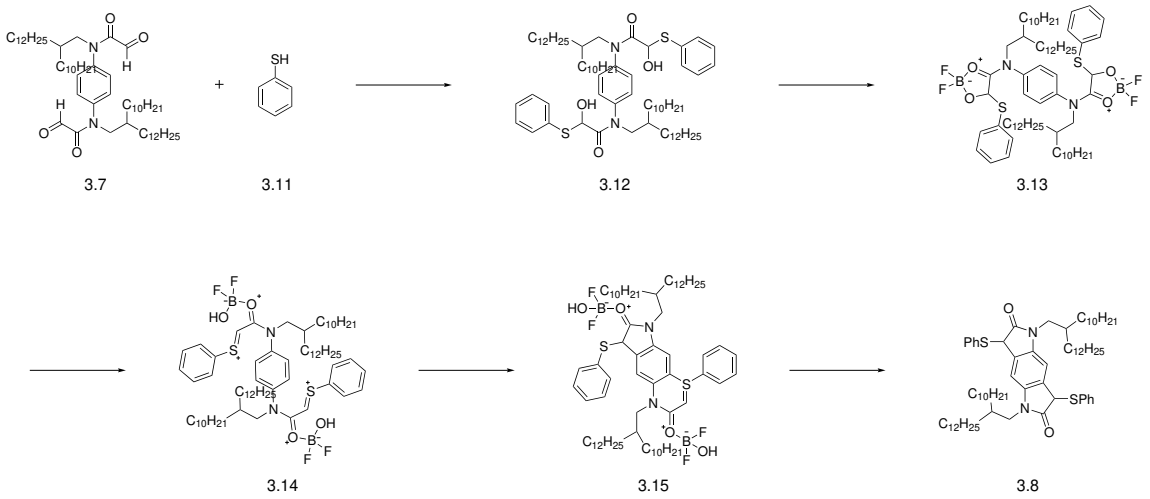

Figure 3.3: A proposed mechanism showing the activating role of BF_3 in the Pummerer-type cyclisation of phenyl bisglyoxamides.

143

alcohol Intramolecular elimination in this intermediates generates dimethyl sulfide and the desired carbonyl.

Oxalyl chloride activation of DMSO in Swern oxidation is preferred to other activators because it often generates the highest yields of oxidised product. We also attempted oxidation of dihydroxyacetamide in Parikh-Doering oxidation reaction where pyridine sulfur trioxide is used rather than oxalyl chloride. The Parikh-Doering oxidations were unsuccessful in oxidising dihydroxyacetamide. DMSO activation with pyridine sulfur trioxide generates a less reactive sulfonium ion, that is subsequently less susceptible to decomposition and ergo less likely to form the methylthiomethyl ether side product. In addition to the Swern oxidation and Parikh-Doering, the Dess-Martin Periodane oxidation and PCC oxidation were performed to give the bisglyoxamides, however it was not possible to obtain the product under these conditions.

Although, the Swern oxidation is a reliable reaction for alcohol oxidation, it is a reaction that benefits from optimisation of the reaction temperature in particular. Activated sulfonium cation is stable until about $-20\ ^oC$. Perhaps conducting the reaction at $-30\ ^oC$ rather that -78 ^oC, to allow for the exothermic substitution reaction of the alcohol, may have improved the yield. Furthermore, Swern oxidation is sensitive to moisture, a combination of these may be the source of the low success rate with this reaction.

After oxidation of dihydroxyacetamide, structure 3.6 in Figure 3.2, the resulting dialdehyde underwent nucleophilic addition with thiophenol and then a Pummerer-type cyclisation initiated by BF_3 to give the thiol-intermediate, compound 3.8.[142,143] Figure 3.3 outlines a proposed mechanism of this transformation.[143,144] Reduction of this thiophenol with samarium iodide generates the C10C12 phenyl bisoxindole, but when oxidised by cerium ammonium nitrate it gives the corresponding bisisatin.

After synthesising the C10C12 phenyl monomers, further literature search revealed a more convenient route to the phenyldiamines.[145] Common reductive amination followed by air oxidation and aromatisation of 1,4-cyclohexanedione dissolved in ethanol with dodocane-1-amine furnished the phenyldiamine.[146] Air was bubbled through the reaction mixture at room temperature which enabled consecutive imine formation reactions and aerial oxidation to give the dialkylbenzene. The mechanism for this transformation is depicted in Figure 3.4. A condensation reaction of the 1,4-cyclohexanedione with alkyl amine gives the imione structure 3.18. This intermediate imione can undergo aerial oxidation to generate a minor side-product compound 3.21. This by-product was not isolated during the synthesis as the reaction was often used immediately as to minimise further oxidation of the p-phenylenediamine. In any case, the aminophenol by-product is generated in low quantities due to the fast second imination reaction step.[146] Aerial oxidation of this di-imine intermediate results in the formation of the product. The reaction time is often short, 4-5 hours, because longer reaction time results in the oxidation of the diamine product. Within four hours reaction time, the reaction was opaque with red precipitates suspended in the flask. The reaction mixture was was immediately concentrated to afford a brown powder. Dialkyl-*p*-phenylenediamines are colourless solids, however fast oxidation of the phenylenediames in air results in the red colored precipitate.[146,147] This atom-economic, green, one-pot route bypasses two reaction steps, but most importantly eliminates a lithal reduction workup.

Rather than proceed with the same synthetic steps as for the C10C12 phenyl bisisatin and bisoxindole, all the limited glyoxal generated was oxidised to C12 phenyl bisisatin. Subsequently to prepare C12 phenyl bisoxindole, N1,N4-didodecylbenzene-1,4-diamine was suspended in DCM and chloroacetyl chloride was introduced drop-wise to the reaction solution.

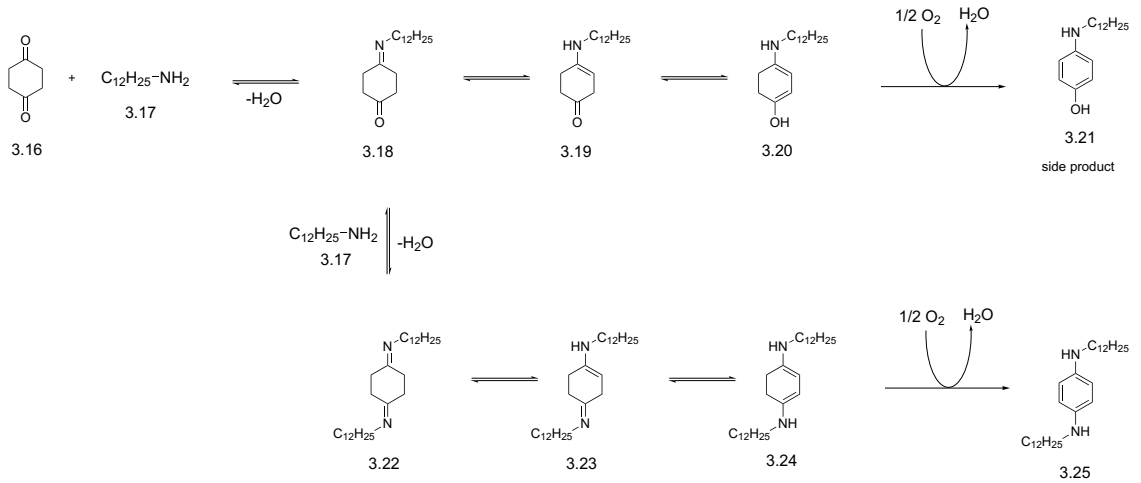

Figure 3.4: Possible mechanism for the reaction for the one-pot synthesis of N,N'-dialkyl-p-phenylenediamines.[146]

The dichloroacetamide precipitated immediately, and the poorly soluble off-white precipitate, dichloroacetamide, was recovered by filtration. A Heck-type cyclisation of this dichloroamide intermediate, compound 3.26, in toluene furnished the dodoceylamine phenyl bisoxindole monomer.[148] Despite the successes with the above synthetic process we found the Heck-type cyclisation reaction of *alpha*-halo or *alpha*-hydroxy acetanilides was challenging and poorly reproducible. It requires a specific ligand and catalyst loading of 12 % 2-(di-*tert*-butylphosphino) biphenyl and 12 % palladium acetate as published by Hennessy and Buchwald in 2003.[148] Other conditions for achieving this cyclisation were attempted; heating the precursor in excess aluminium trichloride without solvent also produced the bisoxindole.[145] This Friedel-Crafts alkylation reaction was practically precarious because the whole reaction vessel required heating to 190 ^oC to prevent much of the aluminium chloride from subliming in the reaction vessel. In the future, an alternative route to this cyclisation may be considered to obviate the use of transition metals and make the overall synthetic route more environmentally benign.

The synthesis of the C12 complementary bisisatin monomer began also with the reductive amination and aerial oxidation of 1,4-cyclohexanedione with dodocane-1-amine. In this case though, the red diamine intermediate was dissolved in DCM then acylated with aceytoxyacetyl chloride rather than chloroacetyl chloride, Figure 3.5, bottom scheme. The diacetate intermediate was purified by flash chromatography to give an off-white solid. This diamide was dissolved in THF/methanol/water mixture prior to the addition of potassium carbonate to in-

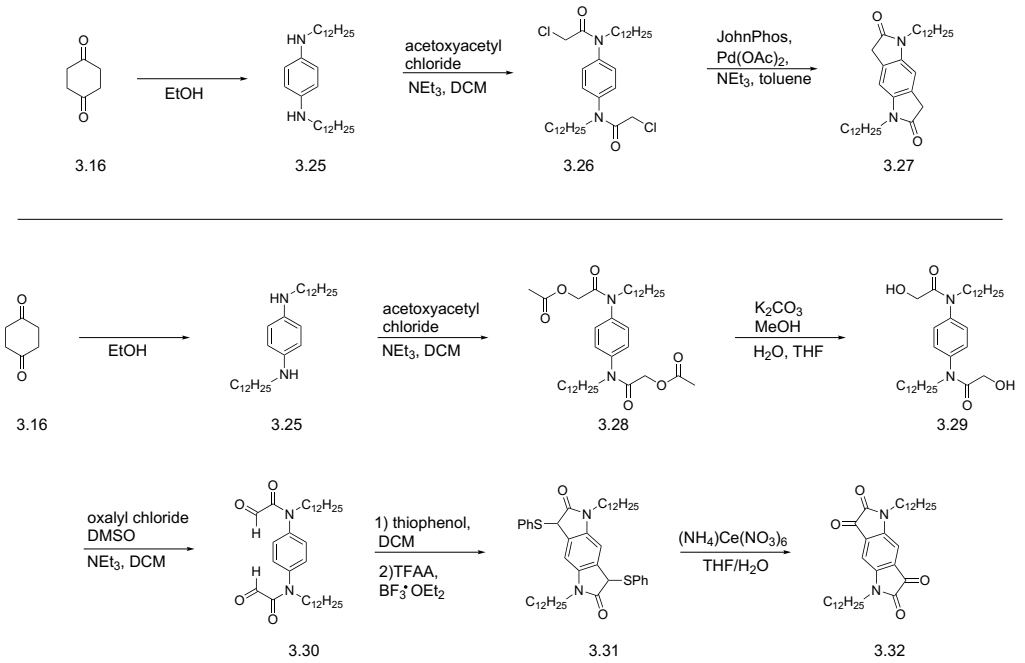

Figure 3.5: Synthetic route to phenyl bisoxindole and bisisatin from 1,4-cyclohexanedione.

duce hydrolysis of the ester group. Once the hydroxyl groups were exposed, a Swern oxidation was carried out to elicit the formation of aldehyde functional groups. The aldehyde groups on this bisglyoxamides intermediate, compound 3.30, were intercepted by thiophenol in DCM. A Pummerer-type cyclisation was then initiated using boron trifluoride in diethyl ether and trifluoroacetic acid anhydride as reported by Procter *et al.*.[142,143] This reaction was conducted for 5 hours before being quenched with water and worked up to give a red solid. This crude material was oxidised using cerium ammonium chloride in a THF and water solvent mixture to furnished C12 phenyl bisisatin, compound 3.32.

Synthesis of Isatins and Oxindoles

Isatins (1*H*-indole-2,3-dione) are naturally occurring motifs.[149,150] Isatin-based compounds can be found in plants, *genus isatis*, *calanthe discolor* lindl and *Couroupita guianensis*, fungi and are present as metabolic derivatives in humans. Pharmaceutical molecules containing isatin motifs have also shown antimicrobial, antiviral, anticancer, anti-convulsant, anti-inflammatory and analgesic activities.[151] With these potential applications open to isatin-containing drugs, there is a steady interest in the wider scientific community for isatin-containing compounds. There

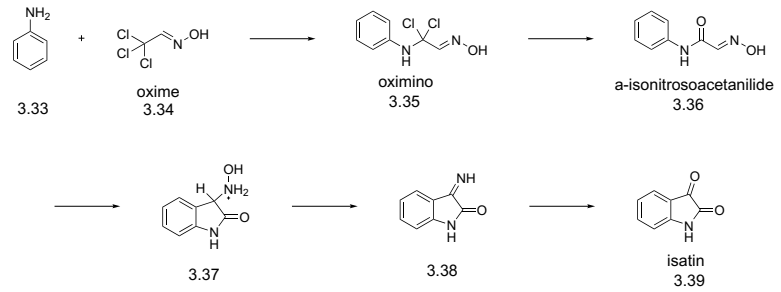

Figure 3.6: An outline of Sandmeyer isatin synthesis mechanism on prototypical aniline.

are also, consequently, well established synthetic routes to isatin units. The five main synthetic routes to isatins being the Sandmeyer isatin; Stolle istain; Martinet isatin; Gassman isatin and the metalation of anilide isatin synthesis.[152] Three of these synthetic routes, unchanged or modified were used in this thesis.

The Sandmeyer isatin synthesis,[153] first reported in 1919, is the reaction of an aryl amine with chloral hydrate and hydroxylamine hydrochloride in aqueous sodium sulphate to form isonitrosoacetanilide.[154] In the reaction, hydroxylamine undergoes nucleophillic addition to chloral hydrate and subsequent proton transfer processes leads to water extrusion and the formation of an oxime, Figure 3.6.[134,155] Nucleophilic substitution of the aryl amine onto the oxime, structure 3.34, forms an oximino that is hydrolysed to the intermediate α-isonitrosoacetanilide. This intermediate is isolated and treated with concentrated sulfuric acid to obtain isatin. This is the industrial method for generating isatin with good yields above 75 %. An attempt was made to generate the phenyl bisisatin unalkylated core through the Sandmeyer isatin synthesis however, only the intermediate α-isonitrosoacetanilide was isolated. It was suspected that the bisoximino was too electron deficient for the cyclisation to occur similarly to the situation of Sandmeyer isatin synthesis of 3,5-bromoaniline.[156] The low solubility of the α-isonitrosoacetanilide intermediate in sulfuric acid could have hindered its cyclisation. In a modified Sandmeyer isatin synthesis, electron deficient 3,5-dibromoaniline was achieved in excellent yield by increasing the solubility of the starting material by adding ethanol to the reaction mixture. The reaction temperature was also lowered and the reaction run time lengthened. Tuning the reaction in this way may be a possibility in the future, as we expect the unalkylated phenyl bisisatin and the intermediate bisisonitrosacetanile to be poorly soluble.

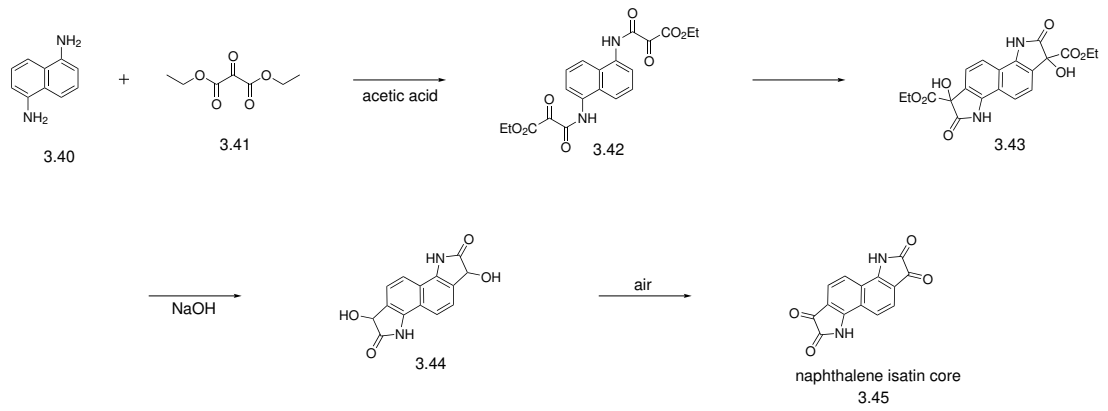

Figure 3.7: A breakdown of the Martinet isatin synthesis on 1,5-diaminonaphthalene. The intermediates were not isolated and overall the naphthalene bisisatin core was obtained at 63 % yield.

Another route to isatin is the Stolle isatin synthesis. It describes the reaction of aniline with oxalyl chloride to make intermediate chlorooxalylanilide which is then cyclised with a Lewis acid such as boron trifluoride, aluminium chloride or titanium trichloride. The Martinet isatin synthesis involves the reaction of an amino aromatic compound with an oxomalonate ester, diethyl ketomalonate, in acidic medium to form 3-(3-hydroxy-2-oxindole) carboxylic acid derivative, structure 3.43 in Figure 3.7.[157] The aryl amine undergoes nucleophilic addition to the ester carbonyl group of diethyl ketomalonate, followed by a proton transfer and ethanol is extruded due to reformation of the carbonyl group. Subsequent proton transfer and tautomerisation leads to the formation of the intermediate 3-(3-hydroxy-2-oxindole) carboxylic acid derivative. Here, the acetic acid solvent is removed under reduced pressure and the red residue dissolved in 1 M sodium hydroxide solution to pH 11-12. The base hydrolyses the ester group in the intermediate and facilitates decarboxylation to furnish the desired isatin. This reaction was particularly difficult, due to the uncertainty of the quantity of isatin present in the final crude material. It was impractical to purify the crude isatin residue due to the large mixture of products present and the poor solubility of the material in common solvents other than methanol. There is a range of possible side products that could be present in the crude material, and this lead to overall lower yields in the alkylation of the isatin cores.

Starting from isatins, an obvious route to oxindoles is the reduction of isatin *via* Wolff-Kishner reduction of the corresponding isatin. This works well for isatins, but less well for bisisatins pri-

marily due to solubility issues and functional group tolerance. Other routes to oxindoles include cyclisation of *o*-aminophenylacetic acid derivatives and radical cyclisations, intramolecular Heck reactions, pyridinium chlorochromate catalysed intramolecular cyclisation or intramolecular arylation of amides or amide enolates.

Synthesis of Naphthalene-Based Monomers

The Martinet isatin synthesis procedure was conducted on 1,5-diaminonaphthalene dissolved in hot glacial acetic acid (Figure 3.7). To this a solution of diethyl ketomalonate in acetic acid was added drop-wise to the reaction at 115 ^oC. The reaction was refluxed for 16 hours after which the brick red reaction mixture with red precipitate was concentrated under reduced pressure. The red residue was dissolved in 1 M sodium hydroxide until the solution was pH 11-12. Air was bubbled through the reaction mixture while it was heated at reflux for 5 hours. After air was bubbled through the reaction for 5 hours, the reaction was allowed to return to room temperature. The reaction was poured onto ice and 6 M hydrochloric acid was then used to acidify the reaction mixture to pH 0. To minimise the problems with filtering an aqueous solution, the suspension was allowed to settle before the red supernatant was decanted and the remaining solution filtered. The purple/black solid was washed with methanol and dried in a vacuum oven for 16 hours.

To synthesize the naphthalene bisisatin monomer, the core naphthalene bisisatin and potassium carbonate were dissolved in DMF at 100 ^oC, before being cooled to 70 ^oC and the alkyl bromide added to the reaction mixture. After heating at 70 ^oC for 6 hours, the reaction was concentrated under low pressure to remove as much DMF as possible before being worked up and purified by flash column chromatography. The blue monomer was isolated from its side product by recrystallisation in hexane.

The C12 naphthalene bisoxindole was obtained by acylating naphthalene-1,5-diamine with C12 acyl chloride. Similarly to the other acylation reactions, the acylation progressed in the presence with triethylamine in DCM. The diacetamide was filtered, washed with ethyl acetate and dried in a vacuum oven. Reduction of diacetamide in THF with 2.5 M solution of lithium alumminium

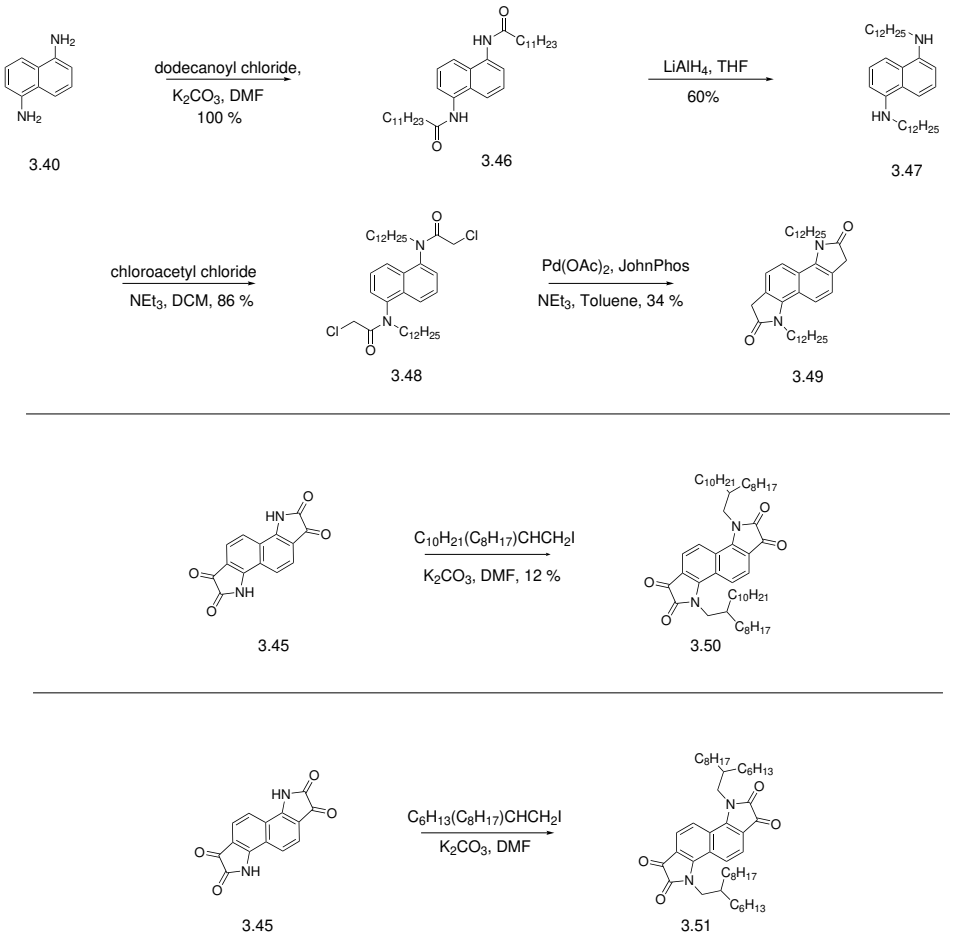

Figure 3.8: Reaction scheme for the synthesis of naphthalene based bisisatin and bisoxindole monomers.

hydride produced C12 naphthalene diamine. The amine isolated from this reduction reaction was acylated with chloroacetyl chloride to give dichloroacetamide. The Heck-type cyclisation on the C12 precursor gave the bisoxindole in 30-40 % yield.

3.2.2 Polymer Synthesis

Once the monomers for each polymer were prepared, the polymerisation reactions were conducted in toluene with 30 % *p*-toluene sulfonic acid relative to the bisisatin monomer. The concentration of the acid, was maintained around 20 mol/L. In preparation for the polymerisation processes, toluene was degassed for 1 hour and injected into a sealed reaction vessel already containing the monomers and *p*-toluene sulfonic acid in argon atmosphere. After injecting toluene, the solution was further degassed for 10 minutes before the reaction vessel was submerged into an oil bath at 120 ^oC. Initially, the polymerisation reactions were conducted with dry molecular sieves to drive the equilibrium forwards as water is the reaction byproduct. It was later found that molecular sieves were unnecessary and that the reaction progressed suitably without a drying agent as the last reaction step is generally irreversible. Although, the extrusion of water in the last step of the mechanism is theoretically reversible, it is considered practically irreversible. Bager *et al.* investigated the equilibrium constant for the elimination of water in aldol reaction of acetone in sulfuric acid and found the reaction became practically irreversible at 67 % w/w sulfuric acid concentration. The relatively high acid catalyst loading here helps to push the equilibrium to the right and make the water elimination practically irreversible.

The polymerisation reaction mixture goes through several colour changes, the reaction begins as a blue solution then colour changes to a dark murky red then to a olive green colour before resting on the final polymer colour of purple. The polymers were isolated by precipitation in methanol. The solids were collected in a cellulose thimble and the polymer subjected to Soxhlet extraction in methanol, acetone, to remove the acid, hexane, DCM, chloroform, toluene and chlorobenzene in succession depending on the polymer molecular weight and solubility. The extraction solution was concentrated under reduced pressure and the polymer re-precipitated in

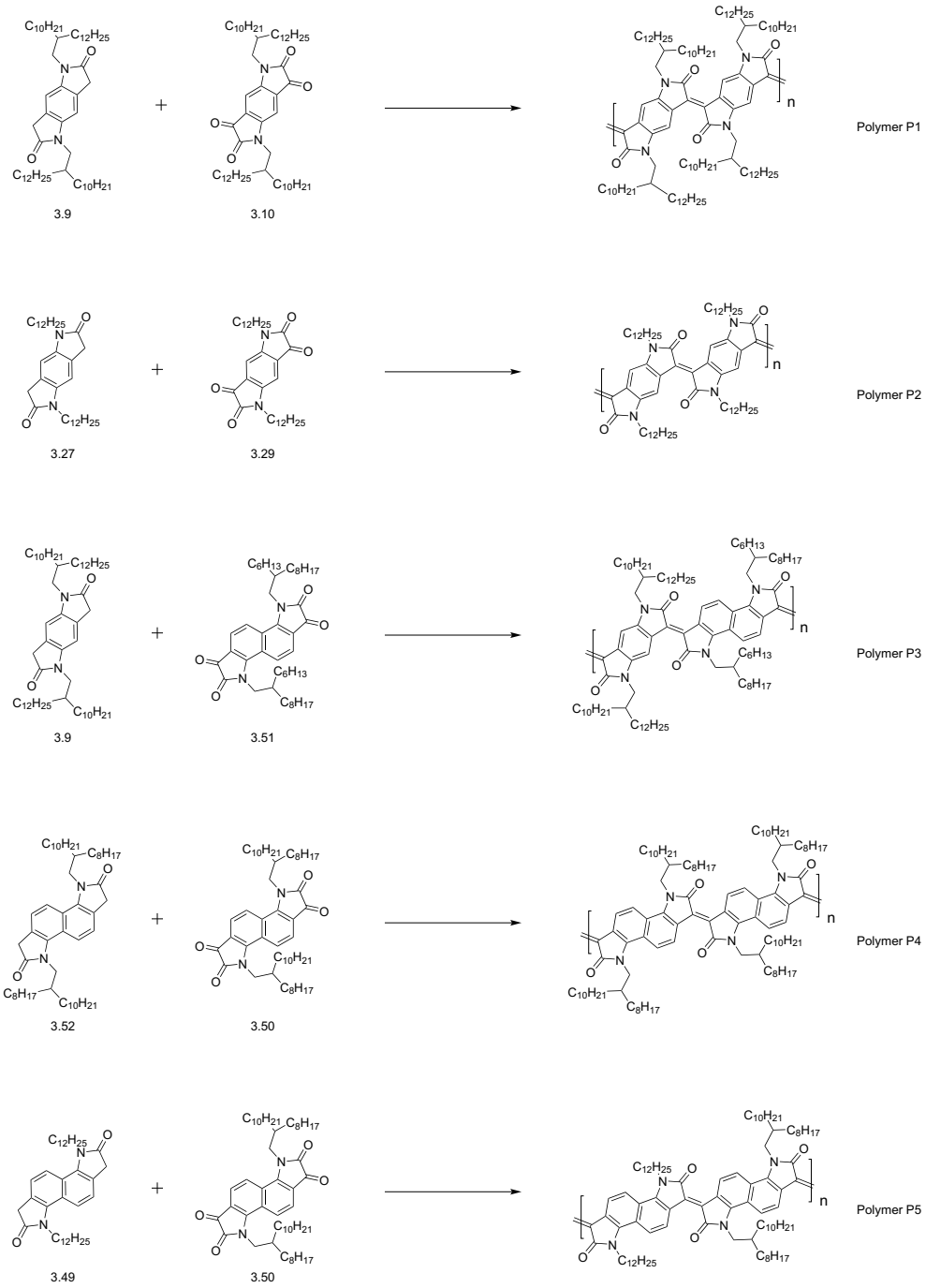

Figure 3.9: Reaction schemes for the synthesis of Polymers P1 to P5 *via* *p*-toluene sulfonic acid catalysed aldol polymerisation.

methanol and then collected by filtration through a 0.25 μm PTFE filter to isolate the purple solid. Polymers P1 and P3 which have large alkyl chain densities were waxy purple solids. The solubility of the polymers were found to vary with the nature and length of the side chain. The benzene-core homopolymer, P2, with linear dodecyl chain was insoluble in common solvents, but partially soluble in hot chlorobenzene. Polymer P2 and P5 were isolated as discrete dry pellets since they are less soluble. Even during the polymerisation reaction it was clear that the polymer would be difficult to solubilise as the polymer partially precipitated out of the reaction mixture prior to termination of the polymerisation reaction. P4 was also slightly waxy due to the large chains.

3.2.3 Polymer Characterisation

The length of the polymers were measured using Gel Permeation Chromatography (GPC), where the molecular weights of the polymers were calculated relative to narrowly dispersed polystyrene standard. Given the physical differences between these polymers, polystyrene is a highly flexible polymer, whilst these polymers may be considered rigid rods, this measurement gives an indication of the polymer molecular weight. The number average molecular weight is reported as Mn and the weight average molecular weight is Mw. The GPC traces of the polymers are included in Appendix 2-6.

Mass Spectrometry offers a precise mode of obtaining the polymer mass data, since it can show the polymer length of each polymer. However, it was not possible to observe these polymers in Mass spectrometry, due to ionisation, acceleration or deflection issues in MALDI experiments. According to GPC, the polymers achieved excellent molecular weights except for polymer P2. Polymer P2, an oligomer, precipitated out of the reaction mixture before the polymerisation reactions was stopped. The lack of soluble polymer end groups resulted in the low molecular weight that is in turn due to the short linear alkyl side chains and lack of branching chains.

Table 3.1: Summary of optoelectronic and physical properties of polymers P1 to P5.

Polymer	Mn /kDa	Mw /kDa	TGA /^oC	$\lambda^{[a]}$ /nm	$E_{opt}^{[b]}$ /eV	$IP^{[c]}$ /eV	$EA^{[d]}$ /eV
P1	58	131	406	900	1.10	-5.60	-4.50
P2	14	19	375	850	1.01	-5.40	-4.40
P3	51	132	374	913, 1001	1.11	-5.45	-4.34
P4	214	697	380	927	1.07	-5.30	-4.20
P5	134	538	376	927	1.01	-5.20	-4.20

[a] Thin films were spin-cast on glass substrates from chlorobenzene solution, λ is the peak of the low energy absorption band of the polymers. [b] Estimated optical gap was calculated using onset of the thin-film absorption spectra ($E_{opt} = 1240/\lambda_{onset}$). [c] IP was measured by PESA. [d] EA was estimated by addition of the UV-vis absorption onset to IP ($EA = IP - E_{opt}$), a protocol that neglects the exciton binding energy.

The processing of polymers often involves heat such as in dissolving the polymers and annealing them post deposition. It is therefore important to know the thermal stability profile of the polymers to avoid polymer decomposition within the processing temperature range. All the polymers displayed excellent thermal stability with a 5 % decomposition temperatures at or above 375 ^oC. Phase transitions in the polymers as they are heated or cooled were investigated by differential scanning calorimetry (DSC). No significant transition temperatures were observed in the DSC traces as the polymers were scanned from -10 to 300 ^oC.

NMR spectra of the polymers showed marked down-field shift in the aromatic proton signals due to increased conjugation along the polymer spine. Figure 3.10 gives the NMR spectra of polymer P1, the protons in the repeat units along the polymer correspond to the aromatic protons of C10C12 phenyl bisisatin. The proton signal in the monomer appear at 7.12 ppm and the same protons now in the polymer produce a signal at 9.27 pm. The NMR spectrum show a ratio of approximately 2:4 for the aromatic protons signal relative to the N-methylene groups of the side chain, supporting our expected polymer structure. The large polymer alkyl chains produce a broad signal at 1.25 ppm. Polymer P5 proton NMR spectrum in 1,1,2,2-tetrachloroethane-d2 solution at 60 ^oC also supports the proposed conformationally-fixed structure of the polymers.

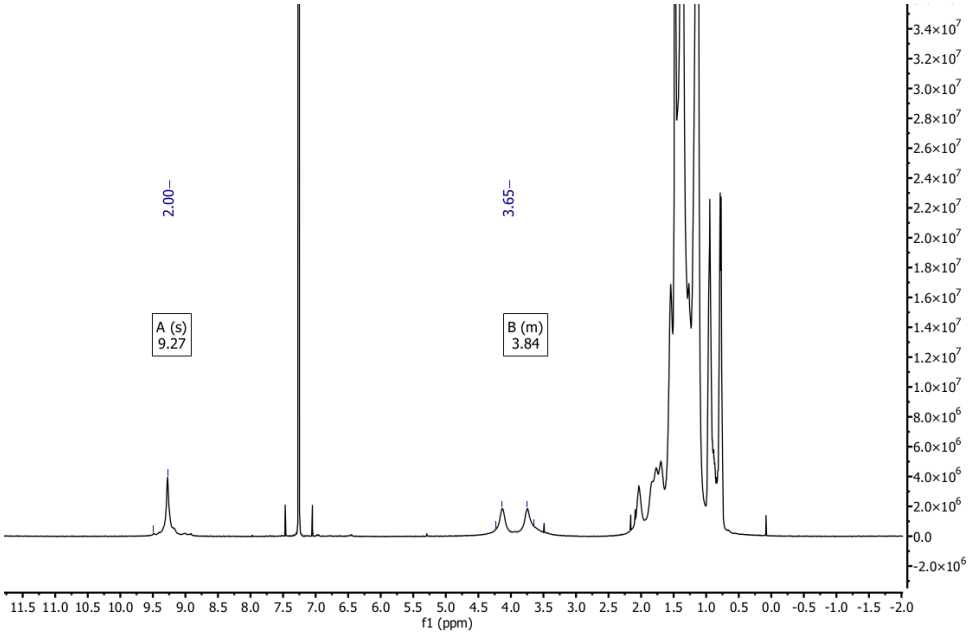

Figure 3.10: NMR spectrum of polymer P1 in chloroform at 400 MHz, ^1H δ (ppm): 9.27 (s, 2H, ArH), 3.84 (m, 2H, NCH_2) and a large alkyl chain multiplex between 2.7 - 0.6 ppm.

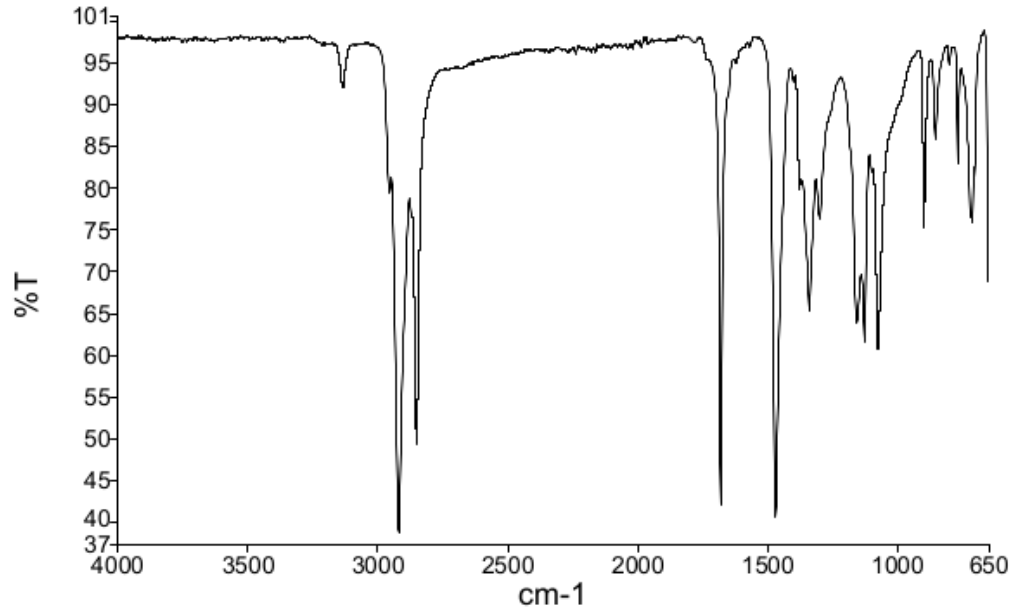

Figure 3.11: FT-IR spectrum of polymer P1 showing the absence of hydroxyl stretch around 3000 cm^{-1}.

Its NMR spectrum is presented in the Appendix 15. As the generation of Michael-adducts are a possible side-reaction, infra-red measurements of the polymer P1 was taken. The absence of a hydroxyl stretching signal in the polymer IR spectrum suggests the absence or low occurrence of Michael-adducts in the polymer that would contain hydroxyl groups.

3.2.4 Optical Properties

In solution, these polymers are a deep purple colour, as evidenced in the UV-vis spectra. Polymer P1 is waxy in the solid state and smears easily due the large greasy alkyl side chains, meanwhile P2 was recovered as pellets of polymer. The less soluble higher Mn polymers have a green sheen in the solid state. Generally, the polymers exhibited two bands in their absorption spectra and displayed absorption profiles that continued into near infra-red region due to the extended conjugation in the polymers. Figure 3.12 gives the UV-vis NIR spectra of polymers P1 to P5. Band I absorption, attributed to $S_0 - S_1$ transitions, occurs in the range of 400-600 nm. It is a broad absorption band, covering the blue, green, yellow and orange regions of the visible spectrum, accounting for the purple colour of the polymer. The absorption properties of the polymers dip around 700 nm before a longer wavelength absorption band around 900 nm.

Polymer P1 displayed the smallest full width at half-maximum in absorption Band I compared to the other polymers. Its first absorption band with λ_{max} at 580 nm is succeeded by smaller absorption bands at 860 and 910 nm respectively. Although polymer P1 and P2 have the same backbone structure, only differing in the nature of their alkyl side chains, there are significant differences in their optical properties, Figure 3.13, top graphs. In the absorption spectra of polymer P2, both absorption bands are broader as well as blue shifted relative to P1. We believe these differences are a consequence of lowering the alkyl chain density between P1 and P2. P1, soluble in hexane because of its large alkyl chains, aggregates less than P2 that is only soluble in hot chlorobenzene, P1 displayed the narrowest absorption bands because it is the most soluble polymer and therefore the least aggregating polymer in solution. We also observed that the two peaks of the second absorption band merged into one peak in the spectrum of Polymer P2. Again, we believe this is a consequence of in-solution aggregation of the polymer.

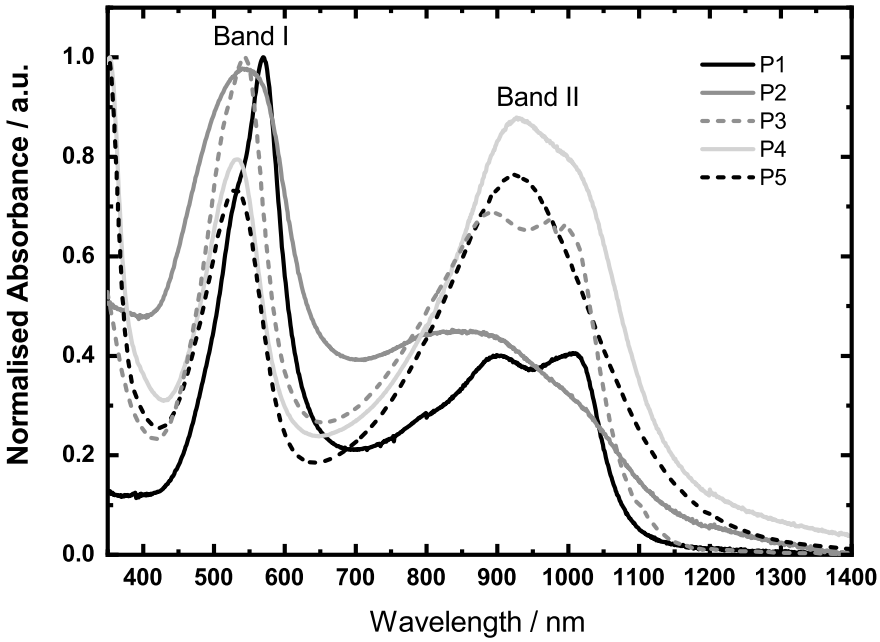

Figure 3.12: Normalised UV-vis NIR absorption spectra of polymers P1 to P5 in chlorobenzene solution.

Polymer P3 is the only polymer with a mixed benzene/naphthalene backbone and consequently its absorption spectra is distinct from that of the other polymers, Figure 3.13. It has absorption peaks at 600 nm and 800 nm respectively. The signal mismatch at 860 nm is an artefact due to a lamp change in the UV-vis NIR spectrometer. Polymer P4 and P5 both have the same naphthyl backbone and similarly to polymers P1 and P2 their UV-vis NIR spectra are similar. Compared to polymers P1 and P2 absorption Band II is the prominent absorption peak in polymers P4 and P5, this is likely due to increased electron delocalisation that enable more low energy transitions along the polymer backbone. P5 is highly aggregated in solution and the single peak observed at 910 nm is reminiscent of the single peak of poorly soluble polymer P2 at 830 nm. On the other hand, a shoulder is present on absorption Band II in the P4 spectrum because it is more soluble than P5 even though it has a much larger Mn.

Generally, there were no significant differences between the solution and thin film absorption spectra of the polymers. This may be due the polymers already achieving high degrees of aggregation in solution and therefore no insignificant energy changes occurred to the frontier

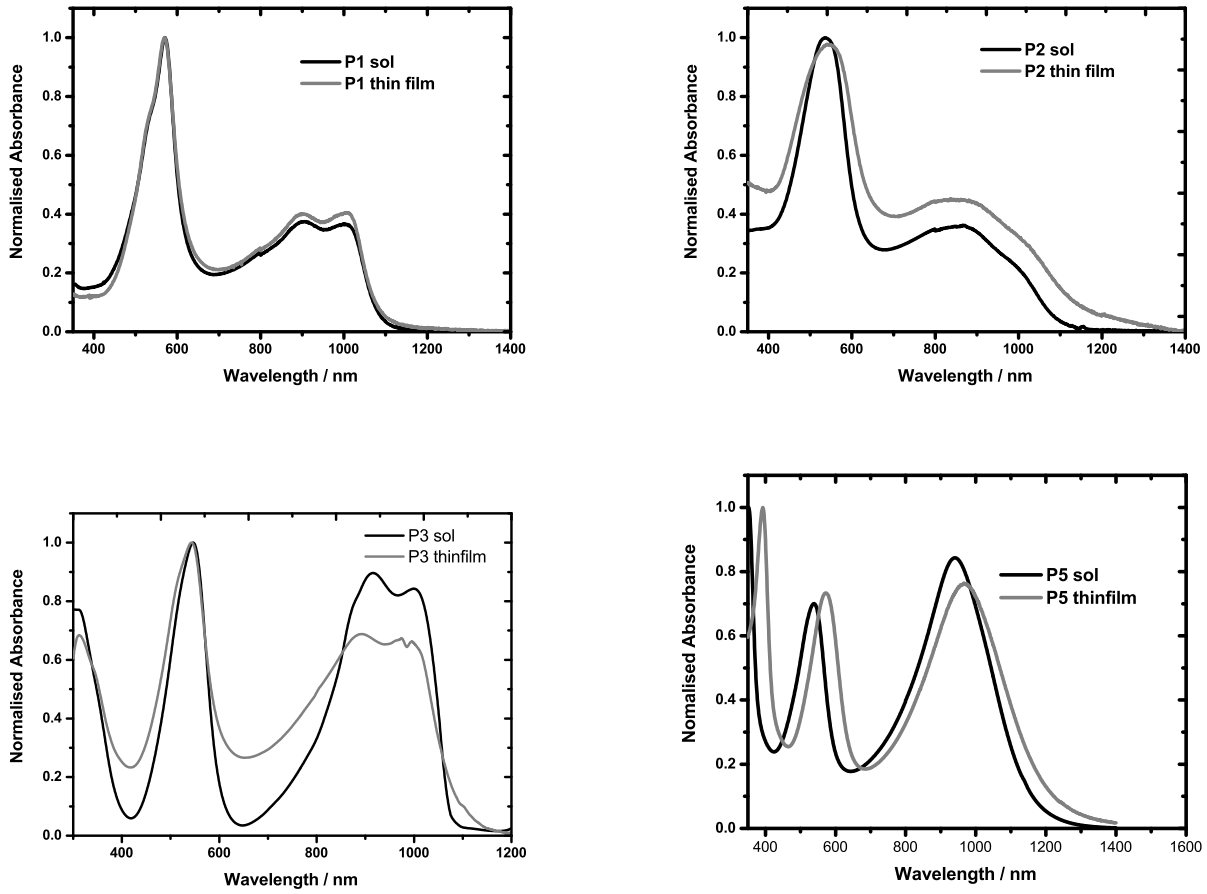

Figure 3.13: Solution and thin film UV-vis NIR absorption profiles for polymers P1, P2, P3 and P5.

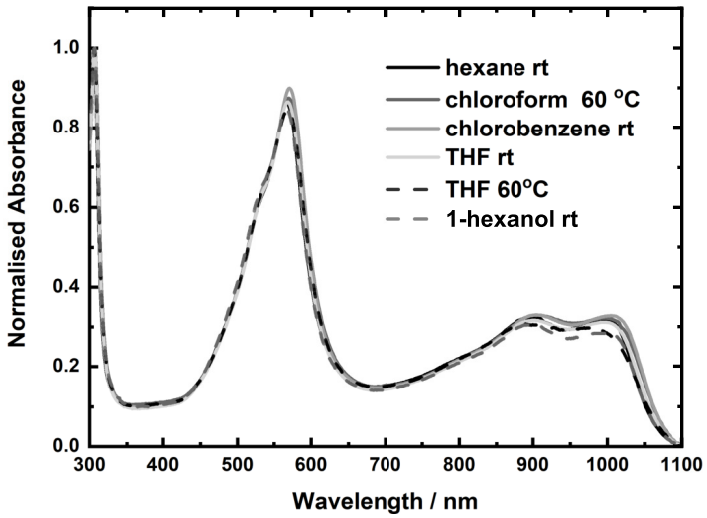

	Dipole Moment / D	Dielectric Constant
Hexane	1.9	0.00
Chloroform	4.8	1.00
Chlorobenzene	5.7	1.54
THF	7.5	1.63
1-Hexanol	1.65	12.50

Figure 3.14: UV-vis absorption spectra of polymer P1 in solvents with a range of solvents. Below: A table showing the dipole moment and dielectric constant of the solvents used.

energy levels upon moving to the solid state. There was though a slight red shift in the UV-vs spectrum of P5 on going to the solid state, as explained by aggregation effect. To gain a better understanding of the origins of the absorption spectrum of the rigid polymers the UV-vis absorption spectra were measured for polymer P1 in different solvents. The solvents were chosen to reflect different types of solvents, non-polar, polar protic and polar aprotic. The dielectric and pKa of the solvents were also noted to observe any effects over a range of values. Solvatochromism refers to the effect of solvent choice on electronic absorption spectra . It occurs when the solvent better solvates one transition state compared to an other during absorption of photons. In the case of conformationally-fixed polymer P1, significant solvatochromism was not observed. Given that P1 was the most soluble polymer, it was practical to use it for these measurements as it would be soluble in the largest range of solvents. As seen in Figure 3.13, there is little changes in the UV-vis absorption spectra of the polymer P1. Band I absorption is the least affected whilst there is small variation in the Band II absorption intensity. Polar protic solvent 1-hexanol had the lowest absorption intensity in both Band I and Band II absorption

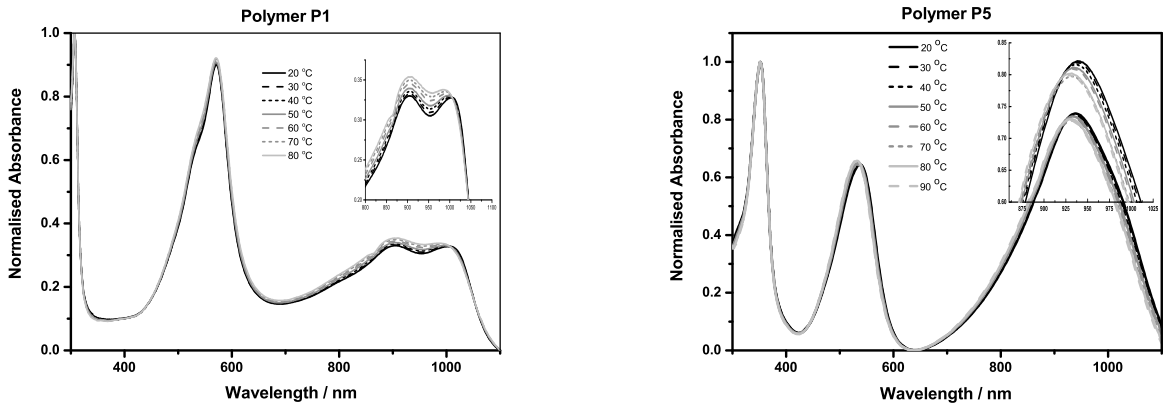

Figure 3.15: UV-vis absorption spectra of polymer P1 and P5 solutions at a range of temperatures.

peaks. Absorption spectrum of P1 in 1-hexanol also displayed the largest separation of the Band II peaks and induced a minor blue shift in the Band II peaks relative to the other polymer solutions. Hexane, chloroform, chlorobenzene and THF at room temperature generated similar absorption spectra. These solvents covered a range of dipole moments from 1.9 to 7.5 D and dielectric constants, 0.0 to 1.63. Interestingly the absorption spectrum of polymer P1 in THF at room temperature differs to that of P1 in THF at 60 ^oC. Higher temperatures increases the polar effect of THF on the polymer. Although the polymer contains strongly polarised groups, the polymer is generally non-polar because it is highly symmetrical. This feature, in addition to the delocalisation of charge in the excited state of the polymer, results in a lack of solvatochromic effect.

The effects of solution temperature on the UV-vis absorption spectra of polymer P1 was also investigated. The absorption spectra of a chlorobenzene solution of P1 was recorded at a range of temperatures from 20 ^oC to 80 ^oC in increments of ten degrees. Again, P1 showed no significant temperature dependent absorption in chlorobenzene. Band I has a slight shoulder due to aggregation of the polymer in solution. The shoulder peak is most distinct at room temperature, as expected. Increasing the solution temperature of the solution causes the shoulder to merge more with the Band I peak. As the solution temperature rises, there are more vibrations in the polymer that results in averaging of transition energies in the polymer, Figure 3.15, left. A similar effect is seen in Band II.

The temperature dependent UV-vis spectra of polymer P5 was also measured. Given that this polymer is much less soluble that P1, we expected more significant differences here, particularly due to potential aggregation shoulder. Here though, aggregation shoulders were not observed. It seems both the absorption bands become blue shifted as the solution temperature increases.

3.2.5 Charge Transport Properties

Transistor devices of polymer P1 and P2 did not show significant semiconducting behaviour in a TGBC geometry. Initially, we argued that polymer P1 displayed no transport properties because its large alkyl side chains prevented close $\pi - \pi^*$ stacking and therefore hindered the formation of ideal charge transporting morphology. Therefore polymer P2 should have had higher charge transport property because its linear chains should facilitate closer polymer packing and the formation of crystalline domains for effective charge transport. However this was not the case and polymer P2 also did not display any charge transport properties. Polymer P3 also did not show considerable improvement on charge transporting properties. P4 on the other hand displayed charge transport of 0.001 $cm^2V^{-1}s^{-1}$ and polymer P5 had maximum electron mobility of 0.03 $cm^2V^{-1}s^{-1}$. This was later further improved to 0.1 $cm^2V^{-1}s^{-1}$ by solution shearing. Figure 3.16 shows the transfer output of P5 in a TGBC transistor at 50 V drain voltage. At 10 V gate potential, the transistor is switched on and as the gate voltage becomes more negative the P5 semiconducting layer accumulates more holes to transport. The hole transport increases moderately with gate voltage. The hole mobility of transistors increases from 10 V for a device under nitrogen and 22 V for a device in air, but by -10 V the hole mobility plateaus at 0.01 $cm^2V^{-1}s^{-1}$. Tuning the gate-voltage positively from 20 V raised the charge mobility as more traps are filled enabling more mobile charges. Over time the turn-on voltage increases from 10 to 25 V as the material degrades and forms more charge traps. Nonetheless the current still rises up to its original value as in a brand new device operating under a nitrogen atmosphere. The electron mobilities increased to a maximum of about 0.03 $cm^2V^{-1}s^{-1}$ at 60 V gate voltage.

N-type organic semiconductors are typically unstable due to the populated LUMO energy

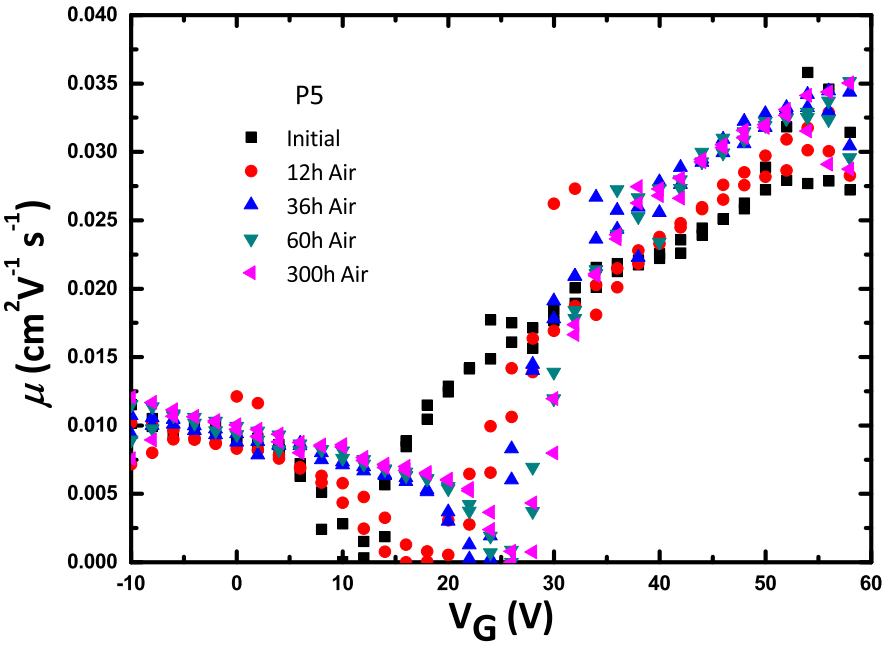

Figure 3.16: A graph of how mobility from the saturation regime varied with gate voltage for polymer P5.

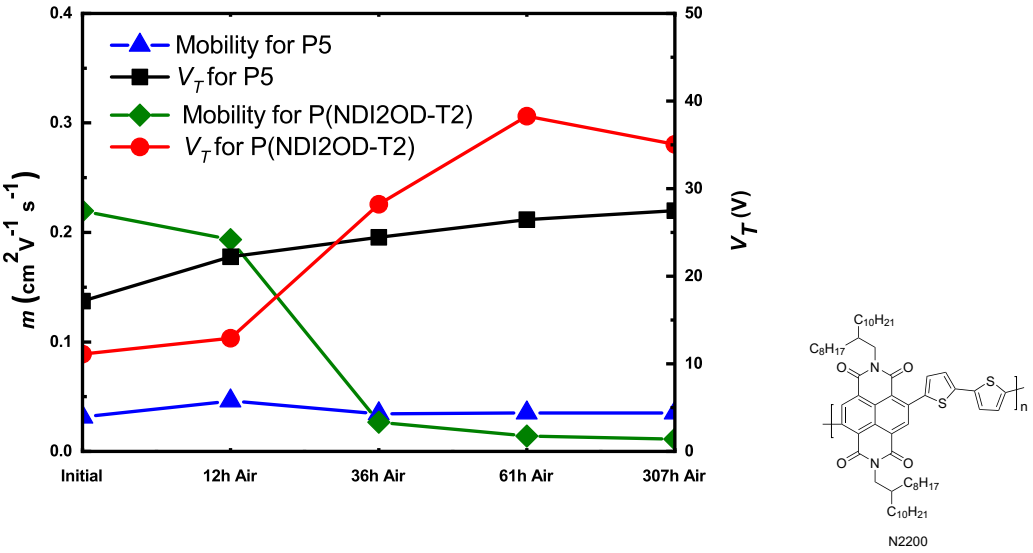

Figure 3.17: Transistor mobility curves showing impressive ambient stability of polymer P5 compared to N2200 (p(NDI2OD-T2))(right).

levels that are susceptible to reactions with water and oxygen. Comparing the stability of N2200 transistor device over 300 hours in air, it is clear that although, N2200 has a higher initial mobility, P5 rigid polymer out performs it after 300 hours operation in air. This is particularly encouraging for the potential of air stable conformationally-fixed polymers by aldol polymerisation.

Polymer Chain length and Mobility

The charge carrier properties of polymers for OFET can be closely linked to the polymer molecular weight. It has been well demonstrated that field-effect mobility in P3HT increases rapidly with its length.[158–161] Oligomers and shorter polymers tend to have more crystallites and longer range crystalline domains than longer polymers.[92] Although it is desirable to have crystalline domains, short polymer chains form numerous small crystallites that are incoherent with other crystallites. Charge transport within these crystallites are fast but the measured material charge mobility is affected significantly by inefficient charge transfer between the multiple crystalline domains. Longer polymers are therefore preferred because of their greater potential for entanglements between crystalline domains. Entanglements describe the interconnectivity between polymer chains and crystallites in the solid state. This interconnectivity facilitate efficient inter-chain charge transfer and charge transfer between crystalline domains.

Batches of polymer P5 were prepared with a range of molecular weights. The table in Figure 3.18 shows the six polymers synthesised and their number and weight average molecular weight as well as their measured mobility. The TGBC transistor architecture used for these polymers consisted of a glass substrate, PMMA dielectric layer and aluminium gate contact and gold source and drain electrodes. The channel length and width were 20 μm and 1 mm respectively. The charge mobility was measured in the saturation region, at $V_D = 60\ V\ and\ V_G = 60\ V$. The n-charge mobility increased linearly with molecular weight. When Mw is above 200 kDa, reduced processability of the polymers prevents device production, as it becomes difficult to generate smooth films of the polymer. In addition to improving the mobility of P5 through molecular weight tuning, optimizing device processing enhanced charge transport. As previ-

Polymer	Mn (kDa)	Mw (kDa)	$\mu\ cm^2V^{-1}s^{-1}$
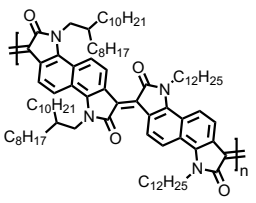	4.7	8.1	0.0008
	15.2	37.2	0.0080
	26.3	75.0	0.0300
	30.2	104.4	0.0400
	55.4	190.7	0.0700
	67.0	266.0	0.1000

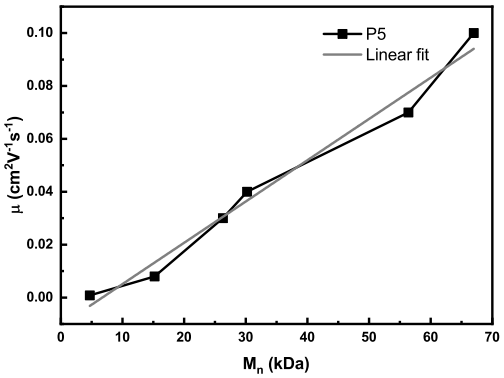

Figure 3.18: A table showing the effect of molecular weight of P5 on mobility. As the weight average molecular weight of polymer P5 increased its mobility also increased to a value of 0.1 $cm^2V^{-1}s^{-1}$. Graphical, the data suggests a linear relationship between polymer length and mobility in conformationally-fixed polymers.

ously discussed, achieving fast charge transport is also closely dependent on transistor components, such as the gate dielectric and fabrication technique. Our collaborators were able to improve on the electron transporting property of P5 by promoting anisotropy in the polymer by solution shearing it rather than spin-coating it onto the substrate. Solution shearing the polymer solution onto the substrate enables the polymers to better align themselves relative to each other. Zone-casting was another depositing technique that improved film morphology. A comparison of the GIWAXS patterns of aligned zone-casted polymer P5 (available in the Appendix 12) and the spin-coated films showed significant reduction in face-on arrangement. There is also a slightly increased proportion of edge-on arrangement between the two scattering patterns. Transistor devices produced by solution shearing achieved electron mobility of 0.1 $cm^2V^{-1}s^{-1}$.

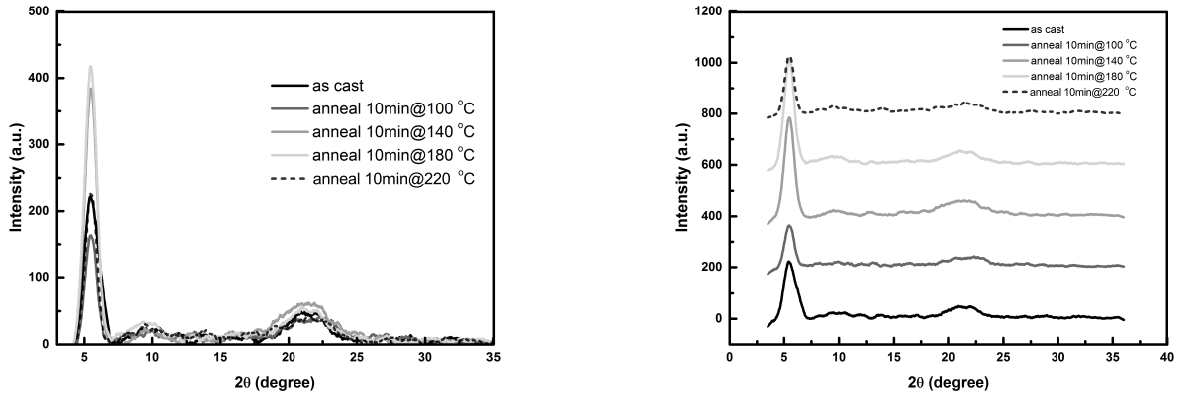

Figure 3.19: X-ray diffraction pattern of polymer P1 film showing the effect of different annealing temperatures.

3.2.6 Morphology and Crystal structure

Grazing-incidence wide-angle X-ray Scattering (GIWAXS) measurement is useful for quantifying the orientation distribution of semiconducting polymers on a surface. It is an X-ray photon scattering technique used to study nano-structured surfaces and thin films. X-ray photons directed at a sample on a spinning stage are scattered by atoms in the thin film in relationship to the incident ray as described by Bragg's law. Peaks are observed as the incidence ray is reflected from the crystal lattice of the material and onto the detector. Higher signal intensities are observed for highly crystalline materials where there are regular repeating layers of atoms in the material. Crystalline materials produce specific patterns of reflected X-rays at specific wavelengths and incident angles. Given that the angle of incidence is equal to the angle of scattering and the path difference is equal to integer number of wavelengths, constructive interference allows for higher peak intensity for highly crystalline materials.

GIWAXS gives insight into the macro-morphological consequence of polymer structure-design strategy and processing. Films samples for GIWAXS measurements were prepared by drop-casting polymer solutions (10 mg/mL hot chlorobenzene) onto ozone-treated undoped silicon wafer. Ozone treatment cleans the silicon surface increasing its surface energy to facilitate wetting of the polymer solution on the surface. Two samples of each polymer was prepared, dried in air, and one sample annealed at 200 ^oC for 10 minutes.

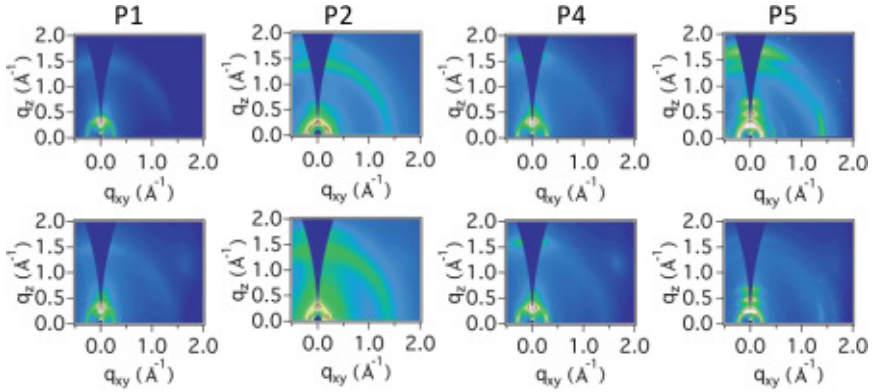

Figure 3.20: GIWAXS imaging of polymers P1, P2, P4 and P5, unannealled (above) and annealled (below). The films were spin-coated from chlorobenzene solutions onto undoped ozone treated silicon substrates.

GIWAXS measurements and analysis were carried out by David Hanifi under the supervision Professor Alberto Salleo at Stanford University. In general, the polymers exhibited an amorphous texture with some face-on tendency and measured coherence lengths between 1.6 - 2.8 nm. This face-on texture maybe be due to templatation of the thin-films onto the silicon substrate. Film thickness is important for reliable scattering patterns from GIWAXS measurements. Nonetheless, the data suggest that there was an increasing degree of edge-on domains in polymers P1 to P5 and this may have contributed to the mobility increase. Polymer P5, in particular, has significant population of edge-on crystallites that upon annealing their coherence lengths increased from 5.5 to 7.1 nm. Figure 3.21, shows 2D-GIWAXS pattern of the edge on texture in P5 along Q_z, The linecut shows strong layering of the (100), (200) and the (010) respectively. Interestingly, with increased conjugation length the $\pi - \pi$ distance actually increased monotonically from 3.36 - 3.76 Å from polymer P1 to P5, and the annealed sample show large $\pi - \pi$ distance relative to the unannealed films.

In Figure 3.19, annealed X-ray diffraction samples of P1 showed insignificant changes in the small quantity of observed edge-on peaks (note the low intensity). Although, thermal annealing induced multiple higher order in-plane layer stacking peaks indicative of a strong face-on texture, this orientation doesn't contribute significantly to charge transport. While side-chain density varied significantly between P1 and P2 it had no impact on in-plane stacking (2.7-2.3 nm), which can primarily be attributed to the higher molecular weight of the polymers.

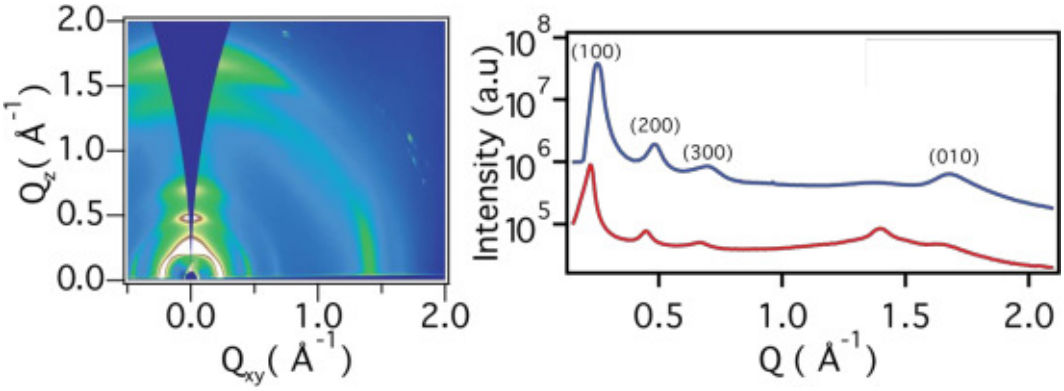

Figure 3.21: GIWAXS diffraction pattern of polymer P5.

3.2.7 Computational Study

Density Functional Theory (DFT) computational analysis can compliment the working hypothesis of a project and aid in explaining the observed properties. Computational calculations were carried out on the polymer structures discussed in this chapter. All the polymers were simplified to six unit oligomers, this number of units was chosen to balance the demand of computation power required and the reliability of the data generated. The polymer side chains were also reduced to methyl groups. The geometries were optimised at $\omega B97XD/6-31G(d,p)$ level theory without any geometrical constraints.

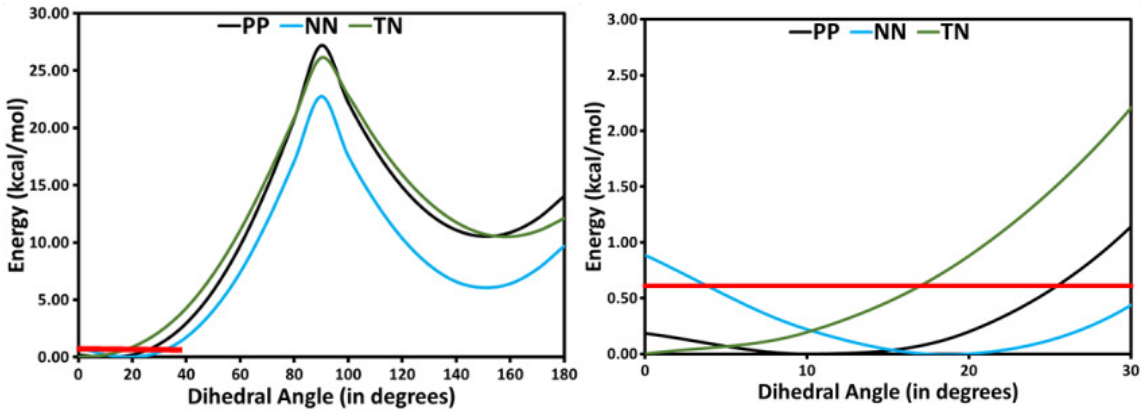

Figure 3.22: DFT simulation of the torsional energy barrier of homophenylene (PP), homonaphthalene (NN) and thienothiophene-naphthyl (TN) based conformationally-fixed polymers. The red line represents kT.

Results from DFT calculations suggest that polymers P1 and P2 with repeating phenylene cores suffer from a torsional twist of 12^o, Fig. 3.23. Steric repulsion between the carbonyl oxygen and the ortho-phenyl hydrogen atoms cause a twist between monomers in the polymer

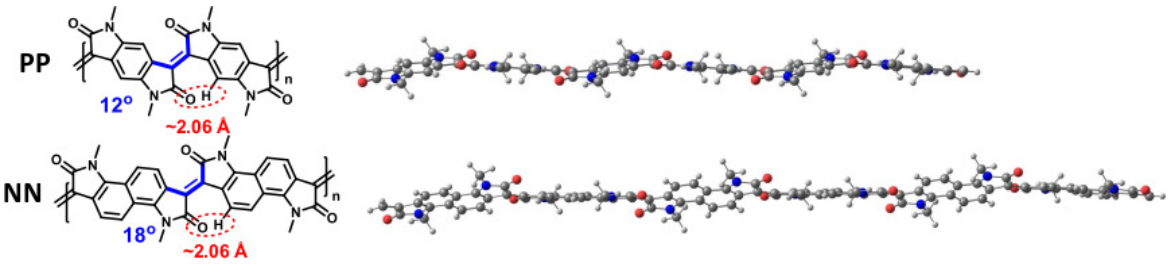

Figure 3.23: DFT calculations showing that homo-phenyl and homo-naphthyl conformationally-fixed polymers have a 12^o and 18^o dihedral angle twist at their lowest energy conformations respectively. There is approximately 2.06 Å distance between the ortho-hydrogen and the lactam oxygen atom. The side profile suggests that the polymers are not coplanar.

backbone. The length of the carbon-carbon double bond between monomers (1.43 Å) facilitate this steric interaction. The resulting large dihedral angle between the monomers produces a non-planar, pluckered polymer that has a detrimental effect on the polymer $\pi - \pi^*$ stacking ability. Although the carbon-carbon double bonds were introduced to planarise the monomer units along the polymer backbone, the double bonds instead plays the detrimental effect of fixing the monomer units in a non-planar conformation because of the size of the aromatic rings. Similarly to the homo-phenylene oligomer(PP), the phenylene-naphthalene polymer and the homonaphthalene (NN) polymers are subject to the same torsional twist due to the size of the aromatic ring. The DFT calculations suggest the phenyl-phenyl homopolymers (P1 and P2) and naphthalene homopolymers (P4 and P5) have a dihedral angle of 12^o and 18^o respectively. This angle is similar to the dihedral angle of 12.8^o measured on our naphthalene bisisatin small molecule (Appendix 1). The torsional barriers of the different polymer cores were also calculated, these are presented in Figure 3.22. The energy of the most stable conformation is taken as the reference energy. Congruent with the torsional angle, the local minima for the three polymer backbones occur at approximately 20^o for the naphthalene-naphthalene oligomer, 12^o for the phenyl-phenyl oligomer and 0^o for a thienothiophene-naphthalene oligomer. The relative energy difference between a coplanar and non-planar torsional angles is approximately 4 kcal/mol. Considering that at room temperature we have $kT = 0.6\ kcalmol^{-1}$, a lot of energy is required to planarise the polymers, however, at room temperature the torsional angles of P1 and P3 and P5 can fluctuate by as much as (plus/minus) 10^o from the minima.

The polymer reorganisation energy, as discussed in the background information, is an important

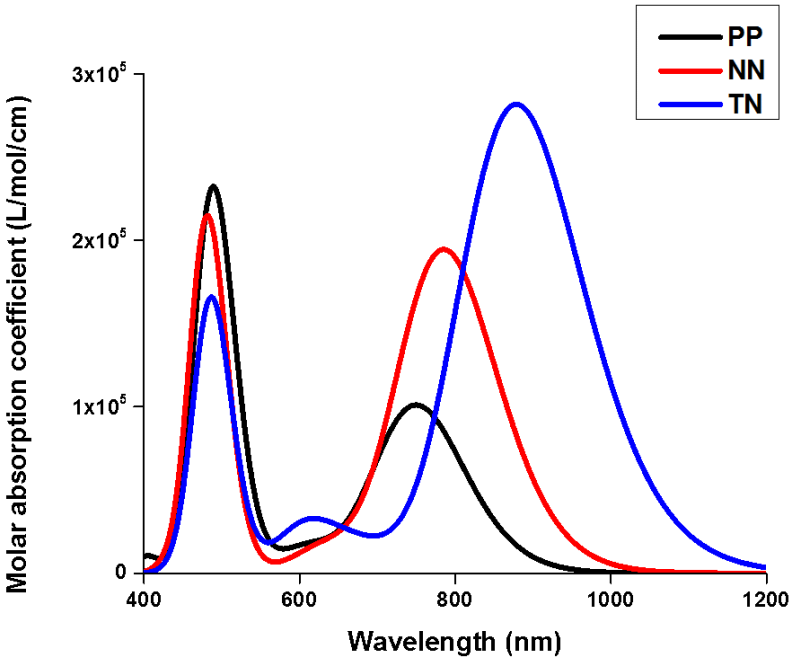

Figure 3.24: DFT calculated UV-vis absorption spectrum of conformationally-fixed polymers where PP, NN and TN represent homophenylene, homonaphthalene and thienothiophene-naphthyl based conformationally-fixed polymers respectively.

Table 3.2: Simulated reorganisation energies of conformationally-fixed polymers with only phenyl or naphthalene backbones.

Polymer Backbone	IP /eV	EA /eV	Reorganisation Energy /meV
PP	6.25	2.47	427
NN	6.00	2.44	327

The IP falls when the polymer backbone is composed of naphthalene units compared to benzene rings, due to the increase electron density of elongating the benzene aromatic core. This also reduces the electron affinity as the carbonyl to aromatic centre ratio decreases. The longer naphthalene-centred polymer was simulated to have lower reorganisation energy which enhances charge transport.

consideration for organic semiconductors for transistors. The reorganisation energies were also calculated for the oligomers of these polymers (Table 3.2). As the conjugation length increases from the phenyl-phenyl oligomer to the naphthalene-naphthalene oligomer, the reorganisation energy decreases. Decreasing the reorganisation energy with conjugation length facilitates charge transfer and thus improved electron mobility.

We also calculated the vertical excited state energies using TD-OT-ωB97XD/6-31g(d,p) theory level. The simulated spectrum, though, was calculated in the gas phase. Naturally, there is some differences between gas phase absorption and absorption in solution. The simulated

spectra show two absorption bands as we observed experimentally. There is a high energy absorption band around 500 nm low energy absorption peak around 800 nm. The calculated spectra also displayed the same trend observed experimentally, that is that as the conjugation length of the polymers increase the lower energy band becomes more dominant. Also as the conjugation length increases the spectra become more red-shifted.

3.2.8 Disorder and Charge Transport in Polymer P5

Sirringhaus *et al.* measured disorder in leading polymers by extracting the Seebeck coefficient and the Urbach energy.[162] The Seebeck coefficient was measured on micro-devices of 20-50 μm channel length with a heater and temperature sensor incorporated in the device. The electromotive force produced across the device is measured when a temperature gradient is applied across the material. The Seebeck coefficient for most leading polymers, such as PBTTT, fitted well with models based on hopping transport in organic semiconductors whilst, the data for IDTBT best fitted narrow-band models where the charge carriers experience low levels of energetic disorder and can consequently access transport sites using K_BT. There is alignment of the monomers on IDTBT that means the polymer behave similarly to a overlapping sheets of ribbons. Consequently even though on the macro level is near-amorphous, it is more ordered than PBTTT for example. There is therefore other methods for quantifying order within polymer films that may reflect intramolecular order, not just macromolecular order between polymer chains. Urbach energy (E_u) data also suggested IDTBT is a low disorder system. The Urbach energy unlike Seebeck coefficient is a bulk-sensitive measurement of the energetic disorder evident in the sub-bandgap tail states. It is measured by photothermal deflection spectroscopy. The Urbach energy, extracted from the optical absorption coefficient near the bandgap, was lowest for the highest mobility polymer IDTBT (E_u = 24 meV) and increased in order of descending mobility, P(NDI2OD-T2) (E_u = 31 meV) and DPPTTT (E_u =33 meV).[162]

The energetic disorder for polymer P1 was probed using photothermal deflection spectroscopy. Figure 3.25 gives the Urbach energy of P1 and IDTBT for comparison. Polymer P1 reported an Urbach energy of 30 meV, similar to high performing polymers P(NDI2OD-T2) and DPPTTT

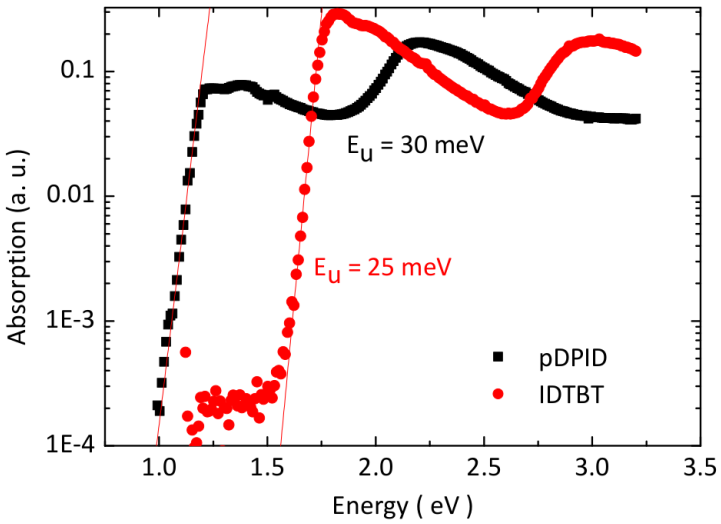

Figure 3.25: The absorption coefficient of P1 and IDTBT films, measured by photothermal deflection spectroscopy. The Urbach Energy calculated from these curves show that polymer P1 has a more disordered polymer backbone than IDTBT.

albeit significantly higher than IDTBT. This in addition to the low fraction of edge-on packing in the polymer film limits charge transport in these conformationally-fixed polymers.

3.3 Conclusion

Here we discussed the synthesis of five polymers *via* metal-free, *p*-toluene sulfonic acid catalysed aldol polymerisation. We were able to achieve a mobility of 0.1 $cm^2V^{-1}s^{-1}$ in polymer P5 by incorporating larger aromatic centers in our polymers, tailoring the polymer chain length and optimising the device fabrication method. The conformationally-fixed polymers prepared displayed good molecular weights. We found that the polymers exhibit absorption into the the near IR. Solvatochromic study and temperature dependent UV-vis absorption spectroscopy showed that the polymers were already as maximum aggregation in solution as in the solid state. Their absorption profiles did not change significantly with solvent or temperature. Extensive computational analysis of the polymers indicated that the absorption spectra is due to possible dihedral fluctuations possible within the polymers at room temperature. The dihedral angle was also calculated to be much larger than expected, at 12-18^oC, the polymers are not co-

planar and we measured increasingly larger $\pi - \pi$ stacking distance by GIWAXS diffraction. Given that the polymers generally displayed amorphous texture due to the systemic polymer backbone torsional strain, we can conclude that the initial electron mobility of 0.03 $cm^2V^{-1}s^{-1}$ observed in polymer P5 is a result of the change in the more edge-on polymer orientation on the substrate as measured by the GIWAXS diffraction. The next steps would be to examine how the electron mobility can be improved through control of the polymer solid state morphology or otherwise.

Chapter 4

Changing Alkyl Chain Density in Conformationally-Fixed Polymers

4.1 Motivations and Objectives

Having established the superiority of the naphthalene homopolymer over the phenyl homopolymers or phenyl-naphthalene polymers, additional methods of controlling their $\pi - \pi$ stacking distance were investigated. Closer $\pi - \pi$ stacking distance between polymers is a well established method of increasing crystalline texture of organic semiconducting polymers in the solid state.[163] Side-chain engineering, introducing linear chains rather than branched alkyl chains can facilitate $\pi - \pi$ stacking between polymers.

Although side-chains are crucial for solubilising polymers, they can also be important for the spatial arrangement of the polymer lamellar in the solid state. Side-chains fall into six broad categories: alkyl side-chains; hybrid side-chains, where the side chain is attached to the polymer backbone by a functional group; ionic side-chains; oligoether side-chains; fluoroalkyl side-chains and latent reactive side-chains. Within alkyl chains, the side-groups can of course be either branched or linear. For linear side-chains, there is an odd-even number effect, although this phenomenon is not confirmed in conjugated polymers, linear chains can promote interchain interdigitation in polymers.[45,164,165]

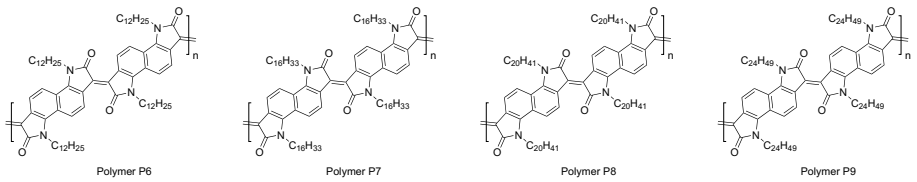

Figure 4.1: A series of naphthalene homopolymers synthesised with linear alkyl side-chains.

Linear side-chains promote self-assembly due to larger local free-volume between adjacent chains, consequently they are less efficient solubilising groups. In branched alkyl side-groups, moving the branching point away from the polymer spine balances the issue of solubilising the polymer and promoting self-assembly.[106,107] When the branching point was moved from carbon-2 to carbon-7 position, Kim *et al.* observed 3-10 fold increases in the hole mobility of DPP-thiophene-selenophene polymers depending on the dielectric material and the post-deposition processing condition.[166] X-ray diffraction of these polymers showed enhanced crystallinity and edge-on packing upon moving the branching point further away from the polymer backbone.

To promote self-aggregation in these conformationally-fixed polymers and thus elicit smaller $\pi-\pi$ distance, naphthalene homopolymers were synthesised with just linear chains. In Chapter 3, improved transport properties was observed when the alkyl chain density was reduced between P4 and P5 and by extending the aromatic core from P1 to P5. The reduction in alkyl chain volume between P4 and P5 resulted in more edge-on packing. By introducing linear alkyl chains, we aimed to promote edge-on polymer orientation on the substrate. This property is likely to affect numerous aspects of the polymers such as the extent of delocalisation of electron density on the aromatic core along the polymer backbone and the interplay between solubility and molecular weight. A decrease in $\pi - \pi$ distance would expedite edge-on packing.[166]

4.2 Results and Discussion

4.2.1 Monomer Synthesis

The monomers synthesised here were made by alkylating naphthalene bisisatin core with various alkyl bromides to obtain the desired monomer. Each alkylation reaction and bisisatin monomer

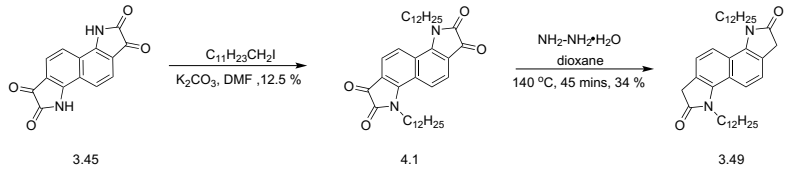

Figure 4.2: Reaction scheme for synthesis of C12 naphthalene bisisatin and bisoxindole monomers.

presented a unique set of challenges due to the physical properties associated with the alkyl side-chains. Each set of synthesis began with the synthesis of the naphthalene bisisatin core *via* the Martinet isatin synthesis. For C12 naphthalene bisisatin, the naphthalene core was alkylated with 1-iododododecane in DMF with potassium carbonate to generate the bisisatin. The C12 naphthalene bisisatin was soluble enough to undergo initial purification by column chromatography with chloroform as eluent. Many impurities were removed from the crude material during the first column, which then enabled the C12 naphthalene bisisatin to be recrystallised easily from a hexane solution. Isolation of this bisisatin monomer was considerably easier than for branched chain bisisatin monomers because it could be purified readily from a hexane solution after one flash column chromatography.

The synthesis of naphthalene bisisatin monomers was complicated by the fact that the desired bisisatin is obtained at low yields. It was proposed that the side-product was the an singly alkylated naphthalene bisisatin due to incomplete cyclisation of the reaction intermediate during the Martinet isatin synthesis. The side-product in the alkylation reaction was isolated at 50 % yield whilst the C12 naphthalene bisisatin monomer was obtained at 12.5 % yield. They closely elute together on a column in multiple solvent mixtures. The side-product is a brown-purple solid that dissolves in chlorinated solvents to give a light purple solution. This side-product was isolated and characterised using multiple techniques to elucidate its structure.

Figure 4.3 shows the IR absorption spectra of the C12 naphthalene bisisatin (top) and the side-product (bottom). There are clear differences between the two spectra, notably the the presence of multiple carbonyl stretches in the side-product at 1700 cm^{-1} and 1650 cm^{-1} compared to the single carbonyl peak at around 1700 cm^{-1} in C12 naphthalene bisisatin. Also, there are two weak peaks at around 3450 cm^{-1} and 3350 cm^{-1} likely due from N-H stretch in the side-product,

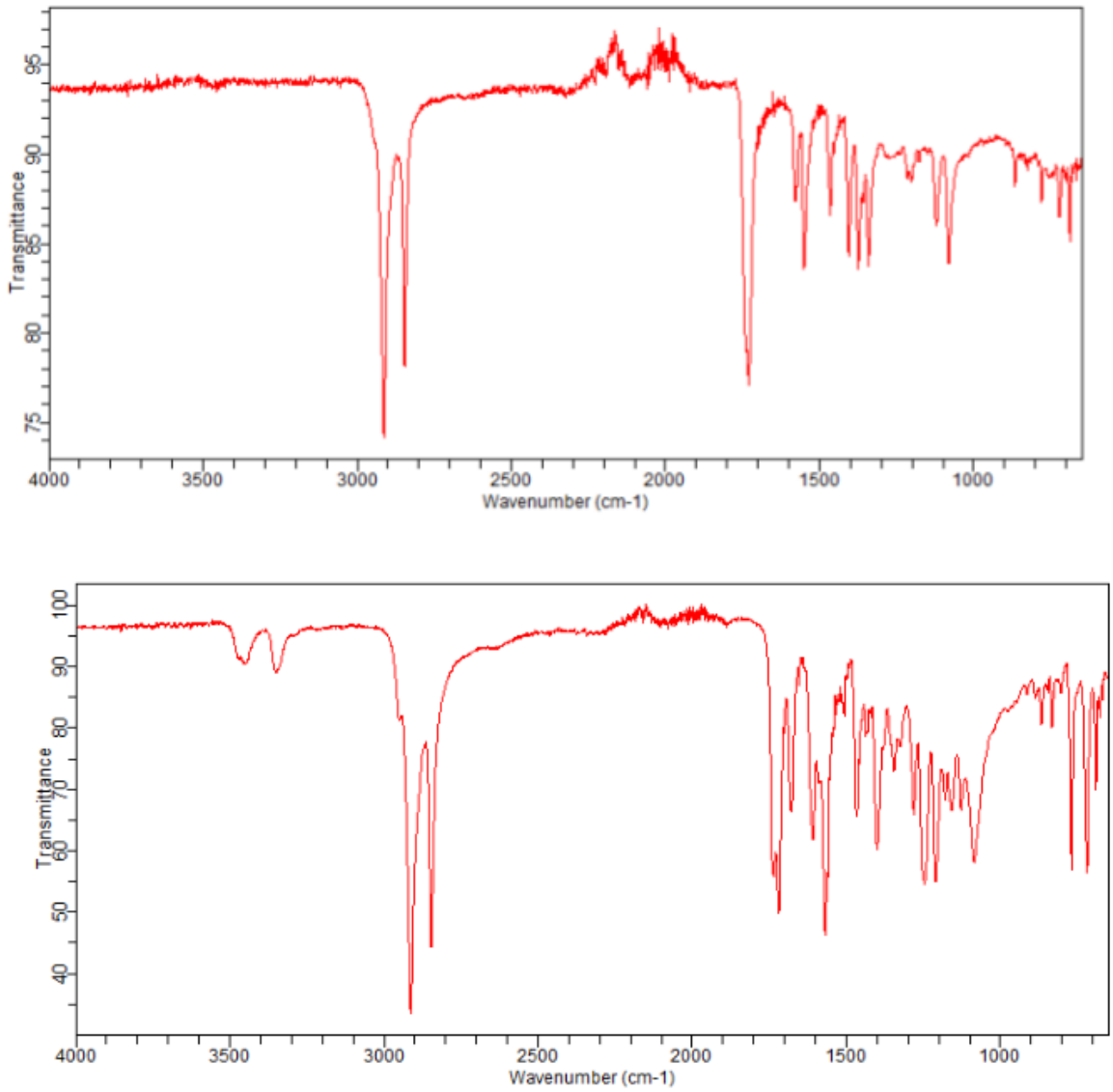

Figure 4.3: IR spectra of C12 naphthalene bisisatin (above) and its side-product (below).

although, they could also be overtones from the carbonyl peaks.

Analysis of the proton NMR spectra makes it possible to identify the structure. There are four aromatic signals in the side-product H^1 NMR spectrum, Figure 4.4. The aromatic signals B and C, resembling a quartet, are actually two doublet signals within similar chemical environments. The protons responsible for this two signals are identified in the structures in figure 4.5. Along with these doublets the other aromatic signals A and D are assigned to the protons H_A and H_D as shown in Figure 4.5. The four aromatic signals allows enabled confirmation of the substituted naphthalene structure 4.2 in Figure 4.5.

Next, the two triplets at 4.33 ppm (signal F) and 4.15 ppm (signal G) are due to the methylene hydrogen atoms from the dodecyl groups bonded to nitrogen atoms that are in two different chemical environments. The NCH_2 is responsible for signal F at 4.33 ppm, whilst NHCH_2 is responsible for signal G at 4.15 ppm. The multiplets at 1.80, 1.40 and 1.32 ppm are from the other methylene groups in the dodecyl chains attached to the nitrogen atoms.

Given that a C12 alkyl chain is attached to both nitrogen atoms in the molecule, structure 4.3 in Figure 4.5 was confirmed. The dashed lines represent unknown substituents on the molecule that are yet to be elucidated. If the broad singlet at 6.90 ppm is from an amine hydrogen, then this is cogent with the IR absorptions at 3450 cm^{-1} or 3350 cm^{-1} corresponding to a secondary amine stretch. As secondary amines only produce one stretching absorption band, one of the peaks could be an overtone band. The broad singlet at 6.90 ppm may be confused for an aromatic signal, but the COSY spectrum shows that it does not interact with any other protons, which supports it being an amine hydrogen atom. This also gives a reason for the alkyl chains to be in different chemical environments. After assigning all these signals, it is clear one proton position is unobserved in the NMR spectrum and this is because the proton had been substituted by a bromine atom. The mass spectroscopy data supports structure 4.4 in Figure 4.5 as the side-product. Rather than navigate the synthetic route to achieve the bisoxindole via the Heck-type palladium catalysed cyclisation. The C12 naphthalene bisisatin was reduced by Wolf-Kishner reduction to furnish C12 naphthalene bisoxindole, structure 3.49, Figure 4.6. Other strategies were attempted to carry out the cyclisation. Wudl et al. achieved this cyclisation in Friedel

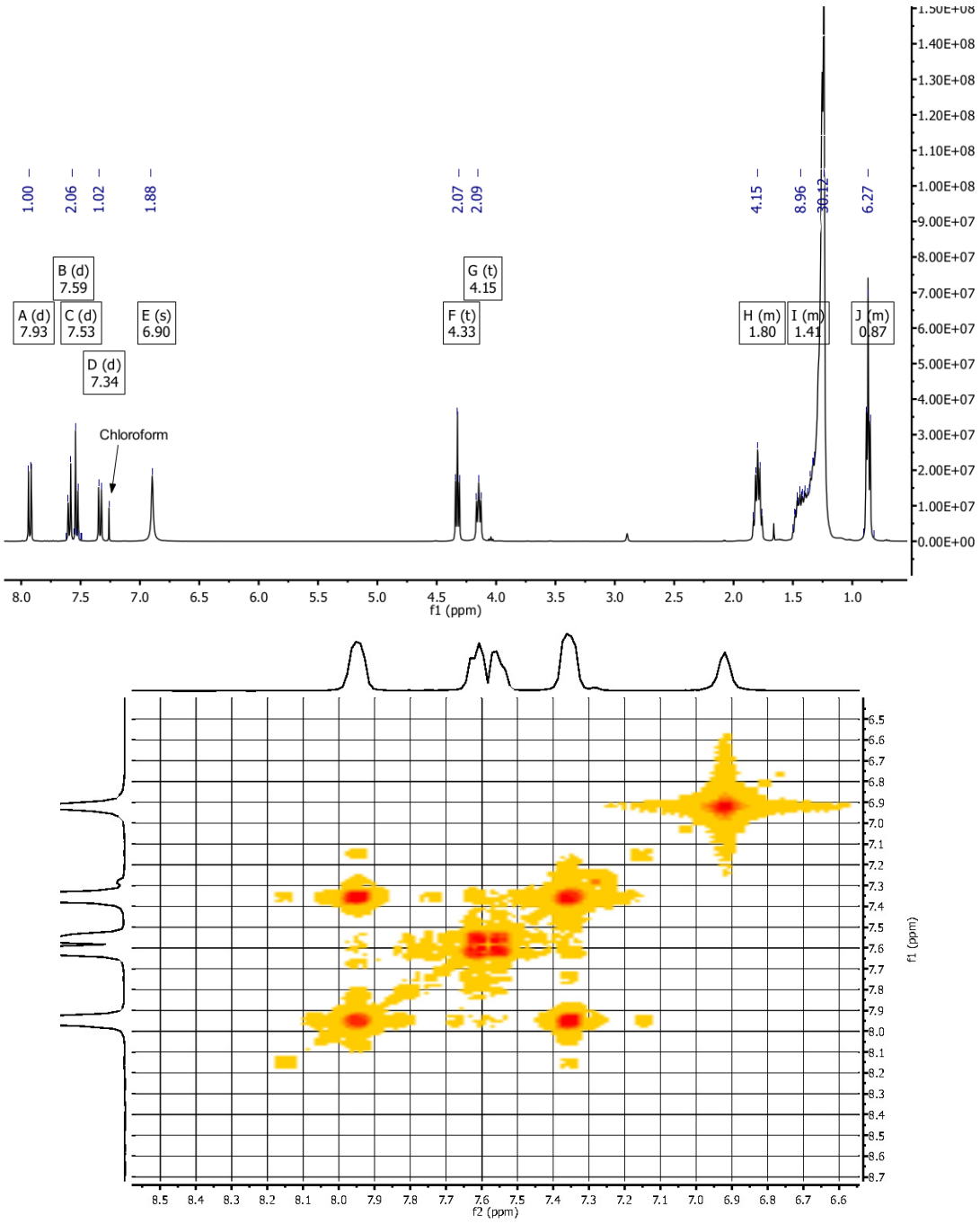

Figure 4.4: Proton NMR and COSY spectrum of C12 naphthalene bisisatin alkylation reaction side-product.

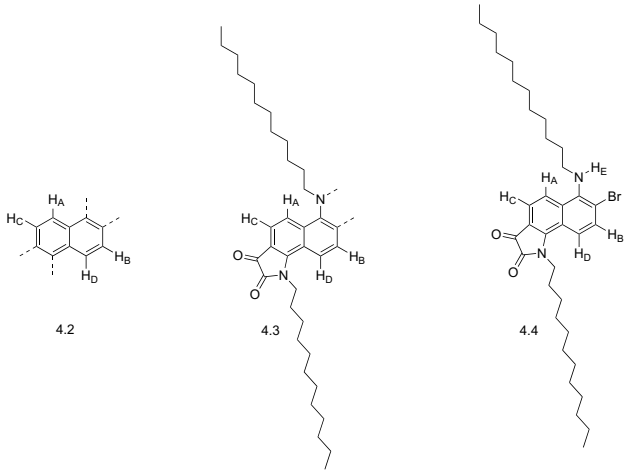

Figure 4.5: Structures 4.2 and 4.3 were identified in the process of determining the naphthalene bisisatin core alkylation side-product (structure 4.4).

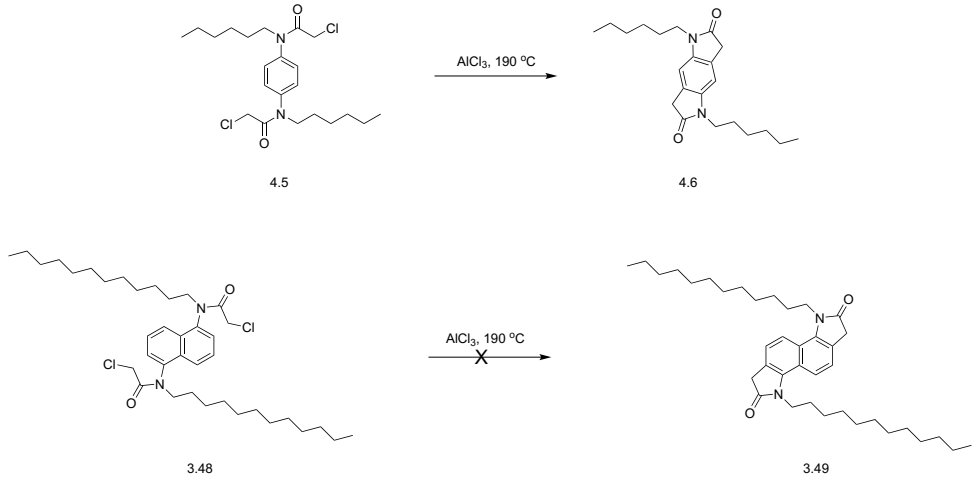

Figure 4.6: Cyclisation of phenyl bis-acetemide (structure 4.5) progressed well in molten $AlCl_3$, however, the corresponding naphthalene monomer decomposed in molten $AlCl_3$ and no reaction occurred when the reaction was conducted in solution.

Crafts alkylation reaction of N,N'-(1,4-phenyl)bis(2-chloro-N-hexylacetamide) in neat $AlCl_3$ at 190 ^oC.[145] The molten $AlCl_3$ activates the halogen carbon bond, enabling nucleophilic aromatic substitution of the halogen. Elimination of the hydrogen atom on the resulting intermediate generates the cyclised product. Although, this reaction proceeded excellently in a test reaction with phenylchloroacetamide 4.5 (Figure 4.6), it failed in the corresponding naphthalene starting material. Naphthalene bisacetamide decomposed when heated in neat $AlCl_3$ due to the more electron rich nature of naphthalene compared to benzene. Less harsh reaction conditions such as heating in solvent only resulted in the recovery of the starting material. Consequently, the Wolff-Kishner reduction[167,168] was conducted on the naphthalene bisisatin monomers. Wolff-

Kisnher reduction involves nucleophilic attack of hydrazine hydrate to a carbonyl group to give a hydrazone intermediate. Reduction of this hydrazone, releases nitrogen and furnishes the desired methylene group and therefore bisoxindole. When the naphthalene bisisatin monomers were subjected to this procedure, the hydrazone intermediate evidently formed as a bright yellow intermediate that lacked methylene proton signals in the proton NMR. However upon addition of potassium hydroxide, the intermediate polymerises, turning green then forming a black clump.

Therefore, in order to generate the bisoxindole, base was eliminated from the reaction procedure and elevated reaction temperatures were used to thermally extrude nitrogen gas. The reactions were carried out in a high pressure vessel that can achieve 240 ^oC. Solvent mixtures of diethylene glycol and dioxane were used to achieve these high temperatures safely. Diethylene gylcol was also beneficial in dissolving the monomers to enable effective solvation of molecules in the reaction.

For the next set of monomers, naphthalene bisisatin core was alkylated with 1-iodohexadacane in DMF and potassium carbonate. And to obtain the corresponding bisoxindole comonomer, the C16 naphthalene bisisatin was reduced in 1,4-dioxane and diethylene glycol. The reaction mixture was purified to give C16 naphthalene bisoxindole at 45 % yield. For the C20 naphthalene bisisatin, the naphthalene bisisatin core was alkylated with 1-iodoicosane and the resulting bisisatin reduced to give the bisoxindole monomer. Here, the concentration of the alkylation reaction was halved because 1-iodoicosane is a waxy solid at room temperature and consequently required larger volume of solvent to dissolve and dilute the reaction. The purification of the C20 naphthalene bisisatin monomer was particularly difficult because although the product crystallised out readily from a dichloromethane solution, the side-product, as identified previously, also crystallised out with it. Multiple long columns in chloroform were run before the naphthaleneicosyl bisisatin was separated from the side-product. Even running the monomer through preparative GPC in chloroform did not separate the products. Two overlapping peaks corresponding to the two products were observed in the first purification cycle, but these coalesced during the second cycle.

Again the C20 naphthalene bisisatin was reduced in 1,4-dioxane and diethylene glycol and hydrazine hydrate to furnish the corresponding bisoxindole. The bisoxindole was simply purified by flash chromatography with toluene as the eluent. Finally, the naphthalene bisisatin core was alkylated with 1-iodotetracosane. Similarly to the C20 naphthalene bisisatin, purification of this monomer required multiple columns. Visually, it is clear these monomers aggregated a great deal more than the C8C10 naphthalene bisisatin or even C12 naphthalene bisisatin because they presented as shiny lilac powder in the solid state rather than a blue powder. The C24 naphthalene bisisatin was reduced *via* Wolff-Kishner reduction to give C24 naphthalene bisoxindole.

4.2.2 Polymer Synthesis

The C12 naphthalene bisisatin (compound 4.1 Figure 4.2) and C12 naphthalene bisoxindole (structure 3.49) were polymerised in toluene with *p*-toluene sulfonic acid to give C12 naphthalene homopolymer P6. The polymerisation reaction lasted 10 minutes and within that time, the polymer precipitated out of the reaction medium. Although the polymer precipitate was extracted from chlorobenzene during Soxhlet, it was highly insoluble and impractical to work with. It was not possible to redissolve the isolated polymer even in boiling hot chlorobenzene. Since the polymer was insoluble in hot chlorobenzene it was not used further. Again the polymerisation time for the C16 naphthalene homopolymer was short, with the polymer precipitating out of the reaction after 10 minutes of reaction. On the second polymerisation attempt, a processable polymer although still poorly soluble was isolated after 7 minutes reaction time.

The polymerisation to give the C20 naphthalene homopolymer P8 was halted after 10 minutes at 120 ^oC by rapidly cooling the reaction in a water bath at room temperature. This prevented further polymerisation as *p*-toluene sulfonic acid is insoluble in toluene at room temperature. The polymer was extracted by Soxhlet in toluene. It displayed greater solubility than C16 naphthalene homopolymer. The polymerisation of C20 naphthalene bisisatin and its corresponding bisoxindole proceeded similarly. This C24 naphthalene homopolymer P9 had superior solubility to the C12 naphthalene homopolymer, as expected, being readily soluble in hot chlorobenzene.

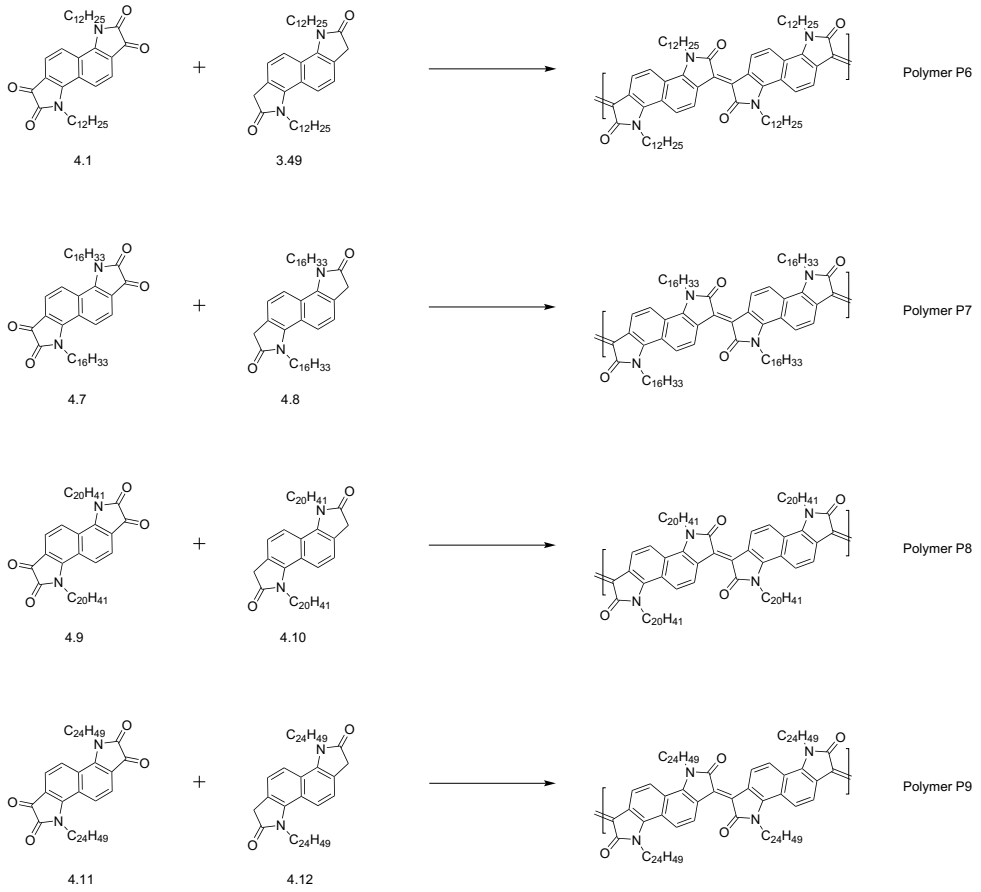

Figure 4.7: Reaction schemes for the synthesis of polymers P6 to P9 *via* *p*-toluenesulfonic acid catalysed aldol polymerisation.

Table 4.1: Summary of optoelectronic and physical properties of polymers P6 to P9.

Polymer	Mn (kDa)	Mw (kDa)	PDI	long $\lambda^{[a]}$ /nm	$E_{opt}^{[b]}$	$IP^{[c]}$ /eV	$EA^{[d]}$ /eV
P6	-	-	-	-	-	-	-
P7	27.2	38.6	1.56	500, 860	1.00	-5.24	-4.24
P8	20.9	29.6	1.42	506, 866	0.97	-5.30	-4.33
P9	11.5	16.0	1.39	496, 840	1.02	-5.31	-4.29

[a] Thin films were spin-coated onto glass substrates from chlorobenzene solution, λ is the peak of the low energy absorption band of the polymers. [b] Estimated optical gap was calculated using onset of the thin-film absorption spectra ($E_{opt} = 1240/\lambda_{onset}$). [c] IP was measured by PESA. [d] EA was estimated by addition of the UV-vis absorption onset to IP ($EA = IP - E_{opt}$), a protocol that neglects the exciton binding energy.

4.2.3 Polymer Characterisation

The improved solubility is likely a combination of the shorter polymer length and the longer alkyl chain. The polymers are short with their Mn decreasing as the length of the linear chain increased. This is likely a function of the reaction time length, acid concentration and polymer *in situ* solubility profile.

Figure 4.8 shows that the thin-film absorption spectra of all the polymers have two absorption bands similar to P5, Band I at at around 500 nm and Band II 850 nm, although the UV-vis spectra of these polymers are broader than P5. A greater propensity to aggregate due to the linear chains on the polymer promotes the electron transitions that culminate in greater full-width-half maxima in this series of polymers compared to P5. There was no significant deviations in the absorption maxima due to the changing alkyl chain length.

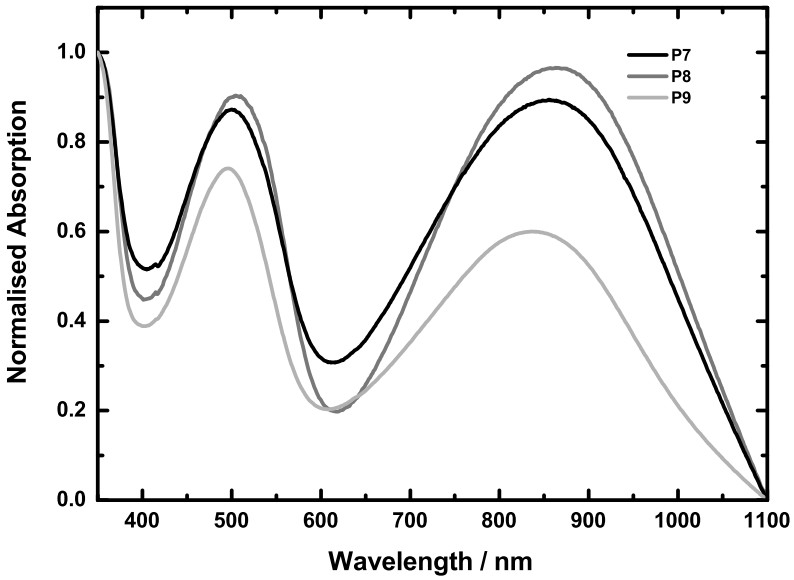

Figure 4.8: Normalised UV-vis absorption spectra of polymers P7 - P9 in chlorobenzene.

4.2.4 Charge Transport Properties

These polymers were fabricated into TGBC transistor devices and tested for charge transporting properties. Figure 4.9 shows transfer curves (top) for C16 naphthalene and C20 naphthalene and C24 naphthalene homopolymer with their mobility curves (bottom). The black curves show the current variation with the gate voltage at 5 V_D and the red curves correspond to 60 V_D. At 60 V_D the polymers show both electron and hole transport whilst there is only electron transport at V_D = 5V. A maximum electron mobility of 0.0006 cm^2V^{-1} was recorded for C16 naphthalene homopolymer for V_D = 5 V and 60 V. A higher hole mobility of approximately 0.0011 cm^2V^{-1} was measured for C16 naphthalene homopolymer at V_D = 60 V .

C20 and C24 naphthalene homopolymer had the same electron mobility of 0.006 cm^2V^{-1} at V_D = 5 V and 60 V. Again the hole mobility of both polymers were marginally higher than the electron mobility. There was an order of magnitude increase in electron mobility from P7 to P8 then the electron mobility plateaued. The lower than expected charge mobilities of these polymers were attributed to difficulties with processing the polymers within a narrow window in which they are dissolved in hot chlorobenzene.

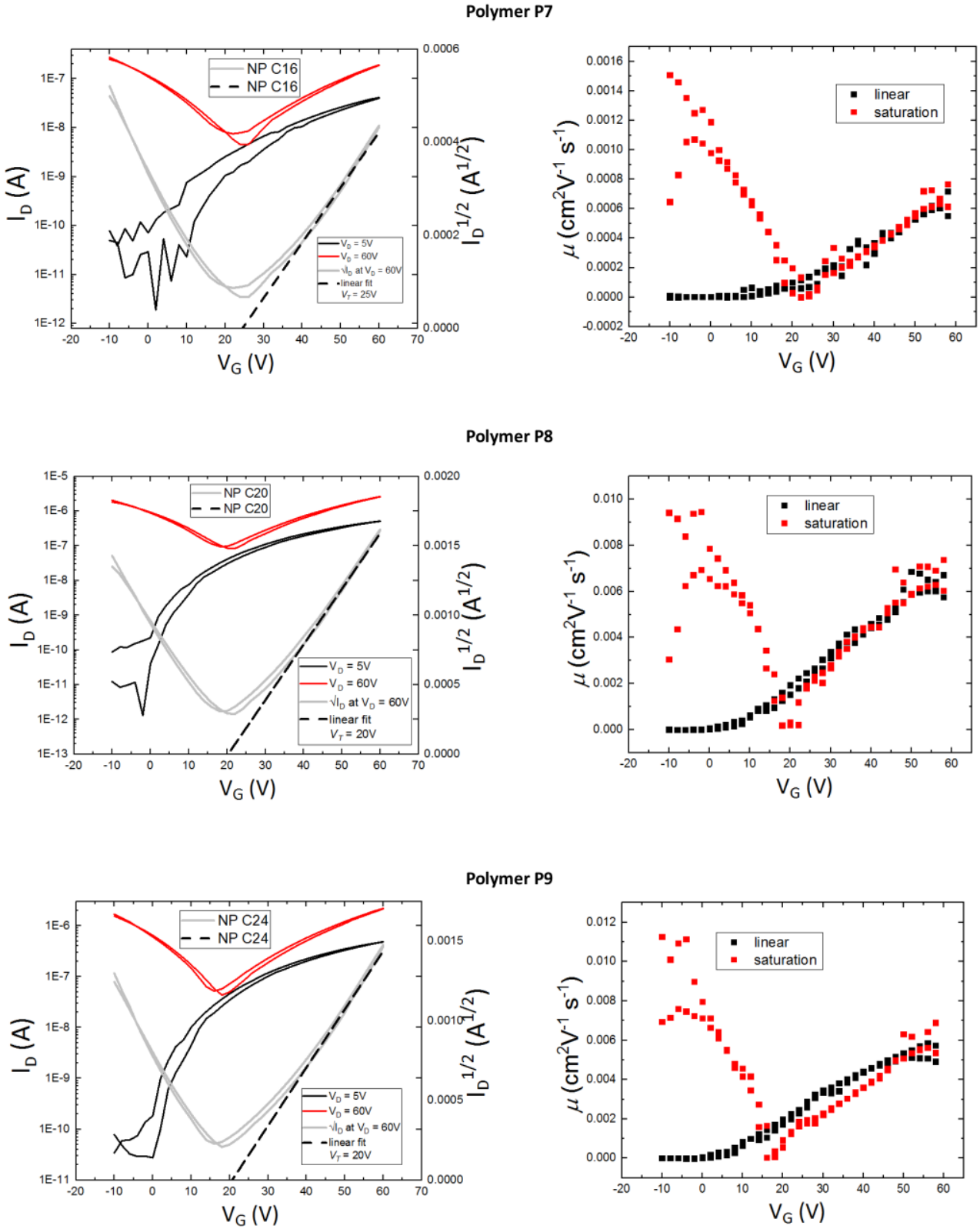

Figure 4.9: Transfer curves and mobility gate voltage curves for polymers P7 (C16 naphthalene polymer), P8 (C20 naphthalene polymer) and polymer P9 (C24 naphthalene) homopolymers.

4.3 Conclusion

Having found that increased conjugation length and reduced alkyl chain density promoted edge-on texture in polymer P5 and subsequently good electron charge transport, we probed the effect of linear alkyl chains on charge transport in on naphthalene spine conformationally-fixed polymers. We synthesised a series of conformationally fixed polymers of naphthalene backbone and systematically increased from 12 to 24 carbon atoms by adding 4 carbon atoms to the preceding polymer. Progressively increasing the length of the alkyl chains served to improve the solubility of the polymer, however there were still considerable processing difficulties that influenced the observed charge mobilities. Both icosyl naphthalene and tetracosyl naphthalene homopolymers achieved maximum electron mobility of 0.006 cm^2V^{-1}, ten times higher than hexadecyl naphthalene polymer electron mobility. The short polymer lengths may also account for lower observed mobility. The tails of long polymers can act are links between the crystalline domains to enable fast charge transfer between crystallites in a film. Although, we demonstrated in the Chapter 3 that mobility of these polymers increased proportionally with the polymer length, it is impractical to further extended the length of these polymers due to solubility issues and working with longer solublising side chain would be synthetically challenging and more importantly the alkyl length can also be detrimental to transport by increasing lamellar packing distance.

Chapter 5

Effect of Dihedral Angle on Conformationally-Fixed Polymer Charge Transport

5.1 Motivations and Objectives

DFT calculations of naphthalene-based conformationally-fixed polymers suggested that the polymers exhibit a torsional strain of 18^o between each monomer. The carbon-carbon double bonds between the monomers force the ortho-hydrogen and the oxygen atom within the same spatial area resulting in steric repulsion. As the electronic repulsion between the two groups is lowest at 18^o dihedral angle, adjacent monomers are not coplanar along the polymer backbone. Subsequently, the polymer strands are less able to arrange into short or long range order suitable for charge transport.

The morphology of organic semiconducting polymers is designed into polymers at the molecular level and therefore reducing the dihedral angles between adjacent monomers in our polymers can be achieved through effective molecular design. A strategy to achieving a near zero dihedral angle is to substitute adjacent six-membered aromatic cycles with five-membered rings.

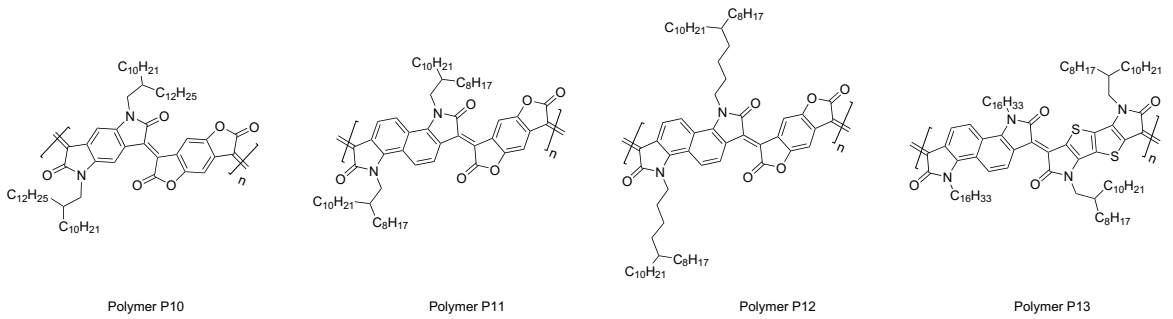

Figure 5.1: Conformational polymers based on phenyl bislactone and thienothiophene bisisatin.

Multiple examples in literature report the introduction of five-membered rings, or spacer units between monomers to enhance morphology and charge transport mobility.[45] In the case of these aldol polymers, five-membered bisisatin monomers are required to lower the dihedral angle. Thiophene is a common planarising copolymerisation moiety in polymers for organic semiconductors. As a five-membered ring it inherently benefits from smaller dihedral angles between its monomers. Furthermore, the thiophene sulfur atom can form short contacts with oxygen to further rigidify and planarise polymers.[44,82] When unalkylated, thiophene as a co-monomer can also facilitate closer polymer strand packing because it allows for an empty space for molecular docking of polymer sections with larger alkyl chain density.[106] Consequently, thiophene is a credible five-membered bisisatin monomer for completely coplanar aldol conformationally-fixed polymers.

Nonetheless, a thiophene bisisatin is an inappropriate monomer because of the curvature of the monomer and the curvature it would introduce to the polymer.[103,106] Pei *et al.* found that anti-centrosymmetrical polymers, an inferred property from the symmetry of the monomers, significantly lowered charge transport properties. To mitigate this, a thienothiophene bisisatin monomer was synthesised. We also explored increasing the degree of polymer coplanarity by introducing non-alkylated, bislactone-based monomers into the polymers. Phenyl bislactone (compound 5.2, Figure 5.2) is a likely candidate because it has been successfully utilised in a number of small isoindigo molecules that exhibited excellent n-transport mobility.[169] Phenyl bislactone-based conformationally-fixed polymers would still have 12^o dihedral angles, however it would not have any side-chains to inhibit close packing of the polymers. In this chapter, three phenyl bislactone copolymers were synthesised in addition to a polymer with thienothio-

phene bisisatin monomer. The optical absorption spectra of these polymers and their transistor behaviour were measured.

5.2 Results and Discussion

5.2.1 Monomer Synthesis

A number of the monomers used in synthesising the polymers discussed in this chapter had been previously utilised in other chapters of this thesis. The C12 phenyl bisisatin monomer was used from a batch synthesised for the study in Chapter 2. The naphthalene C8C10 bisisatin was also taken from the batch in Chapter 2. And the C16 naphthalene bisoxindole monomer was prepared by alkylating naphthalene bisisatin core with 1-bromohexadecane and subjecting the bisisatin to a Wolff-Kishner reduction as described previously. Three new monomers, phenyl bislactone (compound 5.2 in Figure 5.2), an extended C8C10 naphthalene monomer and thienothiophene bisisatin were synthesised to make the polymers reported here. Further details regarding the synthesis are outlined in the Experimental. Phenyl bislactone was synthesised and purified in high yield in a simple one step reaction by refluxing phenylenediacetic acid (compound 5.1 in Figure 5.2) at 100 ^oC in toluene with excess acetic anhydride. It was purified by a pouring it through a short silica plug in toluene to be isolated in high yield of 75 %.

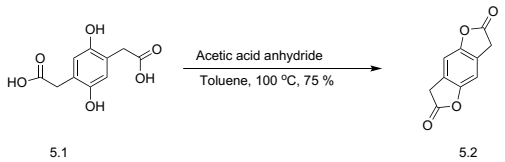

Figure 5.2: Reaction scheme for phenyl bislactone (3,7-dihydrobenzo[1,2-*b*:4,5-*b*']difuran-2,6-dione).

The difficult synthesis of thienothiophene bisisatin begins with bromination of thieno[3,2-*b*]thiophene. Dr. Hung-Yang Chen first conducted this whole synthesis as outlined in Figure 5.3 and further material was later synthesised by Dr Balaji Purushothaman. The bromination was achieved by first lithiating thieno[3,2-*b*]thiophene using *n*BuLi in THF at -78 ^oC.

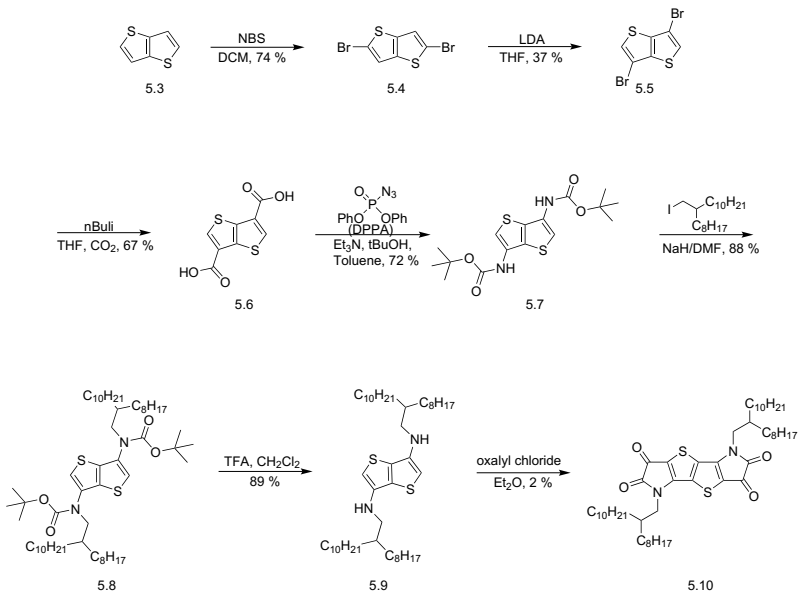

Figure 5.3: Synthetic route to thieno[3,2-*b*]thiophene bisisatin.

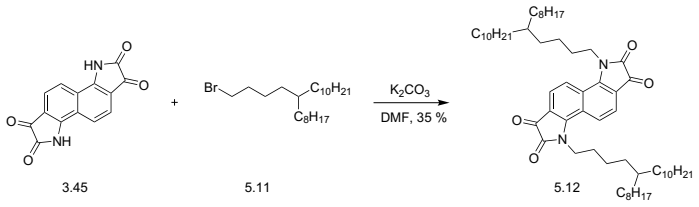

Figure 5.4: Reaction scheme for the alkylation of naphthalene bisisatin core to give extended branching point alkylated naphthalene bisisatin.

N-Bromosuccinamide (NBS) was then added to the reaction mixture to quench the lithiated species to furnish 2,5-dibromo thienothiophene. The lithiation occurs at carbon-2 and 5 position in thieno[3,2-*b*]thiophene as these are the most acidic protons on the molecule. The dibromide intermediate 5.4 was isolated and purified prior to the halogen dance. A halogen dance was initiated by dissolving 2,5-dibromo thienothiophene in THF and adding lithium aluminium amide (LDA) and allowing the reaction temperature to increase to room temperature over 16 hours. During which time successive halogen migration locates the bromine atoms to positions 3 and 4 on thieno[3,2-*b*]thiophene. The white crystalline powder (compound 5.5) was more stable than its precursor and could therefore be stored for longer. An aromatic nucleophilic substitution then takes place with carbon dioxide to furnish dicarboxcylic acid 5.6. Thieno[3,2-*b*]thiophene dicarboxylic acid was then protected as a Boc group by dissolving it in toluene, and adding ethylenediaminetetraacetic acid (EDPA) to the solution. The use of a Boc group circumvents the synthesis and isolation of highly electron rich primary amine of

thieno[3,2-*b*]thiophene. The Boc group reduces the electron density in the intermediate stabilising the intermediate sufficiently for further reactions. Once isolated, Dr Chen found that the thieno[3,2-*b*]thiophene secondary amines rapidly decomposed even when stored at $-4\ ^oC$. The Boc intermediate 5.7 in Figure 5.3 was alkylated in DMF with NaH to deprotonate the amide. After alkylation, the Boc groups were deprotected to expose the amines and enable the immediate cyclisation of compound 5.9, Figure 5.3, in diethyl ether and oxalyl chloride to furnish thienothiophene bisisatin. One-sided cyclisation of similar monomers have been reported in the presence of oxalyl chloride and triethyl amine however Dr Chen found this condition too harsh for the bidirectional electron rich system. This compound was first reported in our Nature Communication paper.

5.2.2 Polymer Synthesis

The aldol polymerisation reaction was conducted with C10C12 phenyl bisisatin and phenyl bislactone to give polymer P10. After 16 hours polymerisation at 120 ^oC, chlorobenezene was added to the polymerisation matrix before the polymer was precipitated into methanol. After precipitating the polymer, a Soxhlet extraction of the polymer was conducted in methanol, acetone, hexane, DCM, chloroform, toluene and chlorobenzene. None of these solvents could extract the polymer. Attempts to dissolve the polymer in tetrachloroethane, a highly potent solvent, was also unsuccessful. Evidently, after the polymer had been precipitated into methanol it was impossible to resolvate the polymer strands. Given that the naphthalene-based aldol polymers outperformed phenyl-based polymers, we decided to polymerise the naphthalene bisisatin with phenyl bislactone. We decided to prepare a polymer from C8C10 naphthalene bisisatin and phenyl bislactone. The polymer P11 was visually different to the phenyl bislactone polymer. It was grey and formed fine polymer sheets, compared to deep purple pellets of phenyl bislactone polymer. The polymer was isolated and underwent Soxhlet using acetone, methanol before the polymer was extracted in boiling hexane. Another phenyl bislactone-based polymer was synthesised using a naphthalene bisisatin monomer with the side-chain branching point at C5. This alkyl chain was synthesised in-house over a six step synthetic process pre-

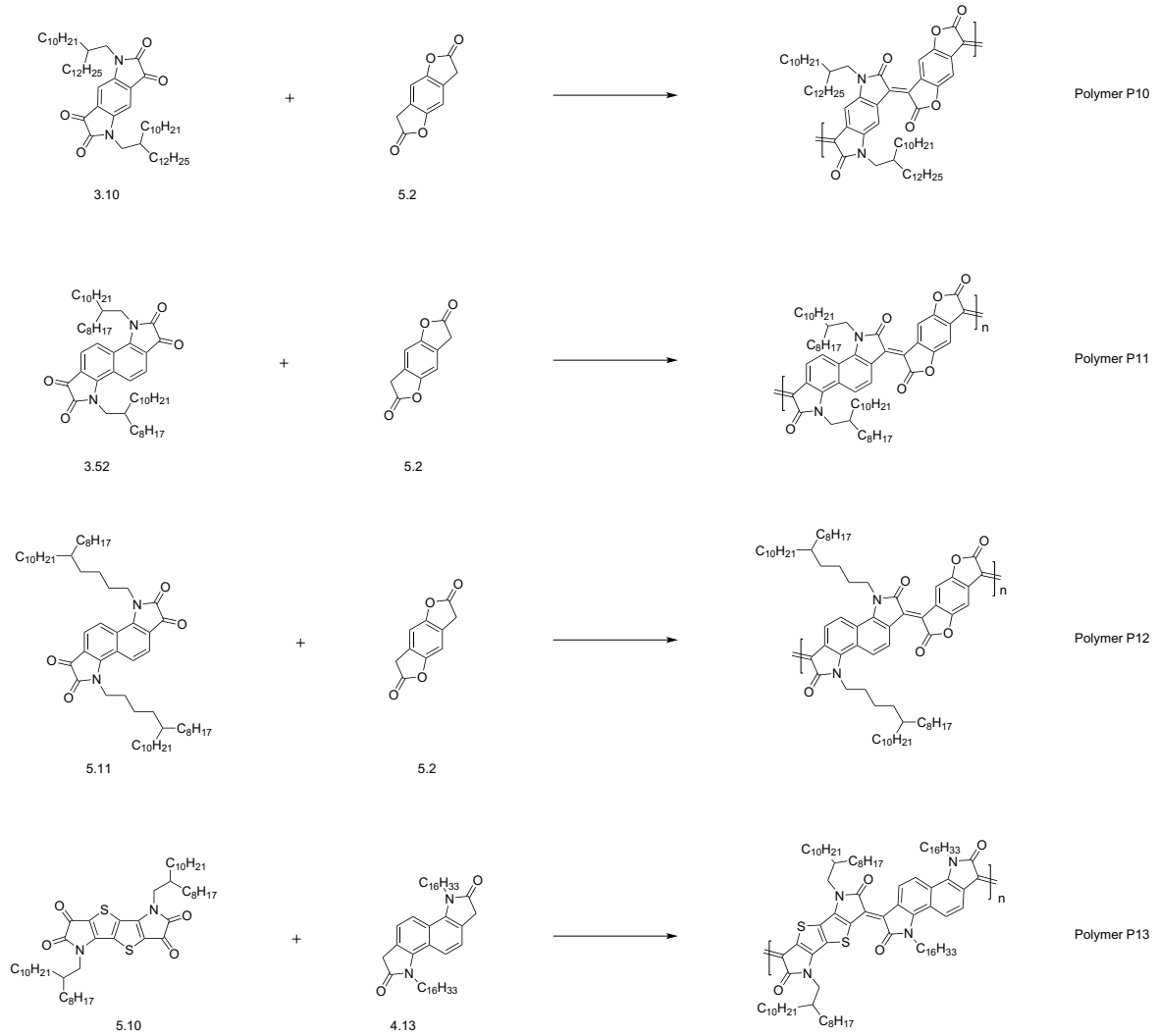

Figure 5.5: Reaction schemes for the synthesis of polymers P10 to 13 *via* *p*-toluene sulfonic acid catalysed aldol polymerisation

Table 5.1: Summary of optoelectronic and physical properties of polymers P10 to P13.

Polymers	Mn (kDa)	Mw (kDa)	PDI	Long $\lambda^{[a]}$	$E_{opt}^{[b]}$	$IP^{[c]}$	$EA^{[d]}$
P10	-	-	-	-	-	-	-
P11	22.1	34.5	1.56	534, 930	0.97	-5.20	-4.23
P12	29.5	49.0	1.66	533, 930	0.95	-5.19	-4.24
P13	8.3	9.0	1.08	548, 1128	0.84	-5.0	-4.16

[a] Thin films were spin-cast on glass substrates from chlorobenzene solution, λ is the peak of the low energy absorption band of the polymers. [b] Estimated optical gap was calculated using onset of the thin-film absorption spectra ($E_{opt} = 1240/\lambda_{onset}$). [c] IP was measured by PESA. [d] EA was estimated by addition of the UV-vis absorption onset to $IP (EA = IP - E_{opt})$, a protocol that neglects the exciton binding energy.

sented in literature.[170] Literature promotes moving the side-chain branching point away from the polymer backbone as a method for obtaining closer polymer aggregation.[106,107]

A polymer of thienothiophene bisisatin with C8C10 side-chains and C16 naphthalene bisoxindole was synthesised. This polymer was polymerised as usual in toluene with p-toluene sulfonic acid. After polymerisation, the polymer matrix was precipitated into methanol and collected in a thimble for Soxhlet. Methanol, acteone, hexane, DCM, chloroform and toluene were used to Soxhlet the polymer. The polymer was extracted in hot toluene and concentrated before the polymer was finally precipitated in methanol, filtered and dried.

5.2.3 Polymer Characterisation

These polymers are generally short, particularly polymer P13 that is only soluble in hot chlorobenzene and easily precipitates out of solution. For the phenyl bislactone containing polymers, P11 and P12, during the polymerisation reactions, we observed crystals on the reaction vial that resembled the phenyl bislactone monomer. If a portion of the monomer was undissolved during the polymerisation reaction, then an imbalance of the Carothers' equation dictates that much shorter polymers would be obtained. As charge mobility of conformationally-fixed polymers scaled with molecular weight, improving the molecular weight of these polymers may also increase the charge transport by orders of magnitudes. The UV-vis absorption spectrum of the polymers, Figure 5.5, display the two absorption band characteristics of the aldol polymers. However, here the low wavelength absorption band is the predominate absorption

band. Furthermore, the absorption extends well into the infrared region with λ_{max} at approximately 1100 nm. In polymer P13, the low energy absorption band is likely the prevalent transition because of the planarising effect of the thienothiophene bisisatin monomer in the polymer.

5.2.4 Optoelectronic Properties

Polymer P12, like P11, showed ambipolar charge transport. Figure 5.7, left, gives the transfer curve and right, the mobility relationship with the gate voltage. Interestingly, the threshold voltage varies depending on the source and drain voltage. The electron mobility of P12 steadily increases to about 0.1 $cm^2V^{-1}s^{-1}$ as the gate voltage was made more positive. The maximum hole transport observed was approximately 0.04 $cm^2V^{-1}s^{-1}$. Polymer P13 displayed near balanced ambipolar charge transport. Sweeping the gate voltage positively from -27 V resulted in n-type charge transport and increasing the gate voltage negatively enabled hole transport. A change in the charge carrier was also observed when the gate voltage was made more positive from approximately 27 V compared to making it more negative, Figure 5.7, right panels. Consequently at zero gate voltage the device is on once there is a potential difference between the source and drain electrodes. Electron charge transport of 0.001 $cm^2V^{-1}s^{-1}$ was achieved for polymer P13 in a TGBC transistor device. Higher mobilities in these polymers may be possible by lengthening the polymer chain. In order to achieve this, the alkyl chain density on the thienothiophene-bisisatin should be increased; as we have observed in the linear chain study, changing the length of linear side-chains does not sufficiently improve polymer solubility. The electron-rich nature of the thienothiophene bisisatin also resulted in less stable electron transport as reported by our collaborator.

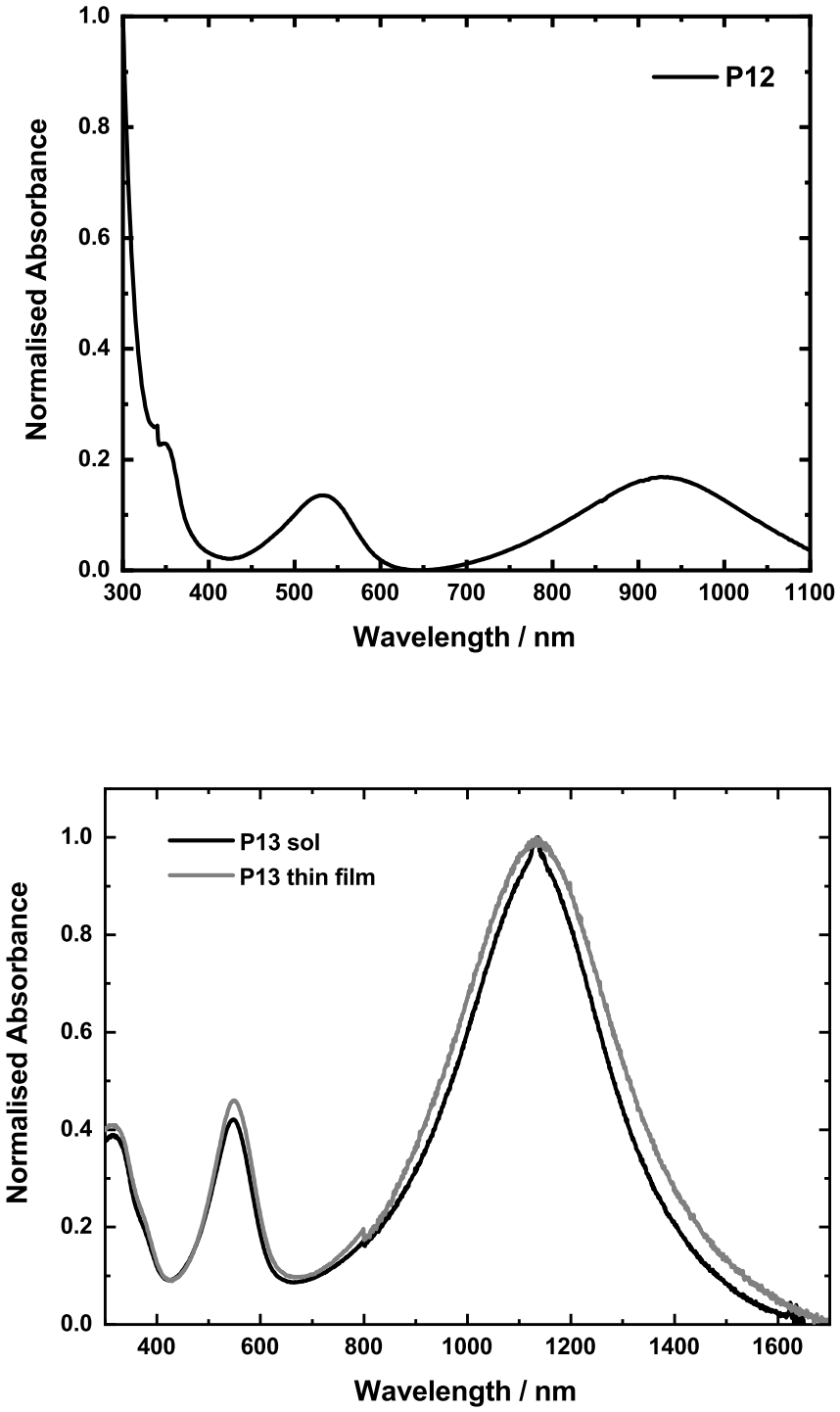

Figure 5.6: UV-vis absorption spectra for polymer P12 (top) and normalised absorption spectra for polymer P13 in chlorobenzene (bottom). The absorption spectra extend well into the near infrared region.

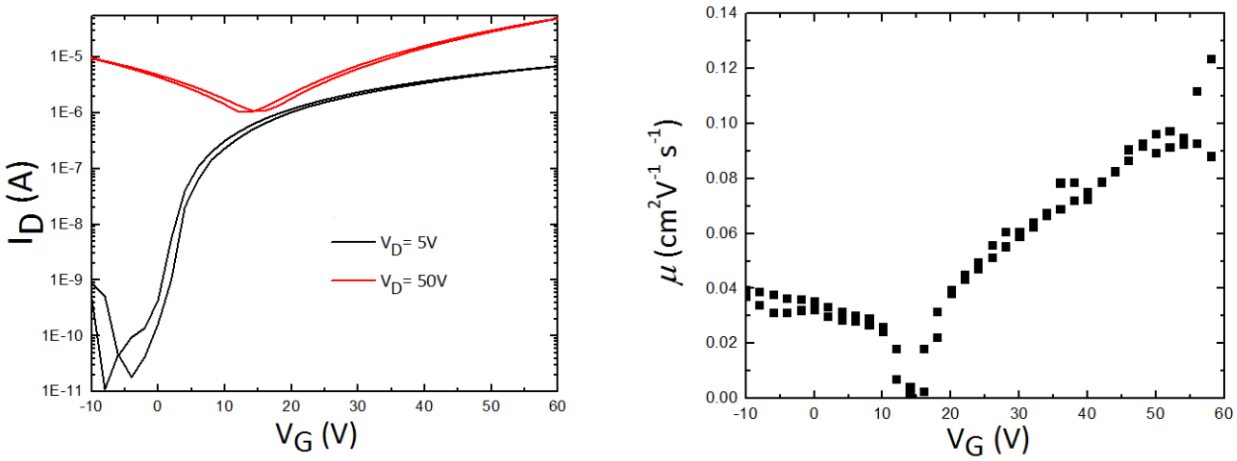

Figure 5.7: Transfer curve (left) and mobility gate-voltage variation (right) for polymer P12.

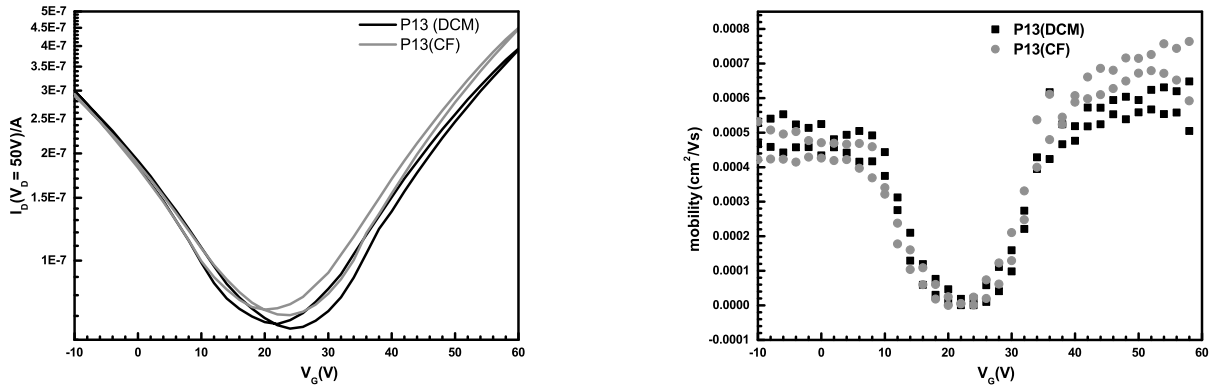

Figure 5.8: Transfer characteristics for batches of polymer P13 obtained from the DCM and chloroform Soxhlet fraction.

5.2.5 X-ray Scattering Pattern

GIWAXS data showed that polymer P13 has strong face-on polymer arrangement relative to silicon substrates. Diffraction from the alkyl chains was also observed. DFT calculations suggest that torsional strain between adjacent naphthalene and thienothiophene bisisatin monomers were part alleviated from the introduction of the 5-membered based bisisatin monomer. $\Omega B97-XD/6-31G(d,p)$ level theory simulations for a thienothiophene-naphthalene conformationally-fixed polymer has a dihedral angle of 0^o between monomer units. Although, this is significantly smaller than for the all naphthalene conformationally-fixed polymers, it didn't translate into higher electron mobility. The short polymer chain length and difficulties in processing the polymer may be responsible for the lower observed charge transport.

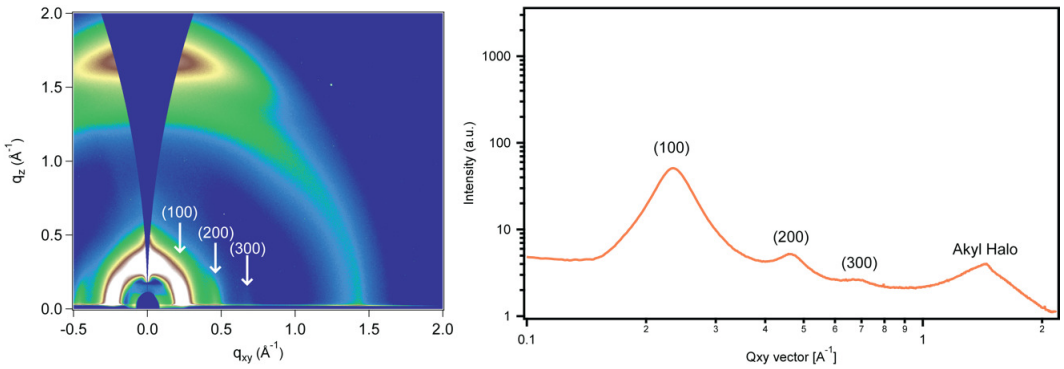

Figure 5.9: Left, a representative 2D-GIWAXS pattern of annealed polymer P13 film displaying strong face-on texture. Right, A horizontal 1D linecut of P13 annealed showing the strong layered ordering (100), (200) and (300) respectively.

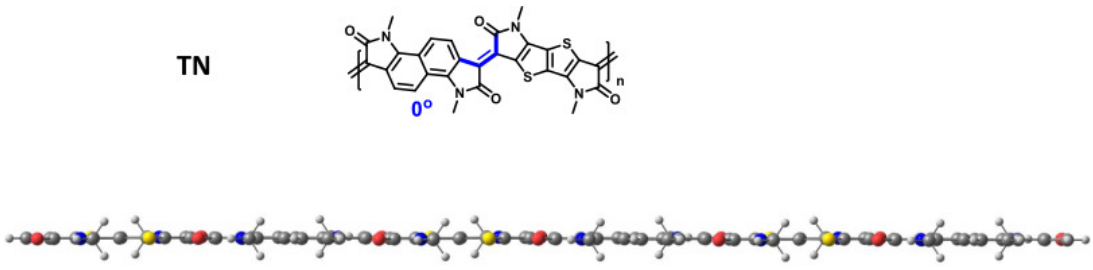

Figure 5.10: DFT calculation of an oligomer of thienothiophene-naphthalene conformationally-fixed polymer calculated at $\omega B97XD/6-31G(d,p)$ level theory simulations, suggesting coplanarity between monomers in the polymer spine.

Other applications such as in photodecting devices were considered for these conformationally-fixed polymers. Photodectors play an important role in technology that require electrical

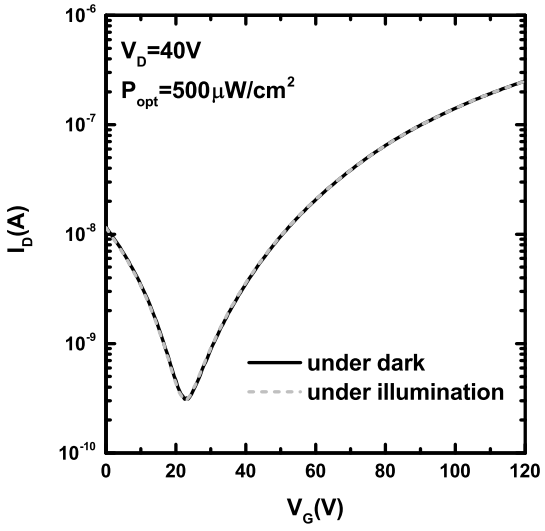

Figure 5.11: Transfer characteristic of photodetector device made from the thienothiophene-naphthalene polymer P13.

responses due to illumination variation such as in biotechnology, telecommunication and atmospheric studies. There are two general device operation modes for photodetectors. In the case of organic semiconductors, photodetectors operate by interband mechanism. Photons with energy greater than the material bandgap generate electron-hole pairs in the semiconducting material. When the material is already under bias, it experiences increased current flow due to excess charge carriers from the illumination. A photodector device made from polymer P13 did not display photo-sensitive current variation, Figure 5.10. The current through the device remained constant when the device was in the dark or under illumination.

5.2.6 Transient Absorption Measurements

In addition to the naphthalene-bislactone polymer P11 and P12, another polymer of the same backbone structure was prepared and its charge recombination mechanism analysed through transient absorption measurements. The parameters for the TA experiments include a pump of 525 nm (FWHM 20nm) with a spot size of 760 by 720 μm. And the probe spot size was 260 by 110 μm, with a repetition rate of 34 kHz. The full spectrum of the polymer is presented in the Appendix 10. Polymer P14 displayed a different decay mechanism depending on the probing

wavelength. It also exhibited picosecond charge decay time when excited. Once excited at that wavelength the injected charge in the polymer undergo recombination in 10s of ps. The longer lived component decayed at around 8 ps and the shorter components at 14-1.5 ps. This ultra-fast charge decay is uncommon for conjugated polymers in the field of organic semiconductors. It supports the extended frontier orbitals analysis of the conformationally-fixed polymers. This is

ıg polymers

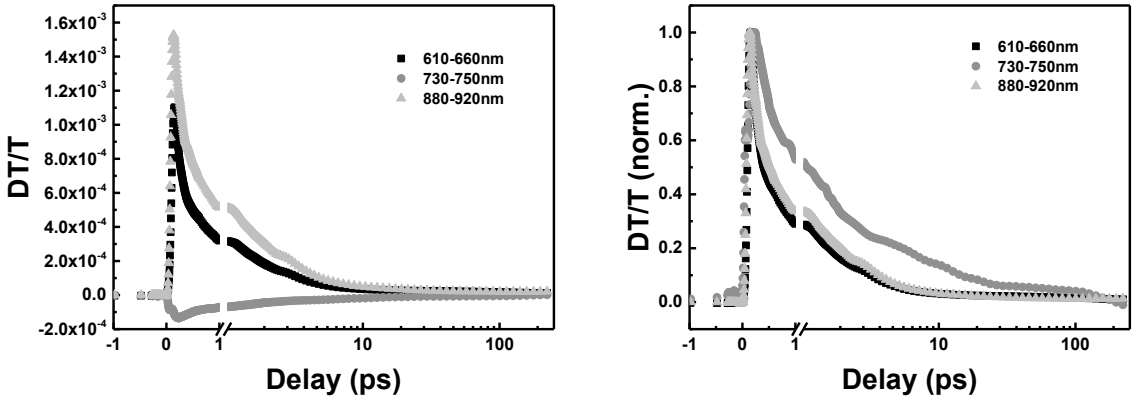

Figure 5.12: The polymer structure of polymer P14 (top) and its transient absorption curves showing the different charge recombination mechanism depending on the probing light wavelength.

5.3 Conclusion

We explored the effect of reducing the dihedral angle between monomer units in aldol polymers on charge transport. In thienothiophene-naphthalene polymer P13 the dihedral angle was decreased from 18^o between two naphthalene-based units to 0^o between a six-membered unit and five-membered bisisatin. Reducing steric repulsion between the monomers in P13 facilitated planarisation of the polymer resulting in oligomeric materials that easily precipitated out from warm chlorobenzene solution. The charge mobility of polymer P13 was decent at 0.001 $cm^2V^{-1}s^{-1}$ given the short polymer length. In the future longer polymers of this backbone structure with larger alkyl chain density are likely to achieve higher electron and hole transport properties. The bislactone-based polymers P11 and P12 maintained the large dihedral angle

between the polymers due to the the nature of the monomers. Nevertheless, there was marked increase in charge transport especially given the short length of the polymers. The bislactone polymers also displayed fast charge recombination times. This property may have been instrumental in hindering the photodetector properties. Reducing the dihedral angle and introducing phenyl bislactone monomers with no alkyl side-chains are a good strategy to enhance the charge mobility of conformationally-fixed aldol polymers.

Chapter 6

Future Work and Conclusion

6.1 Future Work

Polymerisation of bisisatin and bisoxindole monomers *via* p-toluene sulfonic acid catalysed aldol condensation is a metal-free, environmentally benign and reliable synthesis of polymers for organic semiconductors. From the results obtained, it is clearly worthwhile to pursue further polymer structures *via* aldol polymerisation that would enable higher, air stable charge transport and room temperature processability. A number of strategies have already been identified that would improve charge transport properties. Increasing the aromatic core from naphthalene to anthracene would likely improve charge transport as observed in the mobility increase upon going from an all benzene polymer backbone to naphthalene backbone. This has the inevitable effect of raising the electron density of the HOMO, which may impact the material's ambient stability. Introduction of electron withdrawing components into the polymer structure may be necessary to lower the frontier orbitals of more electron rich polymer backbones.

The effect of reducing the dihedral angle between monomers, also discussed, can facilitate polymer arrangements that are capable of faster intermolecular charge transport. Replacement of the acene rings in the bisisatins with thiophene as in the case of thienothiophene bisisatin reduced the dihedral angle between monomers in the polymer. To achieve a completely planar polymer two monomers with flanking 5-membered rings such as thienothiophene

bisisatin and indacenodithiophene-co-benzothiadiazole(IDTBT)-based monomers would be required. IDTBT has been successfully incorporated into polymers with high charge transport characteristics and its bisisatin can be synthesised through the route outlined in Figure 6.1, the same route for making the thienothiophene bisisatin monomer. The shorter synthetic route shown in Fig. 6.1 may be possible if IDTBT diamine intermediate is stable enough for further reactions. The IDTBT bisisatin can be polymerised with its bisoxindole to furnish planar fixed-conformation conjugated IDTBT-based polymer. Large side-chains are necessary to ensure solution processability.

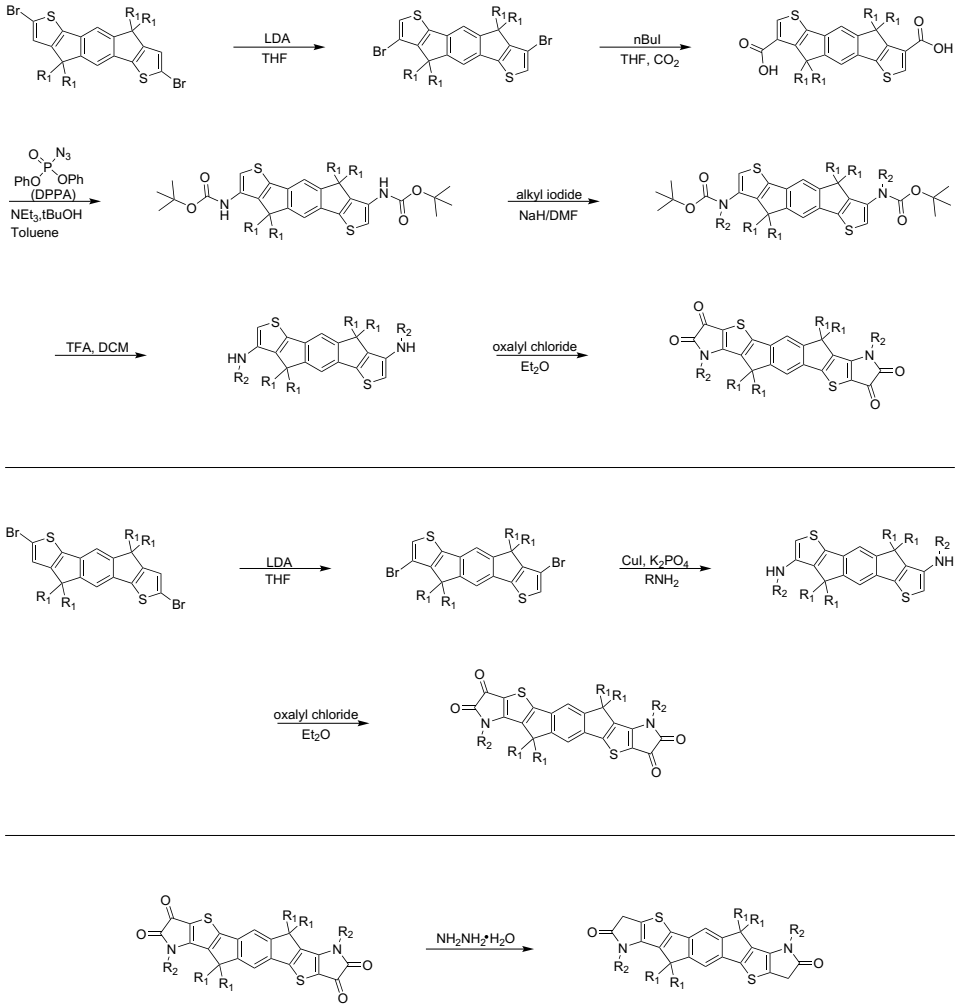

Figure 6.1: Top: synthetic route to IDTBT bisisatin using the same route as for thienothiophene. Middle: another synthetic route to IDTBT bisisatin where brominated IDTBT undergoes halogen migration followed directly by copper catalysed amination and cyclisation to the bisisatin.

IDTBT bisisatin could also be copolymerised with a naphthalene bisoxindole monomer to give

a polymer with dihedral angles of about 15 ^{o} between the monomers. A soluble polymer is expected with side-chains R_1 being an octyl group and R_2 a C8C10 branch alkyl chain.

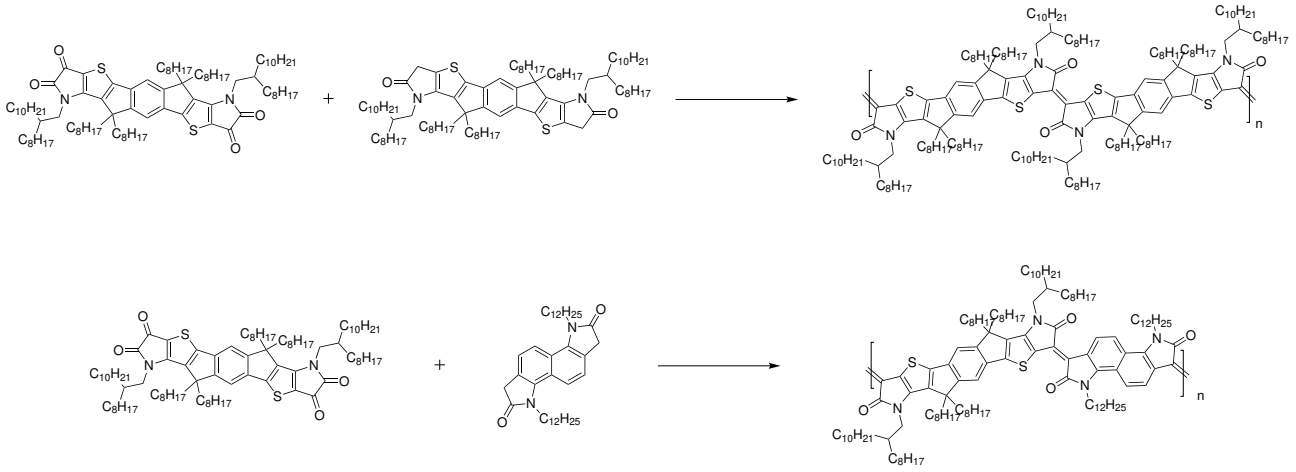

Figure 6.2: Proposed conformationally-fixed polymer from IDTBT bisisatin and bisoxindole, and IDTBT bisisatin and naphthalene bisoxindole.

In addition to synthesising conformationally-fixed polymers by aldol polymerisation, polymers with rotational freedom can also be prepared. Figure 6.3 gives a polymer synthesised from C5 branched naphthalene bisoxindole and thieno[3,2-*b*]thiophene-2,5-dicarbaldehyde. The large side-chain is required because of the lack of solubilising group on the aldehyde and the high possibility of a planar polymer that is difficult to solubilise. Although, this polymer contains a single bond between the monomer, and therefore has a potential for rotation around the single bond. Nonetheless, as of the time of writing this would be a new polymer structure and a polymer made *via* aldol polymerisation would be a more environmentally compatible compared to common polymerisation techniques.

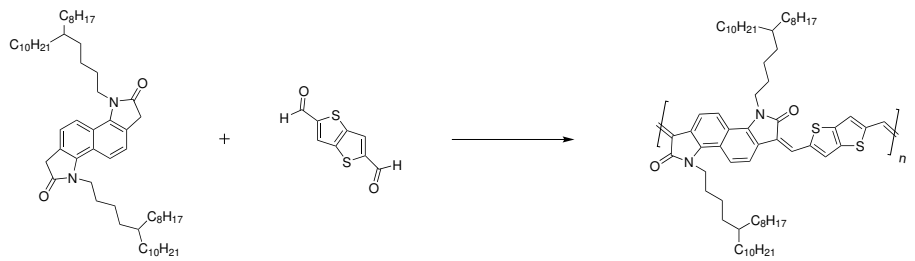

Figure 6.3: Polymerisation of carbon-5 branched alkyl naphthalene bisoxindole with thieno[3,2-*b*]thiophene-2,5-dicarbaldehyde *via* aldol polymerisation.

6.2 Conclusion

Multiple molecular design considerations are required in the field of organic semiconductors. This thesis has investigated a few strands of the structure-property relationships in a new reaction class of polymers for organic semiconductors. The field of Organic Semiconductors is an evolving conversation on many fronts. It certainly has a potential role in technology that can complement recumbent silicon and inorganic electronics. They promise to offer flexible materials that can be mass-produced by cheap high volume manufacturing techniques from solutions at room temperature. There are many overlaps in material function in the field of organic semiconductors that allows for the adaption of one set of materials for alternative applications. For example, considering the good electron charge transports obtained here, attaching glycolated side-chains on these polymers may enable them to be utilised in bioelectronics. In this thesis we added to the field of Organic Semiconducting two fold by introduced a metal free strategy to organic semiconducting polymers and exploring the properties of conformationally-fixed polymers.

The prevailing polymerisation reactions, Suzuki-Miyaura, Negishi, Kumada, Stille, and Sonogashira polymerisation reactions require transition metal catalysts and particularly in the case of the Stille coupling toxic organometallic reagents are also involved. These reactions inherently produce polymers with single carbon-carbon bonds that inherently have a greater degree of freedom along the polymer spine and therefore disorder. We used the aldol reaction in metal-free, p-toluene catalysed reactions to produce conformationally-fixed polymers where double bonds connect monomers. Industrially, aldol polymerisation offers a cleaner polymerisation techniques than established reactions. The acid catalyst used can be recovered and reused after each polymerisation. This reaction also offers excellent control over the polymer molecular weight through monitoring reaction time and catalyst concentration. The catalyst loading can be lowered to slow the reaction time and allow for greater control over the degree of polymerisation.

Strategic molecular design allows us to input desirable characteristics into the polymer. Literature has reported IDTBT-based OS polymers where it was shown that co-planarity between

adjacent monomers, not with-in the polymer, enabled efficient charge transport properties. In this thesis, we found that elongating the aromatic centre on the polymer increased the charge mobility. It also helped to encourage the formation of greater edge-on packing, that is associated with improved charge transport. We achieved a mobility of 0.03 $cm^2V^{-1}s^{-1}$. Improved processing techniques, such as polymer alignment allowed for the charge transport to be further enhanced to 0.08 $cm^2V^{-1}s^{-1}$.

Elongating the aromatic centres in organic semiconductors served to promote aggregation in polymers due to the larger available flat surface areas for Van der Waals interactions to hold polymers together. Long range bulk structuring has been shown to improve charge transport. Another, method to facilitate polymer aggregation is to have linear chains instead of branched or moving the branching point away from the polymer spine. We synthesised four polymers with linear chains, incrementally increasing the polymer chain length to 24 carbons from 12 carbons. The polymers achieved good charge transport of 0.001 $cm^2V^{-1}s^{-1}$. However, the solubility of the polymers limited their solution processability and likely lead to lower observed charge mobilities.

We also synthesised polymers where the side-chain branching position was moved away from the monomer core to create an area for molecular docking, that would enhance aggregation. In addition to the this, a non-alkylated phenylbislactone monomer was incoporated into a polymer that achieved electron mobility of 0.1 $cm^2V^{-1}s^{-1}$ The dihedral angle between the monomers were also reduced by replacing the acene-base monomers with thienothiophene bisisatin, because DFT simulations suggested that there was a high dihedral angle between adjacent monomers due to sterical repulsion. Throughout these studies we have outlined strategies for further increasing the charge transport of these polymers. There is yet plentiful opportunities for conformationally-fixed polymers *via* acid-catalysed aldol polymerisation to achieve high ambient stable electron charge transport.

Chapter 7

Experimental Procedure

7.1 Instruments and Equipment

Numerous instruments were used to measure the properties of the materials made in this thesis. Here is the extensive list of the equipment used. A number of collaborators and partners, specialised in using each technique, were involved in characterising the materials mentioned in this thesis. All our partners involved and their contributions have been outlined in the Contributions section, here we report the materials that were made, equipment and procedures used.

Cyclic Voltammetry of small molecules and polymers were conducted under nitrogen atmosphere in a three-electrode cell at a potential rate scan of $50\,mV/s$. To measure our polymer thin films, indium tin oxide glass substrates were spin coated with polymer solutions in chlorobenzene at 5 mg/mL. Alternatively, a droplet of polymer solution (5 mg/mL in chlorobenzene) was dried onto the platinum work electrode. A platinum mesh was the counter electrode, Ag/Ag^{+} the reference cell and nBu4NPF6 in 0.1 M degassed anhydrous acetonitrile the electrolyte. The measurements were calibrated against ferrocene.

Gel Permeation Chromatography (GPC) data was measured on Agilent Technology 1200. The measurements were run at 80 ^{o}C in chlorobenzene calibrated against narrowly polydispersed polystyrene standard.

Purifications via flash column chromatography were conducted manually using Merck silica gel

(Merck 9385 Kielselgel 60, 230-400 mesh) under positive air pressure with eluent systems as described in the experimental or on **Biotage Isolera**.

Ultraviolet-visible (UV-vis) spectroscopy was performed on UV-1601 Shimadzu UV-vis Spectrometer. Absorption measurements of polymer thin-film measurements were carried out on spin-coated glass substrates of 1mg/mL polymer solutions in chlorobenzene. Agilent Technologies Cary Series UV-vis NIR spectrometer, Cary 5000, was used for measuring the **UV-Vis NIR spectra**.

Mass spectra were recorded by Dr Lisa Haigh at Imperial College London Department of Chemistry Mass Spectrometry Service on a Micromass Autospec Premier/Agilent HP6890 GC.

Nuclear magnetic resonance (NMR) Spectroscopy was used to identify the structure of the molecules synthesised. Proton and carbon NMR measurements were taken on 400 mHz and 500 mHz Bruker DP spectrometers that used an internal deuterium lock at ambient probe temperatures unless otherwise stated. Chemical shifts (δ) are quoted in parts-per million (ppm) relative to tetramethylsilane (TMS) peak at 0.00 ppm. Peak multiplicity are recorded according to standard conventions: bs, broad singlet; s, singlet; d, doublet; t, triplet; q, quartet; m, multiplet. Integration and coupling constants (J) were reported uncorrected in herts (Hz) as appropriate. Residual solvent proton peaks are taken as δ (ppm), 7.26 ppm for $CDCl_3$, 2.52 ppm for DMSO-d^6, 6.00 ppm for TCE-d^2.

Photo-electron Spectroscopy in Air (PESA) was used to obtain the ionisation potentials of polymer films. The results were measured on a Riken Keiki AC-2 PESA spectrometer. The polymer films samples for PESA were prepared by spin coating 5mg/mL polymer solutions in chlorobenzene onto glass substrates. The measurements were run with a light intensity of 5 nW and data processed with a power number of 0.5.

Thermal Gravimetric Analysis curves were obtained from analyses conducted using Perkin Elmer Pyris 1 TGA.

Differential Scanning Calorimetry (DSC) plots were obtained using a TA Instruments DSC Tzero Q20 instrument.

Transistor devices were tested on Agilent 4155C semiconductor parameter. Devices were top-gate-bottom contact (TGBC) structures. The source and drain contacts were Au, PMMA was

the dielectric and Al the gate contact.

Grazing Incidence Wide Angle X-ray Scattering, beamline Specification: X-ray scattering was conducted at the Stanford Synchrotron Radiation Lightsource (SSRL) at 11-3 (2D grazing-incidence wide-angle with MAR225 image-plate area detector). Incident photon energy was 12.732 keV (0.973Å). Helium (g) environments for all measurements were used to minimize air scatter and beam damage to samples. A PANalytical X'Pert-Pro MRD diffractometer equipped with a nickel-filtered Cu K α 1 beam and an X'Celerator detector was used for x-ray diffraction (XRD) measurements.

2D-GIWAXS: 2D grazing-incidence sample-detector distance was 315 mm calibrated with a polycrystalline lanthanide hexaboride (LaB_6) standard at a 3.0^o degree angle with respect to the critical angle of the calibrant. For grazing-incidence geometries, the incidence angle was set below the critical angle of 0.1^o which is above the critical angle underlying native oxide substrate. Data was processed using Nika 2D data reduction homebuilt WxDiff Software. The terms q_{xy} and q_z denote the component of scattering vector in-plane and out-of-plane with the substrate, respectively. Data from 2D grazing-incidence measurements were corrected for the geometric distortion introduced by a flat, plate detector and processed for subsequent analysis with the software WxDiff and GIWAXSTool for Igor.[171]

7.2 Synthetic Procedures

The detailed procedure for synthesising each significant compound in this thesis are recorded here. The molecules are grouped according to the chapters in which they appear. Relevant literature is cited and the compounds are named according to the IUPAC naming system. All solvents, dry or otherwise, were procured from commercial sources and used as purchase unless otherwise specified.

Anhydrous solvents, argon atmosphere, and standard Schlenk technique was used for reactions that necessitated water-free and oxygen-free conditions. Starting materials and appropriate reagents were dried in a vacuum oven overnight prior to the reaction. Glassware for these reactions were oven dried at 140 ^oC and allowed to cool to room temperature under argon flow.

Reaction temperatures should be taken as ambient room temperature approximately 25 ^oC

unless otherwise stated.

Merck aluminium backed precoated silica gel (50 F254) plates were used to monitor reaction progression by thin-layer-chromatography (TLC) . The reaction spots were visualised by ultra-violet light 254 nm or potassium permanganate (VII).

N,N'-(1,4-Phenylene)bis(2-decyltetradecanamide) 3.3

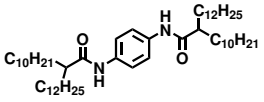

A solution of p-phenyldiamine (1.31 g, 12.1 mmol) in DCM (150 mL) was cooled to 0 ^{o}C, before NEt_3 was added to the reaction mixture. 2-Decyltetradecanoyl chloride (10.3 g, 26.7 mmol) was then added dropwise to the reaction flask and stirred for 4 hours. The product precipitated out of the reaction mixture and was filtered and dried in a vacuum oven overnight to furnish beige poorly soluble solid (9.2 g, 95 %).

N^1,N^4-Bis(2-decyltetradecyl)benzene-1,4-diamine 3.4

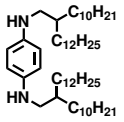

N,N'-(1,4-Phenylene)bis(2-decyltetradecanamide) was suspended in THF (24 ml) and cooled to 0 ^{o}C before 15 mL, 1 M $LiAlH_4$ solution in THF was added to the reaction flask. The reaction was refluxed for 16 hours after which it was placed in an ice bath and 15 M NaOH solution cautiously introduced into the flask. The resulting salted were filtered and washed with copious diethyl ether and the phases separated. The combined organic phase was further washed with water and brine before it was dried using $MgSO_4$ and the solvent removed. Brown solid (1.44 g, 69 %) was obtained.

1,4-Cyclohexanedione (0.6 g, 5.0 mmol) was dissolved in ethanol and 2-decyltetradecan-1-amine added to the solution. Air was bubbled through the reaction mixture for 2 hours before the solvent was removed under reduced pressure. The red residue was purified on basified silica gel with 3 % EtOAc in petroleum ether as eluent to yield 1.8 g, 46 % brown oil. ^{1}H NMR (400 MHz, Chloroform-d) δ (ppm): 6.56 (s, 4H, ArH), 3.19 - 2.68 (m, 4H, NCH_2), 1.72 - 1.50 (m,

2H, CH), 1.50 - 0.99 (m, 80H, CH_2), 0.94 - 0.87 (m, 12H, CH_3). ^{13}C NMR (101 MHz, $CDCl_3$) δ (ppm): 141.18, 114.77, 49.07, 37.95, 32.33, 32.09, 30.25, 29.82, 29.52, 26.90, 22.85, 14.27. MS (ES^+) m/z, M^+ found, 781.8269.

(1,4-Phenylenebis((2-decyltetradecyl)azanediyl))bis(2-oxoethane-2,1-diyl) diacetate 3.5

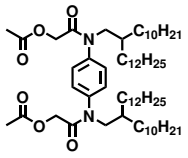

Triethylamine (0.70 mL, 4.99 mmol) was added to a solution of N,N'-bis(2-decyltetradecyl)benzene-1,4-diamine (1.77 g, 2.27 mmol) in anhydrous DCM (22.70 mL) at 0 ^{o}C. Acetoxyacetyl chloride (0.54 mL, 4.99 mmol) was injected into the flask dropwise before the reaction was allowed to warm to room temperature and stirred for 16 hours. The reaction was quenched with $NaHCO_3$ and EtOAc added. The phases were separated and the aqueous phase extracted three times with EtOAc. The combined organic phase was washed with brine dried over $MgSO_4$, the salts filtered and the solvent removed under reduced pressure to give pale yellow solid, 2.00 g, 96 %. ^{1}H NMR (400 MHz, Chloroform-d) δ (ppm): 7.32 (s, 4H, ArH), 4.33 (s, 4H, OCH_2), 3.64 (d, J = 7.0 Hz, 4H, NCH_2), 2.12 (s, 6H, OCH_3), 1.53 - 1.41 (m, 2H, CH), 1.37 - 1.02 (m, 80H, CH_2), 0.94 - 0.79 (m, 12H, CH_3). ^{13}C NMR (101 MHz, $CDCl_3$) δ (ppm): 170.61, 166.56, 141.13, 129.79, 61.79, 53.41, 36.25, 32.06, 31.23, 30.15, 29.82, 29.75, 29.50, 26.39, 22.83, 20.65, 14.25. MS (ES^+) m/z, M^+ found 980.9.

N,N'-(1,4-Phenylene)bis(N-(2-decyltetradecyl)-2-hydroxyacetamide) 3.6

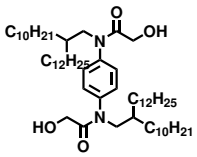

Benzene-1,4-diylbis[(2-decyltetradecyl)imino]-2-oxoethane-2,1-diyl diacetate (3.6 g, 3.7 mmol) in THF (200 mL) and MeOH/water mixture (180 mL, 20 mL respectively). The reaction mixture excess K_2CO_3 was stirred at room temperature for 16 hours before the salt was filtered off. The mixture was concentrated under reduced pressure then water and ethyl acetate added

to the residue. The phases were separated and the aqueous phase extracted three times with ethyl acetate. The combined organic phases were washed with brine dried over $MgSO_4$, filtered and the solvent removed in a rotary evaporator to furnish light yellow oil, 3.1 g, 94 %. ^{1}H NMR (400 MHz, Chloroform-d) δ (ppm): 7.24 (s, 4H), Ar*H*, 3.80 - 3.73 (m, 4H, OCH_2), 3.70 (d, J = 7.1 Hz, 4H, NCH_2), 3.47 - 3.30 (m, 2H, O*H*), 1.52 - 1.37 (m, 2H, C*H*), 1.36 - 1.04 (m, 80H, CH_2), 0.91 - 0.79 (m, 12H, CH_3). ^{13}C NMR (101 MHz, Chloroform-d) δ (ppm): 171.98, 140.31, 129.69, 60.73, 53.47, 36.21, 32.04, 31.23, 30.11, 29.77, 29.71, 29.47, 26.38, 22.80, 14.22. MS ES$^+$ *m/z*, M$^+$ found 898.00.

N,*N*'-(1,4-Phenylene)bis(*N*-(2-decyltetradecyl)-2-oxoacetamide) 3.7

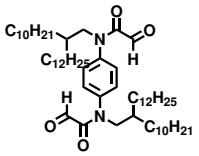

Under argon atmosphere, oxalyl chloride (0.31 ml, 3.89 mmol) was diluted with DCM (4 mL) and cooled to -78 ^{o}C. A solution of DMSO (0.28 mL) in DCM (4.2 mL) was added to the reaction flask at -78 ^{o}C. The reaction flask was stirred for 20 minutes before *N*,*N*'-benzene-1,4-diylbis[*N*-(2-decyltetradecyl)-2-hydroxyacetamide] (1.45 g, 1.62 mmol), diluted in 7 mL DCM, was injected dropwise into the flask. The reaction mixture turned aqua green. After stirring at temperatures below -70 ^{o}C for 1.5 hours, triethylamine (2.26 mL, 16.2 mmol) was added slowly. The reaction was then stirred at -78 ^{o}C for 4 hours before it was warmed to room temperature slowly. The reaction was then stirred for 16 hours before it was quenched with saturated $NaHCO_3$ solution. The phases were separated and the aqueous phase extracted three times with DCM. The combined organic phases were dried with $MgSO_4$, filtered and the solvent removed under vacuum to furnish brown oil, 0.61 g, which was used immediately. ^{1}H NMR (400 MHz, Chloroform-d) δ (ppm): 7.73 (s, 4H, Ar*H*), 3.67 (s, 2H, CH_2), 1.54 (s, 2H, C*H*), 1.36 - 1.03 (m, 83H, CH_2), 0.93 - 0.81 (m, 12H, CH_3).

1,5-Bis(2-decyltetradecyl)-3,7-bis(phenylthio)-5,7-dihydropyrrolo[2,3-*f*]indole-2,6 (1H,3H)-dione 3.8

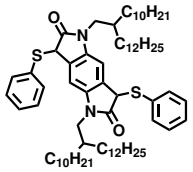

Crude N,N'-(1,4-phenylene)bis(N-(2-decyltetradecyl)-2-oxoacetamide) (1.44 g, 1.61 mmol) was diluted with DCM (6 mL) before thiophenol (0.33 mL, 3.23 mmol) was added to flask. The reaction mixture was then stirred for 16 hours at room temperature. Following this, TFAA (2.01 mL, 14.50 mmol) was added slowly to the reaction and stirred for 1 hour 30 minutes, after which, $BF_3{\cdot}Et_2O$ (0.99 mL, 8.05 mmol) was added to the flask cautiously. Following further stirring for 3 hours, the reaction was cooled to 0 ^{o}C before it was quenched with saturated aqueous $NaHCO_3$ solution. The aqueous phase was extracted with DCM three times and the organic phases combined and washed with brine and dried over $MgSO_4$. The solvent was removed under reduced pressure to furnish red/brown residue as the crude product, which was used without further purification. Yield (1.32 g, 76 %) MS (ES^+) calculated 1077.8244 *m/z* M^+, found 1077.8278.

1,5-Bis(2-decyltetradecyl)-3,7-bis(phenylthio)-5,7-dihydropyrrolo[2,3-*f*]indole-2,6 (1*H*,3*H*)-dione 3.9

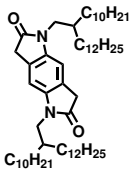

1,5-Bis(2-decyltetradecyl)-3,7-bis(phenylthio)-5,7-dihydropyrrolo[2,3-*f*]indole-2,6(1*H*,3*H*)-dione was dissolved in dry THF (37.0 mL) and 0.1 M SmI_2 in THF (40.0 mL, 4.0 mol) added to the solution at room temperature. Following 16 hours, saturated $NaHCO_3$ (200 mL) was introduced into the reaction mixture and the aqueous phase extracted with ethyl acetate three times. The organic layer was washed with brine, dried over $MgSO_4$, filtered and the solvent removed under reduced pressure. Purification by column chromatography with eluent: 15 % ethyl acetate and 40 - 60 ^{o}C petroleum ether, to afforded beige solid (800 mg, 28 % yield). ^{1}H

NMR (400 MHz, Chloroform-d) δ (ppm): 6.73 (s, 2H, ArH), 3.56 (d, J = 7.9 Hz, 4H, ArCH_2), 3.54 (s, 4H, NCH_2), 1.91 - 1.76 (m, 2H, CH), 1.29 - 1.14 (m, 80H, CH_2), 0.96 - 0.70 (m, 12H, CH_3). ^{13}C NMR (101 MHz, $CDCl_3$) δ (ppm): 174.85, 140.24, 123.92, 106.05, 44.85, 36.41, 36.25, 32.06, 31.68, 30.20, 29.81, 29.49, 26.60, 22.83, 14.26. MS (ES^+) m/z M^+, found 861.9.

1,5-Bis(2-decyltetradecyl)-1,5-dihydropyrrolo[2,3-f]indole-2,3,6,7-tetraone 3.10

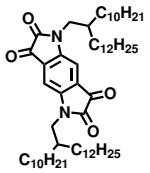

Cerium ammonium nitrate (9.48 g, 17.8 mmol) was added to a solution of 1,5-bis(2-decyltetradecyl)-3,7-bis(phenylthio)-5,7-dihydropyrrolo[2,3-f]indole-2,6(1H,3H)-dione (2.40 g, 2.22 mmol) dissolved in a 6:1 ratio of THF/water (42 mL). Following 30 minutes stirring at room temperature the reaction mixture takes on a deep purple colouration. After 3 hours stirring the reaction mixture was reduced under vacuum. The crude residue was purified by column chromatography at a gradient of 3 - 10 % ethyl acetate in petroleum ether 40 - 60 ^{o}C to furnish the titled compound (300 mg, 15 %). ^{1}H NMR (400 MHz, Chloroform-d) δ (ppm): 7.12 (s, 2H, ArH), 3.62 (d, J = 7.4 Hz, 4H, NCH_2), 1.89 - 1.79 (m, 2H, CH), 1.42 - 1.17 (m, 80H, CH_2), 0.93 - 0.79 (m, 12H, CH_3). ^{13}C NMR (101 MHz, $CDCl_3$) δ (ppm): 183.36, 157.15, 147.85, 123.24, 106.99, 77.16, 45.49, 36.15, 32.06, 31.52, 30.12, 29.79, 29.76, 29.69, 29.47, 26.40, 22.82, 14.25. MS (ES^+), m/z M^+, found 890.2.

N^1,N^4-Didodecylbenzene-1,4-diamine 3.25

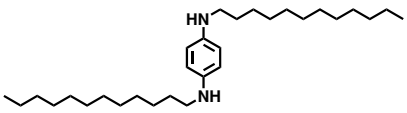

1,4-Cyclohexanedione (5.04 g, 44.6 mmol) was dissolved in ethanol (450 mL) before dodecan-1-amine (16.67 g, 90.0 mmol) was added to the solution and air bubbled through the reaction mixture. After 5 hours, the reaction solvent was removed under reduced pressure to furnish red-brown solid. The crude material, 20.0 g, 50 % yield was used without further purification. ^1H NMR (400 MHz, Chloroform-d) δ (ppm): 6.56 (s, 4H, ArH), 3.30 (br s, 2H, NH), 3.04 (t, J = 7.1 Hz, 4H, NCH_2), 1.64 - 1.52 (m, 4H, NCCH_2), 1.40 - 1.13 (m, 36H, CH_2), 0.93 - 0.82

(m, 6H, CH_3). ^{13}C NMR (101 MHz, Chloroform-d) δ (ppm): 178.26, 151.51, 141.08, 114.95, 92.79, 77.16, 68.11, 45.61, 32.06, 29.77, 29.50, 27.38, 22.83, 14.25, 0.13. MS (ES^+), m/z M^+, found 445.4530.

N, N'-(1,4-Phenylene)bis(2-chloro-N-dodecylacetamide) 3.26

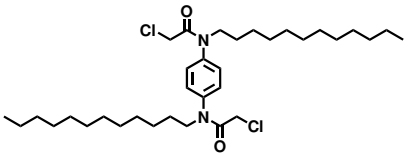

N^1,N^4-Didodecylbenzene-1,4-diamine (2.2 g, 4.88 mmol) was dissolved in DCM (10 ml) and cooled to 0 ^oC. Chloroacetyl chloride (1.55 mL, 19.5 mmol) was added dropwise to the reaction mixture. The reaction was stirred for 4 hours before a saturated solution of the $NaHCO_3$ was used to quench the reaction. The phases were separated and the aqueous phases further extracted using DCM. The combined organic phases were washed with brine, dried over $MgSO_4$, the salts filtered and the solvent removed under reduced pressure. The brown crude product was purified using 20 % ethyl acetate in petroleum ether 40 - 60 ^oC to furnish beige solid. Yield 1.2 g, 41 %. ^1H NMR (400 MHz, Chloroform-d) δ (ppm): 7.32 (s, 4H, ArH), 3.81 (s, 4H, ClCH_2), 3.76 - 3.68 (m, 4H, NCH_2), 1.35 - 1.16 (m, 42H, CH_2), 0.93 - 0.80 (m, CH_3). ^{13}C NMR (101 MHz, Chloroform-d) δ (ppm): 165.82, 141.64, 129.77, 129.31, 116.77, 77.16, 68.08, 50.38, 41.86, 32.02, 29.73, 29.66, 27.72, 26.82, 25.72, 22.79, 14.21, 0.10. MS (ES^+), m/z M^+, found 597.3943.

1,5-Didodecyl-5,7-dihydropyrrolo[2,3-f]indole-2,6(1H,3H)-dione 3.27

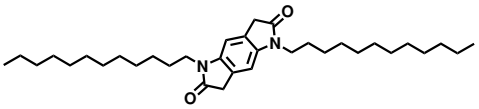

Under argon atmosphere, N, N'-(1,4-Phenylene)bis[2-chloro-N-(2-decyltetradecyl)acetamide] (100 mg, 0.17 mmol), $Pd(OAc)_2$ (4.58 mg, 0.02 mmol) and JohnPhos (12.17 mg, 0.04 mmol) were dissolved with degassed toluene (1.78 mL). The solution was further degassed for 10 minutes and already degassed NEt_3 (0.07 mL, 0.51 mmol) was also added. The reaction was heated for 16 hours at 88 ^oC. The solvent was removed under reduced pressure and the residue purified by flash column chromatography using 10 % EtOAc in petroleum ether 40 - 60 ^{o}C. Beige solid

42 mg was isolated in 42 % yield. ^{1}H NMR (400 MHz, Chloroform-d) δ (ppm): 7.32 (s, 2H, ArH), 3.82 (s, 4H, ArCH_2), 3.7 - 3.65 (m, 4H, NCH_2), 1.63 - 1.46 (m, 2H, CH), 1.34 - 1.17 (br s, 36H, CH_2), 0.95 - 0.78 (m, CH_3). ^{13}C NMR (101 MHz, $CDCl_3$) δ (ppm): 165.83, 141.67, 129.79, 77.16, 50.41, 41.87, 32.05, 29.76, 29.71, 29.68, 29.48, 29.44, 27.76, 26.85, 22.82, 14.25. MS (ES^+), m/z M^+, found 525.4431.

(1,4-Phenylenebis(dodecylazanediyl))bis(2-oxoethane-2,1-diyl) diacetate 3.28

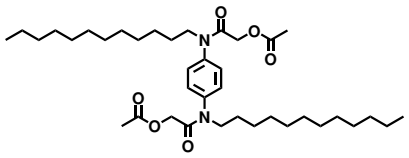

N1,N4-Didodecylbenzene-1,4-diamine(20 g, 45.0 mmol) was dissolved in DCM (400 ml) and cooled to 0 ^{o}C. NEt_3 (13.0 mL, 99.00 mmol) was injected dropwise into the reaction flask before acyl chloride (10.64 mL, 99.00 mmol) was added cautiously to the flask at 0 ^{o}C. The reaction was stirred for 16 hours. A saturated aqueous solution of $NaHCO_3$ was used to quench the reaction at 0 ^{o}C. The phases were separated and the aqueous phase further extracted by DCM. The combined organic phase was washed with brine, dried over $MgSO_4$, filtered and the solvent evaporated under reduced pressure. The crude product was purified using EtOAc/Petroleum spirit 40 - 60 ^{o}C (2:8) to give light yellow solid 20.07 g, 69 %. ^{1}H NMR (400 MHz, Chloroform-d) δ (ppm): 7.32 (s, 4H, ArH), 4.32 (s, 4H, OCH_2), 3.64 (t, J = 7.0 Hz, 4H, NCH_2), 2.12 (s, 6H, OCH_3), 1.58 - 1.45 (m, 4H, NCCH_2), 1.37 – 1.14 (m, 36H, CH_2), 0.94 - 0.83 (m, 6H, CH_3). ^{13}C NMR (101 MHz, $CDCl_3$) δ (ppm): 170.67, 166.12, 141.05, 129.97, 61.76, 49.94, 32.03, 29.74, 29.68, 29.44, 27.81, 26.84, 22.80, 20.64, 14.23. MS ES^+, m/z M^+, found 645.4855.

***N*,*N*'-(1,4-Phenylene)bis(*N*-dodecyl-2-hydroxyacetamide) 3.29**

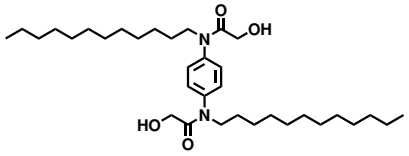

A methanol/water (300 mL) mixture in 9:1 ratio was added to (1,4-phenylenebis(dodecylazanediyl))bis(2-oxoethane-2,1-diyl) diacetate (20.07 g, 31.1 mmol) dissolved in 300 mL THF. To this (42.05 g, 311 mmol) K_2CO_3 was added and the reaction was stirred for 6 hours at room

temperature after which the salts were filtered and the solvent concentrated under reduced pressure and the salts filtered. Water and ethyl acetate was poured into the flask and the phases separated. The aqueous phases was extracted further using ethyl acetate three times. The combined organic phase was washed with brine, dried using $MgSO_4$, the salts filtered and the solvent evaporated. Beige (16.5 g) solid was obtained. ^{1}H NMR (400 MHz, Chloroform-d) δ (ppm): 7.25 (s, 4H, ArH), 3.82 – 3.64 (m, 8H, OCH_2, NCH_2), 1.52 (m, 2H, NCCH_2), 1.36 – 1.13 (m, 38H, CH_2), 0.91 – 0.82 (m, 6H, CH_3). ^{13}C NMR (101 MHz, $CDCl_3$) δ (ppm): 171.47, 140.28, 129.99, 60.70, 49.96, 32.04, 29.75, 29.68, 29.47, 27.88, 26.84, 22.82, 14.24. MS (ES^+), m/z M^+, found 561.4620.

1,5-Didodecyl-5,7-dihydropyrrolo[2,3-f]indole-2,6(1H,3H)-dione 3.30

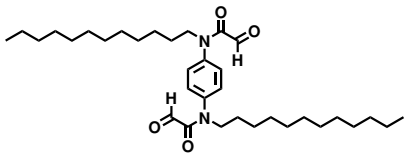

A flask containing 20 mL dry DCM and oxalyl chloride (0.94 mL, 11.8 mmol) was cooled to -78 ^{o}C. To this, a mixture of 1.67 mL anhydrous DMSO in 8 mL DCM was added slowly to the reaction to maintain a solution below -72 ^{o}C. Separately, N,N'-(1,4-phenylene)bis(N-(2-decyltetradecyl)-2-hydroxyacetamide) (3.00 g, 5.35 mmol) was dissolved in 20 mL DCM and added to the reaction flask dropwise. The reaction was stirred for 30 minutes at -72 ^{o}C before NEt_3 (7.46 mL, 53.5 mmol) was added to the reaction flask and the reaction was allowed to warm to room temperature and stirred for 3 hours. Saturated sodium hydrogen carbonate solution was added to the flask to quench the reaction, the phases were separated and the aqueous phases extracted three times with DCM. The combined organic phase was washed with brine, dried over $MgSO_4$, the salt filtered and the solvent removed by rotary evaporated to give a brown solid (2.98 g)

N,N'-(1,4-Phenylene)bis(N-dodecyl-2-hydroxyacetamide) (230 mg, 0.26 mmol) was dissolved in DCM (1.9 mL) and Dess-Martin periodinane (164.9 mg, 0.39 mmol) was added to the solution at room temperature. The reaction was stirred for 2 ours before, saturated aqueous $NaHCO_3$ solution and the phases separated. The aqueous phase was further extracted twice more using DCM. The combined organic phase was washed with brine, dried over $MgSO_4$, the salt filtered and the solvent removed using a rotary evaporator to leave light yellow oil that was confirmed

by proton NMR to be the starting material.

N,*N*'-(1,4-Phenylene)bis(*N*-dodecyl-2-hydroxyacetamide) (100 mg, 0.11 mmol) was dissolved in DCM (1 ml) and pyridinium chlorochromate (98 mg, 0.45 mmol) was added to the reaction mixture.The reaction was stirred at room temperature under argon atmosphere. The reaction was monitored by TLC (20 % EtOAc/PE), and after 2 hours the starting material disappeared and the reaction was quenched with aqueous $NaHCO_3$. The phases were separated and the organic phases extracted twice more with DCM. Proton NMR spectroscopy indicated the presence of a small amount of aldehyde signal at 9.5 ppm, however this signal did not integrate well with other signals in the compound.

1,5-Didodecyl-3,7-bis(phenylthio)-5,7-dihydropyrrolo[2,3-*f*]indole-2,6(1*H*,3*H*)-dione 3.31

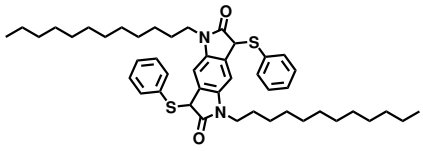

N, *N*′-(1,4-Phenylene)bis(N-dodecyl-2-oxoacetamide) (2.98 g, 5.35 mmol) was dissolved in dry DCM (53.5 mL) and thiophenol (1.09 mL, 10.7 mmol) added to the solution. The reaction was stirred for 16 hours at room temperature. TFAA (6.69 mL, 48.15 mmol) was then introduced into the flask at 0 ^{o}C and the reaction stirred for 1 hour. BF_3OEt_2 solution was injected into the flask and the reaction stirred for a further 16 hours at room temperature. The reaction was quenched with saturated $NaHCO_3$ solution at 0 ^{o}C and extracted with DCM. The organic phase was washed with brine dried over $MgSO_4$ and concentrated on the rotary evaporator to give dark green residue. Th solid was poured though a pad of silica using ethyl acetate to give red solid (3.56 g, 90 % yield). MS *m/z* M^+ found 741.4488.

1,5-Didodecyl-1,5-dihydropyrrolo[2,3-*f*]indole-2,3,6,7-tetraone 3.32

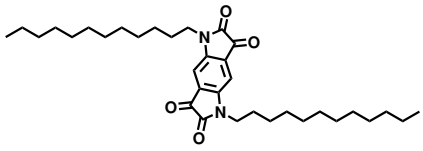

1,5-Didodecyl-3,7-bis(phenylthio)-5,7-dihydropyrrolo[2,3-*f*]indole-2,6(1*H*,3*H*)-dione (1.27 g, 1.49 mmol) was dissolved in THF/water (25 mL) 6:1 mixture and cerium ammonium nitrate

(7.98 g, 14.56 mmol) was added and the reaction stirred for 3 hours at room temperature. The reaction was then concentrated under pressure and the crude material purified by column chromatography in 3-10 % EtOAc in Petroleum ether to furnish the blue product 119 mg, 12 % yield. ^{1}H NMR (400 MHz, Chloroform-d) δ (ppm):7.12 (s, 2H, ArH), 3.62 (d, J = 7.5 Hz, 4H, NCH_2), 1.85 (m, 2H, CH), 1.25 (m, 36H, CH_2), 0.96 - 0.84 (m, CH_3). ^{13}C NMR (101 MHz, $CDCl_3$) δ (ppm):157.16, 107.00, 68.13, 36.16, 32.07, 31.53, 30.14, 29.77, 29.72, 29.51, 29.48, 26.41, 25.77, 22.84, 14.26. MS (ES^+), m/z M^+ found 553.3890.

Polymer P1

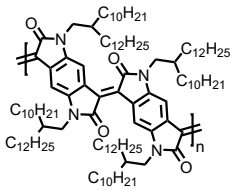

Measured C10C12 phenylbisisatin (50.00 mg, 0.06 mmol) and Lawesson's reagent (22.75 mg, 0.06 mmol) into a microwave vial followed by dry o-xylene (0.56 mL) that had been previously degassed for 1 hour 30 minutes. The solution was further degassed with argon for 15 minutes before the solution was heated to 120 ^{o}C. Within 10 minutes of reaction time, the solution turned brown from the original blue solution. And after 15 minutes reaction time the reaction is reddish brown. The polymerisation was allowed to proceed for 16 hours. It was not possible to precipitate the polymer into methanol. GPC measurement on 80 ^{o}C chlorobenzene: Mn = 2.6 kDa, PDI = 1.6.

Measured C10C12 phenylbisisatin (30.00 mg, 0.03 mmol) into a microwave vial followed by 0.34 mL dry toluene, previously degassed for 1 hour. The blue solution was then degassed prior to the addition of triethylamanio phosphine (0.02 mL, 0.07 mmol) and the solution was stirred at room temperature for 5 hours. The reaction at this time was a purple/red solution, this was then heated to 60 ^{o}C for 16 hours after which the reaction became a dark green solution. Again it was not possible to precipitate the polymer into methanol.

C10C12 phenylbisisatin (100.00 mg, 0.11 mmol), C10C12 phenylbisoxindole (96.86 mg, 0.11 mmol) and p-toluene sulfonic acid (6.45 mg, 0.03 mmol) were all loaded into a microwave vial, along with dried 4 Å molecular sieves. The flask was sealed and purged and backfilled with argon three times. Dry toluene (2.00 mL), already degassed for 1 hour, was injected into the

flask and the reaction mixture further degassed for 30 minutes. The flask was then heated to 140 ^{o}C for 32 hours. The polymer mixture was injected into methanol to precipitate the polymer, and the polymer was filtered. The polymer then underwent sequential Soxhlet extraction in methanol, acetone and hexane. The polymer was extracted in hexane, 159 mg yield 84 %.

Polymer P2

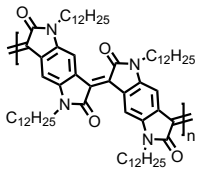

C12 phenylbisisatin (37 mg, 0.07 mmol), C12 phenylbisoxindole (40 mg, 0.07 mmol) and p-toluene sulfonic acid (4.1 mg, 0.02) were all loaded into a microwave vial. The flask was sealed and purged and backfilled with argon three times. Dry toluene (1.00 mL), already degassed for 1 hour, was injected into the flask and the reaction mixture further degassed for 30 minutes. The flask was then heated to 120 ^{o}C for 72 hours. The polymer mixture was injected into methanol to precipitate the polymer, and the polymer underwent sequential Soxhlet extraction in methanol, acetone, hexane, DCM, $CHCl_3$. The polymer was extracted in chloroform, 40 mg.

Naphthalene Bisisatin Core 3.45

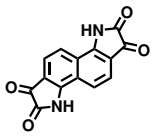

Sandmeyer Isatin Synthesis

Chloral hydrate (11.30 g, 68.32 mmol) was dissolved in 152 mL water. Anhydrous sodium sulphate (7.19 g, 50.61 mmol), 5-diaminonaphtalene (5.00 g, 31.63 mmol) and hydroxylammonium chloride (13.89 g, 199.90 mmol) were also added to the flask. Concentrated HCl (30 mL) was added to the reaction and the mixture was heated at 90 ^{o}C for 10 minutes. The precipitate was filtered and suspended in 25 mL concentrated sulfuric acid and heated at 80 ^{o}C for 1 hour. The highly insoluble precipitate formed was confirmed as mostly starting material by mass spectrometry.

Martinet Isatin Synthesis

1,5-diaminonaphthalene (2.00 g, 12.65 mmol) was refluxed in acetic acid (20 mL) to dissolve it before diethyl ketomalonate (8.11 mL, 53.00 mmol) diluted in acetic acid (10 mL) was added dropwise to the refluxing reaction. The reaction was refluxed for 16 hours. After cooling the reaction to room temperature, the solvent was removed under reduced pressure. The brick red residue was dissolved in 1 M NaOH to pH 11-12 and refluxed for 5 hours with sparging air. The reaction was then poured onto ice, acidified to pH 0 with 6 M HCl, filtered and the purple-red solid dried, 2.19 g, yield 63 %. ^{1}H NMR (400 MHz, DMSO-d6) δ (ppm): 11.77 (d, J = 8.4 Hz, 2H, NH), 7.60 - 7.55 (m, 2H, ArH) ^{13}C NMR (400 MHz, DMSO-d6) d 183.86, 183.53, 160.57, 152.41 124.54, 120.48, 117.67, 117.67, 115.74.

3,8-Bis(2-hexyldecyl)-3,8-dihydroindolo[7,6-*g*]indole-1,2,6,7-tetraone 3.51

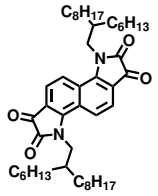

Under argon atmosphere, a flask was charged with 3,8-Dihydroindolo[7,6-g]indole-1,2,6,7-tetraone (500.0 mg, 1.88 mmol) and dry K_2CO_3 (2.58 g, 7.33 mmol). These were dissolved in DMF (10.4 mL) and heated to 100 ^{o}C. 7-(iodomethyl)pentadecane (635.0 mg, 4.7 mmol) was injected into the flask and the reaction heated at 70 ^{o}C for 5 hours. The reaction was poured into water and acidified with 1 M HCl to pH 7 prior to extraction using DCM. The combined organic phase was washed with brine, dried over $MgSO_4$, filtered and the solvent removed under reduced pressure. The crude product was purified by flash chromatography using 1:3 EtOAc/DCM eluent to give 77 mg blue solid, yield 5.5 %. ^{1}H NMR (400 MHz, Chloroform-d) δ (ppm): 7.99 (d, J = 8.7 Hz, 2H, ArH), 7.66 (d, J = 8.6 Hz, 2H, ArH), 4.16 (d, J = 7.3 Hz, 4H, NCH_2), 1.28 - 1.15 (m, 40H, CH_2), 0.90 - 0.80 (m, 12H, CH_3) ^{13}C NMR (101 MHz, $CDCl_3$) d 182.87, 159.46, 152.54, 127.59, 120.23, 120.10, 116.51, 77.16, 68.13, 47.78, 37.73, 31.99, 31.85, 31.25, 30.10, 29.75, 29.61, 29.39, 26.35, 25.77, 22.74, 14.19, 0.14. MS ES^{-}, m/z M^{-}, found found 714.5360

Polymer P3

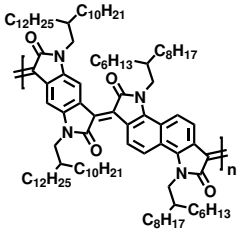

A vial was charged with 3,8-bis(2-hexyldecyl)-3,8-dihydroindolo[7,6-g]indole-1,2,6,7-tetraone (31 mg, 4.34 mmol), 1,5-bis(2-decyltetradecyl)-5,7-dihydropyrrolo[2,3-f]indole-2,6(1H,3H)-dione (37.3 mg, 4.33 mmol) and pTsOH (2.5 mg, 1.3 mmol) before 0.78 mL dry toluene added to the flask. The solution was degassed for 10 minutes and the vial vacated and backfilled with argon before the reaction mixture was heated to 120 ^{o}C for 16 hours. The resulting viscous solution was precipitated into MeOH, filtered and a Soxhlet performed using acetone, followed by hexane. The polymer was extracted in hexane, 63.00 mg, 83 % yield. GPC (chlorobenzene, 80 ^oC): Mn 51 kDa and Mw 132 kDa.

(2E,2'E)-N,N'-(1,4-Phenylene)bis(2-(hydroxyimino)acetamide)

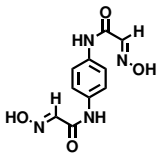

Chloral hydrate (11.68 g, 10.17 mmol) was dissolved in 12 mL water. Anhydrous sodium sulphate (10.5 g, 73.92 mmol), 5-diaminonaphtalene (0.50 g, 4.62 mmol) and hydroxylammonium chloride (2.02 g, 29.1 mmol) were also added to the flask, followed by 3.98 mL of concentrated HCl. The mixture was heated to 90 ^{o}C for 5 minutes the cooled to room temperature and the red precipitate filtered and washed with water. MS (ES^+), m/z MS^+ found: 251.0815

1,5-Dihydropyrrolo[2,3-*f*]indole-2,3,6,7-tetraone

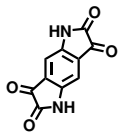

The crude intermediate, (2*E*,2'*E*)-*N*,*N*'-(1,4-Phenylene)bis(2-(hydroxyimino)acetamide) was added to concentrated sulfuric acid and heated at 80 ^{o}C for 20 minutes. When the reaction mixture was at room temperature it was poured onto ice and stirred overnight. The resulting precipitate was filtered to give a dark red powder (60 mg, 6 %).

Benzene-1,4-diamine (2 g, 18.5 mmol) was dissolved in 25 mL glacial acetic acid and heated to reflux. The solution of diethyl ketomalonate (11.3 mL, 73.98 mmol) in 20 mL glacial acetic acid was added dropwise to the refluxing solution. The reaction mixture was refluxed for 16 hours. The reaction mixture was then concentrated and 1 M NaOH solution was added to the residue to give pH 11-12 before the reaction was heated to reflux with sparging air. After sparging with air for 4 hours the mixture was acidified to pH 0 using 6 M HCl. The mixture was then allowed to settle and the acidic medium decanted and the precipitate filtered. The cake was washed with water and methanol and dried to give dark brown solid, 310 mg, 8 % yield.

Polymer P4

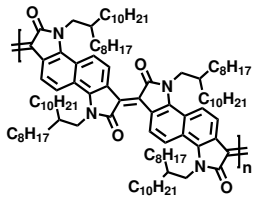

A vial was charged with (N-(2-octyltetradecyl))-naphthalene bisoxindole (41.80 mg, 0.0523 mmol), (N-(2-octyltetradecyl))-naphthalene bisisatin (43.26 mg, 0.0523 mmol) and pTsOH monohydrate (4 mg, 0.3 eq) after which the vial was capped and backfilled with argon three times. Degassed dry toluene (0.5 mL) was added and the mixture was heated at 120 ^{o}C for 2 hours to give a purple solid. Chlorobenzene was added and the polymer was precipitated into methanol. Successive Soxhlet extractions with methanol, acetone, hexane and finally DCM gave a single major polymer fraction, which was reduced to minimum volume and precipitated

into methanol to give 47 mg of a purple solid (56 % yield). GPC (chlorobenzene, 80 ^{o}C): Mn 214 kDa, Mw 677 kDa.

N,*N*'-(Naphthalene-1,5-diyl)didodecanamide 3.46

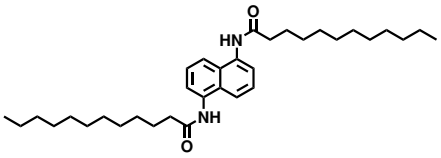

1,5-Diaminonaphthalene (3.0 g, 18.96 mmol) was dissolved in DCM (300 mL) and cooled to 0 ^{o}C, triethylamine (0.3 mL, 45.51 mmol) was added to the flask followed by the dodecanoyl chloride (12.7 mL, 41.71 mmol). The reaction was stirred for 16 hours. The poorly soluble product(12 g, 100 % yield) was filtered and dried in an oven under reduced pressure and used in the next step without further purification.

N1,N5-Didodecylnaphthalene-1,5-diamine 3.47

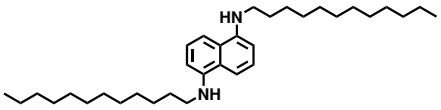

The N,N'-(naphthalene-1,5-diyl)didodecanamide (12.0 g, 18.90 mmol) was suspended in dry THF (160 mL) and cooled to 0 ^{o}C. 1 M lithium aluminium hydride (75.6 mL, 75.6 mmol) was added cautiously to the reaction flask and the reaction was refluxed for 72 hours. To quench, the reaction was cooled to 0 ^{o}C, prior to a slow addition of 1 M NaOH. The quenched mixture was then concentrated under reduced pressure before addition of water and extraction of the aqueous phase with $CHCl_3$. Combined organic phases were dried over $MgSO_4$, the salts filtered and the solvent evaporated under reduced pressure. The brown residue was used without further purification (6.8 g, 60 % yield). ^{1}H NMR (400 MHz, Chloroform-d) δ (ppm): 7.35 - 7.28 (m, 2H, ArH), 7.14 (d, J = 8.5 Hz, 2H, ArH), 6.60 (d, J = 7.5 Hz, 2H, ArH), 4.31 (s, 2H, NH), 3.25 (t, J = 7.1 Hz, 4H, NCH_2), 1.76 (m, 4H, NCCH_2), 1.56 - 1.41 (m, 4H), 1.32 - 1.24 (m, 32H, CH_2), 0.91 - 0.86 (m, 6H, CH_3). 13C NMR (101 MHz, $CDCl_3$) d 144.41, 125.56, 124.02, 108.57, 104.40, 77.16, 68.13, 44.44, 32.08, 29.83, 29.78, 29.61, 29.51, 27.53, 25.77, 14.27, 0.15. MS (ES^+), m/z M^+ found 495.4680.

N,*N*'-(Naphthalene-1,5-diyl)bis(2-chloro-N-dodecylacetamide) 3.48

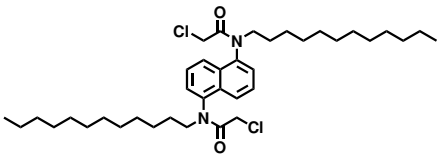

The solution of N1,N5-didodecylnaphthalene-1,5-diamine (3.49 g, 5.6 mmol) in 168 mL DCM was cooled to 0 ^{o}C and triethylamine (1.9 mL, 13.4 mmol) injected into the flask. Chloroacetyl chloride was slowly introduced into the reaction flask. The reaction was allowed to warm to room temperature and quenched with saturated solution of $NaHCO_3$. The phases were separated and the aqueous phases extracted with DCM. The combined organic phases were dried over $MgSO_4$, filtered and the solvent removed under reduced pressure. The brown residue was purified by column chromatography in 1:5 ethyl acetate/petroleum spirit (3.1 g, 86 %) . ^{1}H NMR (400 MHz, Chloroform-d) δ (ppm): 7.90 (d, J = 8.5 Hz, 2H, ArH), 7.64 (m, 2H, ArH), 7.50 (d, J = 7.2 Hz, 2H, ArH), 4.40 - 4.28 (m, 2H,ClCH_2), 3.86 - 3.59 (m, 4H, NCH_2), 3.30 - 3.19 (m, 2H, ClCH_2), 1.77 - 1.59 (m, 4H, NCCH_2), 1.38 - 1.12 (m, 36H, H_2), 0.93 - 0.83 (m, 6H, CH_3). 13C NMR (101 MHz, $CDCl_3$) d 166.55, 138.25, 131.93, 128.05, 127.70, 127.64, 123.84, 123.80, 77.16, 50.30, 50.26, 42.16, 32.01, 29.72, 29.66, 29.44, 28.11, 28.06, 27.07, 26.93, 22.79, 14.22. MS (ES^+), m/z M^+ found 647.4087.

3,8-Didodecyl-1,3,6,8-tetrahydroindolo[7,6-*g*]indole-2,7-dione 3.49

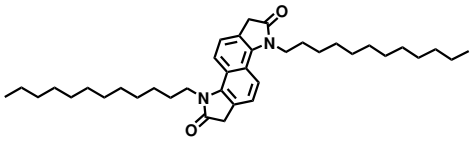

A dry vial was charged with palladium acetate (53.9 mg, 0.24 mmol, 12 mol%), 2-(di-tert-butylphosphino)biphenyl (JohnPhos, 143.2 mg, 0.48 mmol, 24.0 mol %) and *N*,*N*'-(naphthalene-1,5-diyl)bis(2-chloro-N-dodecylacetamide) (1.52 g, 2.0 mmol). The vial was purged and back-filled with argon three times. Degassed dry toluene (16 mL) was then injected into the flask, followed by triethylamine (0.82 mL, 5.88 mmol). The reaction mixture was then heated to 90 ^{o}C for 16 hours. Then the reaction was cooled to room temperature and the solvent removed. The dark residue was purified by flash chromatography with 1:5 ethyl acetate/petroleum spirit 40 - 60 ^{o}C as eluent to furnish off white solid (0.47 g, 34 %). ^{1}H NMR (400 MHz, Chloroform-d) δ (ppm): 7.92 (d, J = 8.7 Hz, 2H, ArH), 7.40 (d, J = 8.6 Hz, 2H, ArH), 4.46 – 4.12 (m,

4H, NCH_2), 3.67 (s, 4H, ArCH_2), 1.81 (p, J = 7.8 Hz, 4H, NCCH_2), 1.45 (m, 4H, NCCCH_2), 1.38 – 1.17 (m, 32H, CH_2), 0.93 - 0.84 (m, 6H, CH_3). ^{13}C NMR (101 MHz, $CDCl_3$) 176.64, 140.76, 122.09, 121.93, 120.43, 115.85, 42.99, 36.21, 32.06, 29.78, 29.71, 29.68, 29.56, 29.49, 29.45, 26.94, 22.84, 14.27. MS (ES^+), *m/z* M^+ found 575.4581.

3,8-Didodecyl-3,8-dihydroindolo[7,6-*g*]indole-1,2,6,7-tetraone (150 mg, 0.18 mmol) was suspended in 1 ml dioxane and hydrazine hydrate solution (0.5 mL) and the mixture refluxed for 3 hours in a high pressure vessel at 180 ^{o}C. The aqueous phase was then extracted with DCM three times. The combined organic phase was washed with brine, dried with $MgSO_4$, filtered and the solvent reduced under reduced pressure. The dark orange crude material was purified by column chromatography on Isolera Biotage with a gradient of 10 - 40 % ethyl acetate and petroleum spirit 40 - 60 ^{o}C. The resulting material was recrystallised from ethyl acetate to give beige solid (45 mg, 31 % yield). ^{1}H NMR (400 MHz, Chloroform-d) δ (ppm): 7.92 (d, J = 8.7 Hz, 2H, ArH), 7.40 (d, J = 8.6 Hz, 2H, ArH), 4.46 – 4.12 (m, 4H, NCH), 3.67 (s, 4H, ArCH_2), 1.81 (p, J = 7.8 Hz, 4H, NCCH_2), 1.45 (m, 4H, NCCCH_2), 1.38 – 1.17 (m, 32H, CH_2), 0.93 - 0.84 (m, 6H, CH_3). ^{13}C NMR (101 MHz, $CDCl_3$) 176.64, 140.76, 122.09, 121.93, 120.43, 115.85, 42.99, 36.21, 32.06, 29.78, 29.71, 29.68, 29.56, 29.49, 29.45, 26.94, 22.84, 14.27. MS (ES^+), *m/z* M^+ found 575.4581.

3,8-Bis(2-decyltetradecyl)-3,8-dihydroindolo[7,6-g]indole-1,2,6,7-tetraone

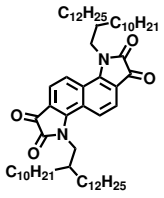

The dark naphthalene naphthalene bisisatin core (1 g, 3.76 mmol), dried K_2CO_3 (4.56 g, 11.26 mmol) were suspended in 10 mL dry DMF and heated to 80 ^{o}C. The reaction was cooled to 60 ^{o}C before 11-(bromomethyl)tricosane (2.08 mL, 15.04 mmol) was injected into the reaction. The reaction was heated for 3 hours at 60 ^{o}C, then quenched by pouring it into water and acidified to pH 7 with aqueous 1 M HCl. The aqueous phase was extracted with DCM dried over $MgSO_4$ and the solvent removed. The brown residue was purified by flash chromatography with 2:3 DCM/petroleum spirit 40 - 60 ^{o}C, followed by recrystallisation in hexane to give blue solid (388 mg, 12.5 % yield). ^{1}H NMR (400 MHz, Chloroform-d) δ (ppm): 8.02 (d, J = 8.7 Hz,

2H, ArH), 7.68 (d, J = 8.6 Hz, 2H, ArH), 4.18 (d, J = 7.3 Hz, 4H, NCH_2), 2.03 – 1.79 (m, 2H, NCCH_2), 1.36 (t, J = 9.9 Hz, 8H), 1.33 (s, 72H), 0.90 (t, J = 6.7 Hz, 6H, CH_3). ^{13}C NMR (101 MHz, $CDCl_3$) 182.86, 159.44, 152.53, 127.57, 120.22, 120.10, 116.49, 68.13, 47.76, 37.76, 32.06, 31.24, 30.12, 29.81, 29.76, 29.68, 29.50, 26.35, 22.84, 14.26. MS ES^-, m/z M^- found 938.7856.

3,8-Bis(2-octyldodecyl)-3,8-dihydroindolo[7,6-g]indole-1,2,6,7-tetraone 3.52

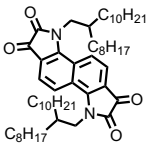

Naphthalene bisisatin core (1 g, 3.76 mmol), dried K_2CO_3(4.56 g, 11.26 mmol) were suspended in 10 mL dry DMF and heated to 80 ^{o}C. The reaction was cooled to 60 ^{o}C before 1-iodo-2-octyldodecane (2.08 mL, 15.04 mmol) was injected into the reaction. The reaction was heated for 3 hours at 60 ^{o}C. The reaction was quenched by pouring it into water and acidified to pH 7 with aqueous 1 M HCl. The aqueous phase was extracted with DCM dried over $MgSO_4$ and the solvent removed. The brown residue was purified by flash chromatography with 2:3 DCM/ petroleum spirit 40 - 60 ^{o}C, followed by recrystallisation in hexane to give blue solid (388 mg, 12.5 % yield). ^{1}H NMR (400 MHz, CDCl3, 300K) δ (ppm): 8.01 (d, J = 8.7 Hz, 2H, ArH), 7.68 (d, J = 8.7 Hz, 2H, ArH), 4.19 - 4.17(m, 4H, NCH_2), 1.87 - 2.01(m, 2H, CH), 1.37 - 1.24(m, 64H, CH_2), 0.90 - 0.87 (m, 12H, CH_3). 13C NMR (101 MHz, CDCl3, 300K) δ (ppm): 182.70, 159.30, 152.39, 127.42, 120.08, 119.94, 116.35, 47.62, 31.09, 29.95, 29.59, 29.52, 26.20, 22.67, 22.65, 14.10. MS (ES^+), calculated for C54H86N2O4: 826.66, m/z M^+ found 827.0.

Polymer P5

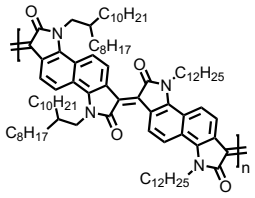

3,8-Didodecyl-3,8-dihydroindolo[7,6-g]indole-1,2,6,7-tetraone (66.37mg, 0.08 mmol), and 3,8-didodecyl-1,3,6,8-tetrahydroindolo[7,6-g]indole-2,7-dione (46.12 mg, 0.08 mmol) and p-toluene sulfonic acid monohydrate (4.0 mg, 0.02 mmol) were loaded into a dry vial and the vial purged and backfilled with argon three times. Degassed anhydrous toluene (1.5 mL) was injected into

the flask and heated at 120 ^{o}C for 12 hours, Soxhlet with chlorobenzene gave purple polymer 102 mg, 92 % yield. GPC (chlorobenzene, 80 ^{o}C): Mn 134 kDa, Mw 538 kDa. ^{1}H NMR (d2-TCE, 403K, 400Hz) δ (ppm): 9.36 - 8.94 ppm (br s), 8.13 - 7.44 ppm (br s), 4.77 - 4.03 ppm (br s), 2.44 - 0.52 ppm (br).

3,8-Didodecyl-3,8-dihydroindolo[7,6-*g*]indole-1,2,6,7-tetraone 4.1

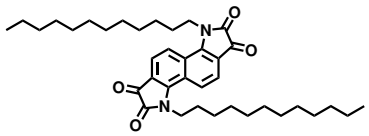

The dark naphthalene naphthalene bisisatin core (1 g, 3.76 mmol), dried K_2CO_3 (4.56 g, 11.26 mmol) were suspended in 10 mL dry DMF and heated to 80 ^{o}C. The reaction was cooled to 60 ^{o}C before 1-bromododecane (2.08 mL, 15.04 mmol) was injected into the reaction. The reaction was heated for 3 hours at 60 ^{o}C. The reaction was quenched by pouring it into water and acidified to pH 7 with aqueous 1 M HCl. The aqueous phase was extracted with DCM dried over $MgSO_4$ and the solvent removed. The brown residue was purified by flash chromatography with 2:3 DCM/petroleum spirit 40 - 60 ^{o}C, followed by recrystallisation in hexane to give blue solid (388 mg, 12.5 % yield). ^{1}H NMR (400 MHz, Chloroform-d) δ (ppm): 7.98 (d, J = 8.7 Hz, 2H, ArH), 7.70 (d, J = 8.7 Hz, 2H, ArH), 4.31-4.20 (m, 4H, NCH_2), 1.91 - 1.77 (m, 4H, NCCH_2), 1.34 - 1.22 (m, 36H, CH_2), 0.94 - 0.83 (m, 6H, CH_3) 13C NMR (101 MHz, $CDCl_3$) d 182.96, 159.18, 152.37, 127.45, 120.41, 119.77, 116.39, 77.16, 68.13, 43.68, 32.05, 29.75, 29.65, 29.60, 29.48, 29.32, 26.82, 25.77, 22.83, 14.26, 0.15. MS (ES^-), m/z M^- found 602.4100.

Polymer P6

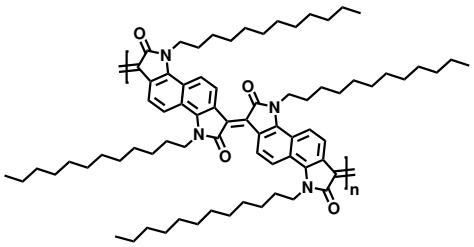

Into an oven dried microwave vial 3,8-didodecyl-3,8-dihydroindolo[7,6-g]indole-1,2,6,7-tetraone (50.00 mg, 0.08 mmol), 3,8-didodecyl-1,3,6,8-tetrahydroindolo[7,6-g]indole-2,7-dione (47.68 mg, 0.08 mmol) and p-toluene sulfonic acid (4.74 mg,0.03 mmol) was loaded. The vial was sealed

and vacated and backfilled with argon three times. Dry toluene (1.5 mL), already degassed for 1 hour, was injected into the vial and the mixture further degassed for 15 minutes. The reaction was heated at 120 ^{o}C for 25 minutes, at which point the polymerisation medium had gelled. Chlorobenzene was introduced into the flask to dissolve the polymer and precipitate it into methanol. Although, the polymer was precipitated into methanol and collected, it was too insoluble for further analysis or device fabrication.

3,8-Dihexadecyl-3,8-dihydroindolo[7,6-*g*]indole-1,2,6,7-tetraone 4.7

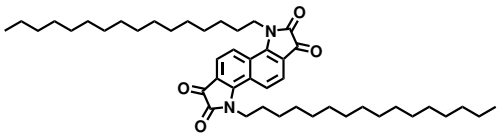

The dark naphthalene naphthalene bisisatin core (1 g, 3.76 mmol), dried K_2CO_3 (4.56 g, 11.26 mmol) were suspended in 10 mL dry DMF and heated to 80 ^{o}C. The reaction was cooled to 60 ^{o}C before 1-bromohexadecane (2.08 mL, 15.04 mmol) was injected into the reaction. The reaction was heated for 3 hours at 60 ^{o}C. The reaction was quenched by pouring it into water and acidified to pH 7 with aqueous 1 M HCl. The aqueous phase was extracted with DCM dried over $MgSO_4$ and the solvent removed. The brown residue was purified by flash chromatography with 2:3 DCM/ petroleum spirit 40 - 60 ^{o}C, followed by recrystallisation in hexane to give blue solid (388 mg, 12.5 % yield). ^{1}H NMR (400 MHz, Chloroform-d) δ (ppm): 7.95 (d, J = 8.7 Hz, 2H, ArH), 7.68 (d, J = 8.6 Hz, 2H, ArH), 4.30 - 4.12 (m, 4H, NCH_2), 1.98 - 1.75 (m, 4H, NCCH_2), 1.51 - 1.39 (m, 4H, NCCCH_2), 1.39 - 1.33 (m, 4H, CH_2), 1.31 - 1.17 (m, 44H, CH_2), 0.93 - 0.84 (m, 6H, CH_3). 13C NMR (101 MHz, $CDCl_3$) d 143.16, 122.09, 77.16, 68.13, 43.00, 36.22, 32.08, 29.85, 29.72, 29.57, 29.52, 29.46, 26.96, 25.78, 22.85, 14.27, 0.15. MS (ES^-), m/z M^- found 714.5322.

3,8-Dihexadecyl-1,3,6,8-tetrahydroindolo[7,6-*g*]indole-2,7-dione 4.8

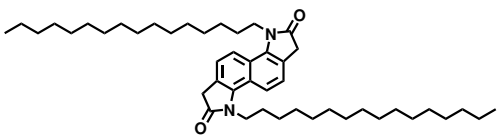

3,8-Dihexadecyl-3,8-dihydroindolo[7,6-g]indole-1,2,6,7-tetraone(150 mg, 0.18 mmol) was suspended in 1 mL dioxane and hydrazine hydrate solution (0.5 mL) and the mixture refluxed for

3 hours in a high pressure vessel at 180 ^{o}C. The aqueous phase was then extracted with DCM three times. The combined organic phase was washed with brine, dried with $MgSO_4$, filtered and the solvent reduced under reduced pressure. The dark orange crude material was purified by column chromatography on Isolera Biotage with a gradient of 10 - 40 % ethyl acetate and petroleum spirit 40 - 60 ^{o}C. The resulting material was recrystallised from ethyl acetate to give beige solid (45 mg, 31 % yield). ^{1}H NMR (400 MHz, Chloroform-d) δ (ppm): 7.93 (d, J = 8.6 Hz, 2H, ArH), 7.40 (d, J = 8.6 Hz, 2H, ArH), 4.37 – 4.13 (m, 4H, NCH_2), 3.67 (s, 4H, ArCH_2/), 1.82 (m, 4H, NCCH_2), 1.39 - 1.49 (m, 4H, NCCCH_2), 1.30 - 1.18 (m, 48H, CH_2), 0.95 – 0.80 (m, 6H, CH_3). ^{13}C NMR (101 MHz, $CDCl_3$) 143.16, 122.09, 68.13, 43.00, 36.22, 32.08, 29.85, 29.72, 29.57, 29.52, 29.46, 26.96, 25.78, 22.85, 14.27. MS (ES^-), m/z M$^-$ found 685.5675.

Polymer P7

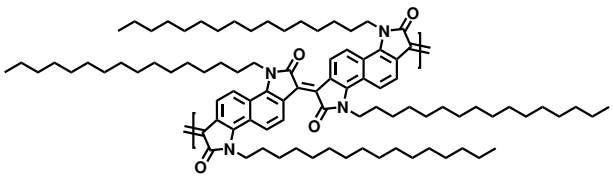

3,8-Dihexadecyl-3,8-dihydroindolo[7,6-g]indole-1,2,6,7-tetraone (50.00 mg, 0.07 mmol), and 3,8-dihexadecyl-1,3,6,8-tetrahydroindolo[7,6-g]indole-2,7-dione (48.04 mg, 0.07 mmol) along with 4.00 mg p-toluene sulfonic acid was charged into a dry microwave vial. The sealed vessel was vacated and backfilled with argon three times before 1.5 mL dry toluene was injected into the vial. The reaction mixture was then degassed for 15 minutes before it was placed in an oil bath at 120 ^{o}C. The reaction was allowed to proceed for 10 minutes before it was cooled rapidly by submerging the vial in water at room temperature. Chlorobenzene was added to the flask to dissolve the polymer to precipitate it in methanol. Successive Soxhlet on the polymer using methanol, acetone, hexane, DCM, chloroform and chlorbenzene. The polymer was extracted in the chlorobenzene fraction to give 61.00 mg purple solid with green sheen, yield 65 %.

3,8-Diicosyl-3,8-dihydroindolo[7,6-*g*]indole-1,2,6,7-tetraone 4.9

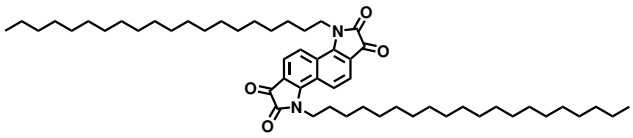

The dark naphthalene 3,8-dihydroindolo[7,6-*g*]indole-1,2,6,7-tetraone solid (1 g, 3.76 mmol), dried K_2CO_3 (4.56 g, 11.26 mmol) were suspended in dry DMF (10 mL) and heated to 80 ^{o}C. The reaction was cooled to 60 ^{o}C before 1-bromoicosane (2.08 mL, 15.04 mmol) was injected into the reaction. The reaction was heated for 3 hours at 60 ^{o}C. The reaction was quenched by pouring it into water and acidified to pH 7 with aqueous 1 M HCl. The aqueous phase was extracted with DCM dried over $MgSO_4$ and the solvent removed. The brown residue was purified by flash chromatography with 2:3 DCM/petroleum spirit 40 - 60 ^{o}C, followed by recrystallisation in hexane to give blue solid (388 mg, 12.5 % yield). ^{1}H NMR (400 MHz, Chloroform-d) δ (ppm): 7.95 (d, J = 8.7 Hz, 2H, ArH), 7.68 (d, J = 8.7 Hz, 2H, ArH), 4.23 (t, J = 7.6 Hz, 4H, NCH_2), 1.89 - 1.76 (m, 4H, NCCH_2), 1.50 - 1.39 (m, 4H, NCCCH_2), 1.38 - 1.14 (m, 64H, CH_2), 0.92 – 0.83 (m, 6H, CH_3). ^{13}C NMR (101 MHz, $CDCl_3$) 32.09, 29.86, 29.77, 29.68, 22.85, 14.28.

3,8-Diicosyl-1,3,6,8-tetrahydroindolo[7,6-*g*]indole-2,7-dione 4.10

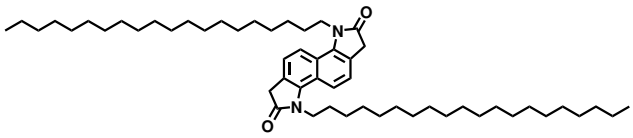

The dark naphthalene 3,8-diicosyl-3,8-dihydroindolo[7,6-*g*]indole-1,2,6,7-tetraone solid (1 g, 3.76 mmol), dried K_2CO_3 (4.56 g, 11.26 mmol) were suspended in dry DMF (10 mL) and heated to 80 ^{o}C. The reaction was cooled to 60 ^{o}C before 1-bromoicosane (2.08 mL, 15.04 mmol) was injected into the reaction. The reaction was heated for 3 hours at 60 ^{o}C. The reaction was quenched by pouring it into water and acidified to pH 7 with aqueous 1 M HCl. The aqueous phase was extracted with DCM dried over $MgSO_4$ and the solvent removed. The brown residue was purified by flash chromatography with 2:3 DCM/petroleum spirit 40 - 60 ^{o}C, followed by recrystallisation in hexane to give blue solid (388 mg, 12.5 % yield). ^{1}H NMR (400 MHz, Chloroform-d) δ (ppm): 7.95 (d, J = 8.4 Hz, 2H, ArH), 7.55 – 7.51 (d, J= 8.5 Hz,

2H, ArH), 4.30 – 4.26 (m, 4H, NCH_2), 3.70 (s, 2H, ArCH_2), 1.32 - 1.12 (m, 72H, CH_2), 0.91 – 0.81 (m, 6H, CH_3). ^{13}C NMR (101 MHz, $CDCl_3$) MS (ES$^+$), m/z M$^+$ found 799.3.

Polymer P8

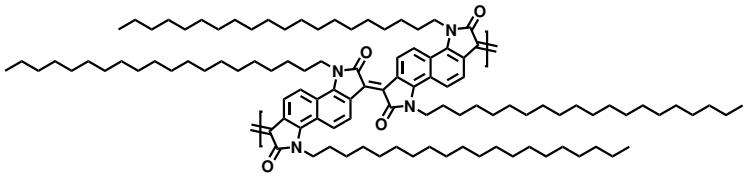

3,8-Diicosyl-3,8-dihydroindolo[7,6-g]indole-1,2,6,7-tetraone (31.05 mg, 0.04 mmol), 3,8-diicosyl-1,3,6,8-tetrahydroindolo[7,6-g]indole-2,7-dione (30.00 mg, 0.04 mmol) along with p-toluene sulfonic acid (2.15 mg, 0.01 mmol) was charged into a dry microwave vial. The sealed vessel was vacated and backfilled with argon three times before dry toluene (1.00 mL) was injected into the vial. The reaction mixture was then degassed for 15 minutes before it was placed in an oil bath at 120 ^{o}C. The reaction was allowed to proceed for 15 minutes before it was cooled rapidly by submerging the vial in water at room temperature. Chlorobenzene was added to the flask to dissolve the polymer to precipitate it in methanol. Successive Soxhlet on the polymer using methanol, acetone, hexane, DCM, chloroform and toluene. The polymer was extracted in the toluene faction to give 49.00 mg purple was isolated from the toluene fraction, yield 84 %.

3,8-Ditetracosyl-3,8-dihydroindolo[7,6-*g*]indole-1,2,6,7-tetraone 4.11

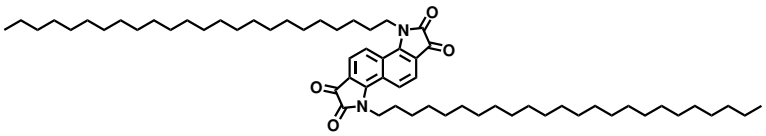

The dark naphthalene 3,8-dihydroindolo[7,6-g]indole-1,2,6,7-tetraone solid (1.00 g, 3.76 mmol), dried K_2CO_3 (4.56 g, 11.26 mmol) were suspended in dry DMF (10 mL) and heated to 80 ^{o}C. The reaction was cooled to 60 ^{o}C before 1-bromotetracosane (2.08 mL, 15.04 mmol) was injected into the reaction. The reaction was heated for 3 hours at 60 ^{o}C. The reaction was quenched by pouring it into water and acidified to pH 7 with aqueous 1 M HCl. The aqueous phase was extracted with DCM dried over $MgSO_4$ and the solvent removed. The brown residue was purified by flash chromatography with 2:3 DCM/petroleum spirit 40 - 60 ^{o}C, followed by recrystallisation in hexane to give blue solid (388 mg, 12.5 % yield). ^{1}H NMR (400 MHz,

Chloroform-d) δ (ppm): 7.95 (d, J = 8.7 Hz, 2H, ArH), 7.68 (d, J = 8.6 Hz, 2H, ArH), 4.34 – 4.11 (m, 4H, NCH_2), 1.87 - 1.76 (m, 4H, NCCH_2), 1.50 - 1.39 (m, 4H, NCCCH_2), 1.39 - 1.16 (m, 80H, CH_2), 0.91 – 0.83 (m, 6H, CH_3). ^{13}C NMR (101 MHz, $CDCl_3$) 127.45, 120.41, 43.68, 32.09, 29.86, 29.68, 29.62, 29.53, 29.33, 26.83, 22.85, 14.28. MS (CI) m/z M^+ found 939.7958.

3,8-Ditetracosyl-1,3,6,8-tetrahydroindolo[7,6-*g*]indole-2,7-dione 4.12

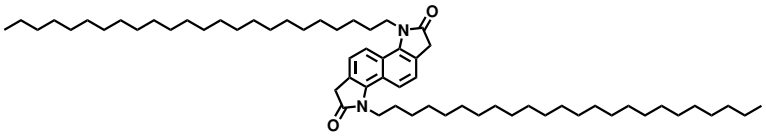

The dark naphthalene 3,8-ditetracosyl-3,8-dihydroindolo[7,6-g]indole-1,2,6,7-tetraone solid (2.50 g, 9.40 mmol), dried K_2CO_3(5.20 g, 38.00 mmol) were suspended in dry DMF (500 mL) and heated to 80 ^{o}C. The reaction was cooled to 60 ^{o}C before 1-bromotetracosane (11.74 g, 28.00 mmol) was injected into the reaction. The reaction was heated for 3 hours at 60 ^{o}C. The reaction was quenched by pouring it into water and acidified to pH 7 with aqueous 1 M HCl. The aqueous phase was extracted with DCM dried over $MgSO_4$ and the solvent removed. The brown residue was purified by flash chromatography with DCM multiple times followed by recrystallisation in DCM to give purple solid (360 mg, 4.1 % yield). ^{1}H NMR (400 MHz, Chloroform-d) δ (ppm): 7.94 (d, J = 8.8 Hz, 2H, ArH), 7.70 (d, J = 8.7 Hz, 2H, ArH), 4.31 (t, J = 7.7 Hz, 4H, NCH_2), 3.73 (s, 4H, NCCH_2), 1.85 (d, J = 7.6 Hz, 4H, NCCCH_2), 1.47 (m, 4H, NCCCCH_2), 1.27 (s, 80H, CCH_2), 0.89 (m, 6H, CH_3). MS (ES^-), m/z, M^+ found 889.7745.

Polymer P9

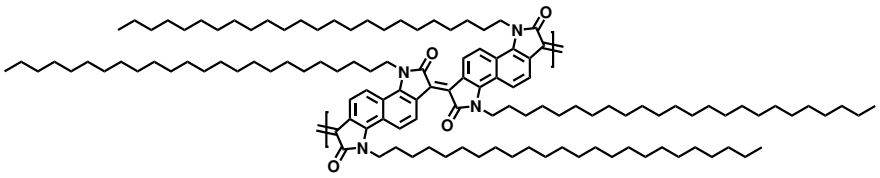

3,8-Ditetracosyl-3,8-dihydroindolo[7,6-g]indole-1,2,6,7-tetraone (39.17 mg, 0.04 mmol) and 3,8-ditetracosyl-1,3,6,8-tetrahydroindolo[7,6-g]indole-2,7-dione (38.00 mg, 0.04 mmol) along with p-toluene sulfonic acid (3.00 mg, 0.02 mmol) was charged into a dry microwave vial. The sealed vessel was vacated and backfilled with argon three times before dry toluene (1.00 mL) was injected into the vial. The reaction mixture was then degassed for 15 minutes before it was

placed in an oil bath at 120 ^{o}C. The reaction was allowed to proceed for 10 minutes before it was cooled rapidly by submerging the vial in water at room temperature. Chlorobenzene was added to the flask to dissolve the polymer to precipitate it in methanol. Successive Soxhlet extraction on the polymer using methanol, acetone, hexane, DCM and chloroform. The polymer was extracted using chloroform to give 54.00 mg purple solid isolated from the toluene fraction, yield 70 %. GPC Mn 11.5 KDa, Mw 16.0 KDa, PD 1.39.

3,7-Dihydrobenzo[1,2-*b*d 4,5-*b*']difuran-2,6-dione 5.2

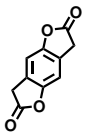

A suspension of 2,2'-(2,5-dihydroxy-1,4-phenylene)diacetic acid (2.00 g, 8.85 mmol) and 20 mL acetic anhydride in toluene (100 mL) was heated at 100 ^{o}C for 5 hours. The reaction was filtered to furnished the desired product 1.27 g, 75 %. ^{1}H NMR (400 MHz, DMSO$-d_6$) d 7.24 (s, 2H, ArH), 3.95 (s, 4H, ArCH_2). 13C NMR (101 MHz, DMSO$-d_6$) d 174.31, 150.10, 123.93, 107.32, 67.00, 39.52, 33.27, 25.11. MS (ES^-), m/z MS^- found 189.0194.

3,8-Bis(5-octylpentadecyl)-3,8-dihydroindolo[7,6-*g*]indole-1,2,6,7-tetraone 5.15

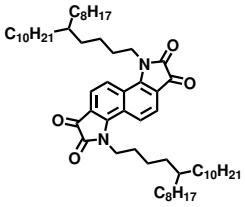

The naphthalene bisisatin core (1.00 g, 3.76 mmol) was dissolved in 12 mL DMF along with K_2CO_3 at 100 ^{o}C for 30 minutes. After this time, the reaction temperature was reduced to 70 ^{o}C and 9-(4-bromobutyl)nonadecane (4.54 g, 11.27 mmol) was introduced into the reaction flask portion-wise. The reaction was stirred for 16 hours at 70 ^{o}C before it was concentrated in a rotary evaporator at high temperatures. Water was added to the residue and the aqueous phase neutralised with 1 M HCl followed by extraction with chloroform. The combined organic phase was washed with brine, dried over $MgSO_4$ and the solvent removed. The brown solid obtained was purified by flash column chromatography in DCM/PE (2:3) eluent. Blue waxy solid (1.2 g) was obtained at 35 % yield. MS (ES^-), m/z M^- found 910.7514.

Polymer P10

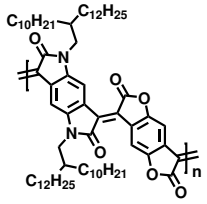

1,5-Bis(2-decyltetradecyl)-1,5-dihydropyrrolo[2,3-*f*]indole-2,3,6,7-tetraone (40 mg, 0.05 mmol) and 3,7-dihydrobenzo[1,2-*b*:4,5-*b'*]difuran-2,6-dione (8.83 mg, 0.05 mmol) and pTsOH (2.8 mg, 0.01 mmol) were charged into to a vial and 1.0 mL dry toluene added to the flask. The solution was degassed for 10 minutes and the vial filled with argon before the reaction mixture was heated to 140 ^{o}C for 48 hours. The resulting viscous solution was precipitated into MeOH, filtered and a Soxhlet extraction performed using acetone, followed by hexane then DCM, hexane/chloroform (2:1), chloroform, each for 2 hours, and then dichlorobenzene for 5 hours. The polymer was not recovered.

Polymer P11

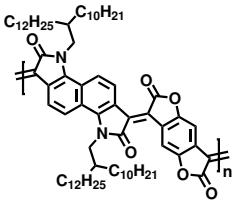

3,8-Bis(2-octyldodecyl)-3,8-dihydroindolo[7,6-*g*]indole-1,2,6,7-tetraone (50.00 mg, 0.06 mmol) and 3,7-dihydrobenzo[1,2-*b*:4,5-*b'*]difuran-2,6-dione (11.49 mg, 0.06 mmol) and p-toluene sulfonic acid (3.45 mg, 0.02 mmol) were loaded into a microwave vial. The sealed system was vacated and backfilled with argon three times. Dry toluene (1 mL) was then injected into the vessel and the mixture degassed for 15 minutes. The reaction was heated at 120 ^{o}C for 16 hours before the reaction matrix was introduced into methanol to precipitate the polymer. Soxhlet extraction of the polymer solid was carried out in methanol, acetone and hexane successively. The polymer was extracted in hexane, the solution reduced to minimum solvent and the polymer re-precipitated in methanol and collected, 46 mg. GPC (Chlorobenzene, 80 ^{o}C): Mn 22.1 KDa, Mw 34.5 KDa, PD 1.56.

Polymer P12

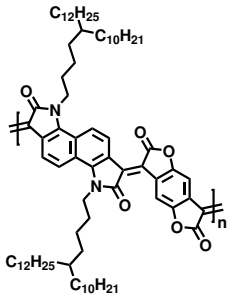

3,8-Bis(5-octylpentadecyl)-3,8-dihydroindolo[7,6-*g*]indole-1,2,6,7-tetraone (50.00 mg, 0.05 mmol) and 3,7-dihydrobenzo[1,2-*b*:4,5-*b'*]difuran-2,6-dione (10.43 mg, 0.05 mmol) and p-toluene sulfonic acid (3.13 mg, 0.02 mmol) were loaded into a microwave vial. The sealed system was vacated and backfilled with argon three times. Dry toluene (1 mL) was then injected into the vessel and the mixture degassed for 15 minutes. The reaction was heated at 120 ^{o}C for 16 hours. The reaction matrix was introduced into methanol to precipitate the polymer. Soxhlet of the polymer solid was carried out in methanol, acetone and hexane successively. The polymer was extracted in hexane, the solution reduced to minimum solvent and the polymer re-precipitated in methanol and collected, 55 mg. GPC (chlorobenzene, 80 ^{o}C): Mn 29.5 KDa, Mw 49.0 KDa, PD 1.66.

2,5-Dibromothieno[3,2-*b*]thiophene 5.4

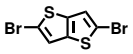

Thieno[3,2-*b*]thiophene (15.0 g, 107.2 mmol) was dissolved in DCM (250 mL) and cooled to 0 ^{o}C before NBS (39.8 g, 225.04 mmol) was added portion-wise to the flask and the reaction was stirred for 16 hours at room temperature. The reaction was quenched with water and the phases separated. The aqueous phase was extracted three times using DCM. The combined organic phase was washed with brine and dried over $MgSO_4$. The solvent was removed under reduced pressure to give brown solid. The solid was recrystallised from ethanol to give pale yellow crystals (23.5 g, 74 %).

3,6-Dibromothieno[3,2-*b*]thiophene 5.5

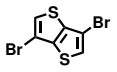

2,5-Dibromothieno[3,2-*b*]thiophene (23.52 g, 79.5 mmol) was suspended in dry THF (620 mL) and cooled to -78 ^{o}C. 2 M LDA (99.4 mL, 198.8 mmol) was added dropwise to the flask and the reaction was stirred at -78 ^{o}C for four hours. The reaction was quenched with cold brine (10 mL) at 0 ^{o}C. The reaction mixture was concentrated on a rotary evaporator and water and diethyl ether added to the flask and the aqueous phase extracted. The combined organic phases were washed with brine and dried over $MgSO_4$ and the solvent was removed in a rotary evaporator to give brown solid (8.63 g, 37 %).

Thieno[3,2-*b*]thiophene-3,6-dicarboxylic acid 5.6

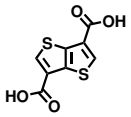

2.5 M nBuLi (10.82 mL, 27.04 mmol) was injected into a lask contining THF (50 mL) at -70 ^{o}C before 3,6-dibromothieno[3,2-*b*]thiophene (4.00 g, 13.5 mmol) dissolved in dry THF (34 mL) was added cautiously into the flask. After 2 hours, crushed carbon dioxide was introduced into the flask and the reaction stirred at room temperature for 16 hours. The reaction was then quenched with water and concentrated in a rotary evaporator. Water and chloroform was added to the flask and the phases separated. The aqueous phase was further extracted with chloroform and the combined phases washed with brine, dried over $MgSO_4$, the salts filtered and the solvent removed under reduced pressure to furnish white solid, yield 67 % ^{1}H NMR (400 MHz, DMSO-d_6) δ (ppm): 13.33 (s, 2H, COO*H*), 8.48 (s, 2H, Ar*H*). ^{13}C NMR (101 MHz, DMSO-d_6) δ (ppm): 163.24, 138.41, 137.69, 126.77. MS (EI^+), *m/z*, M^+ found 228.

Polymer P13

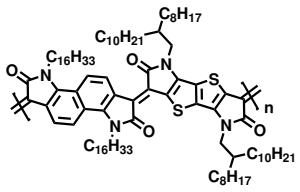

A microwave vial was charged with thieno[3,2-*b*]tjiophene bisisatin (30 mg, 0.04 mmol), 3,8-dihexadecyl-1,3,6,8-tetrahydroindolo[7,6-*g*]indole-2,7-dione (24.56 mg, 0.04 mmol), p-toluene sulfonic acid monohydrate (2.0 mg, 0.01 mmol). The vial was sealed and dry degassed toluene (0.53 mL) injected into it. The reaction was heated at 120 ^oC for 16 hours followed by 16 hours at 140 ^oC. The crude polymer was precipitated in methanol and purified by Soxhlet extraction using methanol, acetone, hexane, dichloromethane and chloroform each in turn. The dichloromethane and chloroform fractions were collected and reduced under vacuum and the polymer precipitated into methanol to give 25 mg and 10 mg respectively. The polymer was filtered and dried. Yield: 35 mg, 66 % dark purple solid. GPC (chlorobenzene, 80 ^oC): Mn 8.3 kDa, Mw 9.0 kDa.

Bibliography

(1) M. Eslamian, *Nano-Micro Letters*, 2016, **9**, 3.

(2) J. Jang, *Materials Today*, 2006, **9**, 46–52.

(3) S. R. Forrest, *Nature*, 2004, **428**, 911–918.

(4) M. Pagliaro, G. Palmisano and R. Ciriminna, *Flexible Solar Cells*, Wiley-VCH Verlag GmbH & Co. KGaA, 2008, pp. 85–106.

(5) C. W. Schlenker and M. E. Thompson, in *Unimolecular and Supramolecular Electronics I: Chemistry and Physics Meet at Metal-Molecule Interfaces*, ed. R. M. Metzger, Springer Berlin Heidelberg, Berlin, Heidelberg, 2012, pp. 175–212.

(6) A. Kitai, T. Davidson-Hall, Y. Kajiyama and H. Aziz, *Organic Light Emitting Device Materials for Displays*, 2017, pp. 1–230.

(7) A. Dodabalapur, *Materials Today*, 2006, **9**, 24–30.

(8) J. T. E. Quinn, J. Zhu, X. Li, J. Wang and Y. Li, *J. Mater. Chem. C*, 2017, **5**, 8654–8681.

(9) M. Chason, P. W. Brazis, J. Zhang, K. Kalyanasundaram and D. R. Gamota, *Proceedings of the IEEE*, 2005, **93**, 1348–1356.

(10) Y.-L. Loo and I. McCulloch, *MRS Bulletin*, 2008, **33**, 653–662.

(11) C. Hilsum, *Philosophical transactions. Series A, Mathematical, physical, and engineering sciences*, 2010, **368**, 1027–1082.

(12) F. M. Insights, *Flat Panel Display Market: Liquid Crystal Display (LCD) Technology Segment Expected to Account for the Highest Market Share of over 85% During the Forecast Period: Global Industry Analysis & Opportunity Assessment 2017 - 2027*.

(13) W. Lee, J. Park, V. Subramanian and H. Takezoe, *Opt. Mater. Express*, 2014, **4**, 1088–1091.

(14) Y. Sun and J. A. Rogers, *Advanced Materials*, 2007, **19**, 1897–1916.

(15) R. A. Street, *Advanced Materials*, 2009, **21**, 2007–2022.

(16) T. Sameshima, *Journal of Non-Crystalline Solids*, 1998, **227-230**, 1196–1201.

(17) A. J. Snell, K. D. Mackenzie, W. E. Spear, P. G. LeComber and A. J. Hughes, *Applied physics*, 1981, **24**, 357–362.

(18) Y. Kuo, *Interface magazine*, 2016, **22**, 55–61.

(19) J. Y. W. Seto, *Journal of Applied Physics*, 1975, **46**, 5247–5254.

(20) W. Xu, H. Li, J. B. Xu and L. Wang, *ACS Applied Materials and Interfaces*, 2018, **10**, 25878–25901.

(21) K. Ide, K. Nomura, H. Hosono and T. Kamiya, *physica status solidi (a)*, 2019, 1800372.

(22) J. Li, Z. Ge, C. Liang and N. An, *Environmental Science and Pollution Research*, 2017, **24**, 16578–16591.

(23) S. velmurugan Manivannan, *Environmental Innovation and Societal Transitions*, 2016, **21**, 69–79.

(24) J. Moltó, S. Egea, J. A. Conesa and R. Font, *Waste Management*, 2011, **31**, 2546–2552.

(25) J. Cao, Y. Chen, B. Shi, B. Lu, X. Zhang, X. Ye, G. Zhai, C. Zhu and G. Zhou, *Journal of Cleaner Production*, 2016, **127**, 311–324.

(26) J. Li, Z. Ge, C. Liang and N. An, *Environmental Science and Pollution Research*, 2017, **24**, 16578–16591.

(27) R. Street, W. Wong, S. Ready, M. Chabinyc, A. Arias, S. Limb, A. Salleo and R. Lujan, *Materials Today*, 2006, **9**, 32–37.

(28) C. Reese, M. Roberts, M.-m. Ling and Z. Bao, *Materials Today*, 2004, **7**, 20–27.

(29) J.-L. Bredas, *Mater. Horiz.*, 2014, **1**, 17–19.

(30) H. C. Longuet-Higgins and L. Salem, *Proceedings of the Royal Society of London. Series A.*, 1959, **251**, 172–185.

(31) A. R. Murphy and J. M. J. Fréchet, *Chemical Reviews*, 2007, **107**, 1066–1096.

(32) A. Facchetti, *Materials Today*, 2007, **10**, 28–37.

(33) F. Lipsett and D. A. J., *Nature*, 1954, **173**.

(34) Z. Rang, A. Haraldsson, D. M. Kim, P. P. Ruden, M. I. Nathan, R. J. Chesterfield and C. D. Frisbie, *Applied Physics Letters*, 2001, **79**, 2731–2733.

(35) H. Klauk, D. J. Gundlach, J. A. Nichols and T. N. Jackson, *IEEE Transactions on Electron Devices*, 1999, **46**, 1258–1263.

(36) G. Horowitz, D. Fichou, X. Peng and F. Garnie, *Synthetic Metals*, 1991, **41**, Proceedings of the International Conference on Science and Technology of Synthetic Metals (ICSM '90), 1127–1130.

(37) Y.-Y. Lin, D. J. Gundlach, S. F. Nelson and T. N. Jackson, *IEEE Electron Device Letters*, 1997, **18**, 606–608.

(38) T. Minakata, H. Imai and M. Ozaki, *Journal of Applied Physics*, 1992, **72**, 4178–4182.

(39) T. Minakata, M. Ozaki and H. Imai, *Journal of Applied Physics*, 1993, **74**, 1079–1082.

(40) G. Turkoglu, M. E. Cinar and T. Ozturk, *Topics in Current Chemistry*, 2017, **375**, 84.

(41) F. Garnier, A. Yassar, R. Hajlaoui, G. Horowitz, F. Deloffre, B. Servet, S. Ries and P. Alnot, *J. Am. Chem. Soc.*, 1993, **115**.

(42) G. Barnes, C. P. Yau and M. Heeney, in *Encyclopedia of Polymeric Nanomaterials*, ed. S. Kobayashi and K. Müllen, Springer Berlin Heidelberg, Berlin, Heidelberg, 2015, pp. 1721–1734.

(43) M. Heeney and I. McCulloch, in *Flexible Electronics: Materials and Applications*, ed. A. Wong, William S.and Salleo, Springer US, Boston, MA, 2009, pp. 261–296.

(44) C. L. Chochos and S. A. Choulis, *Progress in Polymer Science*, 2011, **36**, 1326–1414.

(45) I. McCulloch, M. Heeney, C. Bailey, K. Genevicius, I. MacDonald, M. Shkunov, D. Sparrowe, S. Tierney, R. Wagner, W. Zhang, M. L. Chabinyc, R. J. Kline, M. D. McGehee and M. F. Toney, *Nature Materials*, 2006, **5**, 328–333.

(46) E. Lim, Y. M. Kim, J.-I. Lee, B.-J. Jung, N. S. Cho, J. Lee, L.-M. Do and H.-K. Shim, *Journal of Polymer Science Part A: Polymer Chemistry*, 2006, **44**, 4709–4721.

(47) J. Veres, S. Ogier, G. Lloyd and D. de Leeuw, *Chem. Mater.*, 2004, **16**.

(48) J. Choi, H. Song, N. Kim and F. S. Kim, 2015.

(49) I. Kaur, W. Jia, R. P. Kopreski, S. Selvarasah, M. R. Dokmeci, C. Pramanik, McGruer, N. E. and G. P. Miller, *J. Am. Chem. Soc.*, 2008, **107**, 16274–16286.

(50) L.-L. Chua, J. Zaumseil, J.-F. Chang, E. C.-W. Ou, P. K.-H. Ho, H. Sirringhaus and R. H. Friend, *Nature*, 2005, **434**.

(51) M.-H. Yoon, C. Kim, A. Facchetti and T. J. Marks, *J. Am. Chem. Soc.*, 2006, **128**, DOI: 10.1021/ja063290d.

(52) A. Facchetti, M. Mushrush, H. Katz and T. Marks, *Advanced Materials*, 2003, **15**, 33–38.

(53) A. Facchetti, M. Mushrush, M.-H. Yoon, G. R. Hutchison, M. A. Ratner and T. J. Marks, *J. Am. Chem. Soc.*, 2004, **126**.

(54) H. Usta, A. Facchetti and T. J. Marks, *Accounts of Chemical Research*, 2011, **44**, 501–510.

(55) A. Facchetti, Y. Deng, A. Wang, Y. Koide, H. Sirringhaus, T. J. Marks and R. H. Friend, *Angewandte Chemie International Edition*, 2000, **39**, 4547–4551.

(56) T. Uchida and H. Akamatu, *Bulletin of the Chemical Society of Japan*, 1961, **34**, 1015–1020.

(57) J. R. Ostrick, A. Dodabalapur, L. Torsi, A. J. Lovinger, E. W. Kwock, T. M. Miller, M. Galvin, M. Berggren and H. E. Katz, *J. Appl. Phys.*, 1997, **81**, 6804–6808.

(58) P. R. L. Malenfant, C. D. Dimitrakopoulos, J. D. Gelorme, L. L. Kosbar, T. O. Graham, A. Curioni and W. Andreoni, *Applied Physics Letters*, 2002, **80**, 2517–2519.

(59) R. J. Chesterfield, J. C. McKeen, C. R. Newman, C. D. Frisbie, P. C. Ewbank, K. R. Mann and L. L. Miller, *Journal of Applied Physics*, 2004, **95**, 6396–6405.

(60) A. Rademacher, S. Märkle and H. Langhals, *Chemische Berichte*, 1982, **115**, 2927–2934.

(61) H. E. Katz, J. Johnson, A. J. Lovinger and W. Li, *J. Am. Chem. Soc.*, 2000, **122**.

(62) R. C. Haddon, A. S. Perel, R. C. Morris, T. T. M. Palstra, A. F. Hebard and R. M. Fleming, *Applied Physics Letters*, 1995, **67**, 121–123.

(63) A. Babel and S. A. Jenekhe, *J. Am. Chem. Soc.*, 2003, **125**.

(64) L. E. Chaar, L. lamont and N. E. Zein, *Renewable and Sustainable Energy Reviews*, 2011, **15**, 2165–2175.

(65) R. G. Arns, *Engineering Science and Education Journal*, 1998, **7**, 233–240.

(66) A. Sharma, C. Madhu and J. Singh, *International Journal of Computer Applications*, 2014, **89**, 36–40.

(67) J. Zaumseil and H. Sirringhaus, *Chemical Reviews*, 2007, **107**, 1296–1323.

(68) M. Mas-Torrent and C. Rovira, *Chem. Soc. Rev.*, 2008, **37**, 827–838.

(69) D. Braga and G. Horowitz, *Adv. Mater.*, 2009, **21**, 1473–1486.

(70) C. R. Newman, C. D. Frisbie, D. A. da Silva Filho, J.-L. Brédas, P. C. Ewbank and K. R. Mann, *Chemistry of Materials*, 2004, **16**, 4436–4451.

(71) *Physics of Organic Semiconductors*, ed. W. Brütting, Wiley-VCH, 2005, pp. 1–4.

(72) J.-L. Brédas, D. Beljonne, V. Coropceanu and J. Cornil.

(73) Elmundomike, *English Wikipedia*, Transferred from en.wikipedia to Commons by Gustavocarra., Public Domain, Accessed 18/01/2020.

(74) F. L. J. Vos, D. Aalberts and W. Saarloos, *Physical review. B, Condensed matter*, 1996, **53**, 14922–14928.

(75) A. Heeger, S. Kivelson, J. Schrieffer and W. Su, *Rev. Mod. Phys. 60*, 1988, **60**, 781.

(76) J. S. W.P. Su and A. Heeger, *Physical Review B*, 1980, **22**.

(77) J. S. W.P. Su and A. Heeger, *Physical Review Letters*, 1979, **42**.

(78) I. Botiz and N. Stingelin, *Materials*, 2014, **7**, 2273–2300.

(79) A. a. Virkar, S. Mannsfeld, Z. Bao and N. Stingelin, *Advanced Materials*, 2010, **22**, 3857–3875.

(80) S. Himmelberger, D. T. Duong, J. E. Northrup, J. Rivnay, F. P. V. Koch, B. S. Beckingham, N. Stingelin, R. A. Segalman, S. C. B. Mannsfeld and A. Salleo, *Advanced Functional Materials*, 2015, **25**, 2616–2624.

(81) S. Thankaraj Salammal, J. Chen, F. Ullah and H. Chen, *Journal of Inorganic and Organometallic Polymers and Materials*, 2014, **25**, 12–26.

(82) D. J. Crouch, P. J. Skabara, M. Heeney, I. McCulloch, D. Sparrowe, S. J. Coles and M. B. Hursthouse, *Macromol. Rapid Commun.*, 2008, **29**.

(83) J. Lewis, *Materials Today*, 2006, **9**, 38–45.

(84) S. Y. Son, G.-Y. Lee, S. Kim, W.-T. Park, S. A. Park, Y.-Y. Noh and T. Park, *ACS Applied Materials & Interfaces*, 2019, **11**, 10751–10757.

(85) F. Garnier, *Chem. Phys.*, 1998, **227**, 253–262.

(86) A. Dodabalapur, L. Torsi and H. E. Katz, *Science*, 1995, **268**, 270–271.

(87) M. G. R. Turbiez, R. A. J. Janssen, W. M. Maria, K. H. Juerg, D. Mathias, T. Bernd and Z. Yu, 2008.

(88) C. B. Nielsen, M. Turbiez and I. McCulloch, *Advanced Materials*, 2013, **25**, 1859–1880.

(89) L. Chen, D. Deng, Y. Nan, M. Shi, P. K. L. Chan and H. Chen, *The Journal of Physical Chemistry C*, 2011, **115**, 11282–11292.

(90) X. Zhang, L. J. Richter, D. M. DeLongchamp, R. J. Kline, M. R. Hammond, I. McCulloch, M. Heeney, R. S. Ashraf, J. N. Smith, T. D. Anthopoulos, B. Schroeder, Y. H. Geerts, D. A. Fischer and M. F. Toney, *J. Am. Chem. Soc.*, 2011, **133**, 15073–15084.

(91) P. Sonar, S. P. Singh, Y. Li, Z.-E. Ooi, T.-j. Ha, I. Wong, M. S. Soh and A. Dodabalapur, *Energy Environ. Sci.*, 2011, **4**, 2288–2296.

(92) F. P. V. Koch, J. Rivnay, S. Foster, C. Müller, J. M. Downing, E. Buchaca-Domingo, P. Westacott, L. Yu, M. Yuan, M. Baklar, Z. Fei, C. Luscombe, M. A. McLachlan, M. Heeney, G. Rumbles, C. Silva, A. Salleo, J. Nelson, P. Smith and N. Stingelin, *Progress in Polymer Science*, 2013, **38**, 1978–1989.

(93) T. Maugard, E. Enaud, P. Choisy and M. D. Legoy, *Phytochemistry*, 2001, **58**, 897–904.

(94) T. Mohn, I. Plitzko and M. Hamburger, *Phytochemistry*, 2009, **70**, 924–934.

(95) M. Sassatelli, F. Bouchikhi, S. Messaoudi, F. Anizon, E. Debiton, C. Barthomeuf, M. Prudhomme and P. Moreau, *European Journal of Medicinal Chemistry*, 2006, **41**, 88–100.

(96) F. Bouchikhi, F. Anizon and P. Moreau, *European Journal of Medicinal Chemistry*, 2008, **4**, 755–762.

(97) Q. Yue, Y. Wang, L. Hai, L. Guo, H. Yin and Y. Wu, *Synlett*, 2016, **27**.

(98) X. Wang, L. Wu, P. Yang, X.-J. Song, H.-X. Ren, L. Peng and L.-X. Wang, *Organic Letters*, 2017, **19**, 3051–3054.

(99) R. Stalder, J. Mei and J. R. Reynolds, *Macromolecules*, 2010, **43**, 8348–8352.

(100) E. Wang, W. Mammo and M. R. Andersson, *Advanced materials (Deerfield Beach, Fla.)*, 2014, **26**, 1801–26.

(101) Y. K. Voronina, D. B. Krivolapov, A. V. Bogdanov, V. F. Mironov and I. A. Litvinov, *Journal of Structural Chemistry*, 2012, **53**, 413–416.

(102) X. Guo, A. Facchetti and T. J. Marks, *Chemical reviews*, 2014, **114**, 8943–9021.

(103) T. Lei, Y. Cao, X. Zhou, Y. Peng, J. Bian and J. Pei, *Chemistry of Materials*, 2012, **24**, 1762–1770.

(104) T. Lei, J.-H. Dou, Z.-J. Ma, C.-J. Liu, J.-Y. Wang and J. Pei, *Chemical Science*, 2013, **4**, 2447.

(105) M. L. Tang and Z. Bao, *Chemistry of Materials*, 2011, **23**, 446–455.

(106) T. Lei, J.-y. Wang and J. Pei, *Accounts of Chemical Research*, 2014, **47**, 1117–1126.

(107) T. Lei, J.-H. Dou and J. Pei, *Advanced Materials*, 2012, **24**, 6457–61.

(108) X. Guo, Q. Liao, E. F. Manley, Z. Wu, Y. Wang, W. Wang, T. Yang, Y. E. Shin, X. Cheng, Y. Liang, L. X. Chen, K. J. Baeg, T. J. Marks and X. Guo, *Chemistry of Materials*, 2016, **28**, 2449–2460.

(109) Y. Deng, Y. Chen, X. Zhang, H. Tian, C. Bao, D. Yan, Y. Geng and F. Wang, *Macromolecules*, 2012, **45**, 8621–8627.

(110) I. Osaka, T. Abe, S. Shinamura and K. Takimiya, *Journal of the American Chemical Society*, 2011, **133**, 6852–6860.

(111) O. Knopfmacher, M. L. Hammock, A. L. Appleton, G. Schwartz, J. Mei, T. Lei, J. Pei and Z. Bao, *Nature communications*, 2014, **5**, 2954.

(112) I. Meager, M. Nikolka, B. C. Schroeder, C. B. Nielsen, M. Planells, H. Bronstein, J. W. Rumer, D. I. James, R. S. Ashraf, A. Sadhanala, P. Hayoz, J.-C. Flores, H. Sirringhaus and I. McCulloch, *Advanced Functional Materials*, 2014, **24**, 7109–7115.

(113) S. Xu, N. Ai, J. Zheng, N. Zhao, Z. Lan, L. Wen, X. Wang, J. Pei and X. Wan, *RSC Adv.*, 2014, **5**, 8340–8344.

(114) R. R. Dasari, A. Dindar, C. K. Lo, C.-Y. Wang, C. Quinton, S. Singh, S. Barlow, C. Fuentes-Hernandez, J. R. Reynolds, B. Kippelen and S. R. Marder, *Physical Chemistry Chemical Physics*, 2014, **16**, 19345–19350.

(115) J. Lee, A. J. Kalin, T. Yuan, M. Al-Hashimi and L. Fang, *Chem. Sci.*, 2017, **8**, 2503–2521.

(116) R. L. Van Deusen, *Journal of Polymer Science Part B: Polymer Letters*, 1966, **4**, 211–214.

(117) G. Grem and G. Leising, *Synthetic Metals*, 1993, **57**, 4105–4110.

(118) P. Prins, F. C. Grozema, J. M. Schins, S. Patil, U. Scherf and L. D. A. Siebbeles, *Phys. Rev. Lett.*, 2006, **96**, 146601.

(119) A. L. Briseno, S. C. B. Mannsfeld, P. J. Shamberger, F. S. Ohuchi, Z. Bao, S. A. Jenekhe and Y. Xia, *Chemistry of Materials*, 2008, **20**, 4712–4719.

(120) A. L. Briseno, F. S. Kim, A. Babel, Y. Xia and S. A. Jenekhe, *J. Mater. Chem.*, 2011, **21**, 16461–16466.

(121) N. Wang, A. Yang, Y. Fu, Y. Li and F. Yan, *Accounts of Chemical Research*, 2019, **52**, 277–287.

(122) J. Rumer, Ph.D. Thesis, Imperial College London, 2014.

(123) J. W. Rumer, S. Y. Dai, M. Levick, L. Biniek, D. J. Procter and I. McCulloch, *Journal of Polymer Science, Part A: Polymer Chemistry*, 2013, **51**, 1285–1291.

(124) I. Meager, M. Nikolka, B. C. Schroeder, C. B. Nielsen, M. Planells, H. Bronstein, J. W. Rumer, D. I. James, R. S. Ashraf, A. Sadhanala, P. Hayoz, J.-C. Flores, H. Sirringhaus and I. McCulloch, *Advanced Functional Materials*, 2014, **24**, 7109–7115.

(125) J. W. Rumer, B. C. Schroeder, C. B. Nielsen, R. S. Ashraf, D. Beatrup, H. Bronstein, S. J. Cryer, J. E. Donaghey, S. Holliday, M. Hurhangee, D. I. James, S. Lim, I. Meager, W. Zhang and I. McCulloch, *Thin Solid Films*, 2014, **560**, 82–85.

(126) J. W. Rumer, S.-Y. Dai, M. Levick, Y. Kim, M.-B. Madec, R. S. Ashraf, Z. Huang, S. Rossbauer, B. Schroeder, L. Biniek, S. E. Watkins, T. D. Anthopoulos, R. a. J. Janssen, J. R. Durrant, D. J. Procter and I. McCulloch, *Journal of Materials Chemistry C*, 2013, **1**, 2711.

(127) J. W. Rumer, M. Levick, S.-Y. Dai, S. Rossbauer, Z. Huang, L. Biniek, T. D. Anthopoulos, J. R. Durrant, D. J. Procter and I. McCulloch, *Chemical communications (Cambridge, England)*, 2013, **49**, 4465–7.

(128) A. V. Bogdanov, V. F. Mironov, L. I. Musin, R. Z. Musin, D. B. Krivolapov and I. a. Litvinov, *Monatshefte für Chemie - Chemical Monthly*, 2010, **142**, 81–85.

(129) L. A. Kayukova, P. K. D., V. G. Gut'yar and G. P. Baitursynova, *Russian Journal of Organic Chemistry*, 2015, **51**, 148–160.

(130) G. Kollenz, G. Penn, R. Theuer, W. M. Fabian, H. A. Abd El-Nabi, X. Zhang, K. Peters, E. M. Peters and H. G. Von Schnering, *Tetrahedron*, 1996, **52**, 5427–5440.

(131) R. Shahid, A. Jisk, D. I. James, H. Sirringhaus, R. S. Ashraf, A. J. Kronemeijer, D. I. James, H. Sirringhaus and I. McCulloch, *Chemical communications (Cambridge, England)*, 2012, **48**, 3939–41.

(132) *Ann. Phys. Chem. Ser. 2*, 1838, **44**, 475.

(133) *J. Prakt. Chem.*, 1838, **15**, 129.

(134) Z. Wang, *Sandmeyer Isatin Synthesis*, American Cancer Society, 2010, ch. 557, pp. 2467–2470, 45–51.

(135) E. by Rainer Mahrwald, *Modern Aldol Reactions, Vol. 1: Enolates, Organocatalysis, Biocatalysis and Natural Product Synthesis.* WILEY-VCH Verlag GmbH & Co. KGaA, 2004.

(136) M. T. Casale, A. R. Richman, M. J. Elrod, R. M. Garland, M. R. Beaver and M. A. Tolbert, *Atmospheric Environment*, 2007, **41**, 6212–6224.

(137) S. Lippert, W. Baumann and K. Thomke, *Journal of Molecular Catalysis*, 1991, **69**, 199–214.

(138) J. Mei, Y. Diao, A. L. Appleton, L. Fang, Z. Bao and A. L. Appleton, 2013, DOI: 10.1021/ja400881n.

(139) A. J. Mancuso, S.-L. Huang and D. Swern, *The Journal of Organic Chemistry*, 1978, **43**, 2480–2482.

(140) K. Omura and D. Swern, *Tetrahedron*, 1978, **34**, 1651–1660.

(141) A. J. Mancuso, D. S. Brownfain and D. Swern, *The Journal of Organic Chemistry*, 1979, **44**, 4148–4150.

(142) M. Miller, J. C. Vogel, W. Tsang, A. Merrit and D. J. Procter, *Organic & Biomolecular Chemistry*, 2009, **7**, 589–597.

(143) M. Miller, W. Tsang, A. Merritt and D. J. Procter, *Chem. Commun.*, 2007, 498–500.

(144) V. Cornel and C. J. Lovely, in *Encyclopedia of Reagents for Organic Synthesis*, American Cancer Society, 2007, ch. Boron Trifluoride Etherate, pp. 1–16.

(145) W. Cui and F. Wudl, 2013, **46**, 7232–7238.

(146) L. T. Higham, K. Konno, J. L. Scott, R. Strauss and T. Yamaguchi, 2007, **9**, 80–84.

(147) N. J. Leonard and R. R. Sauers, 1956, **21**, 1187–1188.

(148) E. J. Hennessy and S. L. Buchwald, *Journal of the American Chemical Society*, 2003, **125**, 12084–5.

(149) O. L. Erdmann, *Journal für Praktische Chemie*, 1840, **19**, 321–362.

(150) A. Laurent, *Annales de chimie et de physique*, 1840, **3**, 393–434.

(151) S. Nain, *Medicinal Chemistry*, 2014, **4**, 417–427.

(152) A. V. Kurkin, A. A. Bernovskaya and M. A. Yurovskaya, 2011, **46**, 1208–1214.

(153) T. Sandmeyer, *Helvetica Chimica Acta*, 1919, **2**, 234–242.

(154) P. Sharma, D. Thummuri, T. S. Reddy, K. R. Senwar, V. Naidu, G. Srinivasulu, S. K. Bharghava and N. Shankaraiah, *European Journal of Medicinal Chemistry*, 2016, **122**, 584–600.

(155) B. V. Silva, F. A. Violante, A. C. Pinto and L. S. Santos, *Rapid Communications in Mass Spectrometry*, 2011, **25**, 423–428.

(156) S. J. Garden, J. C. Torres, A. A. Ferreira, R. B. Silva and A. C. Pinto, *Tetrahedron Letters*, 1997, **38**, 1501–1504.

(157) N. M. Randell, P. C. Boutin and T. L. Kelly, *Journal of Materials Chemistry A*, 2016, **4**, 6940–6945.

(158) A. Zen, J. Pflaum, S. Hirschmann, W. Zhuang, F. Jaiser, U. Asawapirom, J. P. Rabe, U. Scherf and D. Neher, *Advanced Functional Materials*, 2004, **14**, 757–764.

(159) R. Kline, M. McGehee, E. Kadnikova, J. Liu and J. Fréchet, *Advanced Materials*, 2003, **15**, 1519–1522.

(160) R. J. Kline, M. D. McGehee, E. N. Kadnikova, J. Liu, J. M. J. Fréchet and M. F. Toney, *Macromolecules*, 2005, **38**, 3312–3319.

(161) R. Zhang, B. Li, M. C. Iovu, M. Jeffries-EL, G. Sauvé, J. Cooper, S. Jia, S. Tristram-Nagle, D. M. Smilgies, D. N. Lambeth, R. D. McCullough and T. Kowalewski, *Journal of the American Chemical Society*, 2006, **128**, 3480–3481.

(162) D. Venkateshvaran, M. Nikolka, A. Sadhanala, V. Lemaur, M. Zelazny, M. Kepa, M. Hurhangee, A. J. Kronemeijer, V. Pecunia, I. Nasrallah, I. Romanov, K. Broch, I. McCulloch, D. Emin, Y. Olivier, J. Cornil, D. Beljonne and H. Sirringhaus, *Nature*, 2014, **515**, 384–388.

(163) J. Mei and Z. Bao, *Chemistry of Materials*, 2014, **26**, 604–615.

(164) P. Keg, A. Lohani, D. Fichou, Y. M. Lam, Y. Wu, B. S. Ong and S. G. Mhaisalkar, *Macromolecular Rapid Communications*, 2008, **29**, 1197–1202.

(165) W. P. Hsu, K. Levon, K. S. Ho, A. S. Myerson and T. K. Kwei, *Macromolecules*, 1993, **26**, 1318–1323.

(166) I. Kang, H.-J. Yun, D. S. Chung, S.-K. Kwon and Y.-H. Kim, *Journal of the American Chemical Society*, 2013, **135**, 14896–14899.

(167) N. J. Kishner, *J. Russ. Phys. Chem. Soc.*, 1911, **43**, 582–595.

(168) L. Wolff, *Justus Liebig's Annalen der Chemie.*, 1912, **394**, 86–108.

(169) J.-H. Dou, Y.-Q. Zheng, Z.-F. Yao, T. Lei, X. Shen, X.-Y. Luo, Z.-A. Yu, S.-D. Zhang, G. Han, Z. Wang, Y. Yi, J.-Y. Wang and J. Pei, *Advanced Materials*, 2015, **27**, 8051–8055.

(170) B. Fu, J. Baltazar, A. R. Sankar, P.-H. Chu, S. Zhang, D. M. Collard and E. Reichmanis, *Advanced Functional Materials*, 2014, **24**, 3734–3744.

(171) S. D. Oosterhout, V. Savikhin, J. Zhang, Y. Zhang, M. A. Burgers, S. R. Marder, G. C. Bazan and M. F. Toney, *Chemistry of Materials*, 2017, **29**, 3062–3069.

Chapter 8

Appendix

8.1 Appendix 1

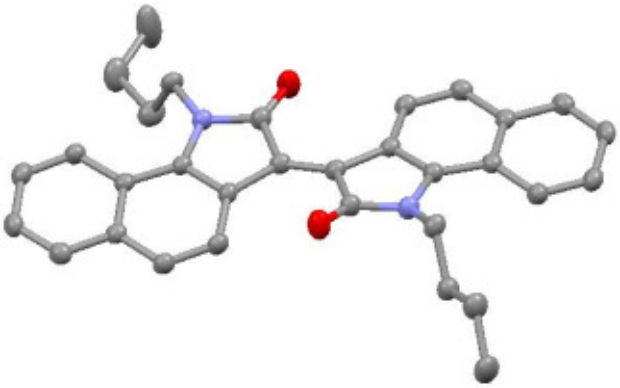

Crystal structure of a naphthalene isoindigo. The dihedral angle across the bridging double bond is 12.8^o.

$Crystaldata : C_{32}H_{30}N_2O_2, triclinicP-1, a : 15.3052(5)$ Å, $b : 15.3815(4)$ Å, $c : 21.1879(6)$ Å, $\alpha : 89.021(2)^o, \beta : 82.798(2)^o, \gamma : 76.127(2)^o, cellvolume : 4803.8(2)$ Å3. $REMR1_all = 0.0974, REMR1_gt = 0.0845, REMwR_ref = 0.2444, REMGOOF = 1.063.$

8.2 Appendix 2

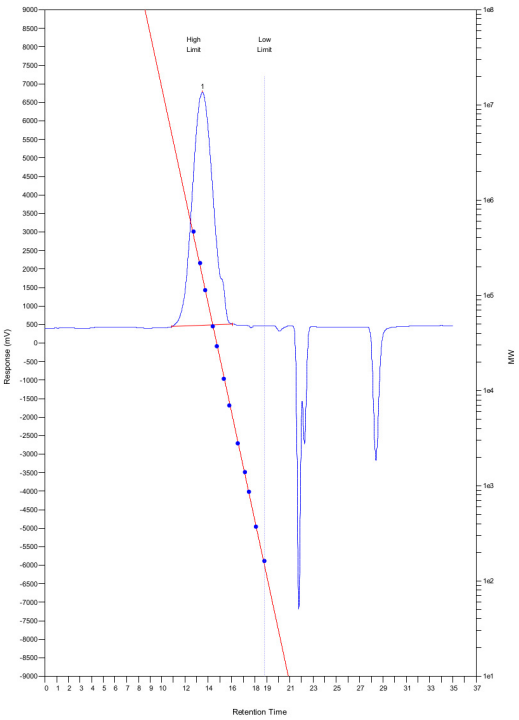

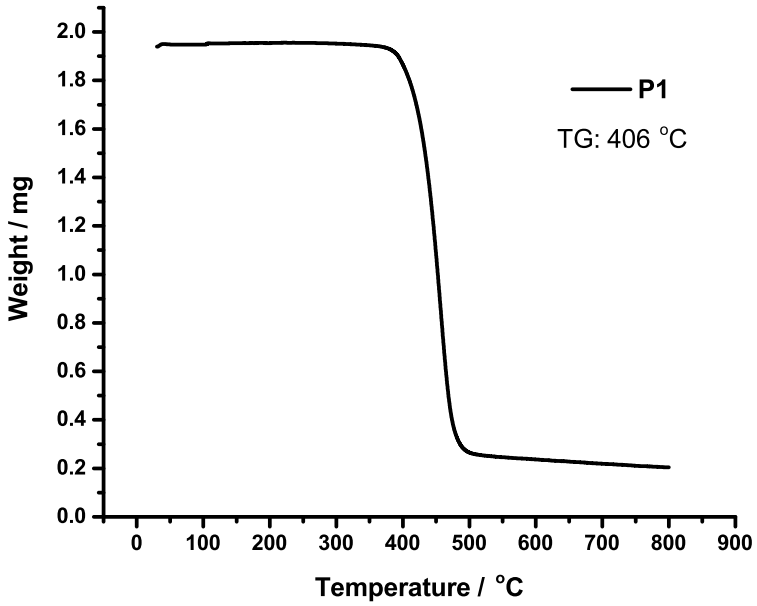

GPC trace of polymer P1 (top) it's TGA trace (bottom) of the polymer, showing 5 % weight loss at 406 ^oC.

8.3 Appendix 3

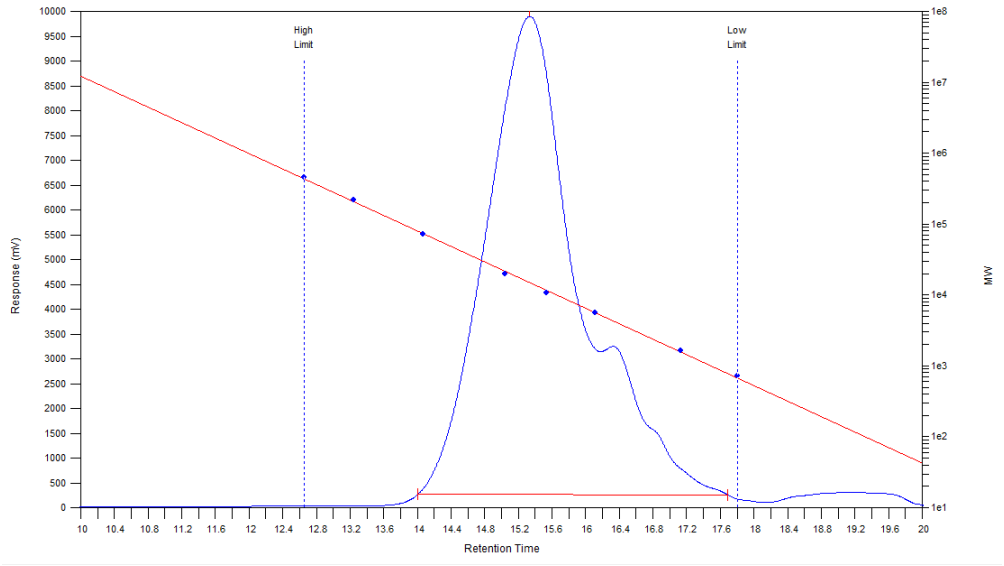

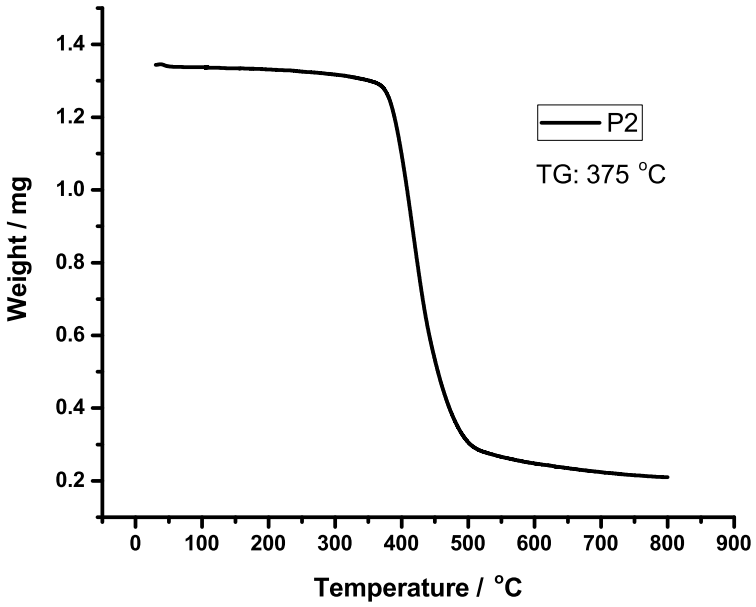

GPC trace of polymer P2 (top) carried out in chlorobenzene at 80 ^oC and the TGA trace of the polymer (bottom), showing 5 % weight loss at 375 ^oC.

8.4 Appendix 4

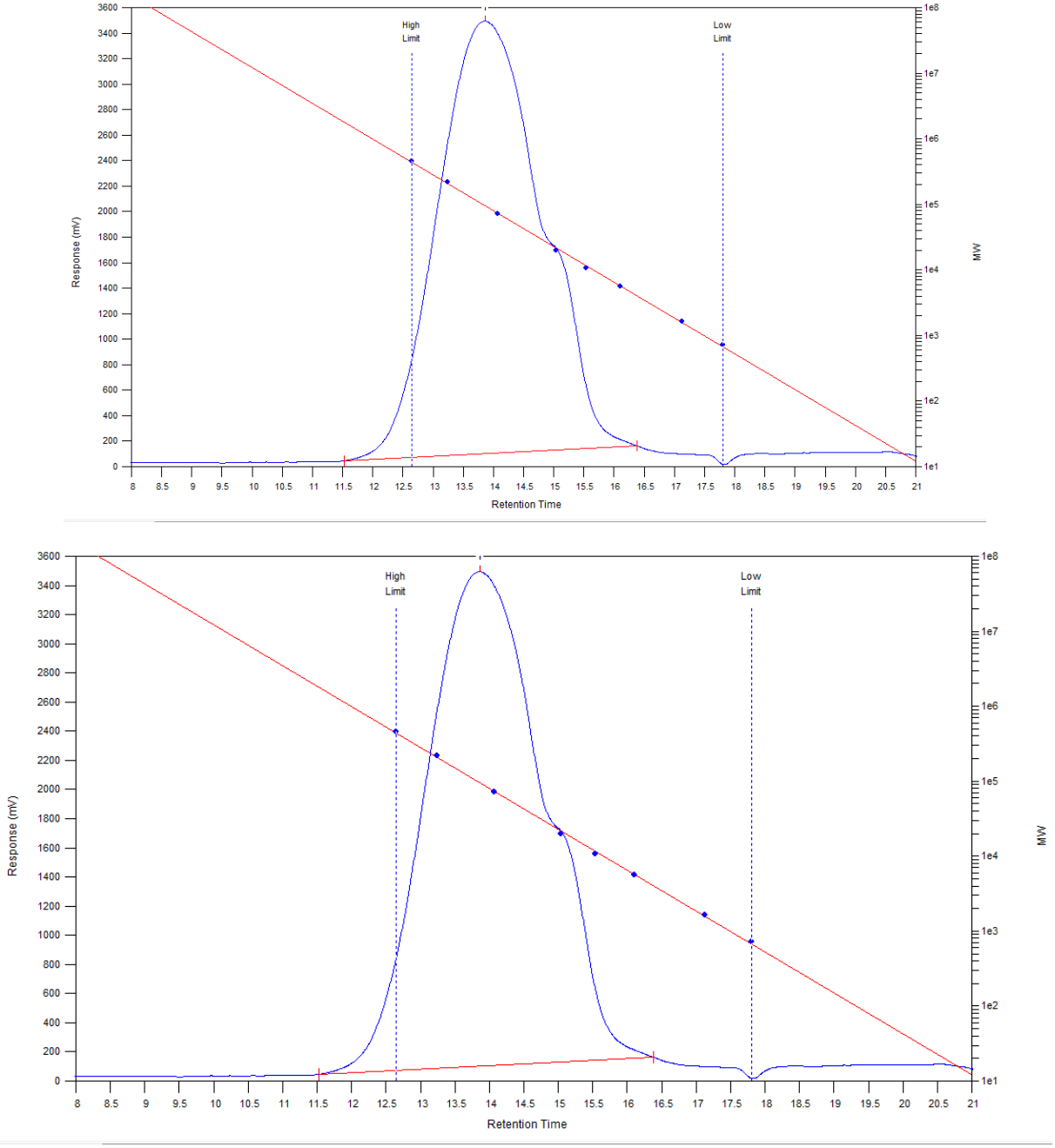

GPC trace of polymer P3 (top) carried out in chlorobenzene at 80 ^oC and the TGA trace of the polymer(bottom).

8.5 Appendix 5

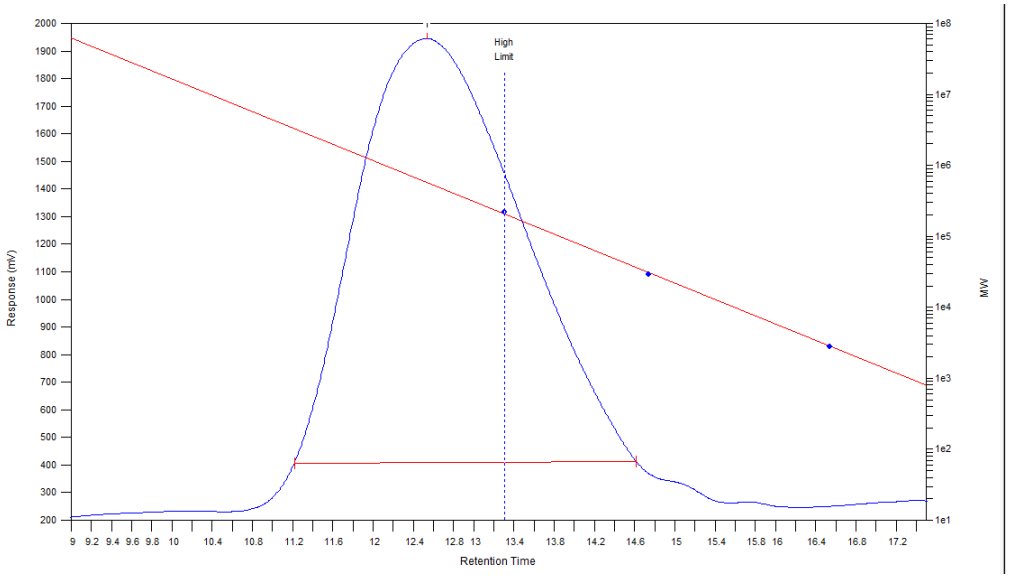

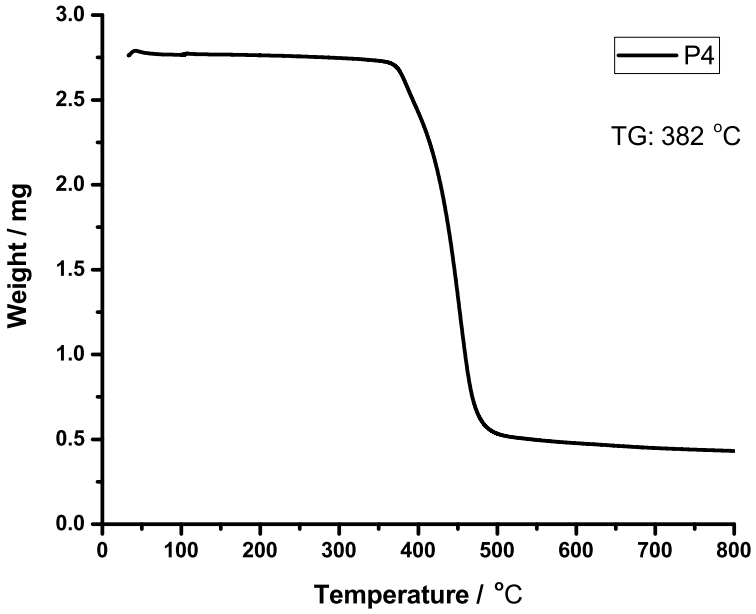

GPC trace of polymer P4 (top) carried out in chlorobenzene at 80 ^oC and the TGA trace of the polymer (bottom), showing 5 % weight loss at 382 ^oC.

8.6 Appendix 6

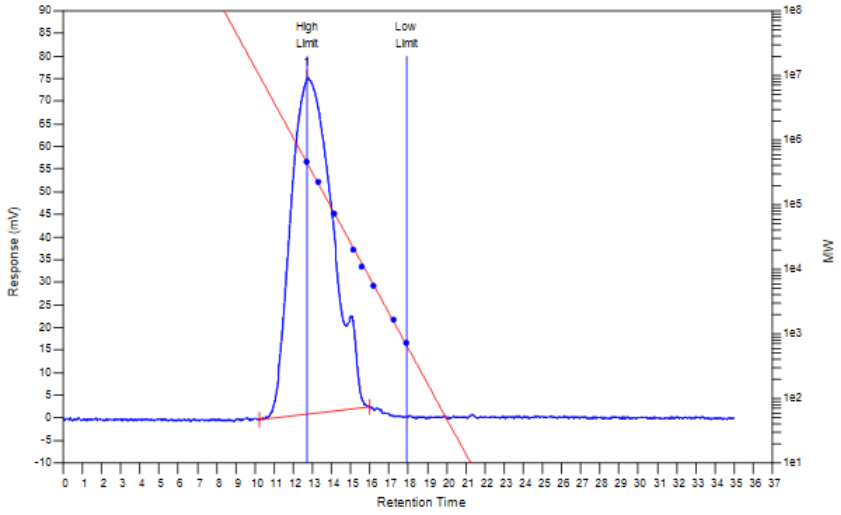

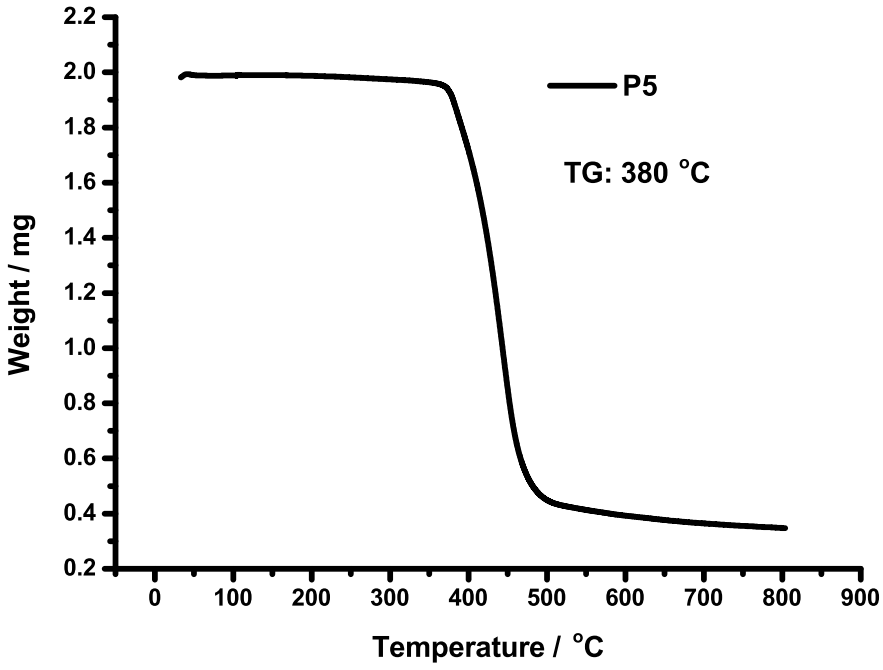

GPC trace of polymer P5 (top) carried out in chlorobenzene at 80 ^oC and the TGA trace of the polymer (bottom), showing 5 % weight loss at 380 ^oC.

8.7 Appendix 7

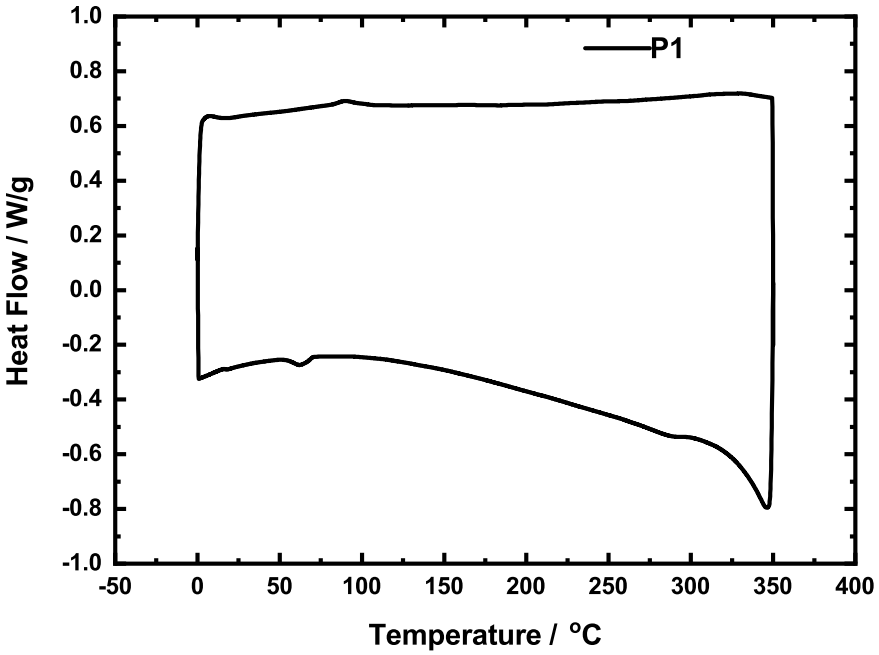

DSC trace of Polymer P1. There were no observable melts or crystallisation in the DSC trace. These polymers in general had featureless DSC traces.

8.8 Appendix 8

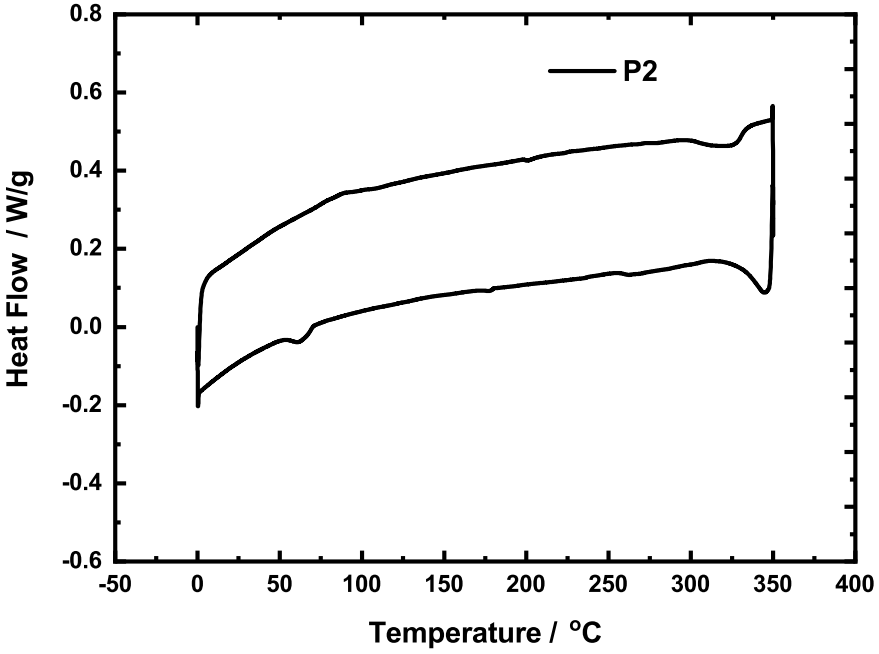

DSC trace of Polymer P2.

8.9 Appendix 9

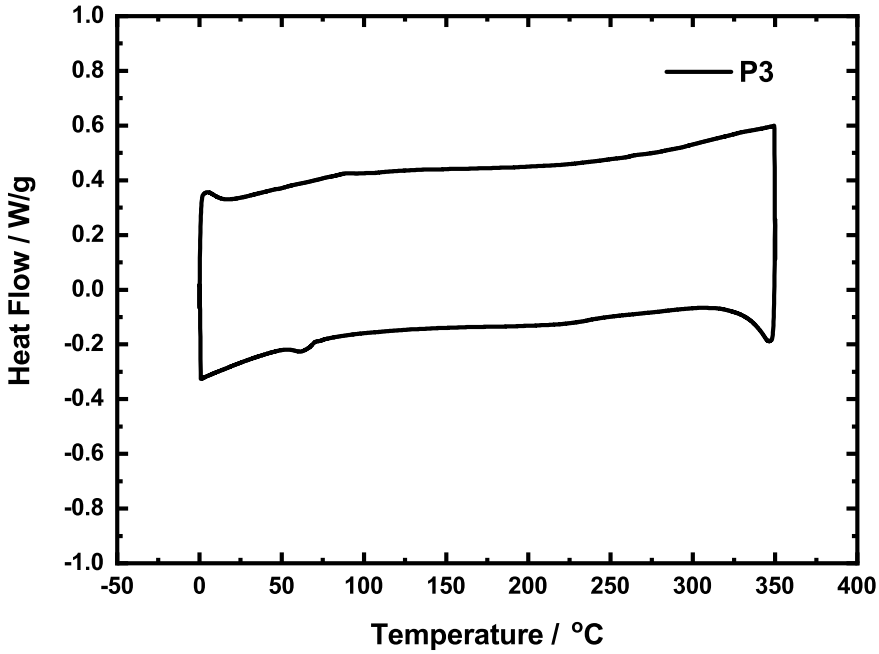

DSC trace of Polymer P3.

8.10 Appendix 10

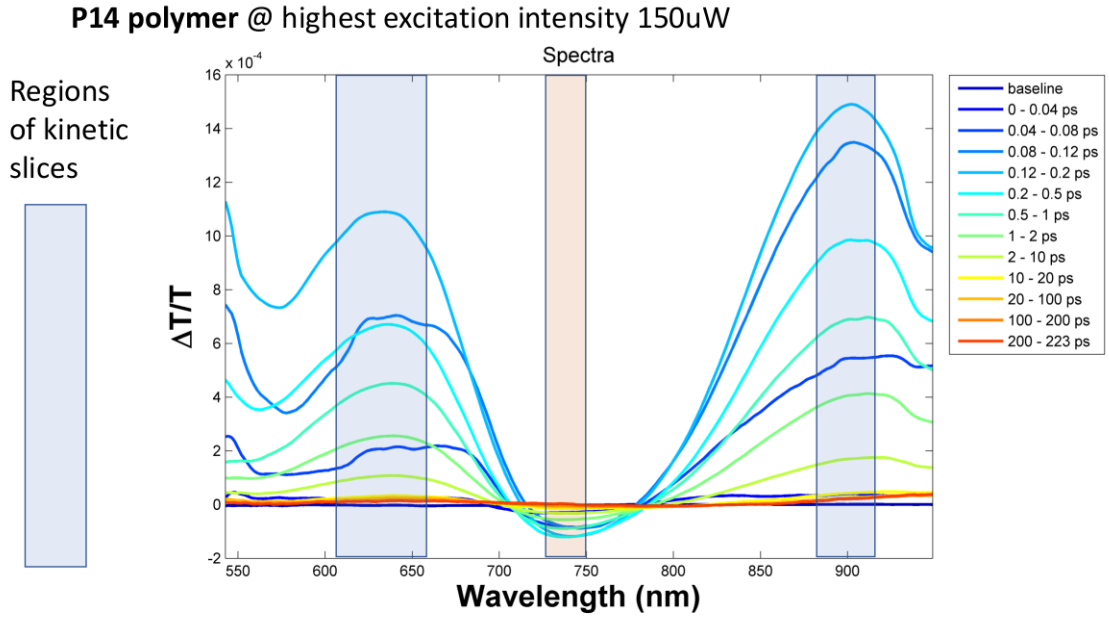

8.11 Appendix 11

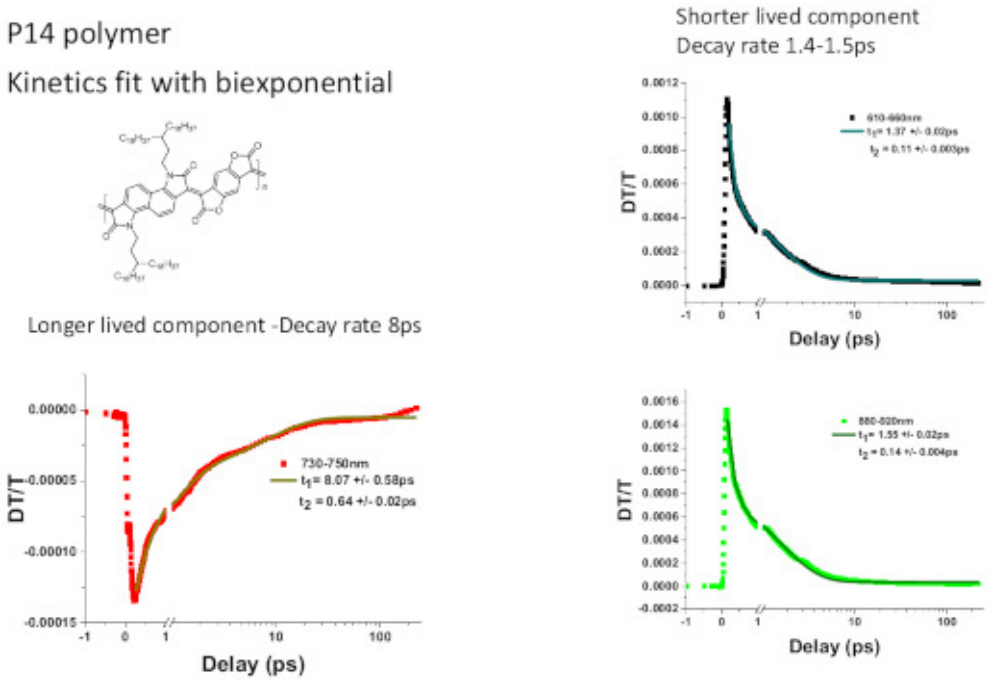

8.12 Appendix 12

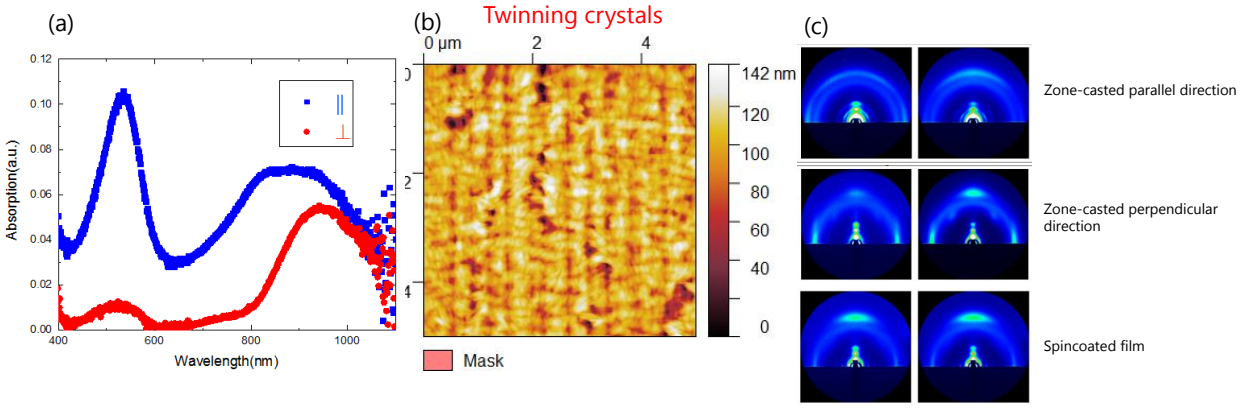

a) Absorption spectrum anisotropy of aligned fused polyisoindigo film. b) AFM image of aligned fused polyisoindigo film showing twinning crystal formation. c) Grazing incidence wide-angle X-ray scattering patterns of spin-coated and aligned films with two GI angles (parallel and perpendicular to alignment direction)

8.13 Appendix 13

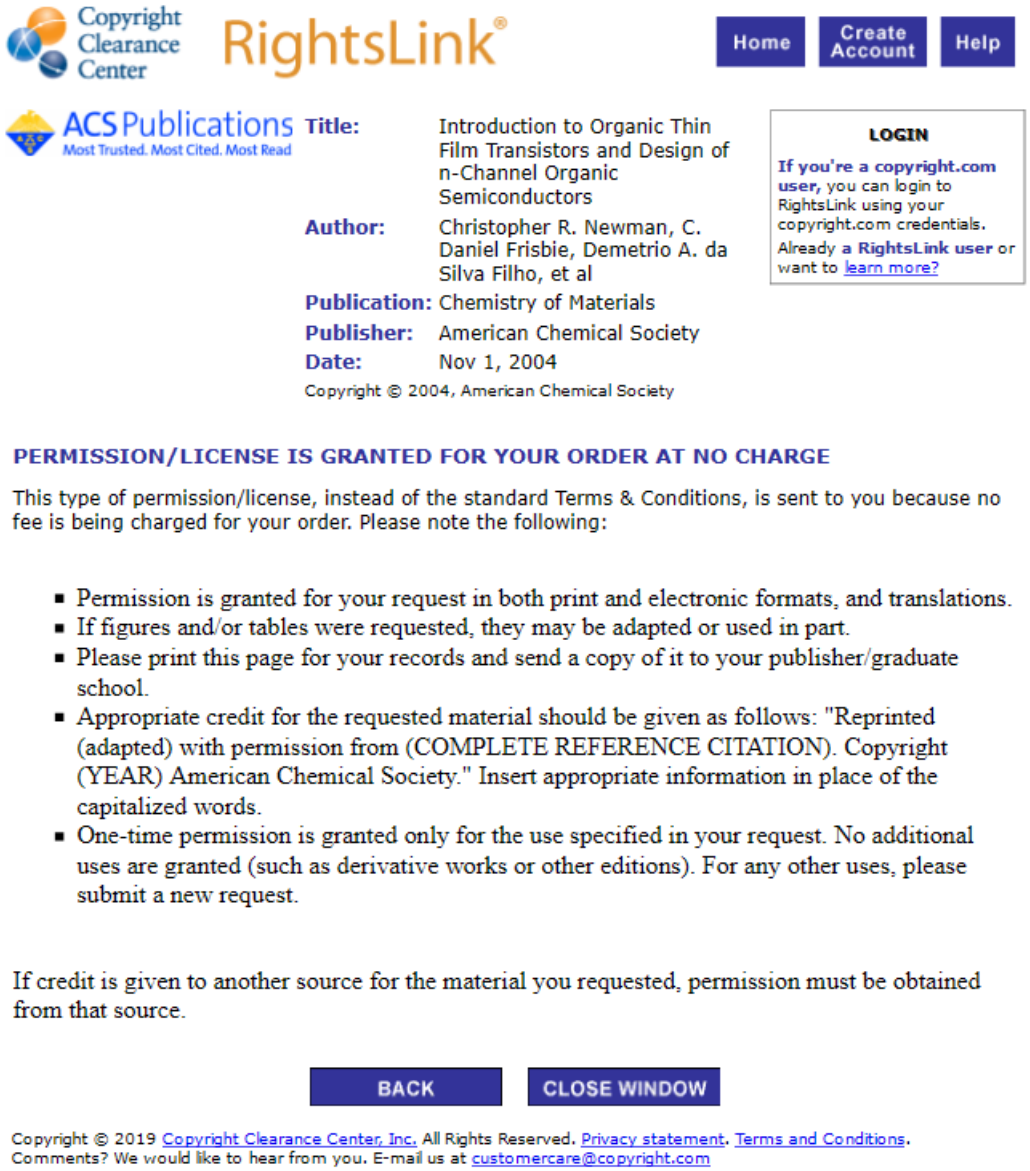

Copyright Clearance Center RightsLink®

Home | Create Account | Help

ACS Publications
Most Trusted. Most Cited. Most Read

Title: Introduction to Organic Thin Film Transistors and Design of n-Channel Organic Semiconductors

Author: Christopher R. Newman, C. Daniel Frisbie, Demetrio A. da Silva Filho, et al

Publication: Chemistry of Materials

Publisher: American Chemical Society

Date: Nov 1, 2004

Copyright © 2004, American Chemical Society

LOGIN

If you're a copyright.com user, you can login to RightsLink using your copyright.com credentials.

Already **a RightsLink user** or want to learn more?

PERMISSION/LICENSE IS GRANTED FOR YOUR ORDER AT NO CHARGE

This type of permission/license, instead of the standard Terms & Conditions, is sent to you because no fee is being charged for your order. Please note the following:

- Permission is granted for your request in both print and electronic formats, and translations.
- If figures and/or tables were requested, they may be adapted or used in part.
- Please print this page for your records and send a copy of it to your publisher/graduate school.
- Appropriate credit for the requested material should be given as follows: "Reprinted (adapted) with permission from (COMPLETE REFERENCE CITATION). Copyright (YEAR) American Chemical Society." Insert appropriate information in place of the capitalized words.
- One-time permission is granted only for the use specified in your request. No additional uses are granted (such as derivative works or other editions). For any other uses, please submit a new request.

If credit is given to another source for the material you requested, permission must be obtained from that source.

BACK | CLOSE WINDOW

Copyright © 2019 Copyright Clearance Center, Inc. All Rights Reserved. Privacy statement. Terms and Conditions.
Comments? We would like to hear from you. E-mail us at customercare@copyright.com

Copyright certificate Figure 1.6.

8.14 Appendix 14

polymer P7

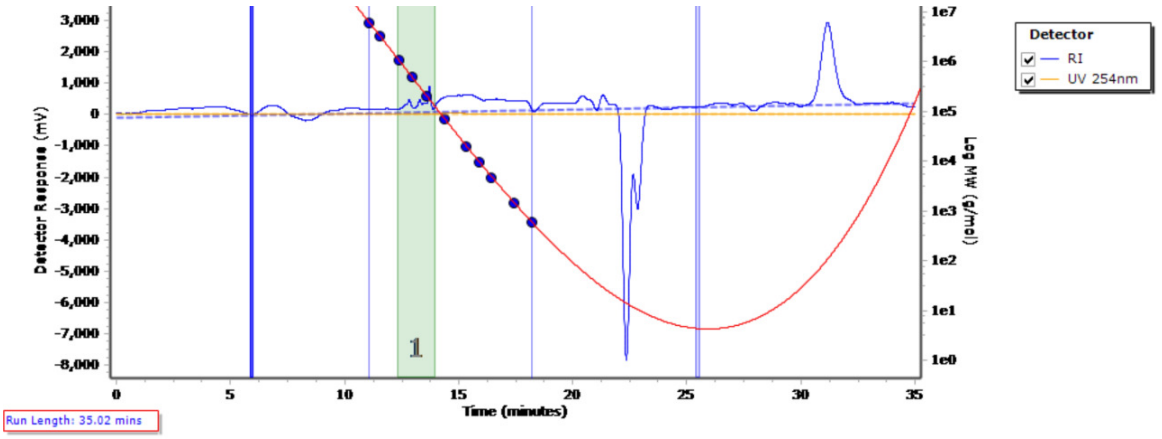

polymer P8

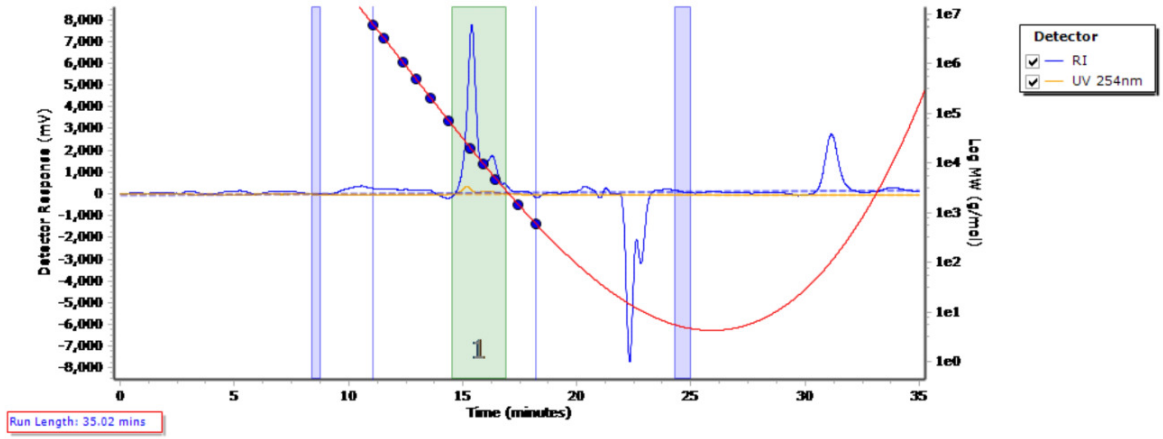

Images of the GPC traces for polymers P7 and P8.

8.15 Appendix 15

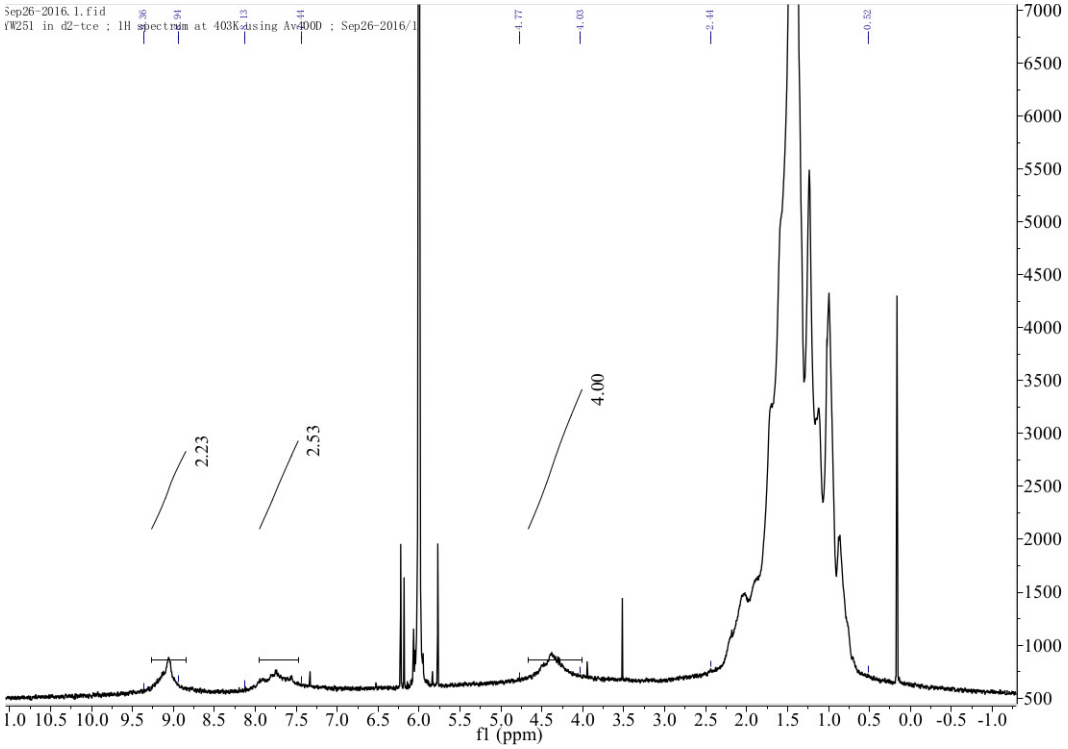

Proton NMR spectrum of polymer P5 in TCE-d^2 measured at 400 K.